PROGRESS AND PROSPECTS ON SKIN IMAGING TECHNOLOGY, TELEDERMATOLOGY AND ARTIFICIAL INTELLIGENCE IN DERMATOLOGY

EDITED BY: Yong Cui, H. Peter Soyer, Paola Pasquali, Je-Ho Mun and Hang Li
PUBLISHED IN: Frontiers in Medicine

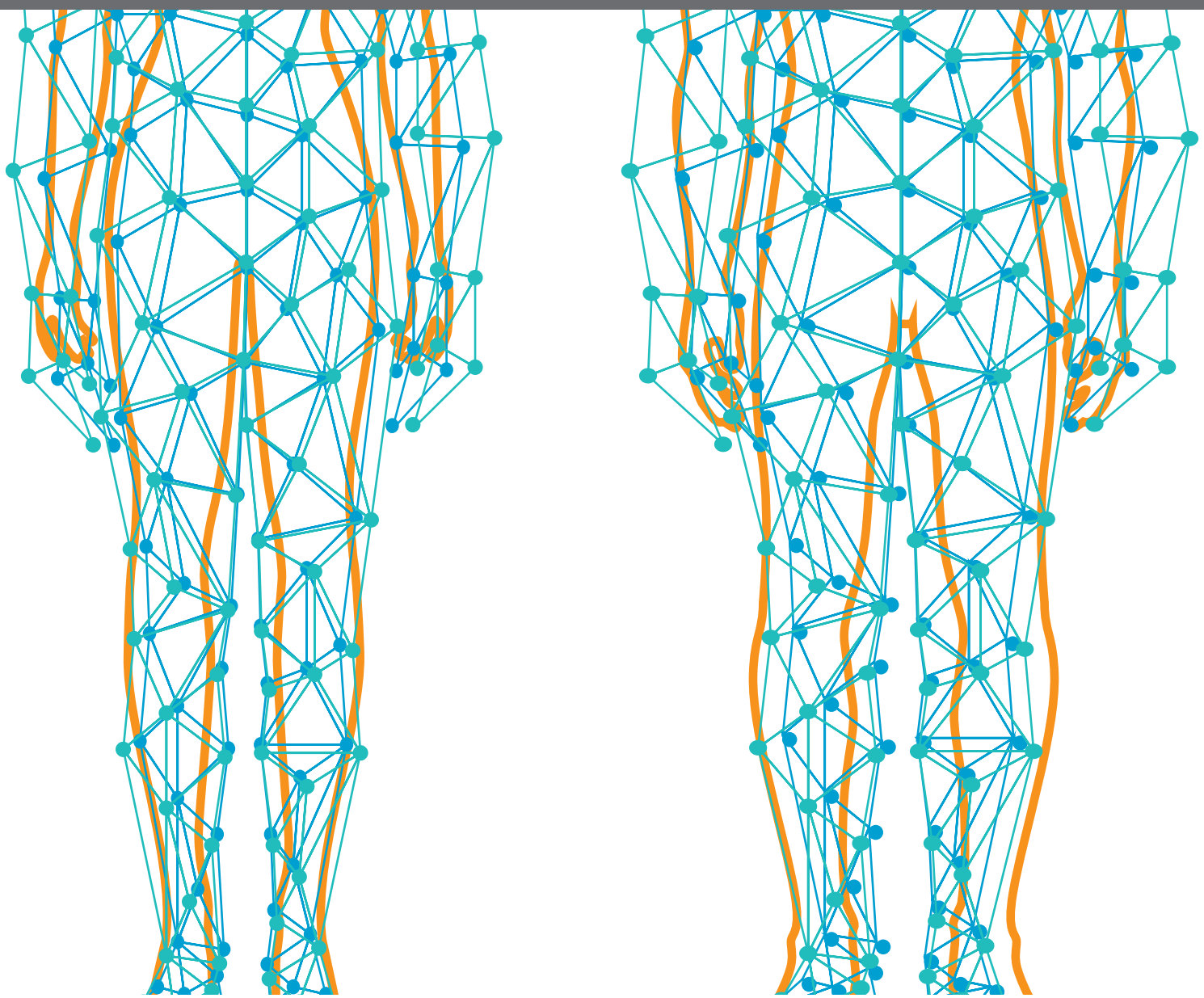

frontiers Research Topics

ISSN 1664-8714
ISBN 978-2-88971-987-7
DOI 10.3389/978-2-88971-987-7

About Frontiers

Frontiers is more than just an open-access publisher of scholarly articles: it is a pioneering approach to the world of academia, radically improving the way scholarly research is managed. The grand vision of Frontiers is a world where all people have an equal opportunity to seek, share and generate knowledge. Frontiers provides immediate and permanent online open access to all its publications, but this alone is not enough to realize our grand goals.

Frontiers Journal Series

The Frontiers Journal Series is a multi-tier and interdisciplinary set of open-access, online journals, promising a paradigm shift from the current review, selection and dissemination processes in academic publishing. All Frontiers journals are driven by researchers for researchers; therefore, they constitute a service to the scholarly community. At the same time, the Frontiers Journal Series operates on a revolutionary invention, the tiered publishing system, initially addressing specific communities of scholars, and gradually climbing up to broader public understanding, thus serving the interests of the lay society, too.

Dedication to Quality

Each Frontiers article is a landmark of the highest quality, thanks to genuinely collaborative interactions between authors and review editors, who include some of the world's best academicians. Research must be certified by peers before entering a stream of knowledge that may eventually reach the public - and shape society; therefore, Frontiers only applies the most rigorous and unbiased reviews.
Frontiers revolutionizes research publishing by freely delivering the most outstanding research, evaluated with no bias from both the academic and social point of view. By applying the most advanced information technologies, Frontiers is catapulting scholarly publishing into a new generation.

What are Frontiers Research Topics?

Frontiers Research Topics are very popular trademarks of the Frontiers Journals Series: they are collections of at least ten articles, all centered on a particular subject. With their unique mix of varied contributions from Original Research to Review Articles, Frontiers Research Topics unify the most influential researchers, the latest key findings and historical advances in a hot research area! Find out more on how to host your own Frontiers Research Topic or contribute to one as an author by contacting the Frontiers Editorial Office: frontiersin.org/about/contact

PROGRESS AND PROSPECTS ON SKIN IMAGING TECHNOLOGY, TELEDERMATOLOGY AND ARTIFICIAL INTELLIGENCE IN DERMATOLOGY

Topic Editors:
Yong Cui, China-Japan Friendship Hospital, China
H. Peter Soyer, The University of Queensland, Australia
Paola Pasquali, Pius Hospital de Valls, Spain
Je-Ho Mun, Seoul National University Hospital, South Korea
Hang Li, Peking University First Hospital, China

Topic Editor H. Peter Soyer is a shareholder of MoleMap NZ Limited and e-derm consult GmbH, and undertakes regular teledermatological reporting for both companies. He is a Medical Consultant for Canfield Scientific Inc., MetaOptima and Revenio Research Oy and also a Medical Advisor for First Derm.

Citation: Cui, Y., Soyer, H. P., Pasquali, P., Mun, J.-H., Li, H., eds. (2021). Progress and Prospects on Skin Imaging Technology, Teledermatology and Artificial Intelligence in Dermatology. Lausanne: Frontiers Media SA.
doi: 10.3389/978-2-88971-987-7

Table of Contents

frontiers in Medicine

EDITORIAL
published: 12 November 2021
doi: 10.3389/fmed.2021.757538

Editorial: Progress and Prospects on Skin Imaging Technology, Teledermatology and Artificial Intelligence in Dermatology

Chengxu Li[1], Je-Ho Mun[2], Paola Pasquali[3], Hang Li[4], H. Peter Soyer[5] and Yong Cui[1]**

[1] Department of Dermatology, China-Japan Friendship Hospital, Beijing, China, [2] Department of Dermatology, Seoul National University College of Medicine, Seoul, South Korea, [3] Department of Dermatology, Pius Hospital de Valls, Tarragona, Spain, [4] Department of Dermatology, Peking University First Hospital, Beijing, China, [5] The University of Queensland Diamantina Institute, The University of Queensland, Dermatology Research Centre, Brisbane, QLD, Australia

Keywords: skin imaging technology, dermoscopy, reflectance confocal microscopy, teledermatology, artificial intelligence in dermatology, big data in dermatology

OPEN ACCESS

Edited by:
Ximena Wortsman, University of Chile, Chile

Reviewed by:
Manu Jain, Memorial Sloan Kettering Cancer Center, United States
Cristian Navarrete-Dechent, Pontificia Universidad Católica de Chile, Chile

***Correspondence:**
H. Peter Soyer
p.soyer@uq.edu.au
Yong Cui
wuhucuiyong@vip.163.com

Specialty section:
This article was submitted to Dermatology, a section of the journal Frontiers in Medicine

Received: *12 August 2021*
Accepted: *20 October 2021*
Published: *12 November 2021*

Citation:
Li C, Mun J-H, Pasquali P, Li H, Soyer HP and Cui Y (2021) Editorial: Progress and Prospects on Skin Imaging Technology, Teledermatology and Artificial Intelligence in Dermatology. Front. Med. 8:757538. doi: 10.3389/fmed.2021.757538

Editorial on the Research Topic

Progress and Prospects on Skin Imaging Technology, Teledermatology and Artificial Intelligence in Dermatology

INTRODUCTION

Dermatology is a clinical discipline based on intuitive features. With the emergence of digital technology, remote transmission, and internet technologies, dermatology has become a very well-suited discipline to integrate these technologies and apply them in clinical practice due to its characteristics. At present, the development of skin imaging technologies [dermoscopy, reflectance confocal microscopy (RCM), optical coherence tomography (OCT), etc.], teledermatology, and artificial intelligence (AI) has profoundly and comprehensively changed the nature, service model, and public recognition of dermatology (1). Skin imaging, as an important technical system in modern dermatology, continues to gain the attention of researchers and the wider community alike. In this spirit, we have proposed a Research Topic titled "Progress and Prospects on Skin Imaging Technology, Teledermatology and Artificial Intelligence in Dermatology" and are very pleased indeed that nine manuscripts on the various aspects of skin imaging technology, five manuscripts on teledermatology, and seven manuscripts on AI in dermatology have been published under the banner of this specific Research Topic. In the current article, we aimed to introduce 21 articles published in this specific Research Topic, so that readers can refer to the articles more pertinently.

UPDATES ON SKIN IMAGING TECHNOLOGY

Skin imaging, as a non-invasive imaging technology, is widely used in disease diagnosis (2), treatment follow-up (3), and surgical boundary determination (4). The combined use of different skin imaging equipment and the combination of skin imaging and AI have further improved the diagnostic accuracy of skin imaging and broadened its application range (5, 6).

In terms of research on dermoscopy, Wang et al. identified new dermatoscopic features through a morphological study of 39 patients with acquired perforating dermatosis. Relative to previously reported dermoscopic features, the newly identified features such as the dam shape uplift at the

periphery may contribute to assist clinical diagnosis. Chen et al. investigated the trichoscopic features of female pattern hair loss in Chinese Han patients, analyzed the difference between different genders and pointed out female pattern hair loss could occur in male with characteristics similar to female. Gao et al. provided a comprehensive summary of the dermoscopic features for four common cutaneous vascular anomalies, namely, infantile hemangioma, cherry angioma, angiokeratoma, and pyogenic granuloma in the Chinese Han population. They described that dermoscopic features of cherry angioma and the other common vascular tumors vary in age stages and different anatomical sites. Chanprapaph et al. used nailfold capillaroscopy technology to investigate nailfold features in patients with systemic lupus erythematosus, dermatomyositis, and systemic sclerosis, and tried to find out which features could distinguish these connective tissue diseases. In addition, the authors explored different capillaroscopic abnormalities and their association with disease activity.

In terms of RCM applications, Feng et al. summarized confocal features of lesions in 11 patients with syringoma on the vulva. The authors compared RCM features with the biopsy findings for histopathological correlation and then highlighted the potential role of RCM in the diagnosis and differential diagnosis of vulva syringoma. Liu et al. studied persistent hypopigmented patches suspicious of early-stage vitiligo or hypopigmented mycosis fungoides with RCM. All the imaged lesions were biopsied and analyzed by histopathology. Their findings indicated that RCM could be a useful tool to screen for hypopigmented mycosis fungoides in hypopigmented lesions underlining. The combined use of dermoscopy and RCM may lead to new diagnostic indications. Wang et al. described dermoscopy and confocal characteristics of two patients with primary cutaneous amyloidosis in two different histopathological subtypes. Although this disease usually is suspected clinically, for cases with an atypical presentation, dermoscopy combined with RCM can be used as a reference for clinicians.

In the application of high-frequency ultrasound, Li et al. conducted a retrospective study to investigate the ultrasonographic features of pilomatricoma and determined the associations of these characteristics with clinical features in different histopathological subtypes. Ultra-high-frequency was proved to be a useful tool to diagnose and stage this disease before surgery. Due to the unique structure and function of the nail unit (NU), it is particularly important to develop useful non-invasive inspection methods. Lipska et al. described that high-frequency ultrasonography was promising in the visualization of the NU structure although in some cases the image quality was insufficient. In addition to ultrasonographic features, the authors measured transonychial water loss by evaporimetry.

All these papers utilizing skin imaging technologies such as dermoscopy, RCM and high-frequency ultrasound, have in common that still numerous inflammatory and neoplastic skin conditions can be studied with imaging technologies leading to a more objective characterization of the morphologic features of the many faces of skin pathologies.

UPDATES ON TELEDERMATOLOGY

Teledermatology is an effective approach to decrease the differences in healthcare quality among regional and metropolitan areas and provide an overall improvement. Teledermatology is enabled by remote transmission technology and internet technology and is gradually changing the way of healthcare access. Endeavors to provide remote consultation and care through telemedicine platforms have started in the last years in several countries. Live interactive technology has enabled remote controlled access to RCM devices and guided clinicians toward diagnosis, breaking through the limitations of existing store-and-forward teledermatology (7). Especially during the COVID-19 pandemic, teledermatology played a very important role and its development was significantly promoted (8).

The following few articles represent a small snapshot on the progress in this field. Edwards et al. summarized the strategy for teledermatology in the COVID-19 period in the dermatology department at Princess Alexandra Hospital, in Brisbane, Australia. A system of telephone consultations and store-and-forward imaging were used to deal with the situation of the epidemic. The efficacy of this system provides experience to develop future telemedicine systems. Giavina-Bianchi et al. compared the consistency of diagnosis made by teledermatologists and in-person dermatologists and presented a high accuracy in the diagnosis of the 20 most frequent inflammatory dermatoses using teledermatology. Besides, their study discovered moderate consistency between teledermatologists, histopathological reports, and in-person dermatologists' diagnosis in skin neoplasms, which reassures the potential of store-and-forward teledermatology being an option for patient care with skin cancer. Polańska et al. present the current applications of 20-MHz ultrasonography in dermatology, including skin tumors and chronic skin diseases. Moreover, the authors analyzed the possibilities for high-frequency ultrasonography being used as a tool in teledermatology, especially in the diagnosis and monitoring of patients with chronic skin diseases, such as psoriasis, atopic dermatitis, vitiligo, or leg ulcers. The convergence of teledermatology with software has driven the management of chronic skin diseases. Stark et al. introduced how IMPROVE 1.0, an android app monitoring psoriasis patients by questionnaires, helped doctors and patients to assess and study disease activity. And it demonstrated smartphone apps' value in disease management and doctor-patient communication.

UPDATES ON ARTIFICIAL INTELLIGENCE IN DERMATOLOGY

Artificial intelligence is strengthening dermatologists (9). Especially for atypical, challenging, or doubtful cases, AI algorithms could be a useful tool for the dermatologists (10). Based on big data made of high-quality skin images (including skin photos, dermoscopy images, skin confocal images, skin pathology images), AI assists dermatologists in making clinical decisions in diagnosis, evaluation, and treatment. Progress

has been achieved through new efforts in the development and application of AI support in dermatology, such as the artificially intelligent diagnosis algorithm for skin cancer by Stanford researchers based on the US data (11), the International Skin Imaging Collaboration (ISIC) with its annual challenges and China's Chinese Skin Image Database (12). Diagnosis of skin diseases is often challenging, and computer-aided diagnostic tools are urgently needed to underpin decision making. Thomsen et al. used non-standardized images to train a VGG-16 model to identify acne from rosacea and cutaneous T-cell lymphoma from eczema. The performance rates reported were equal or superior to those reported for general practitioners with dermatological training, indicating that computer-aided diagnostic models based on the convolutional neural network have the potential in diagnosing multiple-lesion skin diseases. Zhu et al. applied Google's EfficientNet-b4 with pre-trained weights on ImageNet as the backbone of the CNN architecture and trained it using labeled dermoscopic images of 14 common skin diseases. The test results show that the proposed framework has high classification performance, which is superior to previously reported methods. Also, the performance of this CNN model was comparable to 280 board-certified dermatologists in an eight-class diagnostic task, with higher sensitivity in all of the included diseases. Onychomycosis is a common fungal nail infection, and accurate diagnosis is important. Lim et al. reviewed the main characteristics of traditional diagnostic tools for onychomycosis and the newly developed technologies, including dermoscopy, RCM, molecular assays, and AI.

The role of the Digital Imaging and Communications in Medicine (DICOM) standard in AI for skin disease was reviewed. Although DICOM is common in some medical image-producing specialties, the application of DICOM in dermatology imaging has been limited. Caffery et al. discussed the role of DICOM in AI from the perspective of skin imaging and reviewed the current status of AI-specific content in the DICOM standard. DICOM can improve AI workflows by encoding derived objects (e.g., secondary images, visual explainability maps, AI algorithm output) and the efficient curation of multi-institutional datasets for machine learning training, testing, and validation.

Chinese dermatologists' attitudes toward AI have been investigated before, and the vast majority of interviewees believe that the role of AI is to assist dermatologists in diagnosis and treatment (13). Polesie et al. conducted a survey on AI in dermatopathology and reported that 848 dermatopathologists worldwide expected AI for handling narrowly specified tasks, such as automated detection of mitoses and tumor margins as well as for immunostaining evaluation, rather than a global automated suggestion of diagnoses. To understand how to better help dermatologists CNN's inner workings, Dalmau et al. developed an online hands-on pedagogical activity as a tool for beginners to learn about CNNs. Such an attempt is of great significance for clinicians including dermatologists accessing computer science and we encourage and appreciate further solutions in this context.

CONCLUSION

In sum, this special Research Topic of skin imaging technology, teledermatology, and AI in dermatology collects the latest endeavors, progresses, experiences, and challenges in these fields and shows the successful integration of modern information technology into dermatology. Through these studies and investigations, the expectations and positioning of AI in dermatology have been clarified, the applicability of skin imaging techniques has been expanded, and the changes and development of teledermatology in different contexts have been driven. In our estimation, in the future these three essential elements could offer powerful support for patients and doctors alike and even become a mainstream medical model.

AUTHOR CONTRIBUTIONS

All authors listed have made a substantial, direct and intellectual contribution to the work, and approved it for publication.

FUNDING

This work has been supported by the Beijing Municipal Science and Technology Commission Medicine Collaborative Science and Technology Innovation Research Project (No. Z191100007719001). HS holds an NHMRC MRFF Next Generation Clinical Researchers Program Practitioner Fellowship (APP1137127).

REFERENCES

1. Li C, Shen C, Xue K, Shen X, Jing Y, Wang Z, et al. Artificial intelligence in dermatology: past, present, and future. *Chin Med J Peking.* (2019) 132:2017–20. doi: 10.1097/CM9.0000000000000372
2. Fei W, Li C, Cui Y. Diagnostic value of dermoscopy combined with reflectance confocal microscopy for clinically equivocal blue nevus. *Chin Med J Peking.* (2020) 133:2116–8. doi: 10.1097/CM9.0000000000001007
3. Navarrete-Dechent C, Cordova M, Liopyris K, Aleissa S, Rajadhyaksha M, Cohen G, et al. *In vivo* imaging characterization of basal cell carcinoma cutaneous response to high dose ionizing radiation therapy: a prospective study of reflectance confocal microscopy, dermoscopy, and ultrasound. *J Am Acad Dermatol.* (2021) 84:1575–84. doi: 10.1016/j.jaad.2020.07.130
4. Lupu M, Voiculescu VM, Caruntu A, Tebeica T, Caruntu C, et al. Preoperative evaluation through dermoscopy and reflectance confocal microscopy of the lateral excision margins for primary basal cell carcinoma. *Diagnostics.* (2021) 11:120. doi: 10.3390/diagnostics11010120
5. Monnier J, De Carvalho N, Harris U, Garfinkel J, Saud A, Navarrete-Dechent C, et al. Combined reflectance confocal microscopy and optical coherence tomography to improve the diagnosis of equivocal lesions for basal cell carcinoma. *J Am Acad Dermatol.* (2021) 2020:S0190-9622(21)00623-X.
6. Campanella G, Navarrete-Dechent C, Liopyris K, Monnier J, Aleissa S, Minas B, et al. Deep learning for basal cell carcinoma detection for reflectance confocal microscopy. *J Invest Dermatol.* (2021) 2021:S0022-202X(21)01437-8. doi: 10.1016/j.jid.2021.06.015
7. Rubinstein G, Garfinkel J, Jain M. Live, remote control of an *in vivo* reflectance confocal microscope for diagnosis of basal cell carcinoma

at the bedside of a patient 2500 miles away: a novel tele-reflectance confocal microscope approach. *J Am Acad Dermatol.* (2019) 81:e41–2. doi: 10.1016/j.jaad.2019.02.016
8. Su MY, Das S. Expansion of asynchronous teledermatology during the COVID-19 pandemic. *J Am Acad Dermatol.* (2020) 83:e471–2. doi: 10.1016/j.jaad.2020.08.054
9. Tschandl P, Rinner C, Apalla Z, Argenziano G, Codella N, Halpern A, et al. Human-computer collaboration for skin cancer recognition. *Nat Med.* (2020) 26:1229–34. doi: 10.1038/s41591-020-0942-0
10. Muñoz López C, Ramírez Cornejo C, Marchetti M A, Han S S, Del Barrio Díaz P, Jaque A, et al. Performance of a deep neural network in teledermatology: a single-centre prospective diagnostic study. *J Eur Acad Dermatol.* (2021) 35:546–53. doi: 10.1111/jdv.16979
11. Esteva A, Kuprel B, Novoa RA, Ko J, Swetter SM, Blau HM, et al. Dermatologist-level classification of skin cancer with deep neural networks. *Nature.* (2017) 542:115–8. doi: 10.1038/nature21056
12. Li C, Fei W, Shen C, Wang Z, Jing Y, Meng R, et al. Diagnostic capacity of skin tumor artificial intelligence-assisted decision-making software in real-world clinical settings. *Chin Med J Peking.* (2020) 133:2020–6. doi: 10.1097/CM9.0000000000001002
13. Shen C, Li C, Xu F, Wang Z, Shen X, Gao J, et al. Web-based study on Chinese dermatologists' attitudes towards artificial intelligence. *Ann Transl Med.* (2020) 8:698. doi: 10.21037/atm.2019.12.102

Conflict of Interest: HS is a shareholder of MoleMap NZ Limited and e-derm consult GmbH, and undertakes regular teledermatological reporting for both companies. HS is a Medical Consultant for Canfield Scientific Inc., MoleMap Australia Pty. Ltd., Revenio Research Oy, and a Medical Advisor for First Derm.

The remaining authors declare that the research was conducted in the absence of any commercial or financial relationships that could be construed as a potential conflict of interest.

Publisher's Note: All claims expressed in this article are solely those of the authors and do not necessarily represent those of their affiliated organizations, or those of the publisher, the editors and the reviewers. Any product that may be evaluated in this article, or claim that may be made by its manufacturer, is not guaranteed or endorsed by the publisher.

frontiers in Medicine

ORIGINAL RESEARCH
published: 22 September 2020
doi: 10.3389/fmed.2020.574329

Deep Learning for Diagnostic Binary Classification of Multiple-Lesion Skin Diseases

Kenneth Thomsen[1]*, *Anja Liljedahl Christensen*[2], *Lars Iversen*[1], *Hans Bredsted Lomholt*[3] *and Ole Winther*[2,4,5]

[1] Department of Dermatology and Venereology, Aarhus University Hospital, Aarhus, Denmark, [2] Department of Applied Mathematics and Computer Science, Technical University of Denmark, Lyngby, Denmark, [3] Clinical Institute, Aalborg University, Aalborg, Denmark, [4] Center for Genomic Medicine, Rigshospitalet, Copenhagen University Hospital, Copenhagen, Denmark, [5] Department of Biology, Bioinformatics Centre, University of Copenhagen, Copenhagen, Denmark

Background: Diagnosis of skin diseases is often challenging and computer-aided diagnostic tools are urgently needed to underpin decision making.

Objective: To develop a convolutional neural network model to classify clinically relevant selected multiple-lesion skin diseases, this in accordance to the STARD guidelines.

Methods: This was an image-based retrospective study using multi-task learning for binary classification. A VGG-16 model was trained on 16,543 non-standardized images. Image data was distributed in training set (80%), validation set (10%), and test set (10%). All images were collected from a clinical database of a Danish population attending one dermatological department. Included was patients categorized with ICD-10 codes related to acne, rosacea, psoriasis, eczema, and cutaneous t-cell lymphoma.

Results: Acne was distinguished from rosacea with a sensitivity of 85.42% CI 72.24–93.93% and a specificity of 89.53% CI 83.97–93.68%, cutaneous t-cell lymphoma was distinguished from eczema with a sensitivity of 74.29% CI 67.82–80.05% and a specificity of 84.09% CI 80.83–86.99%, and psoriasis from eczema with a sensitivity of 81.79% CI 78.51–84.76% and a specificity of 73.57% CI 69.76–77.13%. All results were based on the test set.

Conclusion: The performance rates reported were equal or superior to those reported for general practitioners with dermatological training, indicating that computer-aided diagnostic models based on convolutional neural network may potentially be employed for diagnosing multiple-lesion skin diseases.

Keywords: deep neural network (DNN), dermatology, skin disease, acne, rosacea, psoriasis, cutaneous T cell lymphoma (CTCL), ezcema

OPEN ACCESS

Edited by:
Je-Ho Mun,
Seoul National University Hospital,
South Korea

Reviewed by:
Irina Khamaganova,
Pirogov Russian National Research Medical University, Russia
Harald Kittler,
Medical University of Vienna, Austria

***Correspondence:**
Kenneth Thomsen
kenthoms@rm.dk

Specialty section:
This article was submitted to Dermatology, a section of the journal Frontiers in Medicine

Received: *19 June 2020*
Accepted: *24 August 2020*
Published: *22 September 2020*

Citation:
Thomsen K, Christensen AL, Iversen L, Lomholt HB and Winther O (2020) Deep Learning for Diagnostic Binary Classification of Multiple-Lesion Skin Diseases. Front. Med. 7:574329. doi: 10.3389/fmed.2020.574329

INTRODUCTION

Skin diseases rank fourth among non-fatal diseases with respect to global burden (1) and are, estimated to account for 12–20% of general practitioner (GP) consultations (2, 3). With more than 1,500 different dermatological diagnoses (4), differential diagnosing can be very challenging. GP diagnostic accuracy in dermatological disease has been estimated to fall in the 48–77% range (5).

For GP's distinguishing between the two morphologically similar and common papulo-pustular skin diseases of acne and rosacea, and between the two common scaly erythematous diseases of psoriasis and eczema can be a challenge. Furthermore, cutaneous t-cell lymphoma (CTCL) is a rare malignant disease of the skin that is often difficult to distinguish from eczematous disease, even for trained dermatologists (6). Low diagnostic accuracy in primary healthcare combined with reports of a growing shortage of dermatologists in rural parts of the US (7) carry a risk of untimely treatment and triaging.

Computer-aided diagnostic (CAD) models based on convolutional neural network (CNN) have been developed with promising results for distinguishing what is typically single-lesion skin diseases, such as malignant melanoma, squamous cell carcinoma, or nail dystrophies (8–11). CAD models developed for these diseases are often trained by standardized imagery such as dermatoscopic images (8). Reports on CAD models for multiple-lesion skin diseases are few and have shown more moderate performance rates (8). A Google-associated research team published results on a combined image and text classifier for dermatology (12). This model achieved a 67–75% sensitivity in diagnosing multiple-lesion skin disease (including acne, eczema, and psoriasis). Recently Wu et al. did show an impressive 95% overall diagnostic accuracy in classifying atopic dermatitis, eczema and psoriasis on selected image material (13). Studies comparing the accuracy of CAD models to clinicians are generally based on image classification equivalent to retrospective analysis, though some head to head studies were conducted with prospective collected image material (12, 14, 15).

Machine learning models, broadly characterized as CNNs, have proven their merits in image classification (16). A CNN is a layered statistical model using two-dimensional convolutions, element-wise non-linearities, and local pooling operations in the convolutional layers. The input to a convolutional layer is a representation of the data from the previous layer. The first layer is the original color image of size "height times width times three" (for the three-color channels). The produced data representations are called feature maps. These maps should ideally capture some property of the original data relevant for the classification. After a number of convolutional layers, the final feature maps are collapsed into a vector that is fed into a number of fully connected layers. The final output layer uses a so-called softmax function to calculate the model's estimation of the class probabilities.

Open source CNN models are available both for training from scratch and for transfer learning (modifying parts of an extant model for a new task). These models are often tested on the ImageNet dataset of more than 1 million labeled high-resolution images, in the yearly ImageNet Large Scale Visual Recognition Challenge (ILSVRC). The VGG-16 model is based on the architecture developed by the Oxfords Visual Geometry Group (VGG) (17) and achieved top performance in the ILSVRC 2014.

TABLE 1 | Data distribution in disease category.

Disease	Included images	Excluded images	Patients included in final dataset
Psoriasis	6,545	1,052	790
Eczema/atopic dermatitis	5,350	977	870
CTCL	2,461	380	157
Acne	581	155	131
Rosacea	1,606	534	394
Total	16,543	3,098	2,342

Data and patient distribution in disease categories after data cleansing, for details on data cleansing see ***Supplementary Table 1****.*

The primary aim of this feasibility study was to investigate a diagnostic tool to assist primarily GPs in distinguishing between patients with common and rare multiple-lesion skin diseases that often have a similar clinical presentation, this in accordance to the STARD guidelines for reporting on diagnostic accuracy (18). We aimed to achieve a differential diagnostic accuracy equal to or above the 48–77% reported for GPs (5, 19). We focused on five multiple-lesion skin diseases and on non-standardized imagery to accommodate the paucity in the scientific literature (8), and—more importantly—to imitate the real-life clinical settings of primary healthcare professionals, where multiple-lesion dermatological diseases are often encountered and access to a dermatoscope is limited (20, 21).

MATERIALS AND METHODS

Dataset

A total of 19,641 images were provided from the local skin image database of the Department of Dermatology, Aarhus University Hospital (AUH), Denmark. The images were collected from 2,342 patients of a Danish population and therefore comprise mainly images of patients with Fitzpatrick skin type II and III, see **Table 1** for the disease distribution of the image data and patients. The database was designed for clinical reference such as disease monitoring and plenum discussion, and therefore certain non-skin images were included. Non-skin images were mainly yellow patient identification slips and skin sensitizers related to contact eczema. The data set was cleansed by a simple CNN model trained on 200 skin and 200 non-skin images. This model was tested on 150 images of both skin and non-skin images and removed all non-skin images from the test set with an accuracy of 99%. The architecture is shown in **Supplementary Figure 1**. After cleansing, 16,453 only-skin images were included for further investigation. A sampling counting 208 random images from the data set showed that 3.7% of the images represented healthy skin. No further effort was made to remove healthy

Abbreviations: AUH, Aarhus University Hospital; AUC, Area under the curve; CAD, Computer aided diagnostic; CNN, Convolutional neural network; CTCL, Cutaneous t-cell lymphoma; GP, General practitioner; ILSVRC, ImageNet Large Scale Visual Recognition Challenge; ICD-10, International Classification of Diseases, 10th Version; NPV, Negative predictive value; PPV, Positive predictive value; STN, Spatial transmitter network; VGG, Visual Geometry Group.

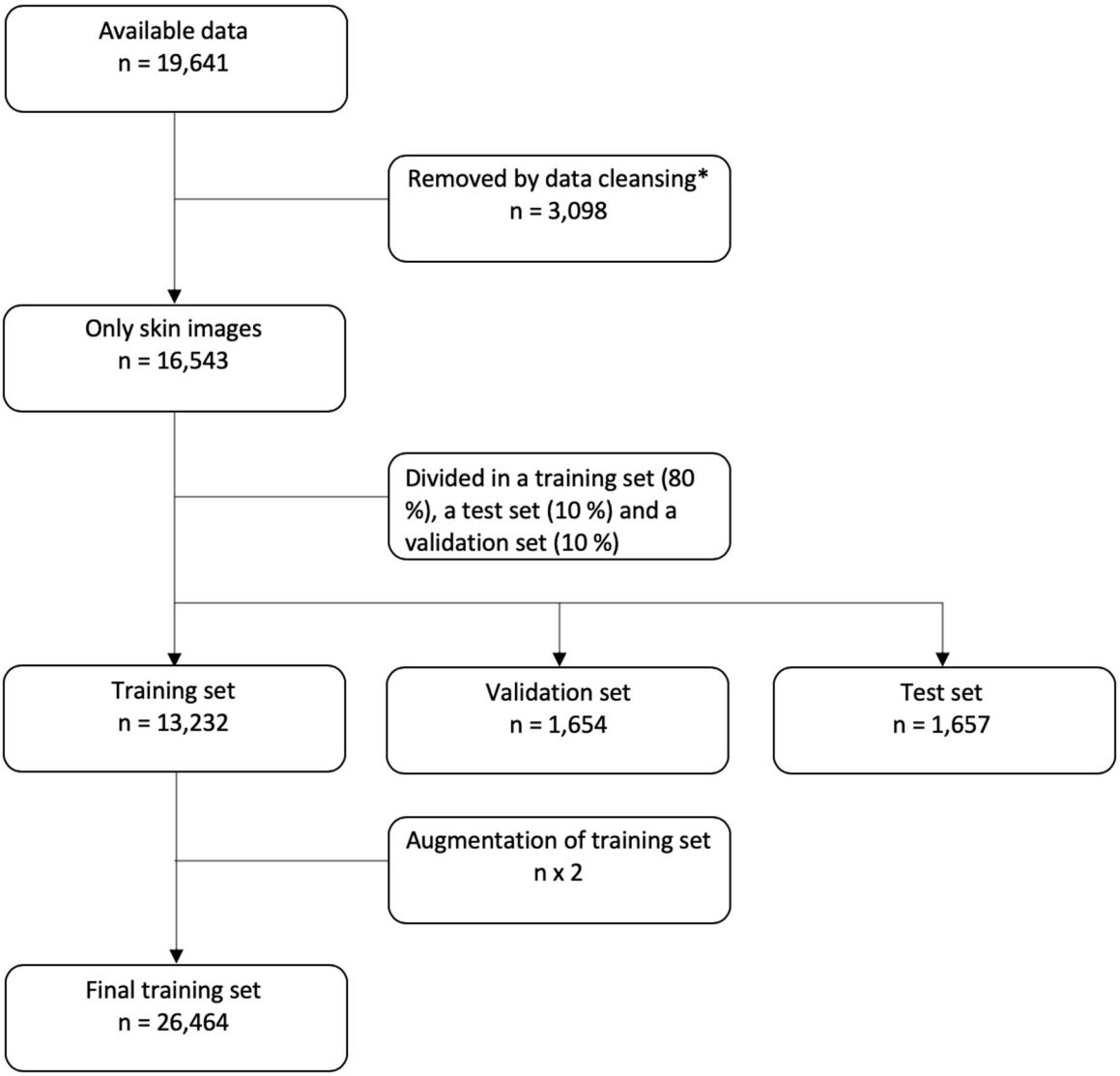

FIGURE 1 | Flowchart of data. *For details on data cleansing, please see the **Supplementary Figure 1**.

skin images from the data. All images were non-standardized photographs, in different resolutions, shot by a clinical photographer using a blue background or by a healthcare worker or by the patients themselves, the latter two with random background.

All images were diagnosed by trained dermatologists from the AUH according to the International Classification of Diseases, 10th Version (ICD-10). For the ICD-10 codes included in each disease category, see the **Supplementary Table 1**. CTCL diagnosis were histologically verified.

In the final data set, 80% of the data were used for training of the CNN, 10% were used as a validation set, and 10% were saved as a test set. For patients with multiple images, all images were placed either in the training, validation or test set. So the same patient will not have images used for both training and testing. The flow of data is shown in **Figure 1**.

Data Augmentation

Data augmentation of the training data set was applied randomly on each of the images to duplicate the samples by randomly either zooming in or out, flipping vertically or horizontally, rotating, or shifting.

Ethics

This study was conducted in concordance with the European General Data Protection Regulation. All relevant governmental bodies were notified of the study and usages of the image database.

The study was approved by the data controller of the clinical image database according to §10 of the Danish privacy act.

The Regional Ethics Committee of the Central Denmark Region (case no. 177/2018) deemed the study as not being a

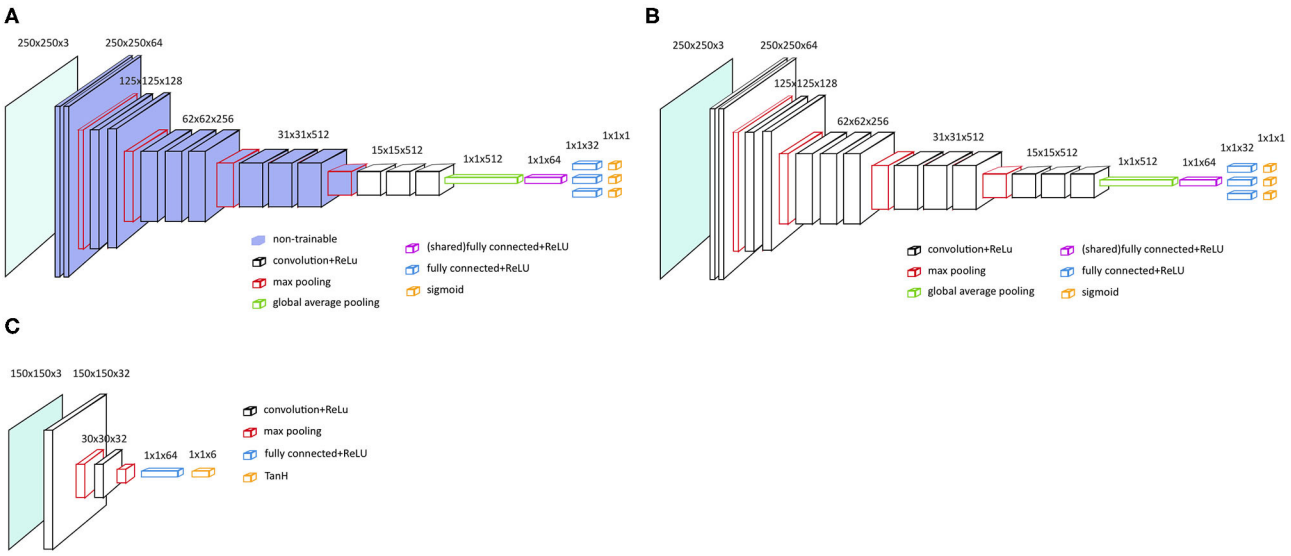

FIGURE 2 | Main architecture of the VGG-16 models. **(A)** VGG-16 model with frozen and pre-trained layers, i.e., VGG-16P and VGG-16PS. **(B)** VGG-16 architecture with no frozen layers and no pre-trained layers, i.e. VGG-16N and VGG-16NS. **(C)** Localization network with two convolutional layers, as applied for VGG-16PS and VGG-16NS.

health care project, and authorized the project to proceed without their approval.

The Danish Patient Safety Authority (case no. 31-1521-68) authorized the usage of the clinical image database without patient consent.

Finally, the study was registered in the Regional Research Study Registry of Central Denmark Region under the Danish Data Protection Agency (case no. 1-16-02-373-19).

Pre-processing

Cropping of noise, i.e., clothes, background and jewelry, in the pictures was done by K-means clustering using the pixel hue values. Using K = 2 clusters, each image was segmented into a skin cluster and a non-skin cluster (22). An image-dependent ratio was used with lower bound of 0.1 and upper bound of 0.3 to avoid under and over cropping, respectively. Examples of image cropping can be found in **Supplementary Figure 2**. All models were tested on original, cropped, and balanced versions of the data.

Tasks

Four binary CNN models were trained using data from all of the five diseases, afterwards model tests were conducted focusing on three separate binary tasks of all four binary models. This method is known as multi-task learning.

Task 1: classification of psoriasis vs. eczema; task 2: classification of acne vs. rosacea; and task 3: classification of CTCL (mainly images of mycosis fungoides, see **Supplementary Table 1** of ICD-10 code distribution) vs. eczema.

The primary outcome was the sensitivity and the specificity of the best model in the binary classification task. The secondary outcome was to define the best model by the area under the curve (AUC) and accuracy.

CNN Models

As a base model we choose VGG-16 with pre-trained parameters from the ILSVRC data set and no spatial transformer network (STN) (VGG-16P) (23). The fully connected layers and softmax layers were removed and replaced by new randomly initialized, fully connected layers and sigmoid layers, see **Figure 2A**. The pre-trained convolutional layers of the VGG-16 model were frozen.

To test if an even better performance could be achieved by training all the parameters from scratch, we also tested the VGG-16 with no pre-trained parameters and no STN (VGG-16N); see the architecture in **Figure 2B**.

To test if addition of a STN would increase the VGG-16 classification performance by assisting the VGG-16 in selecting the region of interest in an image (24), we developed two models similar to the two models described above, but added a STN; VGG-16 with pre-trained parameters and a STN (VGG-16PS) and VGG-16 with no pre-trained parameters and a STN (VGG-16NS).

Initial tests showed that the implementation of a STN was better with a localization network with two convolutional layers (**Figure 2C**).

See **Supplementary Table 2** "hyperparameters and hardware details" for more on this matter.

Data Presentation

In accordance with guidelines for developing and reporting machine learning models in biomedical research, we present our data as AUC, sensitivity, specificity, negative predictive value (NPV), and positive predictive value (PPV) (25). Unlike in medical science, PPV and NPV are not statistical analyses based on the incidence of a certain disease but an internal statistical analysis of the predicted negative or positive value

TABLE 2 | Results of best model; VGG-16P.

Task	Specificity	Sensitivity	PPV	NPV
Psoriasis from Eczema	73.57% (69.76–77.13%)	81.79% (78.51–84.76%)	76.79% (74.18–79.22%)	79.07% (76.03–81.81%)
Acne from Rosacea	89.53% (83.97–93.68%)	85.42% (72.24–93.93%)	69.49% (59.16–78.17%)	95.65% (91.72–97.76%)
CTCL from Eczema	84.09% (80.83–86.99%)	74.29% (67.82–80.05%)	63.16% (58.28–67.78%)	89.90% (87.59–91.83%)

Result of best model, VGG-16P. The 4 parameters shown are the results in distinguishing psoriasis from eczema, acne from rosacea and CTCL from eczema. The 95% confidence interval is in parenthesis. All results are based on cropped images of the test set.

TABLE 3 | Performance of all VGG-16 modifications.

	AUC	Accuracy
Task 1; Psoriasis vs. Eczema		
VGG-16P	**86.07% (83.96–88.18%)**	**77.82% (75.35–80.15%)**
VGG-16N	81.74% (79.34–84.14%)	73.70% (71.10–76.18%)
VGG-16PS	83.47% (81.18–85.76%)	74.87% (72.31–77.32%)
VGG-16NS	81.88% (79.49–84.27%)	73.11% (70.49–75.61%)
Task 2; Acne vs. Rosacea		
VGG-16P	89.89% (81.98–94.80%)	**88.64% (83.68–92.51%)**
VGG-16N	88.70% (82.36–95.04%)	86.82% (81.62–90.99%)
VGG-16PS	**92.74% (87.54–97.94%)**	88.18% (83.16–92.13%)
VGG-16NS	92.03% (86.60–97.46%)	87.73% (82.65–91.75%)
Task 3; CTCL vs. Eczema		
VGG-16P	**88.39% (85.30–91.48%)**	**81.46% (78.55–84.12%)**
VGG-16N	85.55% (82.16–88.94%)	78.90% (75.87–81.71%)
VGG-16PS	86.64% (83.36–89.92%)	78.77% (75.74–81.59%)
VGG-16NS	85.42% (82.02–88.82%)	77.37% (74.27–80.25%)

Results in AUC and accuracy for all model in all three tasks, best results are highlighted. The 95% confidence interval is in parenthesis. All results are based on cropped images of the test set.

which are truly negative or positive, as used in computer science. As is common practice, we also included results in accuracy to reduce complexity in interpreting our findings. All results are presented with a 95% confidence interval in the tables.

RESULTS

Primary Outcome

Results on sensitivity, specificity, NPV, and PPV are presented only for the best model; VGG-16P,. VGG-16P identified acne and rosacea with almost equal success as demonstrated by a specificity and sensitivity of 89.53 and 85.42%, respectively, see **Table 2**. VGG-16P was successful in distinguishing CTCL from eczema with a low rate of false positives (specificity 84.09%), but it proved more difficult to recognize eczema as seen by VGG-16P reaching a sensitivity rate of 74.29% in CTCL versus eczema. Distinguishing psoriasis from eczema was the task with the lowest performance of the VGG-16P. The best outcome came from identifying eczema, with a sensitivity of 81.79%, but the outcome for identification of psoriasis was inferior, with a specificity of 73.57%.

Secondary Outcome

Pre-trained models were superior, as demonstrated by the VGG-16P outperforming the VGG-16N in all analyses. This was further demonstrated by the VGG-16PS being superior to the VGG-16NS with respect to accuracy on all tasks and overall on AUC, see **Table 3**.

The VGG-16 architecture without the addition of a STN was slightly superior, as demonstrated by VGG-16P outperforming VGG-16PS, and the VGG-16N and VGG-16NS having similar outcomes.

For all models, the general trend of best performance was on cropped images in the three defined tasks (see **Supplementary Table 3**), why all results presented in **Tables 2**, **3** are based on cropped images.

DISCUSSION

The present retrospective study is an attempt to develop a CAD for more generalized skin diseases that may be of significant help, especially for GPs. The proposed CAD was based on an extensive dataset of clinical images collected from patients consulting a single dermatological department in Denmark. The best performance was obtained by the VGG-16P model when performing the task of distinguishing acne from rosacea (sensitivity 85.42 and specificity 89.53%). Notably, this model distinguished between the diseases on all three tasks with accuracy above 77%, indicating a clinically relevant accuracy compared with the reported diagnostic accuracy in dermatology in general of primary care physicians (48–77%) (5).

Comparing our results to the sensitivity of 67–75% on common multiple-lesion skin diseases reported for the CAD of Liu et al. (12), we find that the present binary model has a potential role in the field of computer-aided diagnostics for common multiple-lesions skin disease. The CAD model of Lui et al. was a multinomial classifier, why further testing of our system in multinomial classification is indicated for true comparison. Head-to-head comparison of suggested CAD models for dermatology seems warranted but it is challenging due to a general lack of online availability (8). To accommodate this paucity, our classification model can be accessed at: https://github.com/anjalilje/Classification-of-skin-diseases.

High performance in distinguishing CTCL from eczema may indicate a yet unidentified usability of CAD tools in diagnosing rare and malignant multiple-lesion skin diseases.

The published image classifiers for single-lesion skin disease show a higher accuracy than our model. Notably, two

studies combined have outperformed hundreds of trained dermatologists in identifying melanoma in skin images (9, 10). Accordingly, Esteva et al. achieved an AUC of between 91 and 96%. In comparison, the maximum AUC achieved by our VGG-16PS in distinguishing acne from rosacea was 92.74%. Our best model VGG-16P achieved AUCs between 86.07 and 89.89% for the three defined tasks. The superior performance of CAD models classifying single-lesion skin disease compared to CAD models classifying multiple-lesion skin disease indicates that developing a classification model for generalized dermatology on non-standardized imagery may prove to be a more complex task.

Overfitting is a risk in the present study for several reasons: Firstly, acne, rosacea and CTCL were represented only by small datasets, and balancing the data did enhance the classification performance on these three skin diseases, thereby confirming a level of overfitting. Still, the performance enhancement on balanced datasets was only slightly superior to that of unbalanced datasets. Secondly, overfitting due to selection bias is a potential problem of CNN models in dermatology (26). The present retrospective study may therefore suffer from selection bias.

Wu et al. showed that multi-lesion skin disease can be classified at the level of single-lesion skin disease, on highly selected image material (13).

Our study was conducted on a clinical image database, we argue this to be less prone to selection bias, due to our content originating from clinical photographers, patients, and clinicians in non-specific clinical situations.

To which extend the results of this study can be extrapolated to clinical use, could be further investigated by head to head testing of the CAD model and trained physicians, like the man and machine approach from a recent study in single-lesion skin disease classification (15). But there is a need for designs of real-time clinical intervention studies for true estimates of the clinical diagnostic accuracy of CAD models not based on dermatoscopic images. This paucity of prospective clinical tests in the development of CADs in dermatology has been criticized (27, 28). Fourthly, no quantification of unknown biases was conducted, this represents a limitation, as an example a certain diseases may be represented by clinical photography to a higher degree than others. Unknown biases could be tested on an external dataset. Since no external dataset are available for the selected disease categories, this further argues for making CAD models available for online testing.

And finally, the grouping of several ICD-10 codes into major disease categories may result in overfitting, since some subtypes of diseases have less similar morphology than others. Thus, overall, the level of overfitting is considered to be of minor importance.

One limitation of this study was the contents, which comprised both healthy skin images and non-skin images. Non-skin images were cleansed successfully with a 99% accuracy, why the effect of their inclusion was minute. Healthy skin images were estimated to comprise 3.7% of the material in the sampling, which may have had a negative effect on the performance outcome. Hence, the true performance of the models may have been underestimated. Another limitation is racial bias, as the data source consisted primarily of Fitzpatrick skin type II-III patients. Concerns have been raised of racial bias in CAD in dermatology because databases used for machine learning have historically had an overrepresentation of Caucasian data (29).

Grouping ICD-10 codes into major disease categories may not only represent a limitation but could also be considered a strength in our study. Disease categories increase the amount of data, thus enhancing the performance of the models. Moreover, disease categories represent a simpler outcome and may therefore be more clinically relevant for a GP, as the primary purpose of CAD in general dermatology should be to assist correct and early diagnosing, treatment, and triaging.

ICD-10 coding of the images were considered as high quality categorization of the images due to two factors. Firstly, the ICD-10 codes were provided by a physicians employed at the dermatological department of a University Hospital. Secondly, all ICD-10 codes related to the only rare disease included, CTCL, were based on histological verification.

Images used for single-lesion disease classification like malignant melanoma are often taken by highly standardized methods (8). However, CNN models like the present one trained on various types of images with varying quality may perform better in real-life usage. Most dermatological diseases have a more generalized skin manifestation than malignant melanoma, and the sparsity of dermatoscopes in the primary sector is also a limitation (20).

The results obtained in this study are encouraging. Medical students, resident doctors, and GPs with little to no training in the field of dermatology have been shown to perform very poorly in diagnosing dermatological diseases (19) and may benefit from a CAD model performing to the present level.

Furthermore, our findings support that in the future of all dermatological diagnostics, man and machine together will very likely be superior to man alone as seen for CAD models developed for single-lesion skin disease (15). Even so, implementing CAD models in dermatology should be accommodated by thorough prospective clinical testing to ensure true estimates, thus ensuring patient safety, efficacy, and effectiveness.

DATA AVAILABILITY STATEMENT

The datasets presented in this article are not readily available because the datasets consist of clinical images of patients with skin disease, which cannot be shared in accordance to the European General Data Protection Regulation. The skin disease classification algorithm is available only at https://github.com/anjalilje/Classification-of-skin-diseases.

ETHICS STATEMENT

The studies involving human participants were reviewed and approved by The Regional Ethics Committee of Central Denmark Region. Written informed consent from the participants' legal guardian/next of kin was not required to participate in this study in accordance with the national legislation and the institutional requirements.

AUTHOR CONTRIBUTIONS

KT: main contributor to all aspects of the manuscript. AC: software developer, significant contributor to the methods and results sections of the manuscript, and designer of figures of software architecture. LI: main supervisor in the clinical aspects of the manuscript and significant contributions to the introduction and discussion. HL: co-supervisor in the clinical aspects of the manuscript, large contributions especially to the introduction, discussion and to table content. OW: supervisor of software development and significant contributor to all aspects of the manuscript.

SUPPLEMENTARY MATERIAL

The Supplementary Material for this article can be found online at: https://www.frontiersin.org/articles/10.3389/fmed.2020.574329/full#supplementary-material

REFERENCES

1. Hay RJ, Johns NE, Williams HC, Bolliger IW, Dellavalle RP, Margolis DJ, et al. The global burden of skin disease in 2010: an analysis of the prevalence and impact of skin conditions. *J Invest Dermatol.* (2014) 134:1527–34. doi: 10.1038/jid.2013.446
2. Julian CG. Dermatology in general practice. *Br J Dermatol.* (1999) 141:518–20. doi: 10.1046/j.1365-2133.1999.03048.x
3. Verhoeven EW, Kraaimaat FW, van Weel C, van de Kerkhof PC, Duller P, van der Valk PG, et al. Skin diseases in family medicine: prevalence and health care use. *Ann Fam Med.* (2008) 6:349–54. doi: 10.1370/afm.861
4. DermNet NZ. (2019). Available online at: http://www.dermnetnz.org/. (Accessed February 16, 2019).
5. Federman DG, Kirsner RS. The abilities of primary care physicians in dermatology: implications for quality of care. *Am J Manag Care.* (2017) 3:1487–92.
6. Barrett M, Luu M. Differential diagnosis of atopic dermatitis. *Immunol Allergy Clin North Am.* (2017) 37:11–34. doi: 10.1016/j.iac.2016.08.009
7. Feng H, Berk-Krauss J, Feng PW, Stein JA. Comparison of dermatologist density between urban and rural counties in the United States. *JAMA Dermatol.* (2018) 154:1265–71. doi: 10.1001/jamadermatol.2018.3022
8. Thomsen K, Iversen L, Titlestad TL, Winther O. Systematic review of machine learning for diagnosis and prognosis in dermatology. *J Dermatol Treat.* (2019) doi: 10.1080/09546634.2019.1682500
9. Brinker TJ, Hekler A, Enk AH, Klode J, Hauschild A, Berking C, et al. Deep learning outperformed 136 of 157 dermatologists in a head-to-head dermoscopic melanoma image classification task. *Eur J Cancer.* (2019) 113:47–54. doi: 10.1016/j.ejca.2019.04.001
10. Esteva A, Kuprel B, Novoa RA, Ko J, Swetter SM, Blau HM, et al. Dermatologist-level classification of skin cancer with deep neural networks. *Nature.* (2017) 542:115–8. doi: 10.1038/nature21056
11. Han SS, Park GH, Lim W, Kim MS, Na JI, Park I, et al. Deep neural networks show an equivalent and often superior performance to dermatologists in onychomycosis diagnosis: Automatic construction of onychomycosis datasets by region-based convolutional deep neural network. *PLoS ONE.* (2018) 13:e0191493. doi: 10.1371/journal.pone.0191493
12. Liu Y, Jain A, Eng C, Way DH, Lee K, Bui P, et al. A deep learning system for differential diagnosis of skin diseases. *EESS.* (2019) arXiv:1909.05382. doi: 10.1038/s41591-020-0842-3
13. Wu H, Yin H, Chen H, Sun M, Liu X, Yu Y,, et al. A deep learning, image based approach for automated diagnosis for inflammatory skin diseases. *Ann Transl Med.* (2020) 8:581. doi: 10.21037/atm.2020.04.39
14. Kim YJ, Han SS, Yang HJ, Chang SE. Prospective, comparative evaluation of a deep neural network and dermoscopy in the diagnosis of onychomycosis. *PLoS ONE.* (2020) 15:e0234334. doi: 10.1371/journal.pone.0234334
15. Tschandl P, Rinner C, Apalla Z, Argenziano G, Codella N, Halpern A, et al. Human-computer collaboration for skin cancer recognition. *Nat Med.* (2020) 26:1229–34. doi: 10.1038/s41591-020-0942-0
16. Krizhevsky A, Sutskever I, Hinton G. ImageNet classification with deep convolutional neural networks. *Adv Neural Inform Process Syst.* (2012) 1:1097–105. doi: 10.1145/3065386
17. Simonyan K, Zisserman A. Very deep convolutional networks for large-scale image recognition. *ICLR.* (2014) *arXiv*. arXiv:1409.556.
18. Cohen JF, Korevaar DA, Altman DG, Bruns DE, Gatsonis CA, Hooft L, et al. STARD 2015 guidelines for reporting diagnostic accuracy studies: explanation and elaboration. *BMJ open.* (2016) 6:e012799. doi: 10.1136/bmjopen-2016-012799
19. Solomon BA, Collins R, Silverberg NB, Glass AT. Quality of care: issue or oversight in health care reform? *J Am Acad Dermatol.* (1996) 34:601–7. doi: 10.1016/S0190-9622(96)80058-2
20. Fee JA, McGrady FP, Rosendahl C, Hart ND. Dermoscopy use in primary care: a scoping review. *Dermatol Pract Concept.* (2019) 9:98–104. doi: 10.5826/dpc.0902a04
21. Wilmer EN, Gustafson CJ, Ahn CS, Davis SA, Feldman SR, Huang WW. Most common dermatologic conditions encountered by dermatologists and nondermatologists. *Cutis.* (2014) 94:285–92.
22. Bishop CM. *Pattern Recognition and Machine Learning*. New York, NY: Springer-Verlag. (2006).
23. Russakovsky O, Deng J, Su H, Krause J, Satheesh S, Ma S, et al. ImageNet large scale visual recognition challange. *Int J Comput Vis.* (2015) 115:211–52. doi: 10.1007/s11263-015-0816-y
24. Jaderberg M, Simonyan K, Zisserman A, Kavukcuoglu K, editors. *Spatial Transformer Networks*. NIPS (2015). 2015:arXiv:1506.02025.
25. Luo W, Phung D, Tran T, Gupta S, Rana S, Karmakar C, et al. Guidelines for developing and reporting machine learning predictive models in biomedical research: a multidisciplinary view. *J Med Internet Res.* (2016) 18:e323. doi: 10.2196/jmir.5870
26. Dick V, Sinz C, Mittlbock M, Kittler H, Tschandl P. Accuracy of computer-aided diagnosis of melanoma: a meta-analysis. *JAMA Dermatol.* (2019) 155:1291–99. doi: 10.1001/jamadermatol.2019.1375
27. Wise J. Skin cancer: smartphone diagnostic apps may offer false reassurance, warn dermatologists. *BMJ.* (2018) 362:k2999. doi: 10.1136/bmj.k2999
28. Esteva A, Topol E. Can skin cancer diagnosis be transformed by AI? *The Lancet.* (2019) 394:16–22. doi: 10.1016/S0140-6736(19)32726-6
29. Adamson AS, Smith A. Machine learning and health care disparities in dermatology. *JAMA Dermatol.* (2018) 154:1247–8. doi: 10.1001/jamadermatol.2018.2348

Conflict of Interest: The authors declare that the research was conducted in the absence of any commercial or financial relationships that could be construed as a potential conflict of interest.

frontiers in Medicine

ORIGINAL RESEARCH
published: 20 October 2020
doi: 10.3389/fmed.2020.591952

Attitudes Toward Artificial Intelligence Within Dermatopathology: An International Online Survey

Sam Polesie[1,2]*, *Phillip H. McKee*[3], *Jerad M. Gardner*[4], *Martin Gillstedt*[1,2], *Jan Siarov*[2,5], *Noora Neittaanmäki*[2,5] *and John Paoli*[1,2]

[1] Department of Dermatology and Venereology, Institute of Clinical Sciences, Sahlgrenska Academy, University of Gothenburg, Gothenburg, Sweden, [2] Region Västra Götaland, Sahlgrenska University Hospital, Department of Dermatology and Venereology, Gothenburg, Sweden, [3] Retired, Boston, MA, United States, [4] Department of Laboratory Medicine, Geisinger Medical Center, Danville, PA, United States, [5] Department of Pathology, Institute of Biomedicine, Sahlgrenska Academy, University of Gothenburg, Gothenburg, Sweden

OPEN ACCESS

Edited by:
H. Peter Soyer,
The University of Queensland, Australia

Reviewed by:
Joann Elmore,
UCLA David Geffen School of Medicine, United States
Zrinka Bukvic Mokos,
University Hospital Centre Zagreb, Croatia

***Correspondence:**
Sam Polesie
sam.polesie@vgregion.se

Specialty section:
This article was submitted to Dermatology, a section of the journal Frontiers in Medicine

Received: 05 August 2020
Accepted: 21 September 2020
Published: 20 October 2020

Citation:
Polesie S, McKee PH, Gardner JM, Gillstedt M, Siarov J, Neittaanmäki N and Paoli J (2020) Attitudes Toward Artificial Intelligence Within Dermatopathology: An International Online Survey. Front. Med. 7:591952. doi: 10.3389/fmed.2020.591952

Background: Artificial intelligence (AI) has recently surfaced as a research topic in dermatology and dermatopathology. In a recent survey, dermatologists were overall positive toward a development with an increased use of AI, but little is known about the corresponding attitudes among pathologists working with dermatopathology. The objective of this investigation was to make an inventory of these attitudes.

Participants and Methods: An anonymous and voluntary online survey was prepared and distributed to pathologists who regularly analyzed dermatopathology slides/images. The survey consisted of 39 question divided in five sections; (1) AI as a topic in pathology; (2) previous exposure to AI as a topic in general; (3) applications for AI in dermatopathology; (4) feelings and attitudes toward AI and (5) self-reported tech-savviness and demographics. The survey opened on March 13, 2020 and closed on May 5, 2020.

Results: Overall, 718 responders (64.1% females) representing 91 countries were analyzed. While 81.5% of responders were aware of AI as an emerging topic in pathology, only 18.8% had either good or excellent knowledge about AI. In terms of diagnosis classification, 42.6% saw strong or very strong potential for automated suggestion of skin tumor diagnoses. The corresponding figure for inflammatory skin diseases was 23.0% (P_{adj} <0.0001). For specific applications, the highest potential was considered for automated detection of mitosis (79.2%), automated suggestion of tumor margins (62.1%) and immunostaining evaluation (62.7%). The potential for automated suggestion of immunostaining (37.6%) and genetic panels (48.3%) were lower. Age did not impact the overall attitudes toward AI. Only 6.0% of the responders agreed or strongly agreed that the human pathologist will be replaced by AI in the foreseeable future. For the entire group, 72.3% agreed or strongly agreed that AI will improve dermatopathology and 84.1% thought that AI should be a part of medical training.

Conclusions: Pathologists are generally optimistic about the impact and potential benefit of AI in dermatopathology. The highest potential is expected for narrow specified tasks rather than a global automated suggestion of diagnoses. There is a strong need for education about AI and its use within dermatopathology.

Keywords: artificial intelligence, attitude, dermatopathology, machine learning, online survey

INTRODUCTION

Even though artificial intelligence (AI) has been discussed for decades, the unprecedented computer processor development, storage availability, and universal internet access including cloud services have contributed to the recent accelerated research interest in AI in several domains of medicine including pathology (1). AI and machine learning (ML) have recently pervaded every aspect of medical image analysis at an extraordinary pace (2).

While historically restricted to traditional microscopes and glass slides, pathology has recently transitioned to become a more digitally oriented specialty. Within the past decade, the use of whole slide imaging (WSI) has been validated for surgical pathology and dermatopathology (3, 4). Although WSI has not uniformly been well-received among dermatopathologists (5), the diagnostic modality has proven non-inferior to traditional microscopes for most diagnostic classes, except for a subset of melanocytic lesions, in a recent intra-observer validation investigation (6). With the rise of whole slide scanner technology (7), and free-hand smartphone photography (8), large numbers of tissue slides are being captured and archived digitally. For dermatopathology specifically, closed online forums now represent an important piece of continuing medical education and attract thousands of users from multiple countries across the world in all age groups (9). In many centers, all glass slides are routinely scanned and are made available digitally. While the primary diagnosis might still be made by pathologists using traditional microscopes, ancillary diagnoses by ML-based software might only be a few computer maneuvers away, fundamentally changing pathology as we know it.

The immense accumulation of online dermatopathology images represents a substantial resource not only for education, but also for ML research purposes. Recently, Schaumberg et al. presented the first pan-tissue and pan-disease ML-method for predicting disease as well as immunostaining (10). The training set consisted of thousands of images obtained through social media and PubMed articles and was prospectively tested in public on social media. Although in its early stages, the potential seen for ML in dermatopathology have been demonstrated both pertaining to specific tasks as well as diagnosis (11–13). The use of ML within dermatopathology has recently been listed as one of the important dermatological applications of AI (14). Nonetheless, little is known about dermatopathologists' attitudes toward an increased use of AI within their field. In a recent study, including 1,271 dermatologists, investigating the attitudes toward AI within dermatology, the majority of responders were positive toward a development with an increased use of AI. Moreover, only a minority expressed fear toward an increased use. Interestingly, a majority of responders (58.1%) saw either strong or very strong potential for automated detection of skin diseases based on dermatopathology images (15).

Dermatopathology and dermatology depend on one another and collaboration between our disciplines is essential for clinical-pathological correlation. In order to prepare for a future with an increased use of AI, it is our belief that a first inventory of dermatopathologists' views on the topic is important. Ultimately, it is our hope that dermatopathologists together with dermatologists should be the ones who guide and lead the development in our fields. Thus, the following study was performed as an exploratory survey with the aim to specifically address feelings and attitudes toward AI among dermatopathologists.

MATERIALS AND METHODS

An anonymized and voluntary English online survey was prepared and distributed through SurveyMonkey® (www.surveymonkey.com, San Mateo, CA, USA). The survey started with a brief introduction followed by 39 questions (Q1–Q39). The first baseline question (Q1) tested for eligibility (i.e., if the responders worked as a pathologist who regularly analyzed dermatopathology slides/images). If a responder answered "no" to this first question, the survey ended. The rest of the survey questions were divided into five sections: (1) AI as a topic in pathology (Q2-Q3); (2) previous exposure to AI as a topic in general (Q4-Q7); (3) applications for AI in dermatopathology (Q8-Q14); (4) feelings and attitudes toward AI (Q15-Q25) and (5) self-reported tech-savviness and demographics (Q26-Q39). Most of the response options were prepared as Likert-type scales (16). The complete survey as displayed to the responder is available in the **Supplementary Material**. Answers to all questions were required for the survey to be considered complete.

The survey opened on March 13, 2020 and closed on May 5, 2020 (53 survey days). The survey link was advertised on a closed Facebook® (Menlo Park, CA, USA) group called McKee Derm, which is frequently visited by international pathologists, dermatopathologists and dermatologists and has ∼15,000 members (17). The group opened in May 2017 and its main purpose is to share and discuss dermatopathology cases. The survey link was also shared publicly by one of the authors (JMG) on their public Facebook page and Twitter account. Since all responses were obtained voluntarily and anonymously from professional colleagues, the study was exempt from approval by an ethics review board.

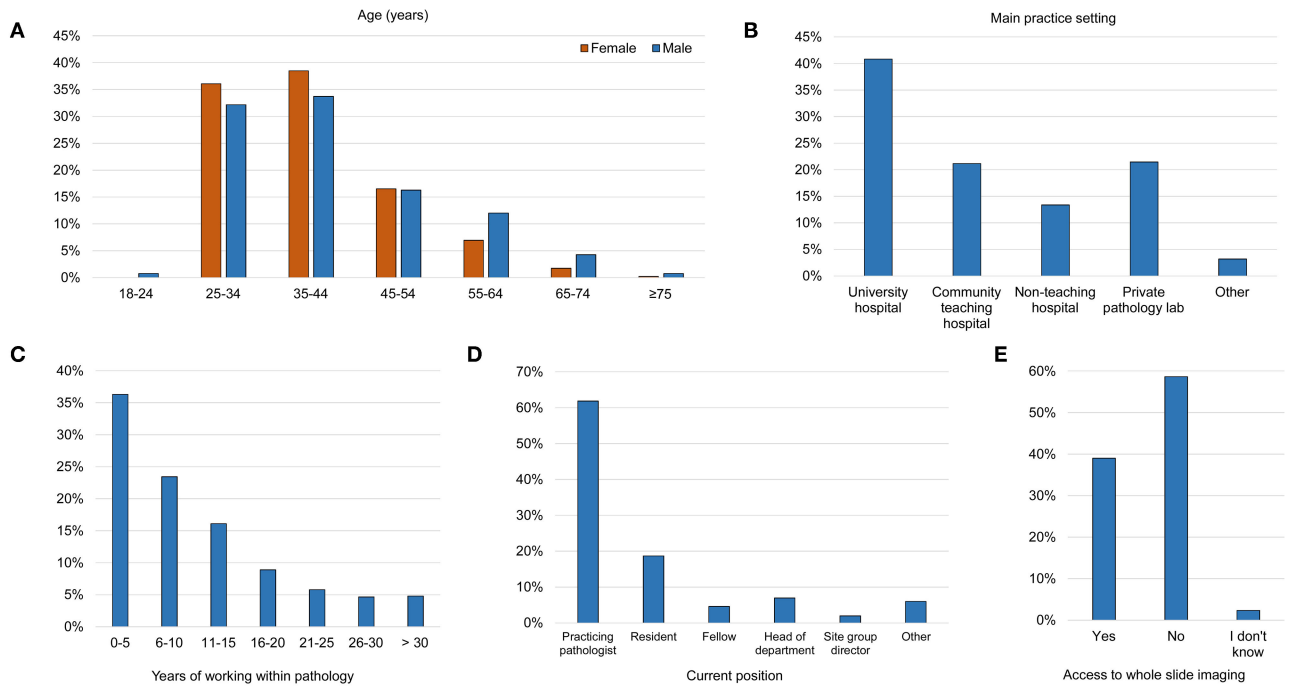

FIGURE 1 | Responder characteristics. **(A)** Age distribution for each sex. **(B)** Proportion in each type of practice setting. **(C)** Distribution of the number of years working within pathology. **(D)** Current position. **(E)** Access to whole slide imaging at work.

Statistical Analysis

All data were analyzed using R version 3.5.3 (https://www.r-project.org/). Fisher's exact test and Wilcoxon's rank sum test were used for two-sample tests. Wilcoxon's signed rank test was used for paired tests. For questions with dichotomous answers, logistic regression was used with "*no*"/"*yes*" as the dependent variable and sex and age group as independent variables. For questions with non-dichotomous answers, linear regression models were used to correlate answers to sex and age group using a score for the answers, for example: "*Strongly disagree*" = 1, "*Disagree*" = 2, "*Neither agree nor disagree*" = 3, "*Agree*" = 4 and "*Strongly agree*" = 5. The age groups (20-24, 25-34, 35-44, 45-54, 55-64, 65-74, and ≥75 years) were used as numeric values in the regression models, i.e., numbers ranging from 1 to 7. P-values were adjusted (P_{adj}) for multiple comparisons using the Holm method (18). All tests were two-sided and $P_{adj} < 0.05$ was considered as statistically significant.

RESULTS

Of 1,263 surveys received, 848 responders worked as pathologists who regularly analyzed dermatopathology slides/images in a clinical setting. Among these, 718 completed the survey resulting in an 84.7% response rate among the eligible audience and these responses were further analyzed. The median time to complete the survey was 6.1 min (interquartile range, 4.7–8.5 min). All aggregated result summaries for Q1-Q38 are available in **Supplementary Material**. An overview of the age and sex distribution of the responders as well as other demographic data are presented in **Figure 1**. Practicing specialists and residents in pathology constituted 80.5% of the responders. The median age (range) was 38 years (22–79 years), 64.1% ($n = 460$) were females and 39.0% ($n = 280$) had access to WSI at work. The great majority of the surveyed dermatopathologists mainly used traditional microscopes for routine diagnostic dermatopathology while only 4% (29 of 718) of the responders mainly used digitally scanned slides. Overall, 91 different countries were represented. The three countries where most responders worked were India ($n = 96$, 13.4%), USA ($n = 80$, 11.1%) and United Kingdom ($n = 35$, 4.9%).

While 81.5% of responders were aware of AI as an emerging topic in pathology, only 18.8% had either good or excellent knowledge about AI within pathology. Younger responders (<40 years) were equally aware of the recent development compared to older responders (≥40 years) with 322 of 400 (80.5%) vs. 263 of 318 (82.7%) claiming awareness ($P = 0.50$, $P_{adj} = 1$). A higher percentage of responders mainly working in a university hospital (255 of 293, 87.0%) were aware of the AI development within pathology compared to those working in other settings (330 of 425, 77.6%) ($P = 0.0017$, $P_{adj} = 0.073$). Males generally had a higher self-reported level of knowledge about AI than females (26.0 vs. 14.8%, $P = 0.003$, $P_{adj} = 0.12$).

Among all responders, 22.3% had used AI as a diagnostic aid in real life within pathology and 11.0% had used AI within dermatopathology in particular. Use of AI was not associated with age nor sex (**Table 1**). Physicians with access to WSI and those with previous use of AI within pathology

TABLE 1 | Distribution of answers to questions regarding background knowledge about AI.

Question	Yes	No				log(OR) for age -group (95% CI)	*P-value*	Holm corrected *P*-value	log(OR) for sex (95% CI) [Ref. Female]	*P*-value	Holm corrected *P*-value
AI is a topic that has become of interest for the pathology community. Were you already aware of this topic in pathology?	585 (81.5%)	133 (18.5%)				0.10 (−0.08, 0.28)	0.28	1	−0.03 (-0.42, 0.37)	0.89	1
Have you read any medical publications regarding AI within dermatopathology?	181 (25.2%)	537 (74.8%)				0.12 (−0.03, 0.27)	0.12	1	0.29 (−0.06, 0.63)	0.11	1
Have you used AI as a diagnostic aid in real life within pathology?	160 (22.3%)	558 (77.7%)				0.09 (−0.07, 0.25)	0.29	1	−0.18 (−0.55, 0.19)	0.35	1
Have you used AI as a diagnostic aid in real life within dermatopathology?	79 (11.0%)	639 (89.0%)				0.18 (−0.03, 0.38)	0.087	1	−0.07 (−0.56, 0.42)	0.78	1
	I have never heard about it	**I have heard about it, but not more**	**Basic knowledge**	**Good knowledge**	**Excellent knowledge**	**Score increase per age interval (95% CI)**	***P-value***	**Holm corrected *P*-value**	**Sex; Score difference (95% CI) [Ref. Female]**	***P***	**Holm corrected *P*-value**
Which degree of knowledge would you say you have when it comes to AI within pathology?	25 (3.5%)	275 (38.3%)	283 (39.4%)	111 (15.5%)	24 (3.3%)	0.06 (0.01, 0.12)	**0.034**	1	0.20 (0.07, 0.33)	**0.003**	0.12

For the questions with dichotomous answers, log-odds ratios, 95% CI and P-values for the logistic regression model (no=0 and yes=1) containing both sex and age group (20-24, 25-34, 35-44, 45-54, 55-64, 65-74, and ≥75 years) are included. The age groups are used as numeric values in the regression model, i.e., numbers ranging from 1 to 7. For the final question with five possible answers, the answer was transformed to a numeric score (1–5) and a linear regression model with both sex and age group was used with the coefficients, 95% CI and P-values included in the table. AI, artificial intelligence; CI, confidence interval; OR, odds ratio. Bold values indicates the singificant values P < 0.05.

and dermatopathology were more knowledgeable about the technique (**Supplementary Table 1**).

Responders with ≤10 years of experience within pathology (339 of 423, 80.1%) were equally aware of the AI development as responders with >10 years of experience (237 of 285, 83.2%) ($P = 0.33$, $P_{adj} = 1$). In the tech-savvy group, 99 of 376 responders (26.3%) reported either good or excellent knowledge about AI within pathology compared to 36 of 342 non-tech-savvy responders (10.5%) ($P < 0.0001$, $P_{adj} < 0.0001$).

When responders were asked about previous exposure to AI as a topic in general (Q4-Q7), 71.0, 74.9, 53.5, and 65.5% had heard about AI from the media, social media, lectures and friends, respectively. Social media and friends were more common sources for younger age groups. Other media was a more common source among men compared to females (**Table 2**).

The aggregated results from Q8-Q14 about seven applications for AI within dermatopathology are summarized in **Figure 2**. In terms of classification of diagnoses, 42.6% ($n = 306$) saw strong or very strong potential for automated suggestion of skin tumor diagnoses. The corresponding figure for inflammatory skin diseases was 23.0% ($n = 165$) ($P < 0.0001$, $P_{adj} < 0.0001$). For specific applications, the highest potential was considered for automated detection of mitosis (79.2%), automated suggestion of tumor margins (62.1%) and immunostaining evaluation (62.7%). The potential for automated suggestion of immunostaining (37.6%) and genetic panels (48.3%) were lower.

Results for feelings and attitudes toward AI (Q15-Q25) are presented in **Table 3**. Age did not impact the overall attitudes toward AI. Males displayed more excitement and less fear about the use of AI within dermatopathology as well as within medicine in general. The level of fear toward a development with an increased use of AI within dermatopathology did not differ between dermatopathologists working mainly at a university hospital compared to those who mainly worked in another setting (16.7 vs. 15.8%, $P = 0.76$, $P_{adj} = 1$). Among 280 responders with known access to WSI, 14.6% ($n = 41$) expressed fear toward a development with an increase use of AI within dermatopathology, which did not differ significantly to expressed fears among 74 of 421 responders without such access (17.6%) ($P = 0.35$, $P_{adj} = 1$). Furthermore, tech-savviness did not influence expressed levels of fear (data not shown). The attitudes toward AI among those with and without access to WSI did not differ, whereas those with previous use of the technique in dermatopathology had generally more positive attitudes (**Supplementary Table 2**).

Only 6.0% (43 of 718) of the responders agreed or strongly agreed that the human pathologist will be replaced by AI in the foreseeable future. Among tech-savvy responders, the corresponding figure was 7.7% (29 of 376, $P = 0.086$, $P_{adj} = 1$). For the entire group, 72.3% agreed or strongly agreed that AI will improve dermatopathology and 84.1% thought that AI should be a part of medical training.

DISCUSSION

Our results indicate a generally positive attitude toward AI within dermatopathology among surveyed pathologists. The majority of responders have not yet used AI tools as a diagnostic aid within dermatopathology, underlining that such tools are still under development and a broad implementation to a large extent still is pending.

Age did not influence the results and, while males generally expressed more excitement and less fear compared to female responders, the differences were small in absolute terms. Nonetheless, some of the differences between the genders, might be due to systematic gaps in confidence levels between men and women (19, 20). The majority of the responders were not afraid of being replaced by AI and felt that AI will improve dermatopathology making it more exciting. Only 4% of the responders mainly worked with digital pathology which could explain the low usage of AI tools. Interestingly, only 25% of the responders

TABLE 2 | Distribution of answers to questions regarding sources about AI applications.

Other applications we use in daily life already use AI (e.g., speech recognition, spam filters, recommendation algorithms). Have you been made aware of the use of AI in such applications?	Yes	No	log(OR) for age -group (95% CI)	*P*-value	Holm corrected *P*-value	log(OR) for sex (95% CI) [Ref. Female]	*P*-value	Holm corrected *P*-value
From the media	510 (71.0%)	208 (29.0%)	0.07 (−0.08, 0.23)	0.37	1	0.53 (0.18, 0.88)	**0.003**	0.14
From social media	538 (74.9%)	180 (25.1%)	−0.30 (−0.46, −0.15)	**0.0001**	**0.004**	0.27 (−0.10, 0.63)	0.15	1
From lectures	384 (53.5%)	334 (46.5%)	0.11 (−0.03, 0.25)	0.12	1	0.17 (−0.14, 0.48)	0.27	1
From friends	470 (65.5%)	248 (34.5%)	−0.16 (−0.30, −0.02)	**0.029**	1	0.37 (0.04, 0.70)	**0.029**	1

A logistic regression model (no = 0 and yes = 1) containing both sex and age group (20-24, 25-34, 35-44, 45-54, 55-64, 65-74, and ≥75 years) was used. The age groups are used as numeric values in the regression model, i.e., numbers ranging from 1 to 7. Log-odds ratios, 95% CI and P-values for the coefficients are included. AI, artificial intelligence; CI, confidence interval; OR, odds ratio. Bold values indicates the singificant values P < 0.05.

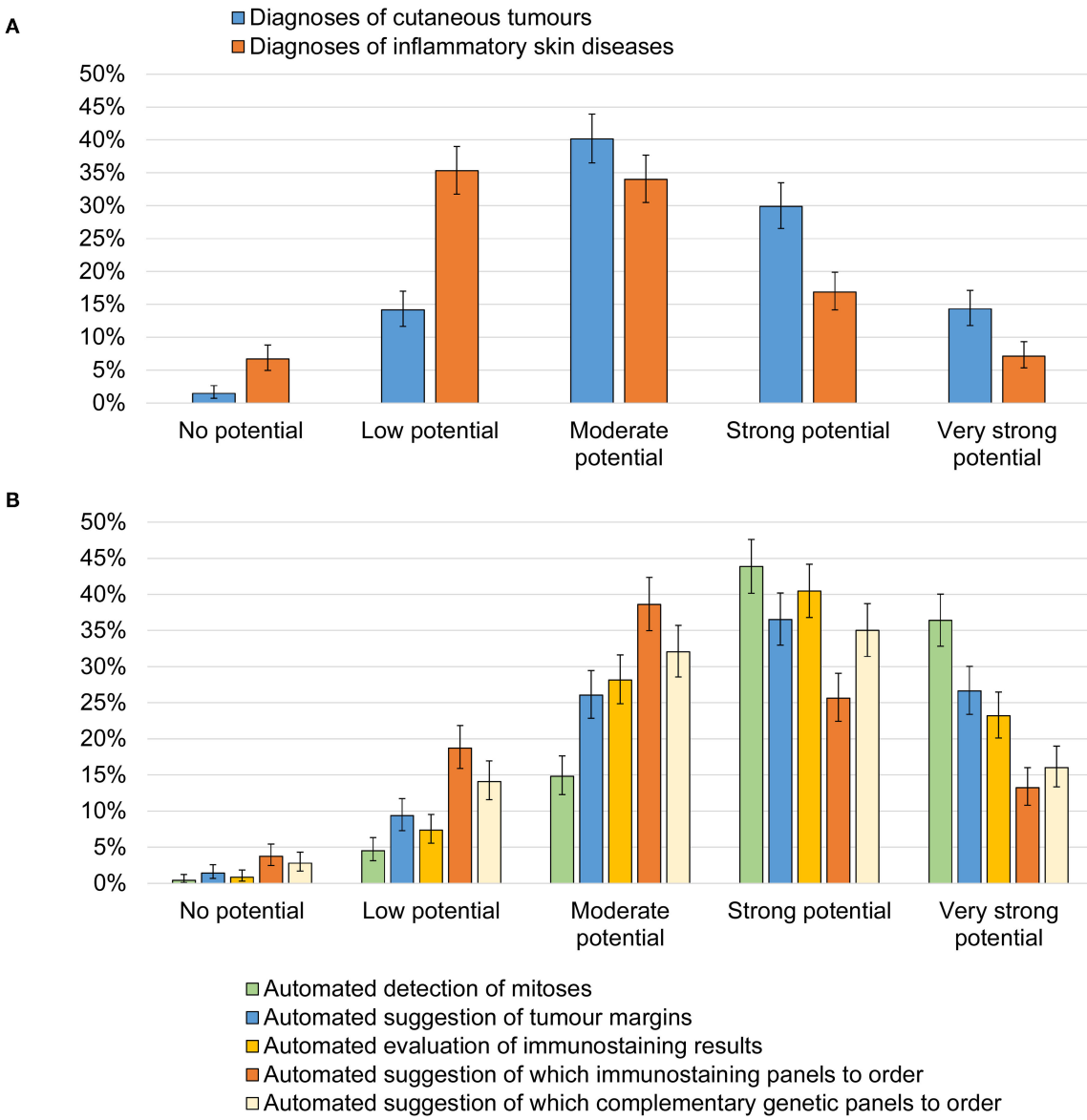

FIGURE 2 | Potential seen for AI within dermatopathology. Regardless of whether you have thought about this before, which potential do you personally see for AI for dermatopathology images regarding each of the following. **(A)** Potential seen for automated suggestion of diagnoses of cutaneous tumors and inflammatory skin diseases. **(B)** Potential seen for specific tasks including; automated detection of mitoses; automated suggestion of tumor margins; automated evaluation of immunostaining results; automated suggestion of which immunostaining panels to order; automated suggestion of which complementary genetic panels to order.

had read a medical publication regarding AI within dermatopathology which may reflect that studies in this field are still rare.

Narrow tasks such as automated detection of mitoses and tumor margins were seen to have higher potential compared to automated diagnosis of both cutaneous tumors and inflammatory skin disorders. This is not surprising since several studies have shown AI's potential in detecting mitoses while evidence in diagnostic use is still rare (21, 22). In regards to AI-driven automated diagnostics, its usefulness for tumors was considered more likely than for dermatoses. In fact, a few studies have shown the potential of AI in differentiating skin tumors in WSI (12, 23). AI has even outperformed pathologists in the classification of melanoma (24). Melanocytic lesions in specific have proven particularly difficult for dermatopathologists, where significant levels of inter- and intra-observer variability have been reported (25). ML-based solutions likely hold strong promise in this domain.

The responders reported a high potential for automated suggestion of tumor margins. Such benefits were observed in a recent study in which fluorescence lifetime imaging and ML

TABLE 3 | Distribution of answers to questions regarding attitudes and feelings about AI.

Question	Strongly disagree	Disagree	Neither agree nor disagree	Agree	Strongly agree	I don't know	Score increase per age interval (95% CI)	*P*-value	Holm corrected *P*-value	Sex; Score difference (95% CI) [Ref. Female]	*P*-value	Holm corrected *P*-value
AI will revolutionize Medicine in general.	3 (0.4%)	59 (8.2%)	122 (17.0%)	405 (56.4%)	129 (18.0%)	0 (0.0%)	0.02 (−0.04, 0.071)	0.56	1	0.21 (0.08, 0.33)	**0.001**	**0.046**
AI will revolutionize dermatopathology.	7 (1.0%)	64 (8.9%)	190 (26.5%)	322 (44.8%)	113 (15.7%)	22 (3.1%)	0.02 (−0.04, 0.08)	0.52	1	0.16 (0.02, 0.30)	**0.023**	0.80
AI will revolutionize dermatopathology more than other subfields within pathology.	22 (3.1%)	217 (30.2%)	304 (42.3%)	96 (13.4%)	37 (5.2%)	42 (5.8%)	−0.01 (−0.07, 0.05)	0.79	1	−0.02 (−0.16, 0.12)	0.74	1
In the foreseeable future all physicians will be replaced by AI.	250 (34.8%)	342 (47.6%)	70 (9.7%)	26 (3.6%)	17 (2.4%)	13 (1.8%)	0.01 (−0.06, 0.07)	0.84	1	−0.01 (−0.15, 0.13)	0.91	1
The human pathologist will be replaced by AI in the foreseeable future.	248 (34.5%)	337 (46.9%)	66 (9.2%)	30 (4.2%)	14 (1.9%)	23 (3.2%)	0.03 (−0.03, 0.09)	0.28	1	0.09 (−0.05, 0.22)	0.23	1
A development with an increased use of AI in dermatopathology frightens me.	78 (10.9%)	320 (44.6%)	204 (28.4%)	93 (13.0%)	23 (3.2%)	0 (0.0%)	−0.01 (−0.08, 0.05)	0.65	1	−0.17 (−0.32, −0.03)	**0.022**	0.79
A development with an increased use of AI in dermatopathology makes dermatopathology more exciting to me.	12 (1.7%)	69 (9.6%)	210 (29.2%)	340 (47.4%)	87 (12.1%)	0 (0.0%)	−0.03 (−0.09, 0.03)	0.35	1	0.18 (0.05, 0.31)	**0.009**	0.34
A development with an increased use of AI makes medicine in general more exciting to me.	8 (1.1%)	60 (8.4%)	186 (25.9%)	371 (51.7%)	93 (13.0%)	0 (0.0%)	0.01 (−0.05, 0.07)	0.73	1	0.17 (0.05, 0.30)	**0.008**	0.33
AI will improve dermatopathology	6 (0.8%)	36 (5.0%)	126 (17.5%)	425 (59.2%)	94 (13.1%)	31 (4.3%)	0.01 (−0.04, 0.06)	0.64	1	0.20 (0.09, 0.32)	**0.001**	**0.034**
AI will improve medicine in general.	3 (0.4%)	20 (2.8%)	93 (13.0%)	464 (64.6%)	116 (16.2%)	22 (3.1%)	0.00 (−0.04, 0.05)	0.84	1	0.26 (0.15, 0.36)	**<0.0001**	**<0.0001**
AI should be part of medical training.	6 (0.8%)	19 (2.6%)	72 (10.0%)	441 (61.4%)	163 (22.7%)	17 (2.4%)	0.06 (0.01, 0.11)	**0.017**	0.62	0.10 (−0.01, 0.21)	0.081	1
I consider myself well-informed about the use of modern technology, especially computers.	3 (0.4%)	59 (8.2%)	122 (17.0%)	405 (56.4%)	129 (18.0%)	0 (0.0%)	−0.03 (−0.09, 0.03)	0.31	1	0.18 (0.05, 0.30)	**0.0064**	0.26

The five possible answers were transformed to a numeric score (1–5) used as the dependent variable and a linear regression model with both sex and age group as predictors was used with the coefficients, 95% CI and P-values included in the table. The age groups are used as numeric values in the regression model, i.e., numbers ranging from 1 to 7. All "I don't know" answers were excluded from the regression model. AI, artificial intelligence; CI, confidence interval. Bold values indicates the singificant values P < 0.05.

were used to visualize tumor margins in excised breast specimens showing high specificity and sensitivity (26). In a previous survey about general pathologists' attitudes toward AI, 75% of the pathologists showed interest or excitement about AI as a diagnostic tool and the vast majority felt it could increase diagnostic efficiency (27). This is in line with the findings in our survey.

As the fields of dermatology and dermatopathology are getting ready for a tremendous transition, we believe inventories of attitudes toward AI are important since it will clarify the potential in specific domains and hopefully unify the community to try to work together. Future ML tools will probably make use of several sources of information simultaneously and parallel systems might provide an even more accurate output. Recently, online dermatopathology forums have collected large amounts of digital cases. This online educational resource could potentially be used to train convolutional neural networks. Ideally, these tools should be available through a web-browser and should be freely available to all users. We believe that pathologists must engage in this development in order to take a leading position in AI. The positive attitudes presented here could certainly help promote this development. Nonetheless, this survey also illustrates that the majority (61.0%) of responders don't yet have access to WSI. A broad implementation of WSI is most likely a prerequisite for an increased use of AI in dermatopathology.

When interpreting our results, it is imperative to remember that the majority of responders received the survey invitation via their social media interest in dermatopathology. The possibility of a selection bias exists and physicians with positive attitudes may have been more likely to have completed the survey. Moreover, AI is a new technique and different responders might have varying ideas of what it includes and represents, particularly since the processes between input and output by the algorithms are not usually clearly defined, and the methods and variable combinations may differ from our own decision-making.

Setting up an online link rather than solely inviting pathologists from a predetermined mailing list also makes it difficult to obtain an exact survey response rate. We acknowledge that attitudes toward new technologies including AI can be fluid and have a tendency to change over time. Therefore, it will also be interesting to reassess attitudes toward AI in follow-up investigations. Moreover, we recognize the inherent difficulties in analyzing and merging the results of attitudes. Undoubtedly, the same question and answer options can represent different meanings to different responders who also have different baseline knowledge about the technology. Finally, ethical and legal aspects, which may vary between countries, were not addressed in our survey.

CONCLUSION

In summary, our results demonstrate an overall optimistic attitude toward AI in dermatopathology among surveyed physicians. Nonetheless, our data also highlight the need for education about AI for pathologists. Surveyed pathologists predict greater potential for automated suggestion of skin tumor diagnoses than for inflammatory skin diseases. The greatest potential of AI in dermatopathology was predicted for automated detection of mitoses and tumor margins as well as for immunostaining evaluation.

DATA AVAILABILITY STATEMENT

The anonymized datasets generated in this survey are available on request to the corresponding author.

ETHICS STATEMENT

Ethical review and approval was not required for the study on human participants in accordance with the local legislation and institutional requirements. Written informed consent for participation was not required for this study in accordance with the national legislation and the institutional requirements.

AUTHOR CONTRIBUTIONS

SP and JP contributed to study concept and design, supervised the project, and wrote the manuscript. SP carried out the implementation, data collection, analysis, and statistics with contributions from MG. MG provided biostatistical advice. PM, JG, JS, and NN contributed to design and distribution of the questionnaire. All authors critically reviewed and edited the questionnaire and the manuscript.

SUPPLEMENTARY MATERIAL

The Supplementary Material for this article can be found online at: https://www.frontiersin.org/articles/10.3389/fmed.2020.591952/full#supplementary-material

Supplementary Material 1 | Complete survey text.

Supplementary Material 2 | Aggregated survey responses.

Supplementary Table 1 | Distribution of answers to questions regarding background knowledge about AI. Proportions of answers to questions on the specific rows stratified according to access to WSI, previous use of AI in pathology and previous use of AI in dermatopathology. P-values are computed with Fisher's exact test.

Supplementary Table 2 | Distribution of answers to questions regarding attitudes and feelings about AI. Proportions of answers to questions on the specific rows stratified according to access to WSI, previous use of AI in pathology and previous use of AI in dermatopathology. P-values are computed with Fisher's exact test.

REFERENCES

1. Tizhoosh HR, Pantanowitz L. Artificial intelligence and digital pathology: challenges and opportunities. *J Pathol Inform*. (2018) 9:38. doi: 10.4103/jpi.jpi_53_18
2. Litjens G, Kooi T, Bejnordi BE, Setio AAA, Ciompi F, Ghafoorian M, et al. A survey on deep learning in medical image analysis. *Med Image Anal*. (2017) 42:60–88. doi: 10.1016/j.media.2017.07.005
3. Bauer TW, Schoenfield L, Slaw RJ, Yerian L, Sun Z, Henricks WH. Validation of whole slide imaging for primary diagnosis in surgical

pathology. *Arch Pathol Lab Med*. (2013) 137:518–24. doi: 10.5858/arpa.2011-0678-OA
4. Fertig RM, Sangueza O, Gaudi S, Gamret AC, Cervantes J, Jukic DM. Whole Slide Imaging. *Am J Dermatopathol*. (2018) 40:938–9. doi: 10.1097/DAD.0000000000001008
5. Onega T, Reisch LM, Frederick PD, Geller BM, Nelson HD, Lott JP, et al. Use of digital whole slide imaging in dermatopathology. *J Digit Imaging*. (2016) 29:243–53. doi: 10.1007/s10278-015-9836-y
6. Kent MN, Olsen TG, Feeser TA, Tesno KC, Moad JC, Conroy MP, et al. Diagnostic accuracy of virtual pathology vs traditional microscopy in a large dermatopathology study. *JAMA Dermatol*. (2017) 153:1285–91. doi: 10.1001/jamadermatol.2017.3284
7. Madabhushi A, Lee G. Image analysis and machine learning in digital pathology: challenges and opportunities. *Med Image Anal*. (2016) 33:170–5. doi: 10.1016/j.media.2016.06.037
8. Morrison AS, Gardner JM. Smart phone microscopic photography: a novel tool for physicians and trainees. *Arch Pathol Lab Med*. (2014) 138:1002. doi: 10.5858/arpa.2013-0425-ED
9. Gardner JM, McKee PH. Social media use for pathologists of all ages. *Arch Pathol Lab Med*. (2019) 143:282–6. doi: 10.5858/arpa.2018-0431-ED
10. Schaumberg AJ, Juarez-Nicanor WC, Choudhury SJ, Pastrián LG, Pritt BS, Prieto Pozuelo M, et al. Interpretable multimodal deep learning for real-time pan-tissue pan-disease pathology search on social media. *Modern Pathol*. (2020). doi: 10.1038/s41379-020-0540-1. [Epub ahead of print].
11. Lang UE, Torres R, Cheung C, Vladar EK, McCalmont TH, Kim J, et al. Ciliation index is a useful diagnostic tool in challenging spitzoid melanocytic neoplasms. *J Invest Dermatol*. (2020) 140:1401–9.e2. doi: 10.1016/j.jid.2019.11.028
12. Olsen TG, Jackson BH, Feeser TA, Kent MN, Moad JC, Krishnamurthy S, et al. Diagnostic performance of deep learning algorithms applied to three common diagnoses in dermatopathology. *J Pathol Inform*. (2018) 9:32. doi: 10.4103/jpi.jpi_31_18
13. Fouad S, Randell D, Galton A, Mehanna H, Landini G. Unsupervised morphological segmentation of tissue compartments in histopathological images. *PLoS ONE*. (2017) 12:e0188717. doi: 10.1371/journal.pone.0188717
14. Gomolin A, Netchiporouk E, Gniadecki R, Litvinov IV. Artificial intelligence applications in dermatology: where do we stand? *Front Med*. (2020) 7:100. doi: 10.3389/fmed.2020.00100
15. Polesie S, Gillstedt M, Kittler H, Lallas A, Tschandl P, Zalaudek I, et al. Attitudes towards artificial intelligence within dermatology: an international online survey. *Br J Dermatol*. (2020) 183:159–61. doi: 10.1111/bjd.18875
16. Likert R. A technique for the measurement of attitudes. *Arch Psychol*. (1932)
17. *McKee Derm* [Last accessed 10 September 2020]. Available online at: https://www.facebook.com/groups/mckeederm/
18. Holm S. A simple sequentially rejective multiple test procedure. *Scand J Stat*. (1979) 65–70.
19. Vajapey SP, Weber KL, Samora JB. Confidence gap between men and women in medicine: a systematic review. *Curr Orthopaed Pract*. (2020) 31:494–502. doi: 10.1097/BCO.0000000000000906
20. Nomura K, Yano E, Fukui T. Gender differences in clinical confidence: a nationwide survey of resident physicians in Japan. *Acad Med*. (2010) 85:647–53. doi: 10.1097/ACM.0b013e3181d2a796
21. Andres C, Andres-Belloni B, Hein R, Biedermann T, Schäpe A, Brieu N, et al. iDermatoPath - a novel software tool for mitosis detection in H&E-stained tissue sections of malignant melanoma. *J Eur Acad Dermatol Venereol*. (2017) 31:1137–47. doi: 10.1111/jdv.14126
22. Nielsen PS, Spaun E, Riber-Hansen R, Steiniche T. Automated quantification of MART1-verified Ki-67 indices: useful diagnostic aid in melanocytic lesions. *Hum Pathol*. (2014) 45:1153–61. doi: 10.1016/j.humpath.2014.01.009
23. Campanella G, Hanna MG, Geneslaw L, Miraflor A, Werneck Krauss Silva V, Busam KJ, et al. Clinical-grade computational pathology using weakly supervised deep learning on whole slide images. *Nat Med*. (2019) 25:1301–9. doi: 10.1038/s41591-019-0508-1
24. Hekler A, Utikal JS, Enk AH, Solass W, Schmitt M, Klode J, et al. Deep learning outperformed 11 pathologists in the classification of histopathological melanoma images. *Eur J Cancer*. (2019) 118:91–6. doi: 10.1016/j.ejca.2019.06.012
25. Elmore JG, Barnhill RL, Elder DE, Longton GM, Pepe MS, Reisch LM, et al. Pathologists' diagnosis of invasive melanoma and melanocytic proliferations: observer accuracy and reproducibility study. *BMJ*. (2017) 357:j2813. doi: 10.1136/bmj.j2813
26. Unger J, Hebisch C, Phipps JE, Lagarto JL, Kim H, Darrow MA, et al. Real-time diagnosis and visualization of tumor margins in excised breast specimens using fluorescence lifetime imaging and machine learning. *Biomed Opt Express*. (2020) 11:1216–30. doi: 10.1364/BOE.381358
27. Sarwar S, Dent A, Faust K, Richer M, Djuric U, Van Ommeren R, et al. Physician perspectives on integration of artificial intelligence into diagnostic pathology. *NPJ Digital Med*. (2019) 2:28. doi: 10.1038/s41746-019-0106-0

Conflict of Interest: The authors declare that the research was conducted in the absence of any commercial or financial relationships that could be construed as a potential conflict of interest.

frontiers in Medicine

ORIGINAL RESEARCH
published: 27 October 2020
doi: 10.3389/fmed.2020.585792

Part I: Accuracy of Teledermatology in Inflammatory Dermatoses

Mara Giavina-Bianchi, Raquel Sousa and Eduardo Cordioli*

Department of Telemedicine, Hospital Israelita Albert Einstein, São Paulo, Brazil

Teledermatology is assuming a progressively greater role as a healthcare delivery method, especially now, during this pandemic time. It is important to know how accurate this tool is for different skin diseases. Most of the studies have focused on skin neoplasms or general dermatology. Studies based on a large number of inflammatory dermatoses have not yet been performed. Such knowledge can help dermatologists to decide whether endorsing this method or not. Our objective was to determine the accuracy of teledermatology in inflammatory dermatoses in a robust number of cases. A retrospective cohort study was conducted in São Paulo, Brazil, from July 2017–18, where a store-and-forward Teledermatology project was implemented under primary-care attention to triage surgical, more complex, or severe dermatoses. A total of 30,976 patients presenting 55,012 lesions took part in the project. Thirteen participating teledermatologists had three options to refer the patients: directly to biopsy, to the in-person dermatologist or back to the general physician with most probable diagnosis and management. In the group referred to the in-person dermatologist, we looked for the 20 most frequent International Classification of Diseases and Related Health Problems- 10th revision (ICD-10) of inflammatory dermatoses, which resulted in 739 patients and 739 lesions. As patients had been triaged by teledermatology previously, we were able to compare ICD-10 codes filled both by teledermatogists and by in-person dermatologists. The proportion of complete, partial, and no agreement rates between the in-person dermatologist's and the teledermatologist's diagnoses was used for accuracy. We also calculated Cohen's kappa, a statistical measure of inter-rater agreement, for complete agreement. The mean complete agreement rate for all twenty dermatoses was 78% (31–100%) and kappa = 0.743; partial agreement 8%; and no agreement 14%, presenting variability according to the disease. Our study showed that teledermatology for inflammatory dermatoses has a high accuracy. This result reassures that it can be a proper option for patient care.

Keywords: teledermatology, accuracy, telemedicine, inflammatory dermatoses, telehealth

OPEN ACCESS

Edited by:
Hang Li,
Peking University First Hospital, China

Reviewed by:
Irina Khamaganova,
Pirogov Russian National Research Medical University, Russia
Artem Vorobyev,
University Medical Center Schleswig-Holstein, Germany

****Correspondence:***
Mara Giavina-Bianchi
marahgbianchi@gmail.com

Specialty section:
This article was submitted to Dermatology, a section of the journal Frontiers in Medicine

Received: *21 July 2020*
Accepted: *30 September 2020*
Published: *27 October 2020*

Citation:
Giavina-Bianchi M, Sousa R and Cordioli E (2020) Part I: Accuracy of Teledermatology in Inflammatory Dermatoses. Front. Med. 7:585792. doi: 10.3389/fmed.2020.585792

INTRODUCTION

Telemedicine, especially in this pandemic moment, is of great value for delivering healthcare. It has the potential to improve access to subspecialty expertise, reduce healthcare costs, and improve the overall quality of care. Dermatology is particularly suitable for this care system. The three main teledermatology delivery platforms are: synchronous (RT: real-time teledermatology),

asynchronous (SF-TD), and hybrid (both synchronous and asynchronous forms). Synchronous teledermatology employs live video conferencing between the patient and the teledermatologist. Asynchronous teledermatology is a method whereby clinical or dermoscopy dermatologic images are obtained, sent to the responding dermatologist, who can review them at later time. Although it provides high-resolution dermatologic images and enables an efficient practice that can be performed across time zones, this modality is limited by the ability of the teledermatologist to obtain additional clinical history while evaluating the case (1).

Rates of diagnostic accuracy by teledermatology vary from study to study; the majority have found rates to be in the range of 75–80%, comparable to those with in-person care (1). Nevertheless, most of the studies were focused on skin neoplasms, especially skin cancer and pigmented lesions (2–5), or on general dermatology (6–10). A recent systematic review concluded that robust implementation studies of teledermatology are needed, with attention to reducing risk of bias when assessing diagnostic accuracy (2). For this reason, we performed a study with the aim of determining the accuracy of teledermatology for inflammatory dermatoses in a robust number of cases, assessing the agreement rate between the in-person dermatologist's and the teledermatologist's diagnoses.

MATERIALS AND METHODS

This was a retrospective cohort study designed to assess concordance between diagnoses made by in-person dermatologists and teledermatologists, approved by the Ethics Committee of Hospital Israelita Albert Einstein (CAAE: 97126618.6.0000.0071). We analyzed the reports of 30,976 patients included in a teledermatology triage project conducted in the city of São Paulo, Brazil, from July 2017 to July 2018.

Teledermatology Triage Project

Since there was a long patients' waiting list for an appointment with a dermatologist in the public health service, the aim of the teledermatology project was to triage the patients, in such a way that the severe, more complex, or surgical cases would be prioritized for biopsy procedure and in-person dermatologists, and the mild cases would be managed in the primary care attention along with the general physician (GP). Briefly, there were 57,832 patients under public primary-care attention who were on a waiting list for an appointment with a dermatologist, after being referred by the primary care physician. All of them were consecutively phoned to go to one of the three public municipal hospitals. Once there, their demographic data, a short clinical history and photographs of their skin lesions were taken by a nurse or a health technician, utilizing a cell phone app created for this purpose. Thirty thousand nine hundred seventy-six individuals responded to the call and attended the project. All their data and images were securely uploaded to a platform accessed by thirteen teledermatologists from Hospital Albert Einstein, authorized to do so through login and password at a later time (store-and-forward telemedicine). The thirteen dermatologists were Brazilian Board-certified to decrease the chance of diagnostic error. Once logged, the teledermatologists evaluated the cases, and they had to elaborate the most probable diagnosis and management. Next, they had to decide among three options to refer the patients: (1) directly to biopsy (with subsequent follow-up with an in-person dermatologist), (2) to an in-person dermatologist and (3) back to the general physician who had referred him/her to the dermatologist in the first place. **Figure 1** shows the frequency of patients included, photographed lesions, and referrals made by the teledermatologists, along with the flow used to select the reports to assess the accuracy. Teledermatologists were Hospital Israelita Albert Einstein employees (a private institution), and in-person dermatologists were public health service employees.

Study Design

We selected only the group referred to in-person dermatologist (12,874). Then, we assessed the reports that had the International Code of Diseases diagnoses filled by the in-person dermatologists (2,290). Next, we separated the reports filled with ICD-10 codes of inflammatory dermatoses (1,227). Afterwards, we looked for the 20 most frequent dermatoses to include in our study (1,143). As the last step, we eliminated duplicity of reports from the same patient, totalizing 739 reports from 739 patients (**Figure 1**).

We classified the rate of agreement as: (1) complete agreement when ICD-10 code used in both reports were the same, (2) partial agreement when ICD-10 used in both reports were different, but in the same group of disease (**Table 1**), posing as a probable differential diagnosis, and (3) no agreement when both reports did not fill the previous two conditions. As many inflammatory diagnoses are based on clinical diagnosis, we considered in-person dermatologist diagnosis as our gold standard diagnosis. For this reason, the rate of agreement between in-person dermatologists and teledermatologists was stated in this research as accuracy.

Statistical Analysis

Rates of concordance were expressed using percentages and Cohen's kappa coefficient, which was used to compare between groups of inter-rater observers (Graph Pad Prism 6.0). The guidelines first created by Landis and Koch (11) used to characterize kappa values are as follows: kappa < 0: no agreement, 0.00–0.20: slight agreement, 0.21–0.40: fair agreement, 0.41–0.60: moderate agreement, 0.61–0.8: substantial agreement, and 0.81–1.00: almost perfect agreement.

RESULTS

Table 2 shows the 26 most frequent inflammatory dermatoses diagnosed by teledermatology according to number of patients, lesions, and sex distribution. This constitutes 78% (24,210/30,976) of the total number of patients and 50% (27,519/55,012) of the lesions diagnosed in the overall teledermatology project. The female and male participation was 70 and 30%, respectively, although the female population accounts for 52.6% in the city of São Paulo (12). The mean number of inflammatory dermatosis lesion per patient was 1.1.

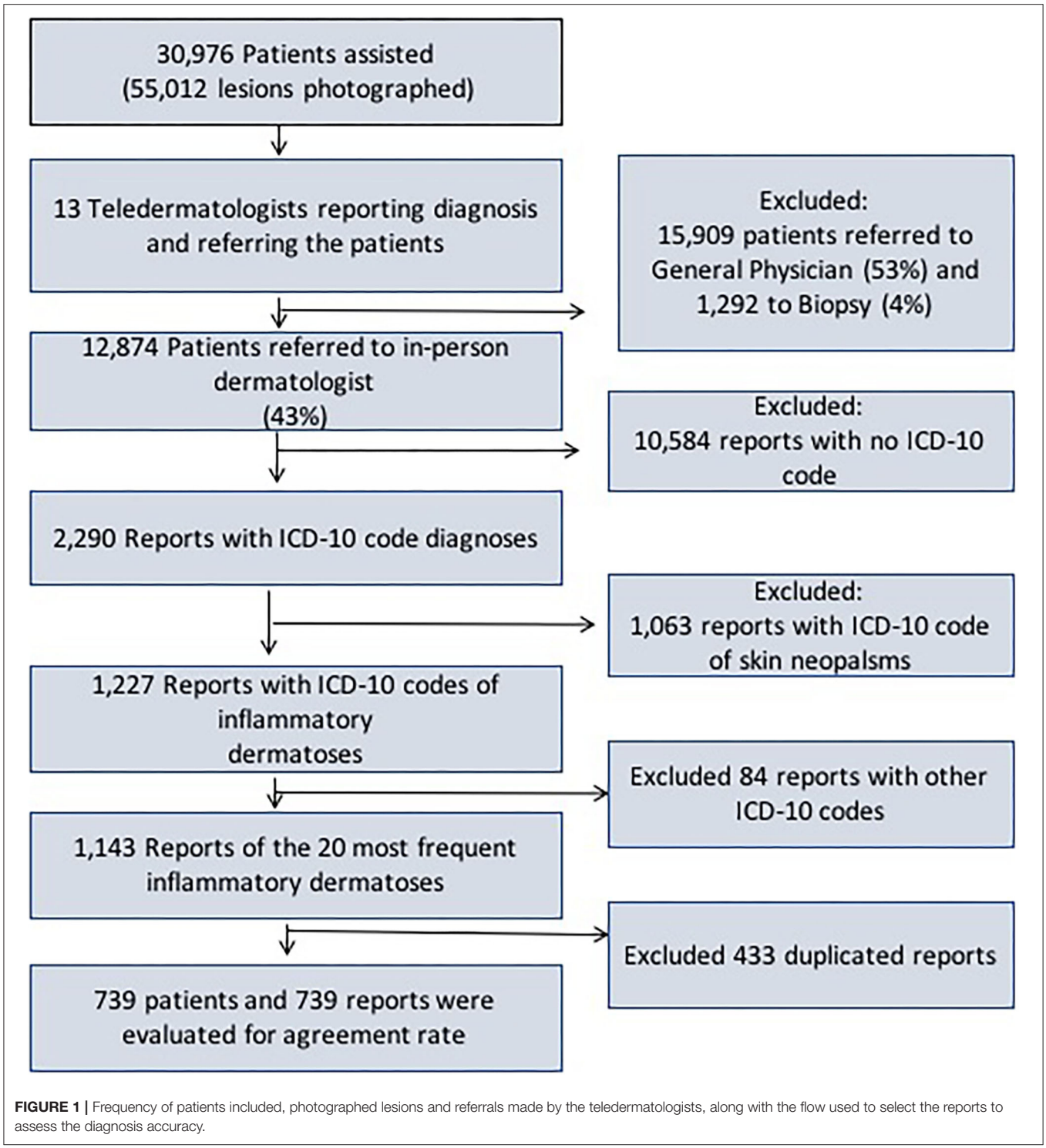

FIGURE 1 | Frequency of patients included, photographed lesions and referrals made by the teledermatologists, along with the flow used to select the reports to assess the diagnosis accuracy.

Table 3 assesses the 20 most frequent inflammatory dermatoses diagnosed by in-person dermatologists of which we were able to recover the ICD-10 codes, along with the accuracy of teledermatology found in our study. The mean frequency of complete agreement was 78% for all 20 dermatoses tested (573/739) and its kappa coefficient was 0.743, which is considered a substantial agreement. Xerosis had the lowest rate (31%; kappa = 0.173) and psoriasis and focal hyperhidrosis showed the greatest (100%; kappa = 1.00). A partial agreement was verified in 8% of all cases (60/739), ranging from 0% (dermatophytosis, atopic dermatosis, molluscum, psoriasis, pityriasis versicolor, and focal hyperhidrosis) to 46% (xerosis). No agreement was

found in 14% (106/739); psoriasis and focal hyperhidrosis with the lowest rate (0%) and pityriasis versicolor with the highest (44%).

TABLE 1 | Group of skin disorders and respective dermatoses present in this study considered as partial agreement between in-person dermatologists' and teledermatogists' diagnosis.

Group of disorder	Dermatoses
Skin adnexal glands (sebaceous, sweat)	Acne, rosacea, hidradenitis
Skin Hyperpigmentation	Chloasma, post-inflammatory hyperpigmentation
Erythematous-scaly patches	Psoriasis, dermatophytosis, pityriasis versicolor, actinic keratosis, seborrheic dermatitis, lupus erythematosus
Skin Hypopigmentation	Vitiligo, leukoderma
Eczematous	Atopic dermatitis, contact dermatitis, dyshidrosis, stasis dermatitis, nummular dermatitis, xerosis, lichen simplex chronicus, pityriais alba, urticaria, photoallergy, seborrheic dermatitis
Alopecia	Androgenetic alopecia, alopecia areata, telogen effluvium, cicatricial alopecia

Partial agreement frequency and the description of each inflammatory dermatoses are shown in **Table 4**. Post-inflammatory hyperpigmentation reached the highest number, with 16 cases, all of them with the same diagnosis. On the other hand, seborrheic dermatitis had 13 cases of partial agreement with 11 different diagnoses.

DISCUSSION

The differences in frequency for the inflammatory dermatoses between **Tables 2** and **3** are due to the fact that although one disease could be very frequently diagnosed by the teledermatologists (**Table 2**), but it could not be referred as frequently to the in-person dermatologists (**Table 3**). That, in fact, was the reason for solar lentigo, leukoderma, pityriasis alba, dyshidrosis, lichen simplex chronicus and stasis dermatitis to be left out of the second table. These dermatoses were mostly referred back to the GP along with the diagnosis/management, and they were present only in few cases for the in-person dermatologist, not included in the 20 most frequent ones as the inclusion criteria.

This fact is also very relevant when discussing accuracy. Since the aim of the teledermatology triage project was to prioritize the severe, more complex, or surgical cases for biopsy and

TABLE 2 | Most frequent inflammatory dermatoses diagnosed by teledermatologists according to number of patients, sex distribution, and number of photographed lesions.

ICD-10 code	Dermatosis	Patients (*n*)	Male (*n*)	Female (*n*)	Photographed lesions (*n*)
B35	Dermatophytosis	3,064	843	2,221	3,496
L70	Acne	2,662	851	1,811	3,217
L81.1	Chloasma	1,749	121	1,628	1,840
L20.9	Atopic dermatitis	1,648	603	1,045	2,058
L85.3	Xerosis	1,632	478	1,154	1,815
L57.9	Solar lentigo	1,584	223	1,361	1,870
L21.9	Seborrheic dermatitis	1,259	426	833	1,421
L23/L24/L25	Contact dermatitis	1,203	325	878	1,333
L81.0	Post-inflammatory hyperpigmentation	1,139	256	883	1,303
L81.5	Leukoderma	1,029	829	200	1,102
L65	Telogen effluvium	881	20	861	891
L30.5	Pityriasis alba	796	282	514	881
L64.9	Androgenetic alopecia	765	135	630	774
B36.0	Pityriasis versicolor	727	264	463	862
L60	Nail disorders	586	94	492	629
L40.0	Psoriasis	551	249	302	760
L80	Vitiligo	550	228	322	694
B08.1	Molluscum contagiosum	366	168	198	423
L30.1	Dyshidrosis	358	84	274	387
L28	Lichen simplex chronicus	340	157	183	368
L63	Alopecia areata	331	135	196	348
L71	Rosacea	248	60	198	257
I83.1	Stasis dermatitis	202	92	110	209
L30.0	Nummular dermatitis	201	59	142	218
L74.5	Focal Hyperhidrosis	200	86	114	209
L50	Urticaria	139	40	99	154
Total		24,210	7,108	17,112	27,519

TABLE 3 | Most frequent inflammatory dermatosis diagnosed by in-person dermatologists and agreement with teledermatology diagnoses.

Diagnoses(*n* =)	Complete agreement *n* (%)	Complete agreement kappa	Partial agreement *n* (%)	No agreement *n* (%)
Acne (122)	113 (93)	0.924	1 (1)	8 (6)
Dermatophytosis (83)	52 (63)	0.564	0 (0)	31 (37)
Atopic Dermatitis (81)	75 (93)	0.923	0 (0)	6 (7)
Post-inflammatory hyperpigmentation (59)	20 (34)	0.206	16 (27)	23 (39)
Contact dermatitis (52)	40 (77)	0.743	5 (10)	7 (13)
Androgenetic alopecia (49)	38 (78)	0.751	8 (16)	3 (6)
Chloasma (36)	32 (89)	0.883	2 (5.5)	2 (5.5)
Molluscum contagiosum (36)	34 (94)	0.943	0 (0)	2 (6)
Vitiligo (30)	27 (90)	0.895	1 (3)	2 (7)
Seborrheic dermatitis (29)	10 (34)	0.213	13 (45)	6 (21)
Psoriasis (26)	26 (100)	1.000	0 (0)	0 (0)
Telogen effluvium (24)	23 (96)	0.957	1 (4)	0 (0)
Alopecia areata (21)	20 (95)	0.951	1 (5)	0 (0)
Rosacea (20)	17 (85)	0.839	1 (5)	2 (10)
Pityriasis versicolor (16)	9 (56)	0.481	0 (0)	7 (44)
Nail disorders (14)	12 (86)	0.847	0 (0)	2 (14)
Focal hyperhidrosis (11)	11 (100)	1.000	0 (0)	0 (0)
Xerosis (13)	4 (31)	0.173	6 (46)	3 (23)
Urticaria (9)	7 (78)	0.754	2 (22)	0 (0)
Nummular dermatitis (8)	3 (37.5)	0.247	3 (37.5)	2 (25)
Total (739)	573 (78)	0.743	60 (8)	106 (14)

TABLE 4 | Differences between teledermatogists' and in-person dermatologists' diagnosis in cases considered partial agreement for inflammatory dermatosis.

Teledermatologist diagnosis	Partial agreement (*n*)	In-person diagnosis
Acne	1	1 hidradenitis
Rosacea	1	1 acne
Contact dermatitis	5	4 atopic dermatitis, 1 lichen simplex chronicus
Nummular dermatitis	3	2 pitiryasis alba, 1 dyshidrosis
Urticaria	2	1 atopic dermatitis, 1 contact dermatitis
Xerosis	6	4 atopic dermatitis, 1 pityriasis alba; 1 photoallergy
Seborrheic dermatitis	13	3 androgenic alopecia, 1 contact dermatitis, 1 psoriasis, 1 dermatophytosis, 1 rosacea, 1 hidradenitis suppurativa, 1 pityriasis alba, 1 phototoxic allergy, 1 perifolicullitis capitis, 1 lupus erythematosus, 1 actinic keratosis
Vitiligo	1	1 leukoderma
Post-inflammatory hyperpigmentation	16	16 chloasma
Chloasma	2	2 post-inflammatory hyperpigmentation
Androgenetic alopecia	8	4 alopecia areata, 3 telogen effluvium, 1 cicatricial alopecia
Alopecia areata	1	1 androgenetic alopecia
Telogen effluvium	1	1 androgenetic alopecia

in-person dermatologists and to manage the mild cases under the primary-care attention along with the GP, the inflammatory disorders diagnosed by in-person dermatologists in **Table 2** have a potential bias of being the most challenging cases. Typical or "regular" inflammatory dermatoses were most likely diagnosed and referred to the GP. Therefore, the rate of agreement found would be probably even higher if the more typical cases were analyzed. The results of our study showed a high agreement rate between diagnoses made by teledermatologists and in-person dermatologists, corroborating the idea that teledermatology is accurate for inflammatory dermatoses. If we add the total (78%) and partial (8%) agreement rates, we will achieve 86% (kappa = 0.846), which is considered an almost perfect agreement, and only 14% of no agreement. This would be remarkable even if we were not discussing the potential bias above. According to literature, SF-TD had an accuracy in general of 64 and 65% in medium size studies (n = 109 and 163, respectively) and 90 and 95% in small size studies (n = 50 and 10, respectively) (6). Another article found an agreement of 90% in 120 cases of SF-TD consultations (7). Lim et al. reported 88% agreement in 53 cases (8). Weingast et al. evaluated 263 patients and found accuracy of 80% (9). O'Connor et al. assessed 40 patients and encountered accuracy of 83% (10).

There were different accuracies among the 20 most frequent dermatoses diagnosed by in-person dermatologists in our study. Eight diseases reached very high complete agreement rate, 90% or above: acne, atopic dermatitis, molluscum contagiosum, vitiligo, psoriasis, telogen effluvium, alopecia areata, and focal hyperhidrosis. Six disorders showed a good total agreement rate, 70–89%: contact dermatitis, androgenetic alopecia, chloasma, rosacea, nail disorders, and urticaria. Six inflammatory dermatoses were less accurate (<60% of total agreement): dermatophytosis, post-inflammatory hyperpigmentation, seborrheic dermatitis, pityriasis versicolor, xerosis, and nummular dermatitis. What were those diseases

mistaken for? In order to verify that, we checked if they could be classified as possible differential diagnosis, which we considered to be a partial agreement.

Examining the six diseases with total agreement ranging from 70–89% and considering the partial agreement rate, three of them would have a considerable change. Contact dermatitis would increase from 77 to 87%, due to five cases that were in fact four atopic dermatitis and one lichen simplex chronicus. Androgenetic alopecia (AGA) would increase from 78 to 94%, due to four alopecia areata, three telogen effluvium and one cicatricial alopecia. Chloasma would also raise from 89 to 94.5% accuracy if we included the two cases of post-inflammatory hyperpigmentation in **Table 4**.

Most interestingly, anyhow, is to look for the diseases showing the least accuracy. Post-inflammatory hyperpigmentation (PIH) should have a separate interpretation once all 16 cases of partial agreement had the same diagnosis: chloasma. One hypothesis is a typing error, because their ICD-10 codes are almost the same (L81.0 and L81.1). Another one is that dermatologists misuse chloasma ICD-10 code for PIH, since chloasma is a very frequent disease and its ICD-10 code may be already known by heart while PIH code would not. Nummular dermatitis and xerosis would at least double the accuracy (37.5–75% and 31–77%, respectively) if we considered the partial agreement diagnosis. Seborrheic dermatitis (SD) was the disease with the highest number of differential diagnosis (13) and considering the partial agreement rate, accuracy would go from 34 to 79%. On the scalp, SD was diagnosed as AGA and perifolicullitis capitis, which could even occur simultaneously, and on the skin, could be confused with many diseases such as psoriasis, eczemas, lupus erythematous, dermatophytosis, rosacea, and actinic keratosis. Dermatophytosis and pityriasis versicolor were the least accurate diagnosis when total and partial agreement were considered, 63 and 56%, respectively. This may be due to some limitation in assessing the lesions through teledermatology or to a great variety of possible differential diagnoses. Again, in our study, the fact that the most typical cases were meant to be treated by teledermatology and not sent to in-person dermatologists could have played an important role in these two dermatoses.

Although this was a retrospective study and much data was missing, we believe this was one of the studies with the largest number of inflammatory diseases included in the literature. The study was performed in two centers and different dermatologists performed the tele and in-person examinations. This is beneficial, in a way that we assessed the agreement between different examiners, but it also may have some bias, since the technical skills in the two groups may be different.

Our study in a large number of patients presenting the most common inflammatory dermatoses showed that the mean accuracy of teledermatology was high, varying according to the disease. This result reassures that store-and-forward teledermatology is as proper option for patient care.

DATA AVAILABILITY STATEMENT

The raw data supporting the conclusions of this article will be made available by the authors, without undue reservation.

ETHICS STATEMENT

The studies involving human participants were reviewed and approved by Ethics Committee of Hospital Israelita Albert Einstein (CAAE: 97126618.6.0000.0071). Written informed consent from the participants' legal guardian/next of kin was not required to participate in this study in accordance with the national legislation and the institutional requirements.

AUTHOR CONTRIBUTIONS

MG-B, RS, and EC were responsible for the study design. MG-B was responsible for writing the article. MG-B and RS were responsible for data analyzes. All authors contributed to the article and approved the submitted version.

REFERENCES

1. Lee JJ, English JC. Teledermatology: a review and update. *Am J Clin Dermatol.* (2018) 19:253–60. doi: 10.1007/s40257-017-0317-6
2. Finnane A, Dallest K, Janda M, Soyer HP. Teledermatology for the diagnosis and management of skin cancer: a systematic review. *JAMA Dermatol.* (2017) 153:319–27. doi: 10.1001/jamadermatol.2016.4361
3. Warshaw EM, Lederle FA, Grill JP, Gravely AA, Bangerter AK, Fortier LA, et al. Accuracy of teledermatology for pigmented neoplasms. *J Am Acad Dermatol.* (2009) 61:753–65. doi: 10.1016/j.jaad.2009.04.032
4. Chuchu N, Dinnes J, Takwoingi Y, Matin RN, Bayliss SE, Davenport C, et al. Teledermatology for diagnosing skin cancer in adults. *Cochrane Database Syst Rev.* (2018) 12:CD013193. doi: 10.1002/14651858.CD013193
5. Markun S, Scherz N, Rosemann T, Tandjung R, Braun RP. Mobile teledermatology for skin cancer screening: a diagnostic accuracy study. *Medicine.* (2017) 96:e6278. doi: 10.1097/MD.0000000000006278
6. Warshaw EM, Hillman YJ, Greer NL, Hagel EM, MacDonald R, Rutks IR, et al. Teledermatology for diagnosis and management of skin conditions: a systematic review. *J Am Acad Dermatol.* (2011) 64:759–72. doi: 10.1016/j.jaad.2010.08.026
7. Lasierra N, Alesanco A, Gilaberte Y, Magallón R, García J. Lessons learned after a three-year store and forward teledermatology experience using internet: strengths and limitations. *Int J Med Inform.* (2012) 81:332–43. doi: 10.1016/j.ijmedinf.2012.02.008
8. Lim AC, Egerton IB, See A, Shumack SP. Accuracy and reliability of store-and-forward teledermatology: preliminary results from the St George Teledermatology Project. *Aust J Dermatol.* (2001) 42:247–51. doi: 10.1046/j.1440-0960.2001.00529.x
9. Weingast J, Scheibböck C, Wurm EM, Ranharter E, Porkert S, Dreiseitl S, et al. A prospective study of mobile phones for dermatology in a clinical setting. *J Telemed Telecare.* (2013) 19:213–8. doi: 10.1177/1357633x13490890
10. O'Connor DM, Jew OS, Perman MJ, Castelo-Soccio LA, Winston FK, McMahon PJ. Diagnostic accuracy of pediatric teledermatology using parent-submitted photographs: a randomized clinical trial. *JAMA Dermatol.* (2017) 153:1243–8. doi: 10.1001/jamadermatol.2017.4280
11. Landis J, Koch G. The measurement of observer agreement for categorical categorical data. *Biometrics.* (1977) 33:159–74. doi: 10.2307/2529310

12. IBGE. *Censo 2010*. (2010). São Paulo. Available online at: https://cidades.ibge.gov.br/brasil/sp/sao-paulo/pesquisa/23/27652 (accessed June 12, 2020).

Conflict of Interest: The authors declare that the research was conducted in the absence of any commercial or financial relationships that could be construed as a potential conflict of interest.

frontiers in Medicine

ORIGINAL RESEARCH
published: 23 November 2020
doi: 10.3389/fmed.2020.598903

Part II: Accuracy of Teledermatology in Skin Neoplasms

Mara Giavina-Bianchi, Maria Fernanda Dias Azevedo, Raquel Machado Sousa and Eduardo Cordioli*

Department of Telemedicine, Hospital Israelita Albert Einstein, São Paulo, Brazil

Teledermatology has been proving to be of great help for delivering healthcare, especially now, during the SARS-CoV-2 pandemic. It is crucial to assess how accurate this method can be for evaluating different dermatoses. Such knowledge can contribute to the dermatologists' decision of whether to adhere to teledermatology or not. Our objective was to determine the accuracy of teledermatology in the 10 most frequent skin neoplasms in our population, comparing telediagnosis to histopathological report and in-person dermatologists' diagnosis. A retrospective cohort study was conducted in São Paulo, Brazil, where a store-and-forward teledermatology project was implemented under primary-care attention to triage surgical, more complex, or severe dermatoses. A total of 30,976 patients presenting 55,012 lesions took part in the project. Thirteen teledermatologists who participated in the project had three options to refer the patients: send them directly to biopsy, to the in-person dermatologist, or back to the general physician with the most probable diagnosis and management. In the groups referred to the in-person dermatologist and biopsy, we looked for the 10 most frequent International Statistical Classification of Diseases and Related Health Problems-10 (ICD-10) of skin neoplasms, which resulted in 289 histopathologic reports and 803 in-person dermatologists' diagnosis. We were able to compare the ICD-10 codes filled by teledermatologists, in-person dermatologists, and from histopathological reports. The proportion of complete, partial, and no agreement rates between the in-person dermatologist's, histopathologic report, and the teledermatologist's diagnosis was assessed. We also calculated Cohen's kappa, for complete and complete plus partial agreement. The mean complete agreement rate comparing telediagnosis to histopathological report was 54% (157/289; kappa = 0.087), being the highest for malign lesions; to in-person dermatologists was 61% (487/803; kappa = 0.213), highest for benign lesions. When accuracy of telediagnosis for either malign or benign lesions was evaluated, the agreement rate with histopathology was 70% (kappa = 0.529) and with in-person dermatologist, 81% (kappa = 0.582). This study supports that teledermatology for skin neoplasms has moderate accuracy. This result reassures that it can be a proper option for patient care, especially when the goal is to differentiate benign from malign lesions.

Keywords: teledermatology, telemedicine, accuracy: skin neoplasms, skin cancer, benign skin lesions, malign skin lesions, tele-health

OPEN ACCESS

Edited by:
Paola Pasquali,
Pius Hospital de Valls, Spain

Reviewed by:
Amanda Oakley,
Waikato District Health Board, New Zealand
David Moreno-Ramírez,
Sevilla University, Spain

****Correspondence:***
Mara Giavina-Bianchi
marahgbianchi@gmail.com

Specialty section:
This article was submitted to Dermatology, a section of the journal Frontiers in Medicine

Received: *25 August 2020*
Accepted: *28 October 2020*
Published: *23 November 2020*

Citation:
Giavina-Bianchi M, Azevedo MFD, Sousa RM and Cordioli E (2020) Part II: Accuracy of Teledermatology in Skin Neoplasms. Front. Med. 7:598903. doi: 10.3389/fmed.2020.598903

INTRODUCTION

As we face this pandemic time around the world, telemedicine has been proving to be of great help for delivering healthcare. Any medical specialty that is based on image analysis, such as dermatology, is especially suitable for this method of care. Teledermatology has the potential to improve access to subspecialty expertise, reduce healthcare costs, and improve the overall quality of care. The three main teledermatology delivery platforms are: synchronous (RT: real-time teledermatology), asynchronous (SF-TD: store-and-forward teledermatology), and hybrid (both synchronous and asynchronous forms). Synchronous teledermatology uses live video conferencing between the patient and the dermatologist. Asynchronous teledermatology is a method whereby clinical or dermoscopy dermatologic images are obtained and sent to the responding dermatologist who can review them at a later time. Although it provides high-resolution dermatologic images and promotes an efficient practice, this modality is limited by the ability of the teledermatologist to obtain additional clinical history while evaluating the case (1). Teledermoscopy involves the use of dermoscopic images for remote consultation and decision-making in skin cancer screening. Its addition significantly improved the results of an internet-based skin cancer screening system, compared with clinical images alone (2).

The majority of studies in teledermatology have found rates of accuracy to be in the range of 75–80%, comparable to those with in-person care (1). Many of the articles were focused on skin neoplasms, especially skin cancer and pigmented lesions (3–6), or on general dermatology (7–11). A recent systematic review concluded that robust implementation studies of teledermatology are needed, with attention to reducing the risk of bias when assessing diagnostic accuracy (3). For this purpose, we performed research with the primary goal of determining the accuracy of teledermatology for skin neoplasms in a robust number of cases, assessing the agreement rate between the histopathological report, in-person dermatologists', and the teledermatologists' diagnoses. The secondary aim was to analyze the differential diagnosis of the lesions.

MATERIALS AND METHODS

This was a retrospective cohort study designed to assess concordance between diagnoses made by in-person dermatologists and teledermatologists, and by histopathological reports and teledermatologists, approved by the Ethics Committee of Hospital Israelita Albert Einstein (CAAE: 97126618.6.0000.0071). We analyzed the reports of 30,976 patients included in a teledermatology triage project conducted in the city of São Paulo, Brazil, from July 2017 to July 2018.

Abbreviations: TD, teledermatology; RT, real time; SF-TD, store and forward; IPD, in-person dermatologist; GP, general physician; ICD-10 code, international code of diseases 10; BCC, basal cell carcinoma; SCC, squamous cell carcinoma; AK, actinic keratosis; SK, seborrheic keratosis; Acro/other benign, acrochordon/other benign neoplasms.

Teledermatology Triage Project

A Teledermatology project implemented from July 2017 to July 2018, in São Paulo. There were 57,832 individuals waiting for a consultation with a dermatologist in the public health system in July 2017. To reduce the waiting list and accelerate the flow of patients with the most severe, complex or surgical dermatoses to in-person dermatologists, the municipal health government requested Hospital Israelita Albert Einstein, a large private hospital in the city with expertise in Telemedicine, to develop a project using Telemedicine to reach these goals. Therefore, an online platform and a mobile app were designed to take photographs with phone cameras and directly upload them to the app and a short clinical history and data of the patient, which were meant to be used by for health technicians or nurses. The photographs and collected information were uploaded to a platform using a secure online process and were accessed only by the 13 Brazilian Board Certified dermatologists associated with this project, for whom the patients were randomly assigned. These 13 dermatologists will be called teledermatologists in this study. All the patients waiting for dermatologist consultations were called consecutively, via phone, by the municipal health care service and scheduled for an appointment in one of the three public city hospitals enabled to carry out the project, depending on the location of the individual's residence. Once there, a short history of the complaint (history of bleeding, pruritus, time from the onset, and location) and demographic data (sex and age) as well as three photographs in different angles and distances from each lesion were taken by a trained health technician: first one at medium distance (50 cm away), second one in close-up (15 cm away) and last one of a lateral view, aiming to evaluate the volume of the lesion. After accessing the patients' pictures and clinical history of the patients, the dermatologists first decided whether the photographs of the lesions were satisfactory for diagnostic purposes. If not, they categorized it under "bad photo," and the patient was referred to a dermatologist for an in-person appointment. If the photo quality was good enough, they formulated the most probable diagnostic hypothesis. They chose one of three options for each lesion assessed: (1) a direct referral for a biopsy (after which the patient would return for an in-person dermatologist appointment), (2) a referral for an in-person dermatologist (IPD) visit, or (3) a referral to go back to the primary care physician (GP) with the most probable diagnosis, treatment and/or recommendation on how to proceed with the investigation and/or management of the lesion. A schematic for this process is shown in **Figure 1**. If the same patient had more than one lesion but different referrals, they were referred to the most specialized one and that would be his/her last referral in terms of statistical accounting. For instance, a biopsy would prevail over a dermatologist visit, which would in turn prevail over general physician referral. This teledermatology project followed the American Medical Association telemedicine policy, adapted for the needs of the Brazilian public health care system (12).

Study Design

We selected the groups referred to IPD (12,874 patients/16,777 lesions) and biopsy (1,292 patients/1,912 lesions). Then, we assessed the reports that had the International Statistical

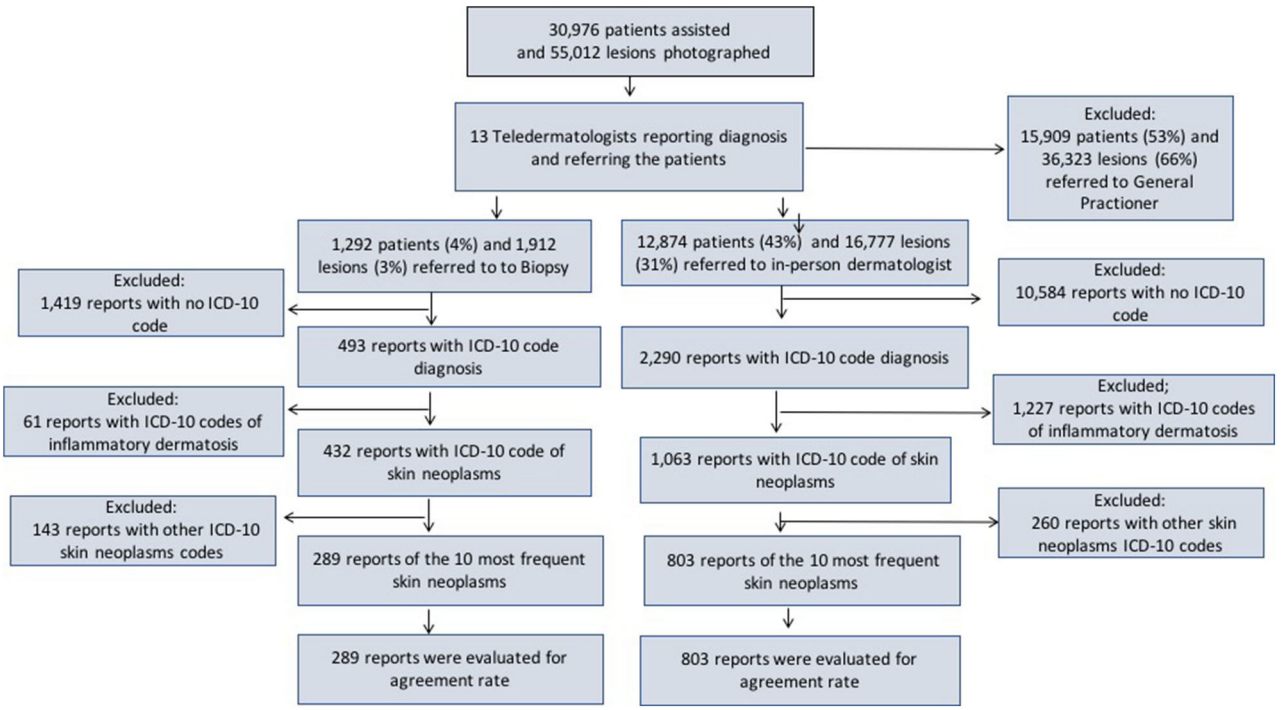

FIGURE 1 | Frequency of patients included, photographed lesions and referrals made by the teledermatologists, along with the flow used to assess the diagnosis accuracy for the 10 most frequent skin neoplasms.

Classification of Diseases and Related Health Problems 10th version (ICD-10 code) (13) diagnoses filled by IPD (2,290) and histopathological reports (HP: 493). Next, we separated the reports filled with ICD-10 codes of skin neoplasms sent to IPD (1,063) and from histopathological reports (432). Afterward, we looked for the 10 most frequent dermatoses in each group, 803 in IPD and 289 to include in our study (803 for IPD and 289 in HP **Figure 1**).

We classified the rate of agreement as follows: (1) complete agreement when the ICD-10 code used in both reports were the same, (2) partial agreement when the ICD-10 code used in both reports were different, but in the same group of disease (malign or benign neoplasms), posing as a probable differential diagnosis, and (3) no agreement when both reports did not fill the previous two conditions. Basal cell carcinoma (BCC), squamous cell carcinoma (SCC), melanoma, and actinic keratosis (AK) were considered the malign group. Nevus, seborrheic keratosis (SK), acrochrodon/other benign neoplasms, cyst, lipoma, and wart were the benign group. If the cases did not belong to one of those 10 classes, it was classified as "other." As the gold standard diagnosis is the histopathological diagnosis, the agreement was stated in this research as accurate.

Statistical Analysis

Rates of concordance were expressed using percentages and Cohen's kappa coefficient, which was used to compare between groups of inter-rater observers (Graph Pad Prism 6.0). The guidelines used to characterize kappa values were created by Landis and Koch (14), as follows: kappa < 0: no agreement, 0.00–0.20: slight agreement, 0.21–0.40: fair agreement, 0.41–0.60: moderate agreement, 0.61–0.8: substantial agreement, and 0.81–1.00: almost perfect agreement.

RESULTS

Table 1 shows the 10 most frequent skin neoplasms diagnosed by teledermatology according to the frequency of lesions, sex, age, and referral distribution. The total amount represents 31% (17,233/55,012) of the lesions diagnosed in the entire teledermatology project. The female and male proportion was 72 and 28%, respectively, although the female population accounts for 52.6% in the city of São Paulo (2010) (15). Lesions diagnosed as benign were 90% (15,496/17,233) and as malign, 10% (1,727/17,233). Among benign neoplasms, 63% (9,849/15,496) were sent to GP for follow-up, 34% (5,242/15,496) were sent to IPD and only 3% (405/15,496) were sent to biopsy. For malign lesions, 3% (4/1,727) was referred to GP, 51% (880/1,727) to IPD and 46% (803/1,727) to biopsy.

Figures 2, **3** demonstrate the comparison between teledermatologists' diagnosis to the histopathological reports and to in-person dermatologists, respectively.

For instance, in **Figure 2**, among the 65 histopathological reports of BCC in this study, the teledermatologists had diagnosed 49 correctly (complete agreement in yellow), 6 as SCC, 2 as melanoma, 3 as AK (all considered partial agreement, in green), 2 as nevus, 2 as SK, and 1 as other (all considered no agreement, in red).

TABLE 1 | Patient's demographics and referrals for the 10 most frequent skin neoplasms diagnosed in the Teledermatology Project in São Paulo from July 2017–2018.

	Sex		Age (years)			Referral			
Skin neoplasm	**M**	**F**	**0–19**	**20–59**	**60+**	**Biopsy**	**IPD**	**GP**	**Total**
BCC	144	274	0	154	264	341	73	4	418
SCC	120	188	5	101	202	267	39	2	308
Melanoma	45	118	7	68	88	117	46	0	163
AK	280	558	2	190	646	78	722	38	838
Nevus	917	3,434	399	2,985	967	166	1,491	2,694	4,351
SK	784	2,251	4	1,124	1,907	75	507	2,453	3,035
Acro/other	889	2,872	275	2,483	1,003	76	539	3,146	3,761
Cyst	738	1,176	119	1,172	623	41	1,059	814	1,914
Lipoma	394	510	26	590	288	3	362	539	904
Wart	592	939	489	722	320	44	1,284	203	1,531
Total	4,903	12,320	1,326	9,589	6,308	1,208	6,122	9,893	17,233

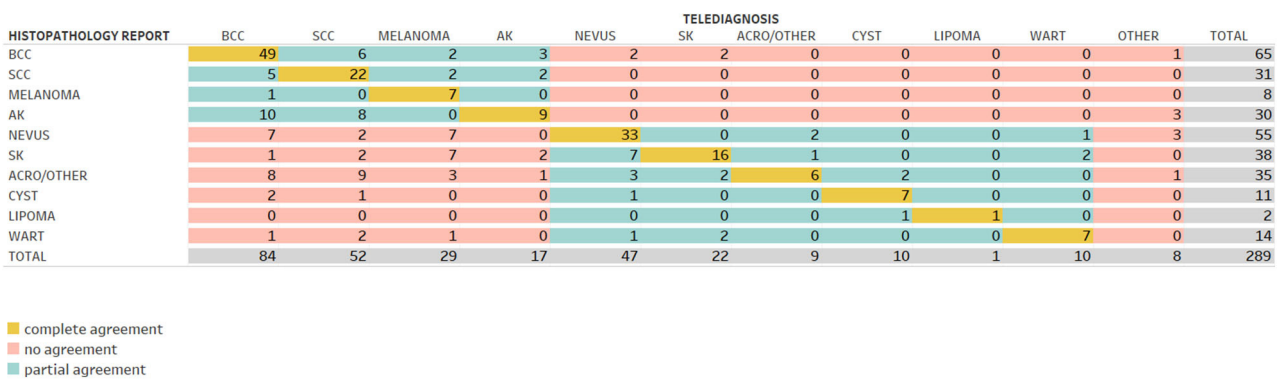

FIGURE 2 | Confusion matrix comparing telediagnosis to histopathology report.

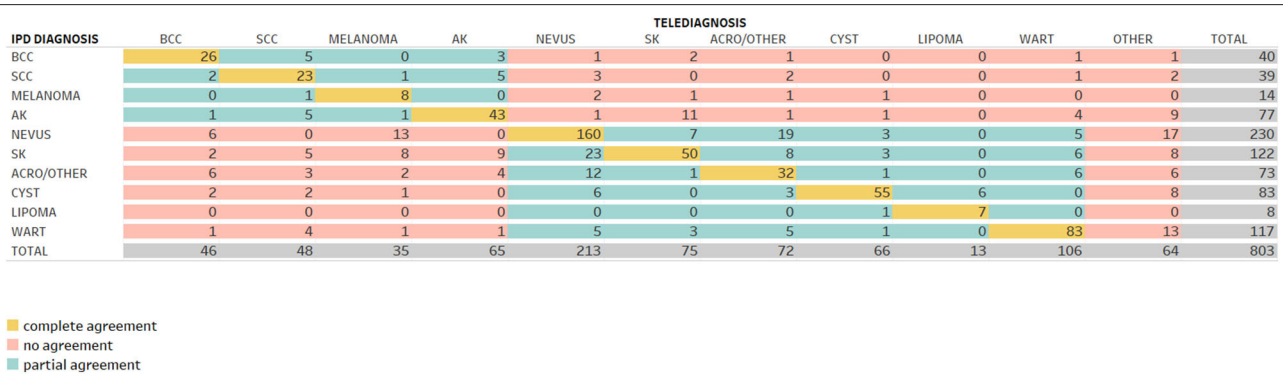

FIGURE 3 | Confusion matrix comparing telediagnosis to in-person dermatologists' diagnosis.

Following the same path, in **Figure 3**, among 40 telediagnosis of BCC, 26 were in agreement with IPD (complete agreement, in yellow), 5 were SCC, 3 were AK (partial agreement, in green) and 1 nevus, 2 SK, 1 acro/other, 1 wart, and 1 other (no agreement, in red).

Table 2 reveals the percentage of accuracy for complete, partial, and no agreement and Cohen's kappa calculations for complete and complete plus partial agreement, comparing the telediagnosis to histopathological reports (upper part) and in-person dermatologists' diagnosis (bottom part). In the upper part, the mean frequency of complete agreement was 54% for all 10 dermatoses tested (157/289) and its kappa coefficient was 0.087), which is considered a slight agreement. Three malign skin tumors had the highest rates of accuracy: melanoma (7/8), BCC (49/65), and SCC (22/31), respectively with 88, 75, and 71% and kappas = 0.060, 0.326, and 0,117. Among benign neoplasms, cyst, and nevus were the most accurate diagnoses, respectively with 64 and 60% and kappas = 0.335 and 0.298 (fair agreement).

TABLE 2 | Agreement between teledermatologists' diagnosis and histopathological reports (upper part) and in-person dermatologists (bottom part).

	Teledermatologists' diagnosis				
Histopathology report	**Complete agreement (%)**	**Cohen's Kappa complete agreement**	**Partial agreement (%)**	**Cohen's Kappa complete + partial agreement**	**No agreement (%)**
BCC	75	0.326	17	0.680	8
SCC	71	0.117	29	0.627	0
Melanoma	88	0.060	12	0.209	0
AK	30	−0.146	60	0.724	10
Nevus	60	0.298	5	0.596	35
SK	42	0.129	26	0.513	32
Acro/other benign	17	−0.078	20	0.195	63
Cyst	64	0.335	9	0.717	27
Lipoma	50	0.400	50	1.00	0
Wart	50	0.189	21	0.676	29
Total	54	0.087	16	0.529	30
In-person dermatologists' diagnosis					
BCC	65	0.213	20	0.472	15
SCC	59	0.067	20.5	0.496	20.5
Melanoma	57	−0.138	7	−0.050	36
AK	56	0.217	9	0.427	35
Nevus	70	0.446	15	0.807	15
SK	41	0.068	34	0.527	25
Acro/other benign	44	−0.117	27	0.642	29
Cyst	66	0.483	22	0.799	12
Lipoma	87.5	0.369	12.5	1.00	0
Wart	71	0.490	12	0.768	17
Total	61	0.213	20	0.582	19

Warts, SK and lipomas showed an intermediate rate, around 50%, and acrochordon and other benign neoplasms had the lowest rate (17%; kappa = −0.078). AK had only 30% of agreement, being the least accurate in the malign group (kappa = −0.146). Partial agreement was verified in 22% of all cases (64/289), ranging from 5% in nevus up to 60% in AK. No agreement was found in 24% (68/289); CBC, SCC, and lipoma had zero no agreements while nevus, SK, warts, and cysts had around 30% of no agreement.

Comparing teledermatologists' to in-person dermatologists' diagnosis accuracy, we found a mean frequency of complete agreement in 61% of all 10 skin neoplasms (487/803) and its kappa coefficient was 0.213, which is considered a fair agreement. Benign skin tumors had the highest rates of accuracy: lipoma (7/8), warts (83/116), and nevus (160/230), with 87.5, 72, and 70% and kappas = 0.369, 0.490, and 0.446, respectively. Among malign neoplasms, all four of them were between 56% (AK) and 65% (CBC). The lowest rate was achieved by SK (41%; kappa = 0.068) and acro/other benign (44%; kappa = −0.117). Partial agreement was verified in 20% of all cases (159/803), ranging from 7% in melanoma up to 34% in SK. No agreement was found in 19% (156/803); lipoma had zero no agreements while melanoma, AK, and acro/other benign had around 36, 35, and 29%, respectively.

DISCUSSION

Analyzing **Table 1**, we can see that most of the benign cases of skin neoplasms in this cohort were not sent to biopsy and in-person dermatologists; they were sent back to the GP to follow-up and, therefore, could not be compared with the teledermatologists' diagnosis. This fact is very relevant when discussing accuracy in this study. As the teledermatology triage project prioritized the severe, more complex, or surgical cases for biopsy and in-person dermatologists, trying to manage the mild cases under the primary-care attention along with the GP, skin neoplasms diagnosed by histopathological analysis or in-person dermatologists have a bias of being the most challenging/difficult cases. Typical or "regular" skin neoplasms were most probably diagnosed and referred back to the GP. In this manner, our results in the rate of agreement would be probably much higher if more typical cases were analyzed.

In terms of health delivery, choosing the proper management of the skin neoplasms is even more important than elaborating the right diagnosis itself. In this way, what is more important than complete agreement (ICD-10 code) is to analyze rates of complete plus partial agreement (benign vs. malign). If the diagnosis fits within the benign neoplasms, an expectant conduct is acceptable, while within the malign neoplasms, a biopsy, or surgery ought to be expected.

Analyzing teledermatogists' diagnosis and histopathological reports' agreement, we showed a mean agreement rate of 70% (54% total + 16% partial agreement rates) and kappa = 0.529 (moderate). Considering studies that compared TD diagnosis and histopathological reports, Silveira et al. (16) included 364 suspected cases of skin malignancy by TD to be confirmed by the biopsy. The majority of the lesions were BCCs with 286 cases, followed by 59 SCCs and 5 melanomas. Two oncologists showed

an overall accuracy of 85.3% for the first and 87.3% for the other in categorizing benign x malign lesions. Our results for malign and benign lesions showed 94% (126/134) and 61% (95/155) of agreement, respectively. In another study, 144 pigmented lesions diagnosed via TD were examined histologically, and 63 (43%) showed complete agreement between the clinical and histological diagnoses (17). Comparatively, our study showed 60 and 88% complete agreement for nevus and melanoma respectively. In another article, 201 biopsies were requested to rule out malignancy via TD, which was confirmed in 45.3% (18). A survey among the teledermatologists participating in the project, after its conclusion, showed that the use of dermoscopy would significantly improve the decision to refer nevus and SK to in-person dermatologists, GP or biopsy and, most probably, the agreement rate too. They felt that many cases referred to biopsy or IPD could have been referred to GP if dermoscopic images were available (19). Melanoma had a fair agreement rate. We believe that happened because, when in doubt, one would rather excise it and send it to histopathological than wait to see how it develops. In this project, with no access to dermoscopic images, there were 112 lesions suspected of melanoma and 8 melanomas confirmed (14 benign lesions:1 melanoma). Other studies show that the number of nevus needed to diagnose one melanoma can vary from 4.5 to 22 (20). Acrochordon/other benign neoplasms had slight agreement rate kappa, probably because of the reasons explained before. Only "weird looking" acrochordons would be sent to biopsy, confirming that they were, in fact, not acrochordons.

The results of our study showed a slightly better agreement rate between diagnoses made by teledermatologists and in-person dermatologists in general. If we summed up complete (61%) and partial (20%) agreement rates, we have reached 81% (kappa = 0.582-moderate), but there was an inversion in the accuracy for benign and malign lesions. The agreement rate for benign lesions was 82% and for malign, 73%. Nevus and acrochordons/other benign neoplasms in this referral were probably more typical than the ones sent to biopsy, and that could explain why the agreement rate for benign skin neoplasms had an improvement compared to the previous one. On the other hand, BCC, SCC, and AK showed lower agreement rate to IPD than histopathological reports. The worst agreement rate was for melanoma. Cohen's kappa coefficient showed no agreement (−0.050). This may reflect the same reasons stated before, the absence of dermoscopy images and also the teledermatologists' fear of letting a melanoma diagnosis go undetected. When compared to the previous studies, Kroemer et al. (21) included 104 pigmented lesions and found a kappa = 0.84. Moreno-Ramirez et al. (22) showed a kappa = 0.81 in 890 cases of skin cancer triage.

According to the latest Cochrane review (2018) about teledermatology in skin cancers, using a more widely defined threshold to identify "possibly" malignant cases or lesions that should be considered for excision is likely to appropriately triage those lesions requeiring face-to-face assessment by a specialist. Despite the increasing use of teledermatology on an international level, the evidence base to support its ability to accurately diagnose lesions and to triage lesions from primary to secondary care is lacking and further prospective and pragmatic evaluation is needed (5).

Although this was a retrospective study and much data was missing, we believe this was one of the studies with the largest number of skin neoplasms included in the literature, comparing teledermatologists' diagnosis both to IPD and histopathological reports. Pathologists were responsible for histopathological reports. The study was performed in two centers and different dermatologists performed the tele and in-person examinations. This is a limitation because there is interoperator variability and the technical skills in the groups may be different. Moreover, teledermatologists could diagnose the lesions differently if they were face-to-face. The profile of 12 out of the 13 teledermatologists involved in the project was shown in a previously study (19). Ten had either subspecialty in dermoscopy or skin cancer, which we thought was very suitable for this study. Six had more than 10 years as Board Certified Dermatologists. Five of them integrated the Skin Oncology outpatient unity at University of São Paulo Dermatology Department. Unfortunately, we do not have the profile of the IPD. The risk of false negative cases, which we could not assess, exists and it is another limitation of this research. Nonetheless, during the project, there was always a physician, either a GP or an IPD, responsible for monitoring the patients.

Our study, performed in a large number of patients presenting the 10 most common skin neoplasms, showed moderate accuracy between teledermatology and histopathological reports, and moderate agreement rate between teledermatologists and in-person dermatologists' diagnosis. Accuracy may differ among skin neoplasms. This reassures that store-and-forward teledermatology can be an option for triage skin neoplasms in primary-care attention.

DATA AVAILABILITY STATEMENT

The raw data supporting the conclusions of this article will be made available by the authors, without undue reservation.

ETHICS STATEMENT

The studies involving human participants were reviewed and approved by Ethics Committee of Hospital Israelita Albert Einstein (CAAE: 97126618.6.0000.0071). Written informed consent from the participants' legal guardian/next of kin was not required to participate in this study in accordance with the national legislation and the institutional requirements.

AUTHOR CONTRIBUTIONS

MG-B and EC: study design. MG-B, RS, MA, and EC: data collection and review of the article. MG-B and MA: data analysis. MG-B and RS: writing. All authors contributed to the article and approved the submitted version.

REFERENCES

1. Lee JJ, English JC. Teledermatology: a review and update. *Am J Clin Dermatol*. (2018) 19:253–60. doi: 10.1007/s40257-017-0317-6
2. Ferrándiz L, Ojeda-Vila T, Corrales A, Martín-Gutiérrez FJ, Ruíz-de-Casas A, Galdeano R, et al. Internet-based skin cancer screening using clinical images alone or in conjunction with dermoscopic images: a randomized teledermoscopy trial. *J Am Acad Dermatol*. (2017) 76:676–82. doi: 10.1016/j.jaad.2016.10.041
3. Finnane A, Dallest K, Janda M, Soyer HP. Teledermatology for the diagnosis and management of skin cancer: a systematic review. *JAMA Dermatol*. (2017) 153:319–27. doi: 10.1001/jamadermatol.2016.4361
4. Warshaw EM, Lederle FA, Grill JP, Gravely AA, Bangerter AK, Frontier LA, et al. Accuracy of teledermatology for pigmented neoplasms. *J Am Acad Dermatol*. (2009) 61:753–65. doi: 10.1016/j.jaad.2009.04.032
5. Chuchu N, Dinnes J, Takwoingi Y, Martin RN, Bayliss SE, Davenport C, et al. Teledermatology for diagnosing skin cancer in adults. *Cochrane Database Syst Rev*. (2018) 12:CD013193. doi: 10.1002/14651858.CD013193
6. Markun S, Scherz N, Rosemann T, Tandjung R, Braun RP. Mobile teledermatology for skin cancer screening: a diagnostic accuracy study. *Medicine (Baltimore)*. (2017) 96:e6278. doi: 10.1097/MD.0000000000006278
7. Warshaw EM, Hillman YJ, Greer NL, Hagel EM, MacDonald R, Rutks IR, et al. Teledermatology for diagnosis and management of skin conditions: a systematic review. *J Am Acad Dermatol*. (2011) 64:759–72. doi: 10.1016/j.jaad.2010.08.026
8. Lasierra N, Alesanco A, Gilaberte Y, Magallón R, García J. Lessons learned after a three-year store and forward teledermatology experience using internet: strengths and limitations. *Int J Med Inform*. (2012) 81:332–43. doi: 10.1016/j.ijmedinf.2012.02.008
9. Lim AC, Egerton IB, See A, Shumack SP. Accuracy and reliability of store-and-forward teledermatology: preliminary results from the St. George Teledermatology Project. *Australas J Dermatol*. (2001) 42:247–51. doi: 10.1046/j.1440-0960.2001.00529.x
10. Weingast J, Scheibböck C, Wurm EM, Ranharter E, Porkert S, Dreiseitl S, et al. A prospective study of mobile phones for dermatology in a clinical setting. *J Telemed Telecare*. (2013) 19:213–8. doi: 10.1177/1357633x13490890
11. O'Connor DM, Jew OS, Perman MJ, Castelo-Soccio LA, Winston FK, McMahon PJ. Diagnostic accuracy of pediatric teledermatology using parent-submitted photographs: a randomized clinical trial. *JAMA Dermatol*. (2017) 153:1243–8. doi: 10.1001/jamadermatol.2017.4280
12. American Medical Association. *AMA Telemedicine Policy*. (2016). Available online at: www.ama-assn.org (accessed october 10, 2020).
13. DATASUS. *CID-10*. (2008). Available online at: http://www.datasus.gov.br/cid10/v2008/webhelp/cid10.htm (accessed May 11, 2017).
14. Landis J, Koch G. The measurement of observer agreement for categorical categorical data. *Biometrics*. (1977) 33:159–74. doi: 10.2307/2529310
15. IBGE. *Censo 2010*, São Paulo: IBGE. (2013). Available online at: https://cidades.ibge.gov.br/brasil/sp/sao-paulo/pesquisa/23/27652 (accessed June 12, 2020).
16. Silveira CE, Silva TB, Fregnani JH, da Costa Vieria RA, Haikel RL Jr., Syrjanen K, et al. Digital photography in skin cancer screening by mobile units in remote areas of Brazil. *BMC Dermatol*. (2014) 14:19. doi: 10.1186/s12895-014-0019-1
17. Jolliffe VM, Harris DW, Whittaker SJ. Can we safely diagnose pigmented lesions from stored video images? A diagnostic comparison between clinical examination and stored video images of pigmented lesions removed for histology. *Clin Exp Dermatol*. (2001) 26:84–7. doi: 10.1046/j.1365-2230.2001.00767.x
18. Tandjung R, Badertscher N, Kleiner N, Wensing M, Rosemann T, Braun RP, et al. Feasibility and diagnostic accuracy of teledermatology in Swiss primary care: process analysis of a randomized controlled trial. *J Eval Clin Pract*. (2015) 21:326–31. doi: 10.1111/jep.12323
19. Giavina Bianchi M, Santos A, Cordioli E. Dermatologists' perceptions on the utility and limitations of teledermatology after examining 55,000 lesions. *J Telemed Telecare*. (2019):1357633X19864829. doi: 10.1177/1357633X19864829
20. Elliott TM, Whiteman DC, Olsen CM, Gordon LG. Estimated healthcare costs of melanoma in Australia over 3 years post-diagnosis. *Appl Health Econ Health Policy*. (2017) 15:805–16. doi: 10.1007/s40258-017-0341-y
21. Kroemer S, Frühauf J, Campbell TM, Massone C, Schwantzer G, Soyer HP, et al. Mobile teledermatology for skin tumour screening: diagnostic accuracy of clinical and dermoscopic image tele-evaluation using cellular phones. *Br J Dermatol*. (2011) 164:973–9. doi: 10.1111/j.1365-2133.2011.10208.x
22. Moreno-Ramirez D, Ferrandiz L, Nieto-Garcia A, Carrasco R, Moreno-Alvarez P, Galdeano R, et al. Store-and-forward teledermatology in skin cancer triage: experience and evaluation of 2009 teleconsultations. *Arch Dermatol*. (2007) 143:479–84. doi: 10.1001/archderm.143.4.479

Conflict of Interest: The authors declare that the research was conducted in the absence of any commercial or financial relationships that could be construed as a potential conflict of interest.

frontiers in Medicine

ORIGINAL RESEARCH
published: 11 January 2021
doi: 10.3389/fmed.2020.609404

The Differential Diagnosis of Hypopigmented Mycosis Fungoides and Vitiligo With Reflectance Confocal Microscopy: A Preliminary Study

Huaxu Liu[1], *Leilei Wang*[2], *Yan Lin*[1], *Xiaofeng Shan*[1] *and Min Gao*[2]*

[1] *Shandong Provincial Institute of Dermatology and Venereology, Shandong First Medical University & Shandong Academy of Medical Sciences, Jinan, China,* [2] *Shandong Cancer Hospital and Institute, Shandong First Medical University & Shandong Academy of Medical Sciences, Jinan, China*

Objective: To investigate the role of reflectance confocal microscopy (RCM) in the differential diagnosis of hypopigmented mycosis fungoides (HMF) and vitiligo.

Methods: Cases with persistent hypopigmented patches, suspicious of early stage vitiligo, or HMF were imaged with RCM. The melanin contents and inflammatory conditions of the epidermis and superficial dermis of the lesions were compared with the same layers of the adjacent skin, and then, the imaged lesions were biopsied and analyzed by histology.

Results: 15 cases were enrolled in this study, and based on the RCM findings, there was just slight or moderate reduction of melanin but no melanin absence in the basal cell layer of HMF lesions. The finding of monomorphous weakly refractile, oval to round cells on the basis of vesicle-like dark space was clearly elucidated in the epidermis of the lesions by RCM, which indicates the Pautrier's microabscesses on histopathology. Among those 15 cases, 13 cases were identified as HMF, and the other two cases were vitiligo, based on RCM findings, which were confirmed by histology analysis.

Conclusions: The RCM findings correlated well with histology results in the screening of HMF, which indicates the RCM is an important tool in the early detection and differential diagnosis of HMF.

Keywords: imaging, reflectance confocal microscopy (RCM), detection, vitiligo, hypo-pigmented mycosis fungoides, differential daignosis

OPEN ACCESS

Edited by:
Yong Cui,
China-Japan Friendship Hospital, China

Reviewed by:
Maria Contaldo,
University of Campania Luigi Vanvitelli, Italy
Salvador Gonzalez,
University of Alcalá, Spain

***Correspondence:**
Min Gao
gmlhx@163.com

Specialty section:
This article was submitted to Dermatology, a section of the journal Frontiers in Medicine

Received: *23 September 2020*
Accepted: *25 November 2020*
Published: *11 January 2021*

Citation:
Liu H, Wang L, Lin Y, Shan X and Gao M (2021) The Differential Diagnosis of Hypopigmented Mycosis Fungoides and Vitiligo With Reflectance Confocal Microscopy: A Preliminary Study. Front. Med. 7:609404. doi: 10.3389/fmed.2020.609404

INTRODUCTION

Mycosis fungoides (MF), the most common primary cutaneous T-cell lymphoma, is a neoplastic disease characterized by classical non-infiltrated lesions (patches), plaques, tumors, and erythrodermic stages (1). Several distinct clinical forms of MF have been described, among which, the granulomatous, pustular, purpuric, hyperkeratotic and verrucous, bullous, invisible, and hypopigmented variants of the disease were included (1). The hypopigmented mycosis fungoides (HMF) was first described by (2, 3). It is an atypical and often misdiagnosed

variant of MF characterized by persistent hypopigmented-to-achromic patches, with a vitiligo-like aspect, which is mainly distributed on the trunk and proximal portions of the extremities (1, 3). Unlike conventional MF, which is regarded as a disease most commonly found in the fifth to sixth decades of life, HMF most commonly affects the pediatric population, especially in Asians (1, 3). Clinically, the diagnosis of HMF is commonly delayed, which may have a potential negative effect on the treatment and prognosis because it is rare, and it may resemble early vitiligo and other hypopigmentary skin disorders (4–6).

Reflectance confocal microscopy (RCM) is a non-invasive imaging technique that provides high-resolution cellular imaging of the epidermis and superficial dermis (7), which has been used in the diagnosis and differential diagnosis of skin tumors and inflammatory diseases for more than two decades with high sensitivity and specificity (8). Agero et al. (9) first investigated the characteristics of MF in the imaging of RCM. The Pautrier's microabscesses in epidermis on histopathology correlated with the vesicle-like dark space filled with collections of monomorphous weakly refractile oval to round cells in epidermis on the RCM images. Other studies (10) verified the correlation of RCM image and histology analysis in the diagnosis of MF.

In this study, we aimed to investigate the role of RCM in the early detection and differential diagnosis of HMF.

MATERIALS AND METHODS

The study was approved by the Ethics Committee of Shandong Provincial Institute of Dermatology and Venereology. The cases with persistent round-to-oval hypopigmentation with mild scales or not, which distributed on the trunk, arms, and legs, wood lamp examination (±) and clinically suspicious of HMF and early vitiligo, were enrolled in the study. Cases with comparatively typical vitiligo lesions were not included in the study.

After written informed consent obtained and the related history recorded, the clinical pictures were taken and the hypopigmentary lesions and adjacent normal skin were imaged with RCM. *In-vivo* RCM imaging was performed with a commercially available, near-infrared, reflectance mode confocal microscope (Vivascope 1500; Lucid Inc., Rochester, NY, USA). A detailed description of the technique and the device used has been published previously (7, 8). At least three areas of hypopigmented lesions were imaged for each case to compare the changes with the perilesional normal skin. The single (0.5*0.5 mm) or mosaic RCM images (2*2 mm, or 3*3 mm) were captured or saved. Then one of the lesions imaged were suggested to be biopsied and analyzed histologically. The excisions were fixed in formalin and embedded in paraffin. After routine processing, slides were stained with hematoxylin and eosin (H–E) and further stained with immune-chemistry methods to detect the changes of CD4 and CD8 molecules.

Based on the previous studies, the RCM features of the lesions were analyzed layer by layer and correlated to the findings of histology analysis.

RESULTS

In total, 15 cases with RCM and histology results were enrolled in the study. Among those enrolled 15 cases, 13 cases were

TABLE 1 | The details of the included cases.

Case	Age	Sex	Main distribution	Duration of evolution (month)	Previous tretments	RCM findings	Pathology findings
1	15	M	Trunk and legs	36	Topical steroids	+	+
2	20	F	Trunk and legs	40	none	+	+
3	14	F	Trunk, arms, and legs	32	Topical steroids	+	+
4	31	F	Trunk and legs	72	none	+	+
5	21	F	Trunk and arms	24	Topical steroids	+	+
6	15	M	Trunk, arms, and legs	12	Topical steroids	+	+
7	22	F	Trunk, arms, and legs	26	Topical steroids	+	+
8	21	M	Trunk, arms, and legs	31	Topical steroids	+	+
9	19	F	Trunk, arms, and legs	37	Topical steroids	+	+
10	17	F	Trunk and legs	16	Topical steroids	+	+
11	18	F	Trunk, arms, and legs	22	Topical steroids	+	+
12	20	M	Trunk and arms	28	Topical steroids	+	+
13	19	F	Trunk, arms, and legs	20	none	+	+
14	16	M	Trunk	5	Topical steroids	Absence of melanin	vitiligo
15	20	F	Trunk	3	Topical steroids	Absence of melanin	vitiligo
Mean	19.2			26.9			

(1) The lesions were mainly located on the trunk and limbs. (2) The duration of evolution was calculated from the early onset of hypopigmented patches, according to the patients' medical histories. (3) The RCM findings was the slight melanin reduction, but not melanin absence in the basal cell layer, and the monomorphous weakly refractile, oval-to-round cells in epidermis and weakly refractive cells with a round-to-oval cellular contour scattered within the papillary dermis or inside dermal papillae rings were the positive findings (+). (4) The histology and immunochemistry findings to confirm those RCM features and diagnosed as HMF was the "+" in the table.

diagnosed as HMF, while two cases as vitiligo, based on our RCM examination, and was demonstrated by histology results, which showed the excellent correlation between RCM and histology findings.

Five of the 15 cases were male, 10 were female, and the average age of the 15 cases was 19.2. The average duration of evolution of the lesions was 26.9 months. The details of the enrolled cases are listed in **Table 1**. Clinically, the persistent, round-to-oval hypopigmentation with mild scales or not were distributed on the trunk, arms, and legs (**Figures 1a–c**).

When the normal skin was imaged with RCM, there were no significant inflammatory condition changes in honeycomb pattern stratum spinosum (**Figure 2a**) and no melanin changes in basal cell layer (**Figure 2b**). While for the lesions of vitiligo, the significant reduction of melanin contents or melanin absence was observed (**Figure 2c**) compared with the adjacent normal skin, and sometimes the slight infiltration of phagocytes and inflammatory cells in the superficial dermis was also recorded. The histology picture (**Figure 2d**) demonstrated the RCM findings.

The HMF lesions showed different changes based on the RCM imaging, as there was only slight reduction of melanin contents but no melanin absence in the basal cell layer. And the other significant changes were founded in stratum spinosum. The finding of monomorphous weakly refractile, oval-to-round cells on the basis of vesicle-like dark space was clearly elucidated in epidermis of the lesions by RCM (**Figures 3a,b**), which indicates the Pautrier's microabscesses on histopathology (**Figure 3c**). And weakly reflective cells with a round-to-oval cellular contour scattered within the papillary dermis or inside dermal papillae rings in the lesions were also observed. Immunohistochemistry analysis (**Figure 3d**) demonstrated the HMF was characterized by CD8+ T cells residing predominantly in the dermal papillae. Thirteen cases with these findings by RCM were confirmed by pathology results.

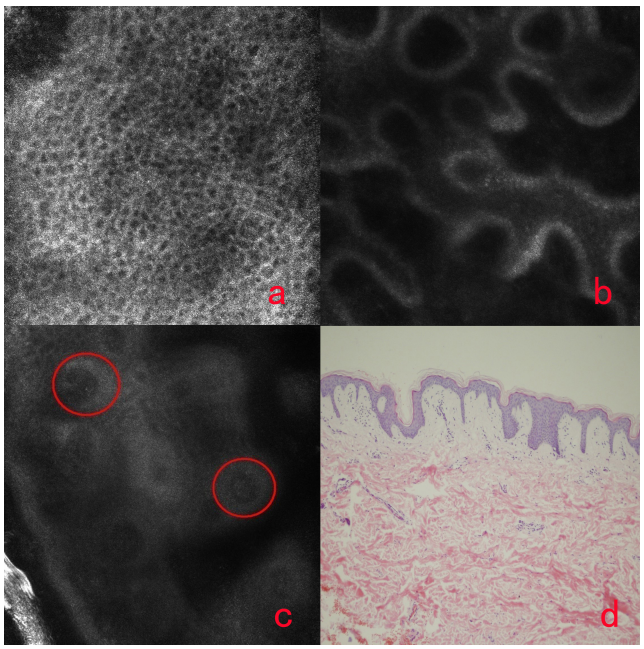

FIGURE 2 | The honeycomb pattern of stratum spinosum **(a)**, the normal basal cell layer, the dermal-epidermal junction of vitiligo **(c)** and the histology of vitiligo. There was no inflammation in the regular arranged honeycomb pattern of stratum spinosum **(a)**. There was no melanin reduction in the basal cell layer of normal DEJ **(b)**. The significant reduction or melanin absence (circles) in the basal cell layer of DEJ of vitiligo **(c)**. There is no melanin in basal cell layer of vitiligo **(d)**.

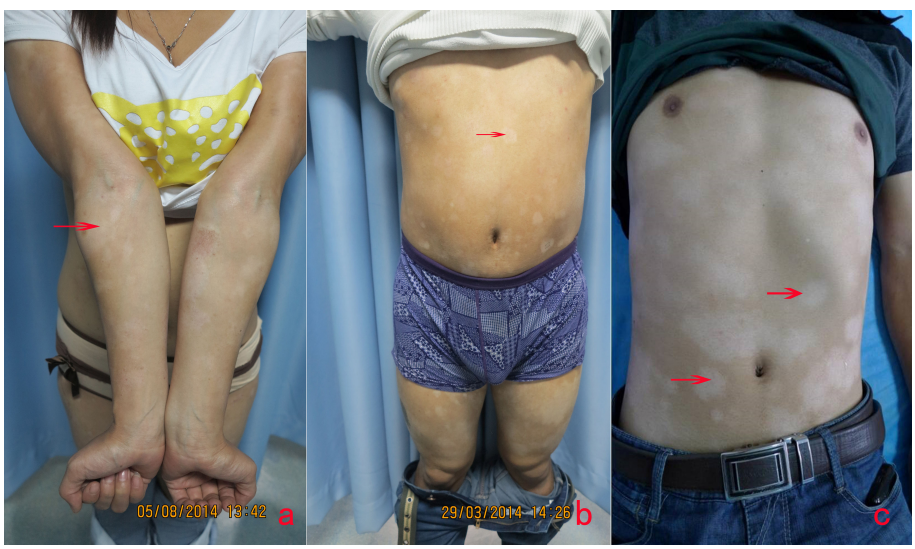

FIGURE 1 | The clinical image of three cases of HMF. An 18-year old woman with the hypopigmented patches for 2 years on arms **(a)** and legs, and a 25-year-old **(b)** and 19-year-old man **(c)**, with generalized lesions on bodies and limbs. The hypopigmentary patches were 2–5 cm in diameter, slightly scaly, with no infiltration (arrows).

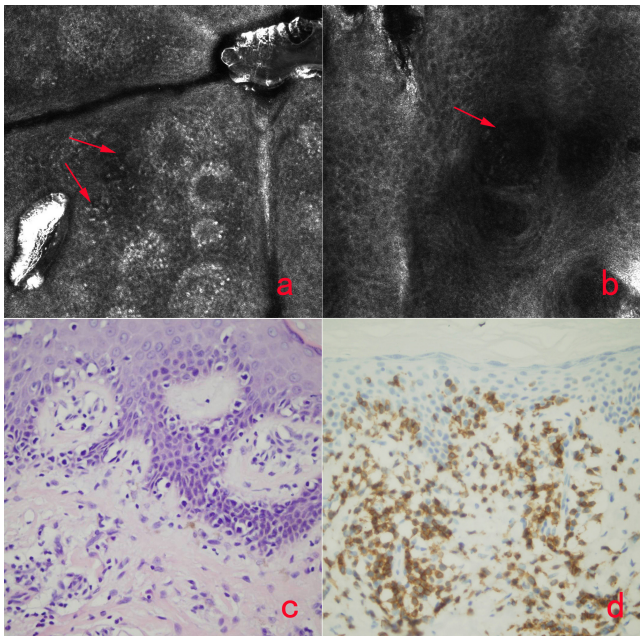

FIGURE 3 | The RCM image of HMF **(a,b)**, the histology of HMF **(c)** and immunochemistry-stained image of HMF **(d)**. The monomorphous weakly refractile, oval-to-round cells (**a,b**, arrows) on the basis of vesicle-like dark spaces were clearly elucidated in epidermis of the lesions by RCM, which indicates the Pautrier's microabscesses on histopathology **(c)**. Immunohistochemical analysis **(d)** demonstrated the HMF was characterized by CD8+ T cells residing predominantly in the dermal papillae.

DISCUSSION

RCM imaging non-invasively shows nuclear and cellular-level morphology in human skin *in vivo* (11, 12). Imaging is based on the detection of single back-scattered photons from the optical section, and contrast is due to the relative variations in refractive indices and sizes of organelles and microstructures (11). Melanin is the natural and strongest contrast in the skin (11, 12), which indicates the significant role of RCM in the imaging of pigmented skin disorders. The cellular changes of the lesion in epidermis and superficial dermis could be imaged and compared with that of the adjacent normal skin. Ardigo et al. (13) first reported the characteristics of vitiligo in confocal images, and other related reports (14) revealed RCM is useful in the diagnosis and differential diagnosis of vitiligo and other hypopigmentary skin disorders. As previously mentioned, RCM has also been reported to be used in the screening of MF and showed relatively specific characteristics in confocal images (9, 10, 15, 16). The migration of abnormal inflammatory cells in the epidermis, the disorder of the basal cell layer, and infiltration of mononuclear inflammatory cells in superficial dermis of MF lesions could be imaged with RCM (15).

The pathology features of HMF are similar to MF. And the histology changes of HMF and vitiligo were located in epidermis and superficial dermis,which was within the penetration depth of RCM.

Our study revealed the melanin contents in the basal cell layer is different based on the RCM findings. Significant melanin reduction or melanin absence was found in vitiligo, while there was a slight reduction of melanin but not melanin loss in HMF. As reported previously, hypopigmentation of HMF may arise from a defect in the transfer of melanosomes from melanocytes to keratinocytes, with reversal of this defect after treatment (4). On the contrary, the significant reduction or total absence of melonosome and melanocytes is the characteristic in the vitiligo lesion (6). The other difference was focused on the stratum spinosum and superficial dermis. The finding of monomorphous weakly refractile, oval-to-round cells on the basis of vesicle-like dark space was regarded as the features of HMF by RCM, while commonly there were no changes in this layer in vitiligo. And weakly refractive cells with a round-to-oval cellular contour scattered within the papillary dermis or inside dermal papillae rings in HMF were also different with that of vitiligo because these changes were the characteristics of HMF in histology level. RCM and histology results had excellent correlation.

Our study highly indicated the role of RCM in the early detection and differential diagnosis of HMF and vitiligo. However, more cases with long time follow-up study were required to confirm our findings.

DATA AVAILABILITY STATEMENT

The original contributions presented in the study are included in the article/supplementary materials, further inquiries can be directed to the corresponding author.

ETHICS STATEMENT

The studies involving human participants were reviewed and approved by Ethics Committee of Shandong Provincial Institute of Dermatology and Venereology. Written informed consent to participate in this study was provided by the participants' legal guardian/next of kin. Written informed consent was obtained from the minor(s)' legal guardian/next of kin for the publication of any potentially identifiable images or data included in this article.

AUTHOR CONTRIBUTIONS

HL and MG designed the study and prepared the manuscript. YL and LW collected the clinical and RCM data. XS collected the histology data. All authors contributed to the article and approved the submitted version.

FUNDING

Supported by National Key Scientific Instruments and Equipment Development Program of China (2016YFF0101606), Project of Shandong Science and Technology Agency (2018GSF118030), and Project from Department of Health of Shandong Province (2018WSA18036).

REFERENCES

1. Jawed SI, Myskowski PL, Horwitz S, Moskowitz A, Querfeld C. Primary cutaneous T-cell lymphoma (mycosis fungoides and Sézary syndrome): part I. Diagnosis: clinical and histopathologic features and new molecular and biologic markers. *J Am Acad Dermatol*. (2014) 70:205. doi: 10.1016/j.jaad.201307049
2. Ryan EA, Sanderson KV, Bartak P, Samman PD. Can mycosis fungoides begin in the epidermis? A hypothesis. *Br J Dermatol*. (1973) 88:419–29. doi: 10.1111/j.1365-2133.1973.tb15444.x
3. Muñoz-González H, Molina-Ruiz AM, Requena L. Clinicopathologic variants of mycosis fungoides. *Actas Dermosifiliogr*. (2017) 108:192–208. doi: 10.1016/j.adengl.201702010
4. Furlan FC, Sanches JA. Hypopigmented mycosis fungoides: a review of its clinical features and pathophysiology. *An Bras Dermatol*. (2013) 88:954–60. doi: 10.1590/abd1806-484120132336
5. Ardigó M, Borroni G, Muscardin L, Kerl H, Cerroni L. Hypopigmented mycosis fungoides in Caucasian patients: a clinicopathologic study of 7 cases. *J Am Acad Dermatol*. (2003) 49:264–70. doi: 10.1067/S0190-9622(03)00907-1
6. El-Darouti MA, Marzouk SA, Azzam O, Fawzi MM, Abdel-Halim MR, Zayed AA, et al. Vitiligo vs. hypopigmented mycosis fungoides (histopathological and immunohistochemical study, univariate analysis). *Eur J Dermatol*. (2006) 16:17–22.
7. Liu H, Lin Y, Nie X, Chen S, Chen X, Shi B, et al. Histological classification of melasma with reflectance confocal microscopy: a pilot study in Chinese patients. *Skin Res Technol*. (2011) 17:398–403. doi: 10.1111/j.1600-0846.201100517x
8. Rajadhyaksha M, Marghoob A, Rossi A, Halpern AC, Nehal KS. Reflectance confocal microscopy of skin *in vivo*: from bench to bedside. *Lasers Surg Med*. (2017) 49:7–19. doi: 10.1002/lsm22600
9. Agero AL, Gill M, Ardigo M, Myskowski P, Halpern AC., González S. *In vivo* reflectance confocal microscopy of mycosis fungoides: a preliminary study. *J Am Acad Dermatol*. (2007) 57:435–41. doi: 10.1016/j.jaad.200702026
10. Mancebo SE, Cordova M, Myskowski PL, Flores ES, Busam K, Jawed SI., et al. Reflectance confocal microscopy features of mycosis fungoides and Sézary syndrome: correlation with histopathologic and T-cell receptor rearrangement studies. *J Cutan Pathol*. (2016) 43:505–15. doi: 10.1111/cup12708
11. Rajadhyaksha M, Grossman M, Esterowitz D, Webb RH, Anderson RR. *In vivo* confocal scanning laser microscopy of human skin: melanin provides strong contrast. *J Invest Dermatol*. (1995) 104:946–52. doi: 10.1111/1523-1747ep12606215
12. Rajadhyaksha M, González S, Zavislan JM, Anderson RR, Webb RH. *In vivo* confocal scanning laser microscopy of human skin II: advances in instrumentation and comparison with histology. *J Invest Dermatol*. (1999) 113:293–303. doi: 10.1046/j.1523-1747.199900690x
13. Ardigo M, Malizewsky I., Dell'anna ML, Berardesca E, Picardo M. Preliminary evaluation of vitiligo using *in vivo* reflectance confocal microscopy. *J Eur Acad Dermatol Venereol*. (2007) 21:1344–50. doi: 10.1111/j.1468-3083.200702275x
14. Lai LG, Xu AE. *In vivo* reflectance confocal microscopy imaging of vitiligo, nevus depigmentosus and nevus anemicus. *Skin Res Technol*. (2011) 17:404–10. doi: 10.1111/j.1600-0846.201100521x
15. Zhu M, Yu W, Wang P, Liu J, Li Z, Dai H, et al. Reflectance confocal microscopy may be included as part of the diagnostic algorithm of early-stage mycosis fungoides. *Skin Res Technol*. (2020) 26:591–598. doi: 10.1111/srt12840
16. Melhoranse Gouveia B, Wells J, Kim J, Consuegra G, Longo C, Fernandez-Penas P. Systematic review and proposal of an *in vivo* reflectance confocal microscopy assessment tool for cutaneous lymphoma. *J Cutan Pathol*. (2020) 47:295–304. doi: 10.1111/cup13598

Conflict of Interest: The authors declare that the research was conducted in the absence of any commercial or financial relationships that could be construed as a potential conflict of interest.

frontiers in Medicine

CASE REPORT
published: 21 January 2021
doi: 10.3389/fmed.2020.619907

Case Report: Diagnosis of Primary Cutaneous Amyloidosis Using Dermoscopy and Reflectance Confocal Microscopy

Xiuli Wang[1,2,3], *Hui Wang*[1,2,3], *Zhenyu Zhong*[1,2,3], *Liyun Zheng*[1,2,3], *Yifan Wang*[1,2,3], *Ze Guo*[1,2,3], *Hui Li*[1,2,3] *and Min Gao*[1,2,3]*

[1] *Department of Dermatology, The First Affiliated Hospital of Anhui Medical University, Hefei, China,* [2] *Key Laboratory of Dermatology (Anhui Medical University), Ministry of Education, Hefei, China,* [3] *Inflammation and Immune Mediated Diseases Laboratory of Anhui Province, Hefei, China*

The dermoscopy and reflectance confocal microscopy (RCM) can provide new insights for diagnosis disease as non-invasive and easy-to-use tool. We described the dermoscopy and RCM characteristics of two patients with primary cutaneous amyloidosis (PCA) respectively. The dermoscopy characteristics were as follows: brownish macules with brown or white centers surrounded by hyperpigmented blotches, and a whitish scar-like center encircled by irregular brownish hyperpigmented spots or patches. The RCM features were increased melanin deposition in the basal layer, highly refractive structures with various shapes in the enlarged papillary dermis, and the increased pleomorphic structure of the dermal papillary ring. This is the first report the dermoscopy and RCM characteristics of PCA. We hope the characteristic dermoscopy and RCM appearances would provide a basis for doctors to diagnose and intervene earlier.

Keywords: primary cutaneous amyloidosis, dermoscopy, reflectance confocal microscopy, non-invasive technique, diagnosis

OPEN ACCESS

Edited by:
Yong Cui,
China-Japan Friendship Hospital, China

Reviewed by:
Salvador Gonzalez,
University of Alcalá, Spain
ZhiQiang Yin,
Nanjing Medical University, China
Huaxu Liu,
Shandong Provincial Hospital of Dermatology, China

***Correspondence:**
Min Gao
ahhngm@126.com

Specialty section:
This article was submitted to Dermatology, a section of the journal Frontiers in Medicine

Received: *21 October 2020*
Accepted: *30 December 2020*
Published: *21 January 2021*

Citation:
Wang X, Wang H, Zhong Z, Zheng L, Wang Y, Guo Z, Li H and Gao M (2021) Case Report: Diagnosis of Primary Cutaneous Amyloidosis Using Dermoscopy and Reflectance Confocal Microscopy. Front. Med. 7:619907. doi: 10.3389/fmed.2020.619907

INTRODUCTION

Primary cutaneous amyloidosis (PCA) is a relatively common disease, but it can cause physical and psychological distress due to itch and potentially disfiguring disorder. There are different subtypes of PCA, including macular amyloidosis, lichen amyloidosis, nodular amyloidosis, or a mixed appearance of macular amyloidosis and lichen amyloidosis, which is described as biphasic amyloidosis (1, 2). We observed two patients with PCA through dermoscopy and reflectance confocal microscopy (RCM). One of them was confirmed by histopathological examination, and the lesions presented as biphasic amyloidosis. Another patient was clinically diagnosed as macular amyloidosis.

Dermoscopy has been proved to be an important noninvasive technique to diagnose cutaneous pigmented diseases, which can magnify the pigmented structures of the epidermis, the dermo-epidermal junction, and the dermis (3, 4). RCM is a valuable, widely used tool for its noninvasive, dynamic real-time and high cellular resolution characteristic (5). These two tools are particularly suitable for disease screening before the histopathological examination, which may avoid some surgical operation.

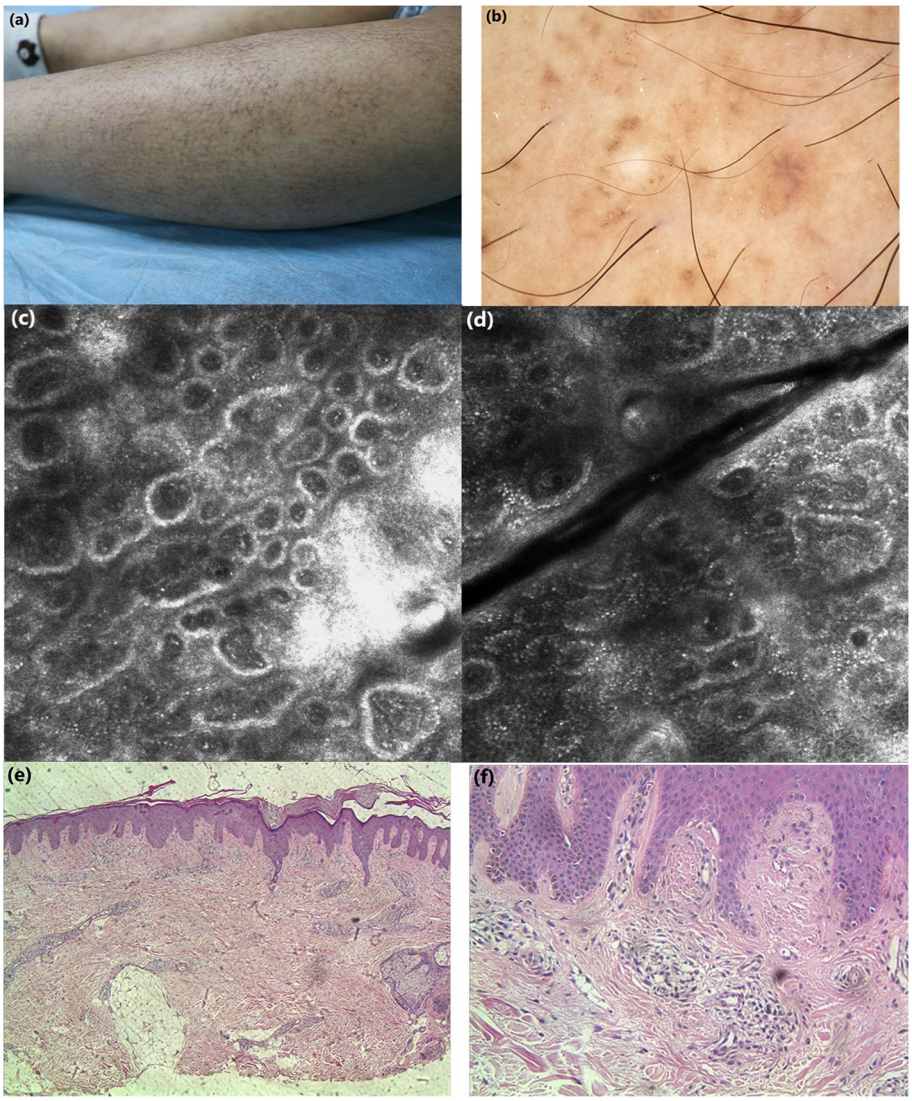

FIGURE 1 | (a) Clinical features: macular hyperpigmentation in a rippling pattern and hyperkeratotic brownish papules. **(b)** Under dermoscopic: irregular brownish macules with brown centers surrounded by hyperpigmented blotches, whitish scar-like center encircled by brownish hyperpigmented patches. **(c,d)** Under RCM: hyperkeratosis, melanin deposition in the basal layer, highly refractive structures inside the enlarged papillary dermis in cloud-like agglomerate shape, some round moderately-highly bright round cells in dermis. **(e, f)** Histopathology: hyperkeratosis in the epidermis, increased melanin deposition in the basal layer, focal deposition of homogeneous acidophilic substance in dermal papilla (H&E stain).

CASE REPORT

Case 1: A 25-years-old woman presented with hyperpigmented macules and maculopapular rash on her lower limbs for 4 years. The lesions were located mainly in the lower legs, which progressed slowly to the thighs and arms, with moderate pruritus. On physical examination, macular hyperpigmentation in a rippling pattern were observed over her limbs, and hyperkeratotic brownish papules in some areas. The patient was otherwise well, with no other skin symptoms or extracutaneous discomfort. The initial clinical diagnosis was consistent with PCA changes, which was more in line with biphasic amyloidosis (because the lesions had both the characteristics of macular amyloidosis and lichen amyloidosus) (**Figure 1a**). Case 2: A 65-years-old woman presented with a 10-year history of tan macules and papules on her back, with a medical history of cardiac disease. The lesions were persistent itching, without other skin discomfort. Physical examination revealed brownish macules fused in a grid pattern. We diagnosed it as macular amyloidosis (**Figure 2a**).

Case 1: Under dermoscopy, the appearance of some smaller brownish macules presented as irregular brown centers

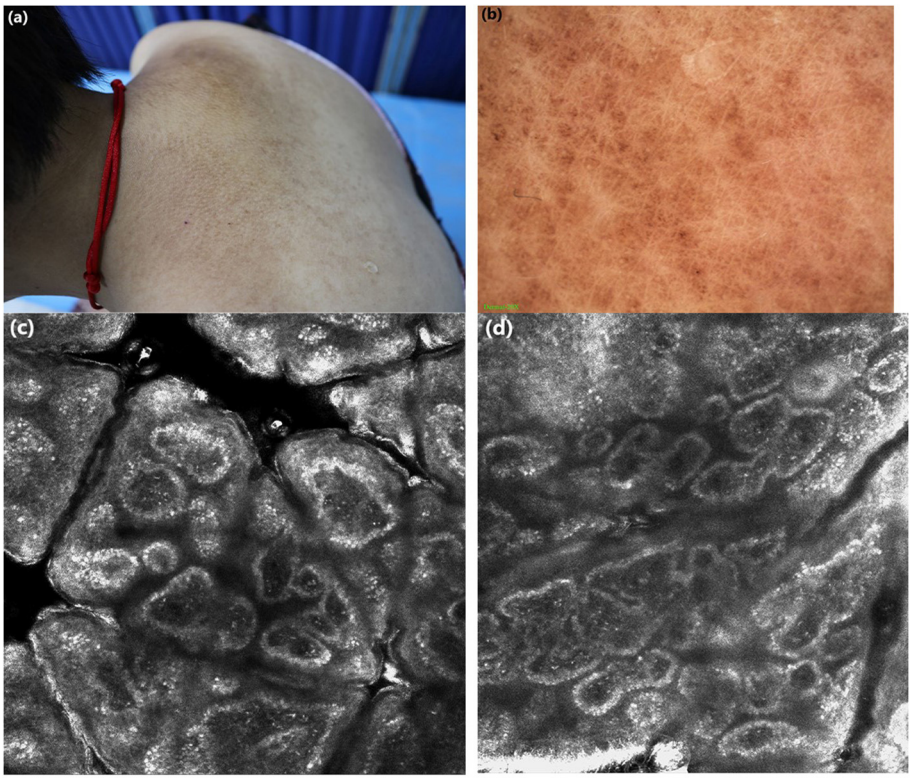

FIGURE 2 | (a) Clinical features: brownish macules fused in a grid pattern. **(b)** Under dermoscopic: white center encircled by hyperpigmented blotches, other pigmented patches were partially fused. **(c,d)** Under RCM: highly refractive structures with various shapes (cloud-like agglomerate, dotted substance, coliform substance) gathered in the enlarged papillary dermis, the increased pleomorphic structure of the dermal papillary ring.

with small brown stripes, surrounded by hyperpigmented blotches, while other macules showed irregular inhomogeneous hyperpigmented blotches. The dermoscopic features of hyperkeratotic brownish papules displayed a whitish scar-like center encircled by irregular brownish hyperpigmented spots or patches (**Figure 1b**). Case 2: On dermoscopic examination, the macula lesions showed white center encircled by hyperpigmented blotches, while other pigmented patches were partially fused (**Figure 2b**).

Case 1: Upon RCM, the examination displayed the hyperkeratosis in the epidermis, the increased melanin deposition in the basal layer, the highly refractive structures with cloud-like agglomerate, and dotted substance inside papillary dermis. Part of the dermal papillary rims were obscured, surrounded by some round, moderately-highly bright round cells (**Figures 1c,d**). Case 2: Under RCM, the appearance of PCA were the highly refractive structures with various shapes (cloud-like agglomerate, dotted substance, coliform substance, and so on) gathered in the enlarged papillary dermis, and the increased pleomorphic structure of the dermal papilla ring (**Figures 2c,d**).

Histopathological examination of case 1 showed hyperkeratosis in the epidermis, epidermal hyperplasia, downward extended of part of the epidermis, increased melanin deposition in the basal layer, and focal deposition of homogeneous acidophilic substance in the enlarged dermal papilla (**Figures 1e,f**).

CONCLUSION

We presented two patient with PCA, and to our knowledge, this is the first report the dermoscopy and RCM characteristics of PCA. The dermoscopic findings of macular amyloidosis often showed a common feature, that is a white or brown central hub surrounded by brownish pigmentation (6). Besides, a white central hub or whitish scar-like center surrounded by pigmentation were often presented in the lichen amyloidosis (6). The RCM features of PCA have not been adequately described in the literature. Only two articles have been published to report the RCM features of PCA (7, 8). Upon RCM, the characteristics of increased melanin in the basal cell layer, cloud-like agglomerate in the dermal papilla, and melanophage infiltrating in the layer of superficial dermis, which were corresponding to histopathological findings: basal hyper pigmentation, amyloid deposition, pigment incontinence (8).

PCA is usually diagnosed clinically. But for cases with atypical presentation, the noninvasive technique, dermoscopy combined with RCM, can be used as a reference for clinicians to diagnose PCA. On our observation, the dermoscopy features

were brownish macules with brown or white centers surrounded by hyperpigmented blotches, and a whitish scar-like center encircled by irregular brownish hyperpigmented spots or patches. The RCM features were increased melanin deposition in the basal layer, highly refractive structures with various shapes (cloud-like agglomerate, dotted substance, coliform substance and so on) in the enlarged papillary dermis, and the increased pleomorphic structure of the dermal papilla. We hope the characteristic dermoscopy and RCM appearances would provide a basis for doctors to diagnose and intervene earlier.

DATA AVAILABILITY STATEMENT

The original contributions presented in the study are included in the article/supplementary material, further inquiries can be directed to the corresponding author/s.

ETHICS STATEMENT

The studies involving human participants were reviewed and approved by Ethical Review Committee of Anhui Medical University. The patients/participants provided their written informed consent to participate in this study. Written informed consent was obtained from the individual(s) for the publication of any potentially identifiable images or data included in this article.

AUTHOR CONTRIBUTIONS

All authors listed have made a substantial, direct and intellectual contribution to the work, and approved it for publication.

REFERENCES

1. Fernandez-Flores A. Cutaneous amyloidosis: a concept review. *Am J Dermatopathol*. (2012) 34:1–14. doi: 10.1097/DAD.0b013e31823465c7
2. Brownstein MH, Hashimoto K, Greenwald G. Biphasic amyloidosis: link between macular and lichenoid forms. *Br J Dermatol*. (1973) 88:25–9. doi: 10.1111/j.1365-2133.1973.tb06667.x
3. Bakos RM, Blumetti TP, Roldan-Marin R, Slareni G. Non-invasive imaging tools in the diagnosis and treatment of skin cancers. *Am J Clin Dermatol*. (2018) 19(Suppl.1):3–14. doi: 10.1007/s40257-018-0367-4
4. Argenziano G, Soyer HP. Dermoscopy of pigmented skin lesions – a valuable tool for early. *Lancet Oncol*. (2001) 2:443–9. doi: 10.1016/S1470-2045(00)00422-8
5. Scope A, Benvenuto-Andrade C, Agero AL, Malvehy J, Puig S, Rajadhyaksha M, et al. *In vivo* reflectance confocal microscopy imaging of melanocytic skin lesions: consensus terminology glossary and illustrative images. *J Am Acad Dermatol*. (2007) 57:644–58. doi: 10.1016/j.jaad.2007.05.044
6. Chuang YY, Lee DD, Lin CS, Chang YJ, Tanaka M, Chang YT, et al. Characteristic dermoscopic features of primary cutaneous amyloidosis: a study of 35 cases. *Br J Dermatol*. (2012) 167:548–54. doi: 10.1111/j.1365-2133.2012.11066.x
7. Ionescu A-M, Ilie M-A, Chitu V, Razvan A, Lixandru D, Tanase C, et al. *In vivo* diagnosis of primary cutaneous amyloidosis -the role of reflectance confocal microscopy. *Diagnostics*. (2019) 9:66. doi: 10.3390/diagnostics9030066
8. Lei W, Ai EX. Reflectance confocal microscopy for the characterization of primary cutaneous amyloidosis: a pilot study. *Skin Res Technol*. (2017) 23:441–3. doi: 10.1111/srt.12343

Conflict of Interest: The authors declare that the research was conducted in the absence of any commercial or financial relationships that could be construed as a potential conflict of interest.

frontiers in Medicine

PERSPECTIVE
published: 10 February 2021
doi: 10.3389/fmed.2020.619787

The Role of DICOM in Artificial Intelligence for Skin Disease

Liam J. Caffery[1,2*], *Veronica Rotemberg*[3], *Jochen Weber*[3], *H. Peter Soyer*[2,4], *Josep Malvehy*[5] *and David Clunie*[6]

[1] Centre for Online, Centre for Health Services Research, The University of Queensland, Brisbane, QLD, Australia, [2] Dermatology Research Centre, The University of Queensland Diamantina Institute, The University of Queensland, Brisbane, QLD, Australia, [3] Dermatology Service, Department of Medicine, Memorial Sloan Kettering Cancer Center, New York, NY, United States, [4] Department of Dermatology, Princess Alexandra Hospital, Brisbane, QLD, Australia, [5] Department of Dermatology, Institut d'Investigacions Biomèdiques August Pi i Sunyer, Hospital Clinic of Barcelona, University of Barcelona, Barcelona, Spain, [6] PixelMed Publishing, Bangor, PA, United States

There is optimism that artificial intelligence (AI) will result in positive clinical outcomes, which is driving research and investment in the use of AI for skin disease. At present, AI for skin disease is embedded in research and development and not practiced widely in clinical dermatology. Clinical dermatology is also undergoing a technological transformation in terms of the development and adoption of standards that optimizes the quality use of imaging. Digital Imaging and Communications in Medicine (DICOM) is the international standard for medical imaging. DICOM is a continually evolving standard. There is considerable effort being invested in developing dermatology-specific extensions to the DICOM standard. The ability to encode relevant metadata and afford interoperability with the digital health ecosystem (e.g., image repositories, electronic medical records) has driven the initial impetus in the adoption of DICOM for dermatology. DICOM has a dedicated working group whose role is to develop a mechanism to support AI workflows and encode AI artifacts. DICOM can improve AI workflows by encoding derived objects (e.g., secondary images, visual explainability maps, AI algorithm output) and the efficient curation of multi-institutional datasets for machine learning training, testing, and validation. This can be achieved using DICOM mechanisms such as standardized image formats and metadata, metadata-based image retrieval, and de-identification protocols. DICOM can address several important technological and workflow challenges for the implementation of AI. However, many other technological, ethical, regulatory, medicolegal, and workforce barriers will need to be addressed before DICOM and AI can be used effectively in dermatology.

Keywords: dermatology, artificial intelligence, DICOM, standards, imaging

OPEN ACCESS

Edited by:
Ivan V. Litvinov,
McGill University, Canada

Reviewed by:
Luís Bastião Silva,
BMD Software, Portugal
Piergiacomo Calzavara-pinton,
University of Brescia, Italy
Carlos Costa,
University of Aveiro, Portugal

***Correspondence:**
Liam J. Caffery
l.caffery@uq.edu.au

Specialty section:
This article was submitted to Dermatology, a section of the journal Frontiers in Medicine

Received: *21 October 2020*
Accepted: *31 December 2020*
Published: *10 February 2021*

Citation:
Caffery LJ, Rotemberg V, Weber J, Soyer HP, Malvehy J and Clunie D (2021) The Role of DICOM in Artificial Intelligence for Skin Disease. Front. Med. 7:619787. doi: 10.3389/fmed.2020.619787

INTRODUCTION

The Digital Imaging and Communications in Medicine (DICOM) standard (1) is a comprehensive, international standard for medical imaging. DICOM defines a standard medical image file format and a metadata model and network services for the storage, transmission, and query and retrieval of objects. DICOM has also specified other network services to improve the efficiency of medical imaging workflows.

The most common DICOM data object is an image file. A DICOM image file consists of metadata and the pixel data of the image melded into a single file. The pixel data may be encoded using the Joint Photographic Expert Group format or other standard compression methods. The metadata model is standardized by object type, meaning there are different metadata models for, say, a magnetic resonance image, and a photographic image. The metadata model is described in an Information Object Definition (IOD). An IOD consists of an amalgamation of modules, where each module is a collection of patient, study, equipment, and image metadata attributes.

Although DICOM is ubiquitous in some medical image-producing specialties (e.g., radiology, cardiology, and radiation therapy), to date, the use of DICOM for dermatological imaging has been limited. There is, however, a growing realization that the adoption of DICOM for dermatological imaging is advantageous compared with other methods of image management (2). Clinical imaging for dermatology can be encoded using the existing, visible light photography IOD. Dermatology-specific IODs for dermoscopy have been developed and included in the DICOM standard. Future work items proposal will be for total body photography and reflectance confocal microscopy (3).

One of the primary motivations for adopting DICOM for dermatology imaging has been interoperability with digital health ecosystems such as electronic medical records, picture archiving and communication systems (PACS), and enterprise imaging repositories. In addition to these interoperability benefits, DICOM adoption is also likely to facilitate the use of artificial intelligence (AI) in clinical dermatology.

The application of AI for dermatology most often uses an image as input into a machine learning algorithm and results in the algorithm outputting a diagnostic or risk prediction of a disease condition. This use of AI is a form of image classification, and convolutional neural networks (CNNs) are becoming the most promising of AI algorithms for dermatology image classification (4). Melanoma diagnosis is a common application of dermatology image classifiers for which several reader studies have found that under experimental conditions, the diagnostic performance of AI can match that of an experienced dermatologist (5–7). Similar results have been reported for psoriasis (8) and onychomycosis (9).

DICOM is an evolving medical imaging standard with continual additions to the standard in the form of supplements and corrections. The increasing interest in AI image classifiers in medical imaging is, in turn, catalyzing the inclusion of AI-specific content in the DICOM standard. The DICOM Standards Committee has a dedicated AI working group (WG 23). The role of this working group is to develop a DICOM mechanism to support AI workflows and encode AI artifacts (10). This paper aims to discuss the role of DICOM in the AI in the context of dermatological imaging and review the current status of AI-specific content in the DICOM standard.

DERIVED OBJECTS

Preprocessing and post-processing of images for prediction analysis by machine learning create derived image objects such as resized or down-sampled images, segmentation images, visual explanation (e.g., saliency maps) images, and the algorithm's output. Research has shown that the output of an AI model influences the clinical decision of even experienced dermatologists (7, 11). Hence, derived objects should form part of the patient's medical record if AI is used in clinical practice to meet the health-care provider's regulatory and legal obligation to retain medical records. In addition to regulatory and legal requirements to store derived objects, there are also ethical aspects. The Joint European and North American Multi-society Statement on the Ethics of AI in radiology (12) recommended that the output of AI algorithms need to be stored in an auditable format to permit the investigation of errors and the monitoring over time to ensure there is no degradation of performance.

In practical terms, encoding the derived objects as DICOM objects with the appropriate identifying and descriptive metadata would allow them to be stored alongside the original image files in the health-care organization PACS or enterprise imaging repositories and visualized in conjunction with the clinical images.

Further, the use of DICOM is likely to improve image acquisition and image review workflows. AI has been shown to substantially reduce the amount of time radiologists spend on image review without compromising diagnostic accuracy (13–15). The same potential exists in dermatology, and the greatest efficiency gains are likely to be achieved for dermatologists reviewing total skin imaging studies. In hospitals, medical imaging infrastructure, including acquisition devices and image repositories, nearly all use DICOM as the underlying communication protocol. Speaking a common language can improve the efficiency of workflows, for example, automatic population of patient demographics at acquisition or the automated storage of images to an image repository. Implementing AI as a standalone product, as opposed to being integrated within the medical imaging ecosystems, may negate the diagnostic efficiencies afforded by using AI.

Original images often need to be resized to a fixed image size before inputting into a CNN. In some instances, we have seen dermoscopic images resized to a fixed resolution of 224 × 224 pixels (7). However, other datasets have reported using a fixed resolution of 448 × 448 pixels (16) or 1,024 × 1,024 pixels (17). Choosing the fixed resolution is a trade-off be computational efficiency and predictive accuracy (18). Therefore, storing the resized or down-sampled images can document the input into the CNN in an auditable and reproducible format.

Visual explanation maps assign each feature in an image a level of importance that the feature contributes to AI algorithm output. An example of two common visual explanation methods is Shapley additive explanation (SHAP) (19), and Gradient-Weighted Class Activation Mapping (Grad-CAM) (20). Examples of these visual explanations are shown in **Figures 1**, **2**. Visual explanation maps can be used by clinicians to help them understand how the AI algorithm came to its output and to assess

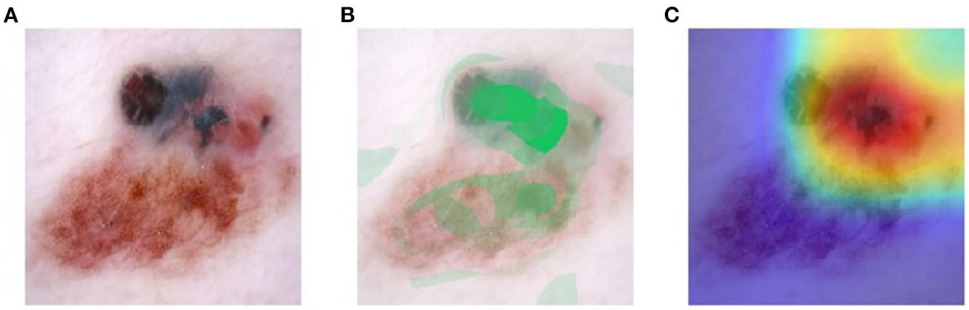

FIGURE 1 | Visual explanation images where AI algorithm correctly classified the skin lesion as melanoma **(A)** original image **(B)** SHAP visual explanation where green indicates the most important area of contribution to the AI result and red indicates the least important area; and **(C)** Grad-CAM visual explanation image where red is the most important area of contribution to AI result and blue is the least important part of the image to AI result. Image courtesy of Sally Shrapnel.

FIGURE 2 | Visual explanation images where the AI algorithm incorrectly classified the skin lesion as benign. Note the pigmented lesion was not considered an important feature by either SHAP or Grad-CAM. Image courtesy of Sally Shrapnel.

the quality of the output (21). Therefore, visual explanation maps can provide insight into potential sources of bias in AI algorithms (22). For example, if an AI algorithm predicted a high probability of melanoma but the visual explanation maps showed that the area of pigmentation in the lesion was not of high importance in determining this, then the clinician may be suspicious of the accuracy of the prediction (see **Figure 2**).

Resized or down-sampled images can be encoded as DICOM photographic or secondary capture objects. DICOM segmentation objects can be used to encode both binary and fractional segmentation images as multi-frame images. The multiple frames include the referenced image instance and segmentation image instances (**Figure 3**). Visual explanation images can be encoded as parametric map objects. A current proposal is to be able to link segmentation objects and parametric map objects to DICOM Structured Reports (SR) for the measurement objects (23). DICOM is also trialing the use of Javascript Object Notation (JSON) for encoding the output of AI algorithms (e.g., risk prediction of skin disease) in DICOM SR format (24). The goal of this trial is to harmonize with the machine learning community where JSON is the preferred format for algorithm output. Additionally, JSON encoding will achieve encoding of ground truth diagnosis that can be used to train, test, and validate future machine learning algorithms.

METADATA

The current use of CNNs for image classification has relied on image data as the only input. However, clinicians also rely on metadata as part of the diagnostic process (4). To emulate this, there have been several studies that have assessed the inclusion of metadata along with images as input into machine learning algorithms. One study found metadata resulted in a small improvement (1–2%) in sensitivity. Improvements were most noticeable in smaller, lower-performing models (25), which may indicate that the metadata compensates for fewer pixel data. A further study found the sensitivity and specificity improved from 82.1 to 95.2% and 86.1 to 91.0%, respectively (26). Both of these studies relied on simple metadata (age, sex, and lesion site). When lesion characteristics of bleeding, pain, and itchiness were added to age and the anatomical site as input, the accuracy of the algorithm improved by around 7% (27).

As previously noted, the DICOM file format (28) is an amalgamation of metadata with the pixel data of the image. The metadata is stored in the DICOM file header. The standardized metadata includes identifying and descriptive patient metadata (e.g., age, sex) and study metadata (e.g., lesion site). Most DICOM viewers allow the metadata encoded in the DICOM file header to be viewed in text format.

FIGURE 3 | Segmentation images **(a)** referenced instance **(b)** binary segmentation instance **(c)** fractional segmentation instance.

The DICOM supplement for dermoscopy has proposed the use of a skin cancer acquisition context. An acquisition context is a method of embedding descriptors of clinical metadata in the DICOM header using codes from standard lexicons [such as SNOMED CT (29)] for both concepts and values (30). The proposed skin cancer acquisition context includes rich clinical metadata such as a personal and familial history of melanoma, *in situ* melanoma, and other skin cancers; Fitzpatrick skin type; the degree of ultraviolet damage; atypical mole syndrome; and other relevant genetic conditions. Furthermore, the skin cancer acquisition context also includes lesion-level metadata such as history of growth, itch, erythema, and other relevant patient-observed changes. As DICOM is extensible, there is the ability to define acquisition contexts for different skin disease classes (e.g., inflammatory disease). There is the potential that using rich metadata stored in the acquisition context as an AI algorithm input will improve the performance of machine learning algorithms, perhaps more so than simple metadata. However, at this time it remains untested. The use of metadata is an area for further research, as it has been shown that not all metadata improve the performance of skin lesion image classifiers, and that selective metadata selection will likely be necessary (31).

DATASETS

One of the main limitations of deep learning is the input data used to train the system (32). AI models trained and validated from the same dataset risk overfitting, which is a phenomenon of "knowing the training data too well (33)." Overfitting results in the predictive output of an AI model only being reliable for the population on which the AI model was trained. To overcome this limitation, external validation or cross-validation is necessary and can be achieved by training the AI model on datasets amalgamated from multiple clinical sources, including different populations and ethnicities. Having images from these disparate sources in a standardized format facilitates the amalgamation of datasets and reduces the cost and effort of dataset curation. The lack of deployment of imaging and metadata standards in dermatology has inhibited the development of large image collections suitable for machine learning (34). DICOM is a universally recognized standard for medical imaging and would be ideal as a standardized image encoding to address this challenge.

The use of metadata-based retrieval (30), using queries based on DICOM metadata attributes, could also facilitate the creation of machine learning datasets with high levels of granularity. For example, to develop an AI algorithm specific to polarized light dermoscopy, one could assemble an appropriate dataset using query (based on DICOM attributes for the dermoscopy image type and polarization) and retrieve images from the repository where they are stored.

The amalgamation of datasets does increase the risk of unauthorized access to patient-identifiable information. DICOM's de-identification profiles (35), which are used to address privacy issues for multi-center clinical trials, can be directly applied to the amalgamation of machine learning datasets. The DICOM Attribute Confidentiality Profiles contain a comprehensive list of attributes that potentially provide identifying information and should be removed to protect the patient's privacy. Adopting an established de-identification profile has many advantages, including avoidance of repeating the same complex technical and legal consideration for de-identification, being less error-prone for participating sites to deploy, and implying a level of rigor that would potentially satisfy ethics committees.

Excluding images from datasets where the DICOM attribute Recognizable Visual Features (0028, 0302) is set is a further way to enhance the privacy of a dataset for machine learning. The Recognizable Visual Features flag is most often set when the subject's face is included in an image. In the forthcoming DICOM supplement for dermoscopy, this attribute is set if the images contain the patient's fingerprints.

DISCUSSION AND CONCLUSION

The increasing use of imaging in dermatology is being driven by many factors, including diagnostic imaging (as opposed to documentary imaging) such as teledermatology, sequential dermoscopic imaging, and melanoma screening using total body photography (36). The ability of DICOM to encode relevant metadata and afford interoperability with the digital health ecosystem has driven the initial interest in the adoption of DICOM for dermatology (2). DICOM can improve AI workflows by encoding derived objects (e.g.,

secondary images, visual explainability maps, AI algorithm output) and the efficient curation of multi-institutional datasets for machine learning training, testing, and validation. This can be achieved using DICOM mechanisms such as standardized image formats and metadata, metadata-based image retrieval, and de-identification protocols.

Currently, the use of DICOM to manage dermatological imaging is not widespread. Further, the use of DICOM to support AI workflows in dermatology is likely more limited still. There has, however, been a successful proof-of-concept trial using DICOM to encode datasets for AI of skin disease (37). DICOM adoption by dermatology may be more challenging than for other medical specialties. Clinical photographs captured on a mobile device constitute most imaging in dermatology. This type of imaging lacks standardization (38). Cameras used for clinical photography in dermatology are often commercial-off-the-shelf products as opposed to dedicated medical devices, hence, unlikely to support DICOM. As opposed to other medical specialties where formal diagnostic reports are produced, dermatology images can be simply viewed, which lessens the importance of integration with PACS. There is a lot of enthusiasm for AI in dermatology (32). More widespread understanding of the role that DICOM has in facilitating the adoption of AI in dermatology may strongly influence the dermatology community to adopt DICOM.

AI workflows for dermatology would require some interoperable actors on a medical imaging network. A potential workflow would be that images are acquired and stored in an image archive using typical DICOM image acquisition and storage workflows. Images could be automatically routed from the archive to an AI evidence creator actor (e.g., CNN). The evidence creator may undertake image post-processing to produce resized or down-sampled images and/or segmentation objects. These images would be encoded as DICOM objects and be automatically stored in the image archive. The AI evidence creator would analyze the image of the skin and create evidence documents (e.g., DICOM SR) containing the risk prediction of skin disease and potentially visual explainability maps. Again, these derived objects would be encoded as DICOM objects and automatically stored in the image archive using DICOM network services. All derived objects created by the AI evidence creator would use the same study identifier as the original images to facilitate linkage. A dermatologist or other clinician could use a DICOM viewer to subsequently query and retrieve an imaging study and display the original images and derived objects (e.g., a structured report containing algorithm output and/or visual explainability maps) that would help with image interpretation. DICOM-facilitated interoperability between AI actors and other devices in a medical imaging network is likely to facilitate workflow efficiencies. In addition to the transmission of images and results, interoperability is likely to play a key role in the continual adaptive learning of machine learning algorithms (39). Interoperability will also allow health-care organizations to use "best-of-breed" AI actors rather than being locked into an existing vendor's product.

The use of DICOM for the management of dermatological images will not guarantee effective clinical use of AI in dermatology. DICOM can address several important technological and workflow challenges for the implementation of AI. However, many other technological, ethical, regulatory, medicolegal, and workforce barriers will need to be addressed before DICOM and AI can be used effectively in dermatology.

DATA AVAILABILITY STATEMENT

The raw data supporting the conclusions of this article will be made available by the authors, without undue reservation.

AUTHOR CONTRIBUTIONS

All authors contributed equally to the preparation of this perspective piece.

FUNDING

HS was supported by an NHMRC MRFF Next Generation Clinical Researchers Program Practitioner Fellowship (APP1137127). VR was supported by the Melanoma Research Alliance Young Investigator Award 614197 and NIH Core Grant (P30 CA008748).

REFERENCES

1. National Electrical Manufacturers Association. *About DICOM: Overview*. National Electrical Manufacturers Association (2020). Available online at: https://www.dicomstandard.org/current (accessed September 01, 2020).
2. Caffery LJ, Clunie D, Curiel-Lewandrowski C, Malvehy J, Soyer HP, Halpern AC. Transforming dermatologic imaging for the digital era: metadata and standards. *J Digit Imaging*. (2018) 31:568–77. doi: 10.1007/s10278-017-0045-8
3. DICOM Standards Committee. *Supplement 221: Dermoscopy (Letter Ballot)*. (2020). Available online at: ftp://medical.nema.org/MEDICAL/Dicom/Supps/LB/sup221_lb_dermoscopy.pdf (accessed October 01, 2020).
4. Wada M, Ge Z, Gilmore SJ, Mar VJ. Use of artificial intelligence in skin cancer diagnosis and management. *Med J Aust*. (2020) 213:256–9.e1. doi: 10.5694/mja2.50759
5. Esteva A, Kuprel B, Novoa RA, Ko J, Swetter SM, Blau HM, et al. Dermatologist-level classification of skin cancer with deep neural networks. *Nature*. (2017) 542:115–8. doi: 10.1038/nature21056
6. Haenssle HA, Fink C, Schneiderbauer R, Toberer F, Buhl T, Blum A, et al. Man against machine: diagnostic performance of a deep learning convolutional neural network for dermoscopic melanoma recognition in comparison to 58 dermatologists. *Ann Oncol*. (2018) 29:1836–42. doi: 10.1093/annonc/mdy166
7. Tschandl P, Rinner C, Apalla Z, Argenziano G, Codella N, Halpern A, et al. Human-computer collaboration for skin cancer recognition. *Nat Med*. (2020) 26:1229–34. doi: 10.1038/s41591-020-0942-0
8. Zhao S, Xie B, Li Y, Zhao X, Kuang Y, Su J, et al. Smart identification of psoriasis by images using convolutional neural networks: a case study in China. *J Eur Acad Dermatol Venereol*. (2020) 34:518–24. doi: 10.1111/jdv.15965
9. Han SS, Park GH, Lim W, Kim MS, Na JI, Park I, et al. Deep neural networks show an equivalent and often superior performance to dermatologists in onychomycosis diagnosis: automatic construction of onychomycosis datasets by region-based convolutional deep neural network. *PLoS ONE*. (2018) 13:e0191493. doi: 10.1371/journal.pone.0191493

10. National Electrical Manufactuerres Association. *AI and DICOM*. (2020). Available online at: https://www.dicomstandard.org/ai (accessed October 01, 2020).
11. Haenssle HA, Fink C, Toberer F, Winkler J, Stolz W, Deinlein T, et al. Man against machine reloaded: performance of a market-approved convolutional neural network in classifying a broad spectrum of skin lesions in comparison with 96 dermatologists working under less artificial conditions. *Ann Oncol*. (2020) 31:137–43. doi: 10.1016/j.annonc.2019.10.013
12. Geis JR, Brady AP, Wu CC, Spencer J, Ranschaert E, Jaremko JL, et al. Ethics of artificial intelligence in radiology: summary of the joint European and North American multisociety statement. *Radiology*. (2019) 293:436–40. doi: 10.1148/radiol.2019191586
13. Booz C, Yel I, Wichmann JL, Boettger S, Al Kamali A, Albrecht MH, et al. Artificial intelligence in bone age assessment: accuracy and efficiency of a novel fully automated algorithm compared to the greulich-pyle method. *Eur Radiol Exp*. (2020) 4:6. doi: 10.1186/s41747-019-0139-9
14. Conant EF, Toledano AY, Periaswamy S, Fotin SV, Go J, Boatsman JE, et al. Improving accuracy and efficiency with concurrent use of artificial intelligence for digital breast tomosynthesis. *Radiol Artif Intell*. (2019) 1:e180096. doi: 10.1148/ryai.2019180096
15. Pesapane F, Codari M, Sardanelli F. Artificial intelligence in medical imaging: threat or opportunity? radiologists again at the forefront of innovation in medicine. *Eur Radiol Exp*. (2018) 2:35. doi: 10.1186/s41747-018-0061-6
16. Mahbod A, Tschandl P, Langs G, Ecker R, Ellinger I. The effects of skin lesion segmentation on the performance of dermatoscopic image classification. *Comput Methods Programs Biomed*. (2020) 197:105725. doi: 10.1016/j.cmpb.2020.105725
17. Combalia M, Codella NC, Rotemberg V, Helba B, Vilaplana V, Reiter O, et al. BCN20000: dermoscopic lesions in the wild. *arXiv*. (2019). *arXiv* 1908.02288v2.
18. Hashemi M. Enlarging smaller images before inputting into convolutional neural network: zero-padding vs. interpolation. *J Big Data*. (2019) 6:98. doi: 10.1186/s40537-019-0263-7
19. Lundberg SM and Lee S-I. A unified approach to interpreting model predictions. In: von Luxburg U, Guyon I, editors. *Proceedings of the 31st International Conference on Neural Information Processing Systems*. Long Beach, CA: Curran Associates Inc., (2017). p. 4765–74.
20. Selvaraju RR, Cogswell M, Das A, Vedantam R, Parikh D, Batra D. Grad-CAM: visual explanations from deep networks via gradient-based localization. *Int J Comput Vision*. (2020) 128:336–59. doi: 10.1007/s11263-019-01228-7
21. Holzinger A, Langs G, Denk H, Zatloukal K, Muller H. Causability and explainability of artificial intelligence in medicine. *Wiley Interdiscip Rev Data Min Knowl Discov*. (2019) 9:e1312. doi: 10.1002/widm.1312
22. Young K, Booth G, Simpson B, Dutton R, Shrapnel S. Deep neural network or dermatologist? In: Suzuki K, Reyes M, Syeda-Mahmood T, et al. editors. *Interpretability of Machine Intelligence in Medical Image Computing and Multimodal Learning for Clinical Decision Support: Proceedings of the Second International Workshop on Interpretability of Machine Intelligence in Medical Image Computing, iMIMIC 2019, and the 9th International Workshop on Multimodal Learning for Clinical Decision Support, ML-CDS 2019, held in conjunction with the 22nd International Conference on Medical Imaging and Computer-Assisted Intervention, MICCAI 2019*. Shenzhen: Springer International Publishing (2019). p. 48–55.
23. DICOM Standards Committee. *CP-1867 Add codes for visual Explanation maps*. (2020). Available online at: https://dicom.nema.org/Dicom/News/September2019/docs/cpack103/cp1867.pdf (accessed October 01, 2020).
24. DICOM Standards Commiteee. *Supplement 219: JSON Representation of DICOM Structured Reports*. (2020). Available online at: ftp://medical.nema.org/medical/dicom/supps/Frozen/sup219_fz_14_JSONSR.pdf (accessed October 01, 2020)
25. Gessert N, Nielsen M, Shaikh M, Werner R, Schlaefer A. Skin lesion classification using ensembles of multi-resolution efficientnets with meta data. *MethodsX*. (2020) 7:100864. doi: 10.1016/j.mex.2020.100864
26. Liu Z, Sun J, Smith M, Smith L, Warr R. Incorporating clinical metadata with digital image features for automated identification of cutaneous melanoma. *Br J Dermatol*. (2013) 169: 1034–40. doi: 10.1111/bjd.12550
27. Pacheco AGC, Krohling RA. The impact of patient clinical information on automated skin cancer detection. *Comput Biol Med*. (2020) 116:103545. doi: 10.1016/j.compbiomed.2019.103545
28. National Electrical Manufacturers Association. *Digital Imaging and Communications in Medicine (DICOM) Standard PS3.10 - Media Storage and File Format for Media Interchange*. (2020). Available online at: https://dicom.nema.org/medical/dicom/current/output/pdf/part10.pdf (accessed October 01, 2020).
29. Donnelly K. SNOMED-CT: the advanced terminology and coding system for eHealth. *Stud Health Technol Inform*. (2006) 121:279–90.
30. Bidgood WD Jr, Bray B, Brown N, Mori AR, Spackman KA, Golichowski A, et al. Image acquisition context: procedure description attributes for clinically relevant indexing and selective retrieval of biomedical images. *J Am Med Inform Assoc*. (1999) 6:61–75. doi: 10.1136/jamia.1999.0060061
31. Li W, Zhuang J, Wang R, Zhang J, Zheng W. Fusing metadata and dermoscopy images for skin disease diagnosis. In: *2020 IEEE 17th International Symposium on Biomedical Imaging (ISBI)*. (2020). p. 1996–2000.
32. Du-Harpur X, Watt FM, Luscombe NM, Lynch MD. What is AI? Applications of artificial intelligence to dermatology. *Br J Dermatol*. (2020) 183:423–30. doi: 10.1111/bjd.18880
33. Chan S, Reddy V, Myers B, Thibodeaux Q, Brownstone N, Liao W. Machine learning in dermatology: current applications, opportunities, and limitations. *Dermatol Ther*. (2020) 10:365–86. doi: 10.1007/s13555-020-00372-0
34. Curiel-Lewandrowski C, Novoa RA, Berry E, Celebi ME, Codella N, Giuste F, et al. *Artificial Intelligence Approach in Melanoma. Melanoma*. New York, NY: Springer (2019). p. 1–31.
35. National Electrical Manufacturers Association Digital Imaging and Communications in Medicine (DICOM). *Standard PS3.15 - Security and System Management Profiles - E.1 Attribute Confidentiality Profiles - De-identifier*. (2020). Available online at: https://dicom.nema.org/medical/dicom/current/output/chtml/part15/chapter_E.html#sect_E.1.1 (accessed October 01, 2020)
36. Rayner JE, Laino AM, Nufer KL, Adams L, Raphael AP, Menzies SW, et al. Clinical perspective of 3D total body photography for early detection and screening of Melanoma. *Front Med*. (2018) 5:152. doi: 10.3389/fmed.2018.00152
37. Rotemberg V, Kurtansky N, Betz-Stablein B, Caffery L, Chousakos E, Codella N, et al. A patient-centric dataset of images and metadata for identifying melanomas using clinical context. *arXiv*. (2020). *arXiv* 2008.07360v1.
38. Quigley EA, Tokay BA, Jewell ST, Marchetti MA, Halpern AC. Technology and technique standards for camera-acquired digital dermatologic images: a systematic review. *JAMA Dermatol*. (2015) 151:883–90. doi: 10.1001/jamadermatol.2015.33
39. Dikici E, Bigelow M, Prevedello L, White R, Erdal B. Integrating AI into radiology workflow: levels of research, production, and feedback maturity. *J Med Imaging*. (2020) 7:016502. doi: 10.1117/1.JMI.7.1.016502

Conflict of Interest: HS is a shareholder of MoleMap NZ Limited and e-derm consult GmbH, and undertakes regular teledermatological reporting for both companies. HS also provides medical consultant services for Canfield Scientific Inc., First Derm by iDoc24 Inc, and Revenio Research Oy. DC provides consultancy to: MITA (editor of DICOM standard), Canfield Scientific, Philips Algotec, Essex Leidos CBIIT NCI, Brigham and Women's Hospital NCI Imaging Data Commons (IDC), University of Leeds Northern Pathology Imaging Co-operative (NPIC) and is on the advisory board of maiData.

The remaining authors declare that the research was conducted in the absence of any commercial or financial relationships that could be construed as a potential conflict of interest.

frontiers in Medicine

REVIEW
published: 22 February 2021
doi: 10.3389/fmed.2021.619965

High-Frequency Ultrasonography—Possibilities and Perspectives of the Use of 20 MHz in Teledermatology

Adriana Polańska[1], Dorota Jenerowicz[2], Elżbieta Paszyńska[3], Ryszard Żaba[1], Zygmunt Adamski[2] and Aleksandra Dańczak-Pazdrowska[2]*

[1] Department of Dermatology and Venereology, Poznań University of Medical Sciences, Poznań, Poland, [2] Department of Dermatology, Poznań University of Medical Sciences, Poznań, Poland, [3] Department of Integrated Dentistry, Poznań University of Medical Sciences, Poznań, Poland

High-frequency ultrasonography (HF-USG) is a non-invasive and *in vivo* method of visualization of the skin and upper part of subcutaneous tissue based on ultrasounds above 20 MHz. Although initially HF-USG was introduced to measure skin thickness, it currently gained widespread acceptance in dermato-oncology, primarily when used to determine skin tumor margins. Moreover, its application in different dermatology fields is known, particularly as a rapidly evolving method in the objective evaluation of the severity of various chronic skin diseases. Among different specialties, teledermatology belongs to leading and continually developing areas of successful telemedicine applications. Various skin conditions are visible to the human eye, which makes them particularly suitable for telemedicine. However, HF-USG enables specialists to look into deeper skin layers, thus extending diagnostic options. On the other hand, teledermatology creates the possibility of sending images for consultation and facilitates the therapeutic decision as HF-USG can be used in an asynchronous store and forward manner. It seems that HF-USG and teledermatology may be regarded as a truly matched pair. The aim of this work is to present current applications of 20-MHz ultrasonography in dermatology, including skin neoplasms and chronic skin diseases. Moreover, the authors aimed to analyze the possibilities of HF-USG use as a valuable tool in teledermatology, especially in diagnosing and monitoring patients suffering from long-lasting skin conditions.

Keywords: teledermatology, melanoma, atopic dermatitis, mycosis fungoides, high-frequency ultrasonography

OPEN ACCESS

Edited by:
H. Peter Soyer, The University of Queensland, Australia

Reviewed by:
Katie June Lee, University of Queensland, Australia
Marika Quadri, University of Modena and Reggio Emilia, Italy

****Correspondence:***
Adriana Polańska
adriana-polanska@wp.pl

Specialty section:
This article was submitted to Dermatology, a section of the journal Frontiers in Medicine

Received: *21 October 2020*
Accepted: *11 January 2021*
Published: *22 February 2021*

Citation:
Polańska A, Jenerowicz D, Paszyńska E, Żaba R, Adamski Z and Dańczak-Pazdrowska A (2021) High-Frequency Ultrasonography—Possibilities and Perspectives of the Use of 20 MHz in Teledermatology. Front. Med. 8:619965. doi: 10.3389/fmed.2021.619965

INTRODUCTION

According to the World Health Organization (WHO), telemedicine utilizes communication technologies in healthcare to exchange medical information for the diagnosis, treatment, prevention, research, evaluation, and education over a distance (1). Therefore, it can be considered a merge of expertise and communication technology, giving patients the possibility of being examined, monitored, and managed by a medical expert in a distant location. Electronic transfer of information may be accomplished in various ways. Still, two basic types currently in practice are "real-time" or "live interactive" (LI) (enables direct communication sender–recipient with an immediate result) and "store-and-forward" (SAF) telemedicine (digital images and patient data are

captured, transferred, and stored) (2–4). Teledermatology belongs to the earliest and leading areas of the successful use of telemedicine solutions. Nowadays, it is applied among all kinds of medical facilities, including hospitals, primary care, or nursing homes (5, 6).

The principle aim of teledermatology seems to be to consult and to educate. Digital communication brings possibilities for the exchange of medical information between the patient and the specialist. What is more, a recent modality—"patient-assisted teledermatology," or "home-based teledermatology"—has been vigorously developing (7). After the first visit and face-to-face diagnosis by the dermatologist, a patient is then supposed to send pictures documenting the skin's condition. This form combines SAF teledermatology and mobile technology tools. It is particularly useful for patients with chronic diseases, such as psoriasis, atopic dermatitis, vitiligo, or leg ulcers.

One of the emerging technologies that may find application in teledermatology and implement WHO assumptions seems to be high-frequency ultrasonography (HF-USG). Although initially HF-USG was introduced to measure skin thickness, currently it has gained widespread acceptance in dermato-oncology, particularly to determine margins of skin tumors (8–10). Moreover, its application in different dermatology fields is known, particularly as a rapidly evolving method in the objective evaluation of the severity of the various chronic skin diseases (11–13). The possibility of sending images for consultation may facilitate therapeutic decisions as HF-USG can be used in a SAF manner.

We present the actual applications of 20-MHz ultrasonography in dermatology and analyze the possibility of its use as a valuable tool in teledermatology, especially in managing patients suffering from chronic skin diseases.

BASIC PRINCIPLES OF HF-USG

The pioneering use of the ultrasound beam in dermatology was carried out in the 1980s by Alexander and Miller with a 15-MHz probe (8). As is known, routine imaging of the abdominal organs is possible with the use of ultrasound waves in the 3–5-MHz range, while for the assessment of more superficial structures (such as lymph nodes, testes, or the thyroid gland), frequencies in the range 7.5–15 MHz are needed. The imaging of the skin became possible with the invention of transducers emitting waves with higher vibration ranges, and now ultrasound scanners of 20 MHz (High Frequency Ultrasonography, HF-USG) and higher (Ultra High Frequency Ultrasonography, UHF-USG) are used for skin examination (14). According to the Guidelines for Performing Dermatologic Ultrasound Examinations, the minimum frequency for dermatological analysis should be 15 MHz (15). However, considering the multifrequency property of available probes, the use of the range from 15 to 22 MHz for better visualization of deeper lesions is suggested (15).

The use of 20-MHz heads allows for images of structures at a depth of 8–10 mm and, according to some manufacturers, even up to 15 mm (14, 16). The higher the frequency, the better the picture resolution. The axial resolution is defined as the minimum distance that can be differentiated between two reflectors located parallel to the ultrasound beam's direction. In comparison, the lateral one is the minimum distance that can be distinguished between two reflectors situated perpendicular to the ultrasound beam's path. Fifty MHz can achieve 20 and 100 μm resolution, respectively, while 20 MHz can achieve 80 and 200 μm (17). The emission of an ultrasound beam by a piezoelectric transducer and its reception enables the analysis of echoes in various presentations. The oldest presentation is of the A-type—it analyzes the echo amplitude as a function of time and allows measurements to be made. However, most often, the B-type presentation is used to analyze the ultrasound image, which is an overlay of many A-type presentations in real time, in which echoes have been converted into glowing spots and mapped on the screen using a grayscale (256-degree grayscale) (18, 19). Thanks to the B-type presentation, it is possible to analyze the echogenicity. The echogenic structures appear bright on ultrasound images (the higher the amplitude of the reflected wave, the brighter the pixel) (14, 16, 18).

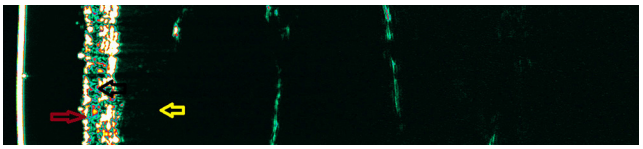

FIGURE 1 | The HF-USG image of healthy skin of the forearm. Red arrow—the echo from the surface of the epidermis; black arrow—dermis; yellow arrow—subcutaneous tissue.

The ultrasound image of healthy skin corresponds to the skin layers visible on histological examination. We can distinguish three layers that differ in echogenicity (14, 18, 19) (**Figure 1**). The first layer, usually called entrance echo, is hyperechoic and reflects the upper (mainly dead) parts of the epidermis. Below, there is a layer of less echogenicity—which corresponds to the lower layers of the epidermis, the dermoepidermal border, and, above all, the dermis, within which echoes of varying intensity are visible. The lowest layer can be easily distinguishable because it is hypoechogenic in nature and corresponds to the subcutaneous tissue, which (depending on the anatomical location and sex) can be visualized to various depths (14, 18, 19).

DIAGNOSTIC PROPERTIES OF HF-USG IN TELEDERMATOLOGY

According to an interesting report by Warshaw et al. (20), performed for The American Veterans Health Services Research, in-person dermatology diagnostic accuracy is of a higher quality than teledermatology. While overall management accuracy rates seem to be equivalent, in the case of malignant and premalignant lesions, rates for teledermatology and teledermatoscopy are inferior to the usual care. It is then recommended to be cautious when using teledermatology in such cases. These observations have to be considered in regard to implementing HF-USG in

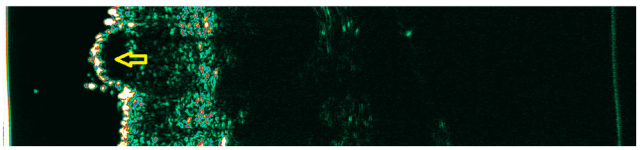

FIGURE 2 | Cellular nevus. Yellow arrow—hypoechogenic mass corresponding to the nevus.

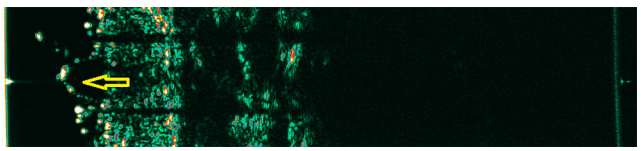

FIGURE 3 | Melanoma. Yellow arrow—hypoechogenic mass corresponding to the melanoma.

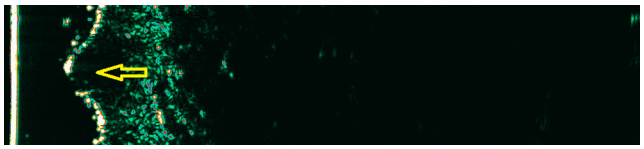

FIGURE 4 | Basal cell carcinoma. Yellow arrow—hypoechogenic mass corresponding to the basal cell carcinoma.

teledermatology modalities, particularly concerning pigmented lesions and tumors.

Various skin pathologies change the echogenicity of its individual layers, which can be used to analyze the ultrasound image. However, the lack of sufficient resolution does not allow a full interpretation of the image with microscopic examination accuracy. Hypoechoic structures can be both of neoplastic and inflammatory origin (14, 21, 22). Moreover, an identical ultrasound image is observed in melanoma and a benign melanocytic nevus. Due to the insufficient resolution of HF-USG, the process cannot be distinguished at the cell level (**Figures 2**, **3**). Although literature has tried to identify more specific features for various skin neoplasms, the final diagnosis should still be supported by histological examination. In melanoma, echolucent areas can be observed, with a shape depending on the subtype. The nodular form may have a spherical arrangement, while superficial spreading melanoma presents as an echolucent area parallel to the entry echo. However, there are no ultrasonographic features pathognomonic for melanoma (14).

What is more, the accuracy of ultrasound analysis may be increased with a Color Doppler ultrasound. This modality is recommended, especially for discriminating between vascular or non-vascular lesions and recognizing the benign or malignant nature of skin tumors (15, 23, 24). In previous studies, vascular signal use in assessing melanoma correlated with the Breslow index and metastatic potential (23). The addition of Color-Doppler in pigmented lesion analysis may have a significant prognostic value (25, 26).

In basal cell carcinoma (BCC), the HF-USG can detect the presence of hyperechoic spots, the so-called cotton flowers; however, in the authors' opinion, this is not a phenomenon that occurs in all tumors and therefore cannot be defining for BCC (14, 21, 27) (**Figure 4**). In squamous cell carcinoma (SCC) and actinic keratosis, scaling may disturb the image's interpretation. This seems to be a crucial limitation of HF-USG in evaluating hyperkeratotic tumors (10, 18, 19).

It is worth noting that the usefulness of HF-USG for assessing the thickness of BCC and melanoma infiltration has been well-documented and is now considered a recognized indication for HF-USG (14, 28–32). The preoperative determination of the surgical margins determines the future management and patients' prognosis (particularly in the case of melanoma). Previous studies confirm the agreement between a histological and ultrasonographic measurement with a high compliance rate (28–33). Therefore, the HF-USG assessment of tumor size may be then transferred to a dermato-oncologist or surgeon during teleconsultation to plan the future procedure. This way, teledermatology may globally contribute to better outcomes and radical treatment. However, it should be considered that the thickness of the tumor determined by ultrasound is slightly greater than the thickness determined histologically, due to shrinkage of the material during histological preparation and accumulation of inflammatory cells underneath the tumor (10, 24, 28). Another limitation of the proper margin assessment is the tumor size, mainly when it crosses the dermis border and penetrates the subcutaneous tissue, which is also hypoechogenic. However, the use of a multifrequency probe may reduce this limitation. The preoperative evaluation of the tumor margins may also be difficult in patients with evident photoaging, where elastosis decreases the skin echogenicity, similarly to the neoplasmatic cells (14).

Due to the low diagnostic properties of HF-USG in oncodermatology, the combination of this method with a preliminary dermoscopic evaluation may be extremely useful. Therefore, an initial diagnosis of probable pathology should be performed using a dermoscope, followed by an evaluation of disease extent using HF-USG. Acquired data, provided in the form of telecommunication, may significantly improve the diagnostic and therapeutic process. These observations remain consistent with teledermatology's role in the process of triaging (particularly the SAF method), which influences the cost-effectiveness of therapies and may limit waiting time in the case of urgent patients (34). Moreover, the inclusion of dermatoscopic images improves triaging decisions, including a need for an excision for both melanomas and other skin cancers (35).

THE MONITORING PROPERTIES OF HF-USG IN TELEDERMATOLOGY

Due to the limited diagnostic value of ultrasonography, the monitoring properties of HF-USG are noteworthy. They allow for observing changes dynamically—occurring in the skin over

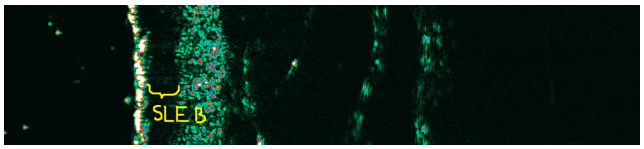

FIGURE 5 | Subepidermal low echogenic band (SLEB) within the plaque of mycosis fungoides before treatment (the hypoechogenic band corresponding to the SLEB was marked).

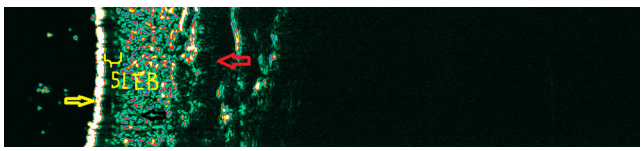

FIGURE 6 | The thinning of the SLEB after treatment. Lack of complete disappearance of SLEB still shows the presence of neoplastic T cell infiltrations (the hypoechogenic band corresponding to the SLEB was marked).

time, mainly due to the introduced treatment (**Figures 5**, **6**). Inflammatory and neoplastic cells cause a reduction of skin echogenicity and may result in the formation of a linear band underneath the entry echo, known as the subepidermal low echogenic band (SLEB) (11, 12, 14). Originally, SLEB was observed in photodamaged skin due to glycosaminoglycan accumulation, which possesses an increased water-binding capacity (14, 18). The SLEB formation was well-documented in inflammatory diseases, including psoriasis and atopic dermatitis (11–13, 36, 37). It is not a parameter specific for any skin disease, but its changes over time are of prognostic significance, especially in patients with chronic skin diseases. The areas of reduced echogenicity are mainly related to swelling of the skin and inflammatory cell infiltration. The SLEB thickness in atopic dermatitis correlated with the degree of several histopathologic findings like epidermal hyperplasia, epidermal hyperkeratosis, the degree of parakeratosis, and the degree of spongiosis as well as the intensity of inflammatory infiltrates (38). However, in psoriatic plaque, SLEB's uniformity can be disturbed by streaky shadows perpendicular to the entry echo (most likely caused by air bubbles trapped between the scales). It is observed that SLEB thickness corresponds to the severity of skin lesions and can be used to monitor patients, also potentially as a teledermatology consultation (14, 39).

In one of our first studies, monitoring properties of HF-USG were assessed for atopic dermatitis and so-called proactive therapy, using tacrolimus ointment (40). Six-month ultrasound monitoring was performed in a group of 39 patients with atopic dermatitis (mean age 26 years). It revealed the significant decrease of SLEB value during the undergone therapy, which correlated with the disease severity assessed by measuring scales (40). We found that HF-USG allowed clinicians to visualize pathologic changes of all skin *in vivo*. As a non-invasive and independent of subjective judgment method, HF-USG should be added to the overall patient evaluation, especially in the era of evidence-based medicine (41). We presented that SLEB was detected within lesional skin and in non-affected skin regions, revealing the presence of subclinical inflammation (42, 43). Such patients may significantly benefit most from proactive treatment (40, 42). Information on the decrease of SLEB or lack of its change could be provided in the form of a teleconference to the attending physician with information about the need to intensify the treatment process. It could also be combined with an emerging teledermatology branch—patient-assisted teledermatology (also called home-based teledermatology)—which involves the SAF method and mobile technology tools. It is regarded as especially useful for patients with chronic dermatoses (psoriasis, atopic dermatitis, vitiligo, leg ulcers) and allows the specialist to monitor the phase and the degree of skin lesions. The above method is relatively new (started in 2009) and is used for both diagnosis and follow-up (20, 35).

SLEB thickness objective measurement as a useful, accurate parameter for skin assessment was also performed in psoriasis (14, 36). Queille-Roussel et al. (36) evaluated an innovative aerosol foam formulation's anti-psoriatic effect and analyzed this parameter's thickness. They found a reduction of SLEB in week 4. We also assessed monitoring properties of HF-USG in a prospective, observational study, which included 58 patients diagnosed with recurrent chronic small plaque psoriasis treated with a two-compound ointment containing calcipotriol and betamethasone dipropionate or NB-UVB (311 nm) (11). The SLEB was significantly decreased in both treated groups. The lack of its decrease, similarly to atopic dermatitis, indicated no improvement in the dermatological condition or the need to change/intensify therapy (11, 14). Such information could be consulted with a dermatologist without the need to travel and access the specialist advice more easily, especially in rural areas. What is essential, a high correlation between SLEB and PASI index indicates that HF-USG quickly complements the measurement of the severity of skin lesions in psoriasis in an objective way (11).

Monitoring properties of HF-USG seem to be particularly useful in assessing the therapeutical outcomes in patients with mycosis fungoides. They can be used in teleconsultations also with a non-dermatologist (i.e., hematologist). Neoplastic cells are responsible for decreasing echogenicity, which in mycosis fungoides also manifests in the form of SLEB, similarly to inflammatory diseases (12, 14, 44–46). We have found strong correlations between SLEB thickness and the thickness of subepidermal infiltration in histopathological examination (47). As it is known, in mycosis fungoides, the proper staging is essential in planning the therapy. It should include a detailed evaluation of the skin lesion types and an assessment of the pathological process' extent (45, 47). For 5 years, we followed up patients based on HF-USG, where SLEB was the assessed parameter (48). We evaluated well-known forms of therapies in mycosis fungoides (the effectiveness of UVA1 and PUVA). We monitored these patients' clinical responses compared to the modified Severity Weighted Assessment Tool (mSWAT) (12). Complete response in examined patients correlated with the entire disappearance of SLEB (12, 48). SLEB thickness was associated with disease severity and was wider in stage IIA

patients than in stage IA and IB patients (48). For the first time, we revealed that HF-USG is a tool for evaluating the patient's response and can be applied in routine clinical practice.

What is more, using HF-USG, there is a possibility to distinguish a lesion of the type of post-inflammatory hyper/hypopigmentation from a non-specific infiltrative lesion (12, 47, 48). Performing ultrasound measurements enables the patient to be consulted with a dermatologist/hematologist without a face-to-face visit and can significantly improve the therapeutic process. In the case of irradiated patients, a routine practice in our clinic is the ultrasound supervision of patients and making decisions about additional radiation if a visible SLEB is still observed. Again, collected data can be then sent to a photodermatology center.

The practical application of HF-USG is its use in hidradenitis suppurativa (49). Recent studies proposed this method to optimize staging, treatment planning, and monitoring patients suffering from this chronic disease (49). Wortsman et al. (50) proposed a three-point sonographic scoring system for hidradenitis suppurativa, based on the number and distribution of fluid collections, fistulous tracts, and pseudocystic nodules, widening of the hair follicles, and alterations in the dermal thickness/echogenicity. According to the authors, the proper staging of these patients resulted in a management modification in 82% of cases (51). It seems that HF-USG in relation to hidradenitis suppurativa may also be conducted in the form of teleconsultation with other specialists (diagnostic and radiological center, dermatological surgeons). The possibility of an ultrasound consultation can improve diagnosis and help choose an appropriate therapeutic option (depending on the severity of skin lesions).

THE ADVANTAGES AND LIMITATIONS OF HF-USG

The most significant advantages of HF-USG in a monitoring examination are non-invasiveness, safety, and the possibility of multiple scans without the need to prepare the patient in advance. It seems that in the era of scrupulously determined scales determining the extent and severity of skin lesions during various treatments of skin diseases, especially to qualify patients for biological therapies and research programs, HF-USG can find an application. In the case of teledermatology, the possibility of transmitting images in between clinicians and of archiving images and analyzing them over time contributes an extremely useful visual *in vivo* method. Teleconsultation with the use of HF-USG may improve the treatment process of chronic dermatological diseases requiring long-term care. The possibility of simultaneous dermoscopy and ultrasound of the skin may have a prognostic significance in skin tumors.

Among the main limitations of HF-USG, its high price should be mentioned, as well as restricted availability of the apparatus in a doctor's office. As in the case of dermoscopy, acquiring the ability to interpret an ultrasonographic image requires appropriate training. Lately, also other techniques of non-invasive skin visualization are gaining interest in regard to associations with teledermatology—for example, reflectance confocal microscopy (RCM). RCM allows an *in vivo* evaluation of various skin lesions on the cellular level—nearly to histologic resolution. In comparison to this technique, it has to be emphasized that HF-USG does not possess sufficient resolution and its diagnostic properties are much lower (52).

AUTHOR CONTRIBUTIONS

All authors listed have made a substantial, direct and intellectual contribution to the work, and approved it for publication.

ACKNOWLEDGMENTS

The authors are entirely grateful to Dr. Tomasz Maksymiuk (MD, Ph.D.), who provided English grammar editing and really improved the quality and understanding of the whole manuscript.

REFERENCES

1. *Telemedicine: Opportunities and Developments in Member States: Report on the Second Global Survey on eHealth 2009*. World Health Organization (2010).
2. Waller M, Stotler C. Telemedicine: a primer. *Curr Allergy Asthma Rep*. (2018) 25:54. doi: 10.1007/s11882-018-0808-4
3. Bischoff A. Benefits and risks from telemedicine. *MMW Fortschr Med*. (2016) 158:18–9. doi: 10.1007/s15006-016-8250-9
4. Zaba R. Telemedycyna w dermatologii. *Medicus Mundi Polonia*. (2009) 28:7–8.
5. Coates SJ, Kvedar J, Granstein RD. Teledermatology: from historical perspective to emerging techniques of the modern era: part I: history, rationale, and current practice. *J Am Acad Dermatol*. (2015) 72:563–74. doi: 10.1016/j.jaad.2014.07.061
6. Jankowski M, Klimczak-Wieczorek A, Kloc M, Matuszewski M, Rozum J. *Telemedycyna w Polsce – mozliwości i szanse rozwoju*. Fundacja im. Lesława A. Pagi, Warszawa (2016).
7. Kanthraj GR. Patient-assisted teledermatology practice: what is it? When, where, and how it is applied? *Indian J Dermatol Venereol Leprol*. (2015) 17:136–43. doi: 10.4103/0378-6323.152172
8. Alexander H, Miller DL. Determining skin thickness with pulsed ultrasound. *J Invest Dermatol*. (1979) 72:17–9. doi: 10.1111/1523-1747.ep12530104
9. Pellacani G, Seidenari S. Preoperative melanoma thickness determination by 20-MHz sonography and digital videomicroscopy in combination. *Arch Dermatol*. (2003) 139:293–8. doi: 10.1001/archderm.139.3.293
10. Hoffmann K, el-Gammal S, Winkler K, Jung J, Pistorius K, Altmayer P. Skin tumours in high-frequency ultrasound. In: Altmeyer P, el-Gammal S, Hoffmann K, editors. *Ultrasound in Dermatology*. Berlin; New York, NY: Springer- Verlag (1992). p. 181–202.
11. Polańska A, Gaura T, Bowszyc-Dmochowska M, Osmola-Mańkowska A, Olek-Hrab K, Adamski Z, et al. Calcipotriol/betamethasone ointment compared to narrow-band UVB in plaque psoriasis: first clinical and ultrasonographic study. *Int J Dermatol*. (2019) 58:108–13. doi: 10.1111/ijd.14150
12. Polańska A, Osmola-Mańkowska A, Olek-Hrab K, Molińska-Glura M, Adamski Z, Zaba R, et al. High-frequency ultrasonography in objective evaluation of the efficacy of PUVA and UVA 1 phototherapy in mycosis fungoides. *Arch Dermatol Res*. (2017) 309:645–51. doi: 10.1007/s00403-017-1767-7

13. Wortsman X, Moreno C, Soto R, Arellano J, Pezo C, Wortsmanet J. Ultrasound in-depth characterization and staging of hidradenitis suppurativa. *Dermatol Surg*. (2013) 39:1835–42. doi: 10.1111/dsu.12329
14. Polańska A, Dańczak-Pazdrowska A, Jałowska M, Adamski Z, Zaba R. Current applications of high-frequency ultrasonography in dermatology. *Adv Dermatol Allergol*. (2017) 6:535–42. doi: 10.5114/ada.2017.72457
15. Wortsman X, Alfageme F, Roustan G, Arias-Santiago S, Martorell A, Catalano O, et al. Guidelines for performing dermatologic ultrasound examinations by the DERMUS group. *J Ultrasound Med*. (2016) 35:577–80. doi: 10.7863/ultra.15.06046
16. Dill-Müller D, Maschke J. Ultrasonography in dermatology. *J Dtsch Dermatol Ges*. (2007) 5:689–707. doi: 10.1111/j.1610-0387.2007.06453.x
17. Ng A, Swanevelder J. Resolution in ultrasound imaging. *Continuing Educ. Anaesthesia Crit Care Pain*. (2011) 11:186–92. doi: 10.1093/bjaceaccp/mkr030
18. Jasaitiene D, Valiukeviciene S, Linkeviciute G, Raisutis R, Jasiuniene E, Kazyset R. Principles of high-frequency ultrasonography for investigation of skin pathology. *J Eur Acad Dermatol Venereol*. (2011) 25:375–82. doi: 10.1111/j.1468-3083.2010.03837.x
19. Jemec GB, Gniadecka M, Ulrich J. Ultrasound in dermatology. Part I: high frequency ultrasound. *Eur J Dermatol*. (2000) 10:492–7.
20. Warshaw E, Greer N, Hillman Y, Hagel E, MacDonald R, Rutks I, et al. *Teledermatology for Diagnosis and Management of Skin Conditions: A Systematic Review of the Evidence*. VA-ESP Project #09-009 (2009).
21. Wortsman X, Jemec GBE. High resolution ultrasound applications in dermatology. *Rev Chilena Dermatol*. (2006) 22:37–45.
22. Harland CC, Kale SG, Jackson P, Mortimer PS, Bamberet JC. Differentiation of common benign pigmented skin lesions from melanoma by high-resolution ultrasound. *Br J Dermatol*. (2000) 143:281–9. doi: 10.1046/j.1365-2133.2000.03652.x
23. Scotto di Santolo M, Sagnelli M, Mancini M, Scalvenzi M, Delfino M, Schonauer F, et al. High-resolution Color-Doppler ultrasound for the study of skin growths. *Arch Dermatol Res*. (2015) 307:559–66. doi: 10.1007/s00403-015-1538-2
24. Catalano O, Roldán FA, Varelli C, Bard R, Corvino A, Wortsman X. Skin cancer: findings and role of high-resolution ultrasound. *J Ultrasound*. (2019) 22:423–31. doi: 10.1007/s40477-019-00379-0
25. Catalano O, Voit C, Sandomenico F, Mandato Y, Petrillo M, Franco R, et al. Previously reported sonographic appearances of regional melanoma metastases are not likely due to necrosis. *J Ultrasound Med*. (2011) 30:1041–9. doi: 10.7863/jum.2011.30.8.1041
26. Lassau N, Lamuraglia M. Prognostic value of angiogenesis evaluated with high frequency and Color-Doppler sonography for preoperative assessment of primary cutaneous melanomas: correlation with recurrence after a 5 year follow-up period. *Cancer Imaging*. (2006) 25:24–9. doi: 10.1102/1470-7330.2006.0009
27. Wang SQ, Liu J, Zhu QL, Zhao CY, Qu T, Li F, et al. High-frequency ultrasound features of basal cell carcinoma and its association with histological recurrence risk. *Chin Med J*. (2019) 132:2021–6. doi: 10.1097/CM9.0000000000000369
28. Tacke J, Haagen G, Hornstein OP, Tacke J, Haagen G, Hornstein P, et al. Clinical relevance of sonometry-derived tumour thickness in malignant melanoma: a statistical analysis. *Br J Dermatol*. (1995) 132:209–14. doi: 10.1111/j.1365-2133.1995.tb05015.x
29. Lassau N, Koscielny S, Avril MF, Margulis A, Duvillard P, De Baere T, et al. Prognostic value of angiogenesis evaluated with high-frequency and color Doppler sonography for preoperative assessment of melanomas. *Am J Roentgenol*. (2002) 178:1547–51. doi: 10.2214/ajr.178.6.1781547
30. Serrone L, Solivetti FM, Thorel MF, Eibenschutz L, Donati P, Catricalàet C. High frequency ultrasound in the preoperative staging of primary melanoma: a statistical analysis. *Melanoma Res*. (2002) 12:287–90. doi: 10.1097/00008390-200206000-00013
31. Guitera P, Li LX, Crotty K, Fitzgerald P, Mellenbergh R, Pellacani G, et al. Melanoma histological Breslow thickness predicted by 75-MHz ultrasonography. *Br J Dermatol*. (2008) 159:364–9. doi: 10.1111/j.1365-2133.2008.08681.x
32. Bobadilla F, Wortsman X, Muñoz C, Segovia L, Espinoza M, Jemec G. Pre-surgical high resolution ultrasound of facial basal cell carcinoma: correlation with histology. *Cancer Imaging*. (2008) 22:63–72. doi: 10.1102/1470-7330.2008.0026
33. Seidenari S. High-frequency sonography combined with image analysis: a non-invasive objective method for skin evaluation and desription. *Clin Dermatol*. (1995) 13:349–59. doi: 10.1016/0738-081X(95)00074-P
34. Congalton AT, Oakley AM, Rademaker M, Bramley D, Martin R. Successful melanoma triage by a virtual lesion clinic (teledermoscopy). *J Eur Acad Dermatol Venereol*. (2015) 29:2423–8. doi: 10.1111/jdv.13309
35. Kanthraj GR. Classification and design of teledermatology practice: what dermatoses? Which technology to apply? *J Eur Acad Dermatol Venereol*. (2009) 23:865–75. doi: 10.1111/j.1468-3083.2009.03136.x
36. Queille-Roussel C, Olesen M, Villumsen J, Lacour J. Efficacy of an innovative aerosol foam formulation of fixed combination calcipotriol plus betamethasone dipropionate in patients with psoriasis vulgaris. *Clin Drug Investig*. (2015) 35:239–45. doi: 10.1007/s40261-015-0269-7
37. Yazdanparast T, Yazdani K, Humbert P, Khatami A, Nasrollahi SA, Firouzabadi LI, et al. Biophysical measurements and ultrasonographic findings in chronic dermatitis in comparison with uninvolved skin. *Indian J Dermatol*. (2019) 64:90–6. doi: 10.4103/ijd.IJD_464_17
38. Polańska A, Dańczak-Pazdrowska A, Silny W, Wozniak A, Maksin K, Jenerowicz D. Comparison between high-frequency ultrasonography (Dermascan C, version 3) and histopathology in atopic dermatitis. *Skin Res Technol*. (2013) 19:432–7. doi: 10.1111/srt.12064
39. Gupta AK, Turnbull DH, Harasiewicz KA, Shum DT, Watteel GN, Foster FS, et al. The use of high-frequency ultrasound as a method of assessing the severity of a plaque of psoriasis. *Arch Dermatol*. (1996) 132:658–62. doi: 10.1001/archderm.1996.03890300076011
40. Polańska A, Silny W, Jenerowicz D, Knioła K, Molińska-Glura M, Dańczak-Pazdrowska A. Monitoring of therapy in atopic dermatitis- observations with the use of high-frequency ultrasonography. *Skin Res Technol*. (2015) 21:35–40. doi: 10.1111/srt.12153
41. Osmola-Mańkowska A, Polańska A, Silny W, Zaba R, Adamski A, Dańczak-Pazdrowska A. Topical tacrolimus vs medium-dose ultraviolet al phototherapy in the treatment of atopic dermatitis—a preliminary study in relation to parameters of the epidermal barrier function and high-frequency ultrasonography. *Eur Rev Med Pharmacol Sci*. (2014) 18:3927–34.
42. Dańczak-Pazdrowska A, Polańska A, Silny W, Sadowska A, Osmola-Mańkowska A, Czarnecka-Operacz M, et al. Seemingly healthy skin in atopic dermatitis: observations with the use of high-frequency ultrasonography, preliminary study. *Skin Res Technol*. (2012) 18:162–7. doi: 10.1111/j.1600-0846.2011.00548.x
43. Polańska A, Dańczak-Pazdrowska A, Silny W, Jenerowicz D, Olek-Hrab K, Osmaola-Mańkowska A. Nonlesional skin in atopic dermatitis is seemingly healthy skin - observations using noninvasive methods. *Wideochir Inne Tech Maloinwazyjne*. (2013) 8:192–9. doi: 10.5114/wiitm.2011.33633
44. Polańska A, Osmola-Mańkowska A, Olek-Hrab K. Do we need high-frequency ultrasonography in mycosis fungoides? *Abstract Book* P1065, EADV 2016 Vienna.
45. Mandava A, Koppula V, Wortsman X, Catalano O, Alfageme F. The clinical value of imaging in primary cutaneous lymphomas: role of high resolution ultrasound and PET-CT. *Br J Radiol*. (2019) 92:20180904. doi: 10.1259/bjr.20180904
46. Olek-Hrab K, Silny W, Dańczak-Pazdrowska A, Osmola-Mańkowska A, Sadowska A, Polańska A, et al. Ultraviolet A1 phototherapy for mycosis fungoides. *Clin Exp Dermatol*. (2013) 38:126–30. doi: 10.1111/ced.12001
47. Polańska A, Bowszyc-Dmochowska M, Olek-Hrab K, Adamski Z, Zaba R, Dańczak-Pazdrowska A. High-frequency ultrasonography a new quantitative method in evaluation of skin lymphomas-first comparative study in relation to histopathology. *Skin Res Technol*. (2019) 25:720–4. doi: 10.1111/srt.12708
48. Polańska A, Dańczak-Pazdrowska A, Olek-Hrab K, Osmola-Mańkowska A, Bowszyc-Dmochowska M, Zaba R, et al. High-frequency ultrasonography-new non-invasive method in assessment of skin lymphomas. *Skin Res Technol*. (2018) 24:517–21. doi: 10.1111/srt.12450
49. Lacarrubba F, Dini V, Napolitano M, Venturini M, Caposiena Caro DR, Molinelli E, et al. Ultrasonography in the pathway to an optimal standard of care of hidradenitis suppurativa: the Italian Ultrasound Working Group experience. *J Eur Acad Dermatol Venereol*. (2019) 33:10–4. doi: 10.1111/jdv.15847

50. Wortsman X. Imaging of hidradenitis suppurativa. *Dermatol Clin*. (2016) 34:59–68. doi: 10.1016/j.det.2015.08.003
51. Nazzaro G, Passoni E, Guanziroli E, Casazza G, Muratori S, Barbareschiet M, et al. Comparison of clinical and sonographic scores in a cohort of 140 patients with hidradenitis suppurativa from an Italian referral centre: a retrospective observational study. *Eur J Dermatol*. (2018) 28:845–7.
52. Witkowski A, Łudzik J, Soyer P. Telediagnosis with confocal microscopy: a reality or a Dream? *Dermatol Clin*. (2016) 4:505–12. doi: 10.1016/j.det.2016.05.013

Conflict of Interest: The authors declare that the research was conducted in the absence of any commercial or financial relationships that could be construed as a potential conflict of interest.

frontiers in Medicine

ORIGINAL RESEARCH
published: 24 February 2021
doi: 10.3389/fmed.2021.649438

Imaging of Vulva Syringoma With Reflectance Confocal Microscopy

Lin Feng[1], Yan Lin[2], Leilei Wang[3], Hongxiao Chen[4], Min Gao[3], Huaxu Liu[2] and Hongyu Yang[5]*

[1] Chongqing Hospital of Traditional Chinese Medicine, Chongqing, China, [2] Shandong Provincial Institute of Dermatology and Venereology, Shandong First Medical University & Shandong Academy of Medical Sciences, Jinan, China, [3] Shandong Cancer Hospital and Institute, Shandong First Medical University & Shandong Academy of Medical Sciences, Jinan, China, [4] Linyi People's Hospital, Linyi, China, [5] Department of Pathology, St. Vincent Evansville Medical Center, Evansville, IN, United States

Objectives: To investigate the application of reflectance confocal microscopy (RCM) imaging in diagnosis of vulva syringoma.

Methods: Patients with lesions suspicious of syringoma on vulva were enrolled in the study. After informed consent was taken, the lesions were photographed and imaged with RCM. The features of the lesion in confocal images were then analyzed and compared with the biopsy findings for histology correlation.

Results: Eleven cases in total were included in the study. The typical RCM features observed in syringoma are the presence of round to oval high refractive, and relatively monomorphous mass of varying sizes in the superficial and middle dermis, usually surrounded with 1–2 layers of light-dark line structures, which were further confirmed by histological evaluation. Ten cases showed classic features of syringoma and 1 case exhibited milia in RCM images.

Conclusions: Syringoma has distinct features in RCM imaging, which correlates well with histological findings, highlighting the potential role of RCM in the diagnosis and differential diagnosis of vulva syringoma.

Keywords: *in vivo* imaging, reflectance confocal microcopy, vulva, syringoma, histology, differential diaenosis

OPEN ACCESS

Edited by:
Yong Cui,
China-Japan Friendship Hospital, China

Reviewed by:
ZhiQiang Yin,
Nanjing Medical University, China
Irina Khamaganova,
Pirogov Russian National Research Medical University, Russia

****Correspondence:***
Min Gao
gmlhx@163.com

Specialty section:
This article was submitted to Dermatology, a section of the journal Frontiers in Medicine

Received: *04 January 2021*
Accepted: *03 February 2021*
Published: *24 February 2021*

Citation:
Feng L, Lin Y, Wang L, Chen H, Gao M, Liu H and Yang H (2021) Imaging of Vulva Syringoma With Reflectance Confocal Microscopy. Front. Med. 8:649438. doi: 10.3389/fmed.2021.649438

INTRODUCTION

Syringoma is a benign sweat gland tumor derived from eccrine ducts and it occurs predominantly in women at puberty or later in life (1). The typical lesions of syringoma present as multiple, small, firm, skin-colored papules, usually 1–3 mm in diameter, and symmetrically distributed on the periorbital region (1, 2). Although the most common site of localized involvement is periorbital, syringoma in other areas have also been reported, including the vulva, penis, palms, scalp, and axillae (2, 3). The classification criterion of syringoma proposed by Friedman and Butler (4) was based on clinical features and consists of 4 variants: localized, familial (5), a form associated with Down Syndrome (DS), and a generalized variant, including multiple and eruptive syringoma (6).

The characteristics of lesions on the eyelids and forehead can be easily identified, while lesions in other areas especially on the vulva were not easily identifiable and the definitive diagnosis was usually made by histological examination. However, the invasive biopsy procedure for histology analysis reduced the compliance of the patients with suspicious vulva lesions, therefore developing a

non-invasive skin imaging modality in the diagnosis and differential diagnosis of syringoma seems more appealing to potential patients.

The reflectance confocal microscopy (RCM) is a non-invasive skin imaging modality with high "cellular" resolution (7), which could compare the cellular changes of epidermis and superficial dermis *in vivo* in real time, and its accuracy is comparable with the histological evaluation of syringoma. In this study, we investigated the role of RCM in the diagnosis of vulva syringoma.

PATIENTS AND METHODS

The study had been approved by Ethics Committee of Shandong Cancer Hospital and Institute and was conducted from 2018 to 2019. Cases with lesions suspicious of syringoma on vulva (**Figures 1a**, **2a**, **3a**, **4a**) were enrolled in the study. After written informed consent was signed, the lesions were photographed and imaged by a commercially available, reflectance mode confocal microscope (Vivascope 1500; Caliber Imaging & Diagnostics, Inc. formerly Lucid, Inc., Rochester, NY, USA). The captured horizontal images in a 500 × 500 μm field, and viva-block image of 3 × 3 mm at different layers were obtained. A detailed description of the technique and the device has been published previously (7, 8). After imaging with RCM, the same lesions were biopsied and fixed in phosphate-buffered neutral formalin, embedded in paraffin, and stained with hematoxylin-eosin (HE), then analyzed using an optical microscope to investigate the accuracy of RCM imaging.

RESULTS

A total of 11 female adults were enrolled in the study (**Table 1**). The average age of the cases was 30.5 years old, and the average duration of the lesion was 17 months.

On clinical examination, multiple small, light brown papules are scattered in the vulva area (**Figures 1a**, **2a**, **3a**, **4a**), or in a "beaded" distribution along the outer margin of labia Majora. The main characteristics of lesions from the patients observed

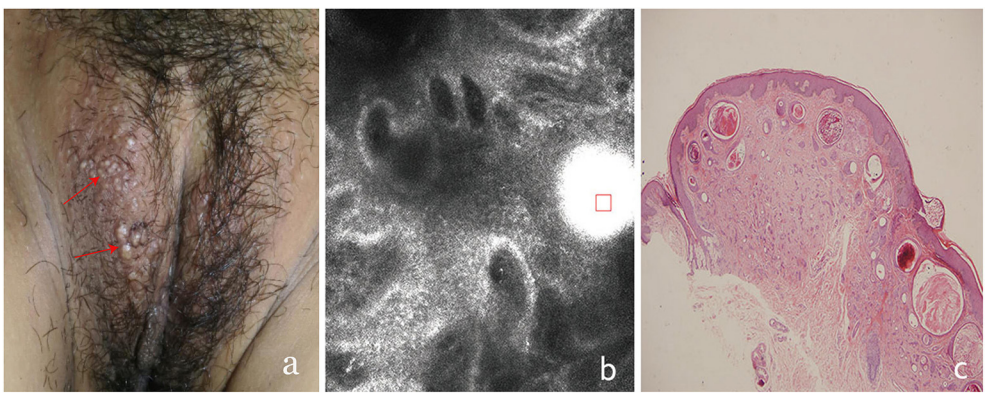

FIGURE 1 | The clinical presentation, RCM findings and histology of vulva syringoma (case 1). **(a)**, the clinical image of case 1, **(b)**, the RCM image findings; **(c)**, the histology findings. The presence of round to oval high refractive, and relatively monomorphous mass of varing sizes (the red square)was prensent in the superficial dermis, with 1–2 layers of surrounding light-dark line structure (red arrowhead) in **(b)**.

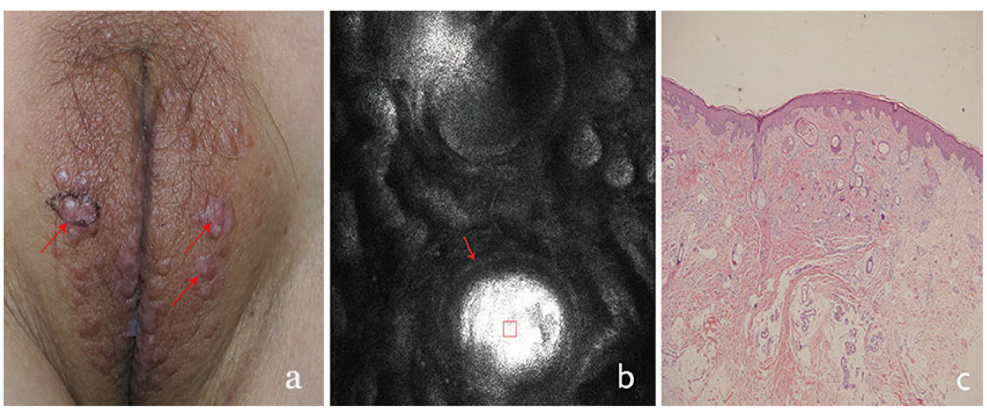

FIGURE 2 | The clinical presentation, RCM findings and histology of vulva syringoma (case 2). **(a)**, the clinical image of case 2, **(b)**, the RCM image findings; **(c)**, the histological findings. The presence of round to oval high refractive, and relatively monomorphous mass of varing sizes (the red square) was present in the superficial dermis, with 1–2 layers of surrounding light-dark line structure (red arrowhead) in **(b)**.

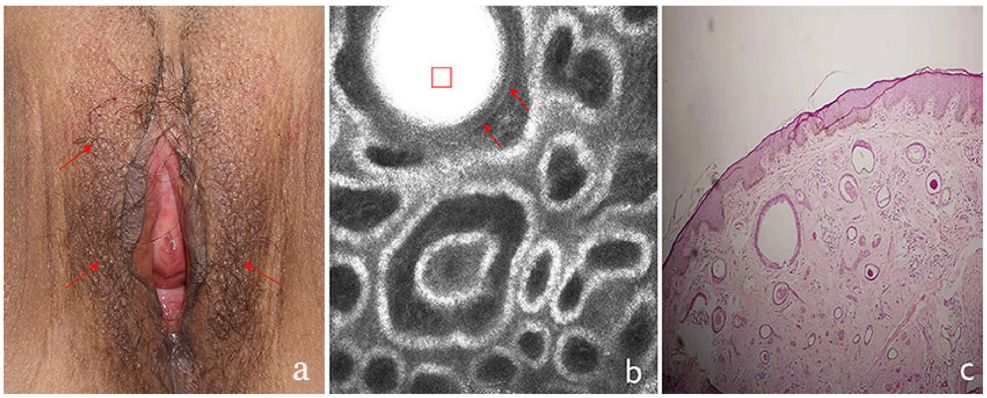

FIGURE 3 | The clinical presentation, RCM findings and histology of vulva syringoma (case 3). **(a)**, the clinical image of case 3, **(b)**, the RCM image findings; **(c)**, the histological findings. The presence of round to oval high refractive, and relatively monomorphous mass of varing sizes (the red square)was present in the upper dermis, with 1–2 layers of surrounding light-dark line structures (red arrowhead)in **(b)**.

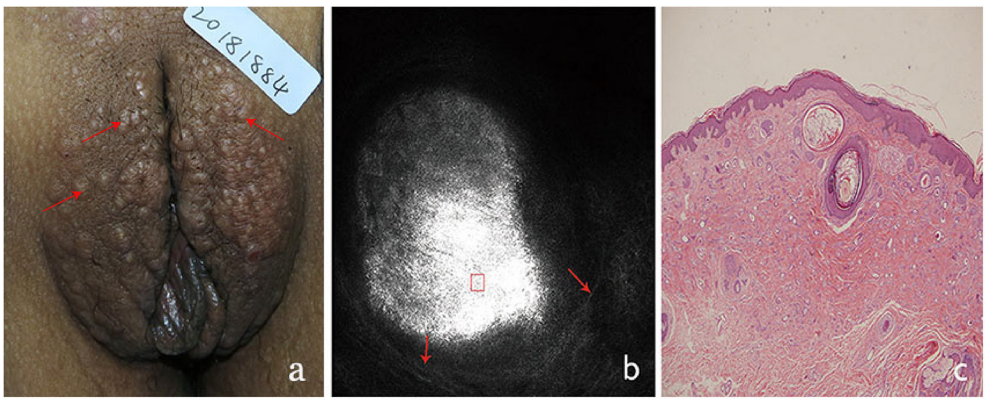

FIGURE 4 | The clinical presentation, RCM findings and histology of vulva syringoma (case 4). **(a)**, the clinical image of case 4, **(b)**, the RCM image findings; **(c)**, the histological findings.

TABLE 1 | The age and medical history of the patients enrolled in the study.

Case number	Age	Medical history (month)	RCM imaging (+ or –)	Histology results (+ or –)
1	23	12	+	+
2	32	16	+	+
3	44	20	+	+
4	21	30	+	+
5	32	23	+	+
5	34	14	+	+
7	25	11	+	+
8	27	17	+	+
9	28	9	+	+
10	31	13	+	+
11	39	22	-(milia)	-(milia)
Average	30.5	17		

+ with significant changes of syringoma in RCM or histology images.
– other changes.

by RCM were very similar. There were no significant cellular changes in superficial epidermis, and the keratinocytes appeared regular and small, and the architectural pattern of the honeycomb was similar with the peri-lesional normal skin. Deeper level imaging showed brighter keratinocytes in the basal cell layer in lesional zone and the melanin contents in the basal cell layer were also increased compared with the adjacent normal skin.

The most characteristic changes were observed in the upper and middle dermis. Evenly distributed varying sizes of round to oval structures show high refractive mass with surrounding light-dark lines (**Figures 1b**, **2b**, **3b**, **4b**). In comparison, there was just mild to moderate refracted collagen in upper and middle dermis in adjacent non-lesional areas.

The definitive histological diagnoses were all confirmed by biopsy finding in all cases studied, which show classic findings of syringoma with superficial to mid-dermal nests of eccrine ducts and tadpole-like structures embedded in fibrous stroma. clear cell changes of epithelial cells were occasional present. The ductal lumina are filled with an amorphous, periodic

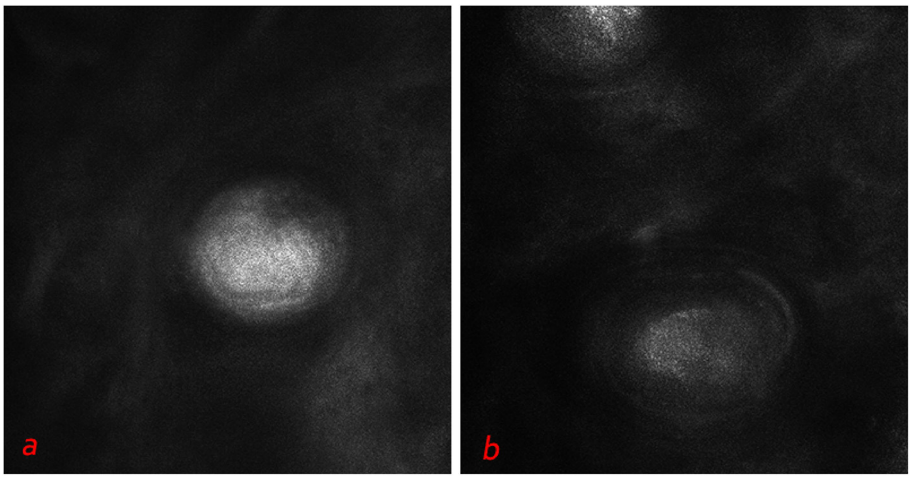

FIGURE 5 | Deeper level imaging of syringoma of vulva area **(a,b)** showed that the refraction of the round structures tends to be slightly decreased as they go deep.

acid-Schiff-positive material (**Figures 1c**, **2c**, **3c**, **4c**), Deeper level imaging showed that the refraction of the round structures tends to be slightly decreased as they go deep (**Figures 5a,b**).

DISCUSSION

Syringoma occurs more frequently in adult female with distinct histopathologic features (1, 2). In cases with characteristic clinical presentation, syringoma can be easily diagnosed clinically. For lesions on unusual sites such as the genital area, the clinical manifestation was usually atypical. They need to be confirmed by biopsy and histological diagnosis. However, the invasive biopsy procedure would reduce the compliance of the patients, and a non-invasive method for the diagnosis and differential diagnosis of syringoma on vulva sites is definitely sought after by various medical professionals.

The application of dermoscopy imaging in diagnosis of syringoma has been reported and dermoscopy may contribute to the imaging diagnosis of syringoma by revealing multiple bright cystic enlargements in dermis (9). While comparing with dermoscopy, RCM provides more details of those lesions studied with more sensitivity and specificity.

The RCM is also non-invasive and dynamically shows the cellular-level morphology in human skin *in vivo* (7, 10). Imaging is based on the detection of single back scattered photons from the optical section and contrast due to the relative variations in refractive indices and sizes of organelles and micro-structures (7). The cellular changes of the lesion in epidermis and superficial dermis could be imaged and compared with that of the adjacent normal skin. The RCM had been widely used in the screening of skin tumors, such as melanoma (10, 11), basal cell carcinoma (12), and actinic keratosis (13). In recent years, the RCM was reported to be useful in the diagnosis, differential diagnosis, and follow-up of pigmented and inflammatory skin disorders (14, 15) with high sensitivity and specificity.

The typical changes of syringoma are in mostly confined to superficial and mid-dermis, which is in the imaging depth of RCM. And we found the presence of round to oval, high refractile, and relatively evenly distributed substances of varying sizes in the superficial and mid-dermis with surrounding light-dark line structures based on RCM imaging to be characteristic for synringomas, which were confirmed by histology results. The well-demarcated high refractile substances noted in confocal image correlate with the amorphous, periodic acid-Schiff-positive material in the ductal lumina in histological findings, while the surrounding 1–2 layers of light-dark line structures seen in confocal images correlate with the lining epithelial cells and myoepithelial cells seen in histological images.

Vulva areas can be affected by many papular skin lesions, which should be differentiated from syringoma, those entities include milia, Fox-Fordyce disease, epidermal cysts, lichen planus, and lichen simplex chronicus (9, 16, 17). The confocal images of milia showed relatively high refractile, but unevenly distributed keratin in superficial dermis (18), which is more superficial compared with syringoma in confocal image findings. The major difference between syringoma and milia in confocal images is the "evenly" refractile substance in dermis and the presence of surrounding 1–2 layers of light and dark lines noted in the former and not present in the latter (18). Our observations are all confirmed with the histological findings. As to other cutaneous adnexal tumors, the RCM could also detect the changes around the follicles and cellular changes in epidermis and superfical dermis, which is useful in the screening and differential diagnosis of those lesions.

A recent case report of syringoma considered the dark areas surrounded by rims of epithelia as the characteristic of syringoma based on RCM findings (19). They interpreted the encircling hollow dark areas as lumina. However, in our study, we identified the round to oval, high refractile, and relatively monomorphous substances of varying sizes in the superficial and middle dermis to represent lumina. And future studies with a larger sample size coupled with histological analysis is needed to confirm our findings.

Our preliminary study showed the novel features of syringoma in RCM imaging, which could be useful as a non-invasive "*in*

vivo" tool in the screening and differential diagnosis of suspicious vulva syringomatous lesions. The appropriate clinical application of RCM or other skin imaging methods will potentially reduce the invasive biopsy procedure and related medical cost, and in the end benefit the patients.

DATA AVAILABILITY STATEMENT

The raw data supporting the conclusions of this article will be made available by the authors, without undue reservation.

ETHICS STATEMENT

The studies involving human participants were reviewed and approved by The ethic committe of Shandong Provincial Hospital for Skin Diseases. The patients/participants provided their written informed consent to participate in this study.

AUTHOR CONTRIBUTIONS

LF, YL, and LW collected the cases and che clnical and RCM data. HC collected the histology data. MG and HL designed the study and prepared the manuscript. HY revised the manuscript. All authors contributed to the article and approved the submitted version.

FUNDING

This work was supported by national key scientific instruments and equipment development program of China (2016YFF0101606), Science and Technology Department of Shandong province (2018GSF118030), Shandong Medical, Health Science and Technology Development Plan Project (2018WSA18036) annd clinical research training program of Shanndong Cancer Hospital (2020).

REFERENCES

1. Ghanadan A, Khosravi M. Cutaneous syringoma: a clinicopathologic study of 34 new cases and review of the literature. *Indian J Dermatol.* (2013) 58:326. doi: 10.4103/0019-5154.113956
2. Williams K, Shinkai K. Evaluation and management of the patient with multiple syringomas: a systematic review of the literature. *J Am Acad Dermatol.* (2016) 74:1234–40. doi: 10.1016/j.jaad.2015.12.006
3. Ciarloni L, Frouin E, Bodin F, Cribier B. Syringoma: a clinicopathological study of 244 cases. *Ann Dermatol Venereol.* (2016) 143:521–8. doi: 10.1016/j.annder.2015.06.025
4. Friedman S, Butler D. Syringoma presenting as milia. *J Am Acad Dermatol.* (1987) 16:310–14. doi: 10.1016/S0190-9622(87)70041-3
5. Lau J, Haber RM. Familial eruptive syringomas: case report and review of the literature. *J Cutan Med Surg.* (2013) 17:84–8. doi: 10.2310/7750.2012.12027
6. Soler-Carrillo J, Estrach T, Mascaró JM. Eruptive syringoma: 27 new cases and review of the literature. *J Eur Acad Dermatol Venereol.* (2001) 15:242–6. doi: 10.1046/j.1468-3083.2001.00235.x
7. Rajadhyaksha M, Marghoob A, Rossi A, Halpern AC, Nehal KS. Reflectance confocal microscopy of skin *in vivo*: from bench to bedside. *Lasers Surg Med.* (2017) 49:7–19. doi: 10.1002/lsm.22600
8. Liu H, Lin Y, Nie X, Chen S, Chen X, Shi B, et al. Histological classification of melasma with reflectance confocal microscopy: a pilot study in Chinese patients. *Skin Res Technol.* (2011) 17:398–403 doi: 10.1111/j.1600-0846.2011.00517.x
9. Corazza M, Borghi A, Minghetti S, Ferron P, Virgili A. Dermoscopy of isolated syringoma of the vulva. *J Am Acad Dermatol.* (2017) 76:S37–S9. doi: 10.1016/j.jaad.2016.06.009
10. Farnetani F, Manfredini M, Longhitano S, Chester J, Shaniko K, Cinotti E, et al. Morphological classification of melanoma metastasis with reflectance confocal microscopy. *J Eur Acad Dermatol Venereol.* (2019) 33:676–85. doi: 10.1111/jdv.15329
11. Uribe P, Collgros H, Scolyer RA, Menzies SW, Guitera P. *In vivo* reflectance confocal microscopy for the diagnosis of melanoma and melanotic macules of the lip. *JAMA Dermatol.* (2017) 153:882–91. doi: 10.1001/jamadermatol.2017.0504
12. Couzan C, Cinotti E, Labeille B, Vercherin P, Rubegni P, Cambazard F, et al. Reflectance confocal microscopy identification of subclinical basal cell carcinomas during and after vismodegib treatment. *J Eur Acad Dermatol Venereol.* (2018) 32:763–7. doi: 10.1111/jdv.14650
13. Peppelman M, Nguyen KP, Hoogedoorn L, van Erp PE, Gerritsen MJ. Reflectance confocal microscopy: non-invasive distinction between actinic keratosis and squamous cell carcinoma. *J Eur Acad Dermatol Venereol.* (2015) 29:1302–9. doi: 10.1111/jdv.12806
14. Ardigo M, Agozzino M, Franceschini C, Lacarrubba F. Reflectance confocalmicroscopy algorithms for inflammatory and hair diseases. *Dermatol Clin.* (2016) 34:487–96. doi: 10.1016/j.det.2016.05.011
15. Cinotti E, Perrot JL, Labeille B, Cambazard F. Reflectance confocal microscopy for cutaneous infections and infestations. *J Eur Acad Dermatol Venereol.* (2016) 30:754–63. doi: 10.1111/jdv.13254
16. Heller DS. Benign tumors and tumor-like lesions of the vulva. *Clin Obstet Gynecol.* (2015) 58:526–35. doi: 10.1097/GRF.0000000000000133
17. Naveen KN, Pai VV, Sori T. Syringoma masquerading as steatocystoma multiplex. *Indian J Dermatol Venereol Leprol.* (2012) 78:365–6. doi: 10.4103/0378-6323.95458
18. Gao M, Lin Y, Wang L, Yu Y, Zhou Y, Chen S, et al. The differential diagnosis of syringoma and milia based on the imaging of reflectance confocal microscopy. *Skin Res Technol.* (2020) 26:951–3. doi: 10.1111/srt.12879
19. Jiménez MR, Rocchetto H, Ferreira PS, Sangueza M, Lourenço SV, Nico MMS. Evaluation of syringomas by *in vivo* reflectance confocal microscopy: a report of two cases. *Am J Dermatopathol.* (2017) 39:845–8. doi: 10.1097/DAD.0000000000000751

Conflict of Interest: The authors declare that the research was conducted in the absence of any commercial or financial relationships that could be construed as a potential conflict of interest.

frontiers in Medicine

MINI REVIEW
published: 04 March 2021
doi: 10.3389/fmed.2021.644327

Convolutional Neural Network for Skin Lesion Classification: Understanding the Fundamentals Through Hands-On Learning

*Marta Cullell-Dalmau[1], Sergio Noé[1], Marta Otero-Viñas[2], Ivan Meić[1,3] and Carlo Manzo[1]**

[1] The QuBI Lab, Facultat de Ciències i Tecnologia, Universitat de Vic – Universitat Central de Catalunya, Vic, Spain, [2] Tissue Repair and Regeneration Laboratory, Facultat de Ciències i Tecnologia, Universitat de Vic – Universitat Central de Catalunya, Vic, Spain, [3] University of Zagreb, Zagreb, Croatia

Deep learning architectures for the classification of images have shown outstanding results in a variety of disciplines, including dermatology. The expectations generated by deep learning for, e.g., image-based diagnosis have created the need for non-experts to become familiar with the working principles of these algorithms. In our opinion, getting hands-on experience with these tools through a simplified but accurate model can facilitate their understanding in an intuitive way. The visualization of the results of the operations performed by deep learning algorithms on dermatological images can help students to grasp concepts like convolution, even without an advanced mathematical background. In addition, the possibility to tune hyperparameters and even to tweak computer code further empower the reach of an intuitive comprehension of these processes, without requiring advanced computational and theoretical skills. This is nowadays possible thanks to recent advances that have helped to lower technical and technological barriers associated with the use of these tools, making them accessible to a broader community. Therefore, we propose a hands-on pedagogical activity that dissects the procedures to train a convolutional neural network on a dataset containing images of skin lesions associated with different skin cancer categories. The activity is available open-source and its execution does not require the installation of software. We further provide a step-by-step description of the algorithm and of its functions, following the development of the building blocks of the computer code, guiding the reader through the execution of a realistic example, including the visualization and the evaluation of the results.

Keywords: convolutional neural networks, skin lesion analysis, classification, melanoma, deep learning

OPEN ACCESS

Edited by:
Je-Ho Mun,
Seoul National University Hospital, South Korea

Reviewed by:
Luis Puig,
Autonomous University of Barcelona, Spain
Philippe Lefrançois,
McGill University, Canada

****Correspondence:***
Carlo Manzo
carlo.manzo@uvic.cat

Specialty section:
This article was submitted to Dermatology, a section of the journal Frontiers in Medicine

Received: *20 December 2020*
Accepted: *10 February 2021*
Published: *04 March 2021*

Citation:
Cullell-Dalmau M, Noé S, Otero-Viñas M, Meić I and Manzo C (2021) Convolutional Neural Network for Skin Lesion Classification: Understanding the Fundamentals Through Hands-On Learning. Front. Med. 8:644327. doi: 10.3389/fmed.2021.644327

INTRODUCTION: BACKGROUND AND RATIONALE FOR THE EDUCATIONAL ACTIVITY INNOVATION

Over the last two decades, convolutional neural networks (CNNs) (1) have become established as an invaluable tool for biomedical image classification and have been proposed as an instrument for clinical diagnosis in disciplines such as radiology, histology, ophthalmology, and dermatology (2).

The rapid spread of CNNs and other deep learning techniques, has created the need for non-experts to become familiar with these complex tools and understand their principles of

operation. There is a broad literature of introductory articles offering basic reviews on CNNs principles and applications. However, on the practical side, tutorials to start working with CNNs often require a familiarity with terms and concepts that could discourage readers without a solid background in mathematics and/or computer programming to obtain a further understanding of these techniques.

In this scenario, we aim to close this gap by offering a hands-on activity based on the step-by-step execution of a computer code involving all the procedures carried out when implementing a CNN classification, along with their description. Similar educational activities have been recently proposed for other research fields (3). The activity guides the student through two complete examples based on images of skin lesions, starting from the pre-processing of the dataset, and leading through the steps of data augmentation, the choice of the network architecture and its fine-tuning, until the final evaluation of the results.

In our opinion, this hands-on activity can help students to obtain an intuitive understanding of the operations performed by the CNN building blocks, e.g., by visualizing the effect of image convolution with a specific kernel, the feature map generated at specific network layers, or even by performing the network training and exploring the effect of different hyperparameters on the results. The activity can be performed at different levels of difficulty, depending on the user expertise in programming. At the basic level of execution, the students can interactively play with the different sections just by changing input parameters from simple form fields and can run the program by pushing the play button, without even visualizing the code. At the intermediate/advanced levels, students can unfold cells to show, read and (possibly) modify portions of the code. In both cases, the use of the Google Colab and GitHub platforms allows to run the activity in the cloud from any internet browser, without any software installation, strongly simplifying configuration requirements and enabling the capability to use hardware accelerators.

PEDAGOGICAL FRAMEWORK AND LEARNING ENVIRONMENT

We aimed at developing a hands-on activity mainly directed to students (medical school, biomedical engineering), but with the potential of being of interest also for clinicians and other professionals willing to get acquainted with deep learning and CNNs. Four major developments make such a learning-by-doing experience nowadays possible, even for non-experts. First, the creation of specific software libraries, which have reduced the complexity and length of the code necessary to implement these networks, thus allowing their use to operators with a basic knowledge of computer programming. Secondly, the distribution of pre-trained classical CNN under license for reuse has enabled the possibility to perform transfer learning further simplifying the coding and speeding up the training. Third, the free availability of cloud computing on virtual machines with graphics (GPUs) and tensor processing units (TPUs), which has played an important role in speeding up training procedures. The last development of note is the accessibility of databases containing labeled images for training.

Along these lines, for the proposed activity we use Keras (4), an open-source framework developed by Francois Chollet. Several open-source frameworks are nowadays available for deep learning such as PyTorch or Caffe. However, Keras is recommended for beginners since it is relatively easy to use and has a high-level API that permits to build complex models by writing a few lines of code. In addition, Keras has several models of the best performing architecture (Alexnet, ResNet, VGGNet, Inception, etc.) pre-trained on large datasets (e.g., the one used for the ImageNet Large Scale Visual Recognition Challenge (ILSVRC, http://image-net.org) containing millions of photographs from 1,000 categories) that have thus achieved very general classification capabilities. These trained networks can be "reconverted" to the classification of different target images in few simple steps and their learnable parameters (weights and biases) are fine-tuned to provide high classification accuracy, through a procedure called transfer learning.

The code for the activity is provided on the Google Colaboratory platform (Colab, https://colab.research.google.com/notebooks/intro.ipynb). Colab is a free cloud service that enable coding in Python and program execution in a web browser, in a highly interactive fashion. In addition, it requires a minimum number of configuration steps, offers free access to GPUs and TPUs, and allows sharing of contents in a straightforward manner. The notebooks and metadata necessary for the activity are shared on GitHub (www.github.com), a free hosting service for software development and version control.

Deep learning requires a massive amount of information in the form of labeled images. Several repositories contain high-quality images associated to dermatology, available as research tools in clinical training and computer science. For example, the archive of the International Skin Imaging Collaboration (ISIC, https://isic-archive.com/), or the Edinburgh Dermofit Library (https://licensing.edinburgh-innovations.ed.ac.uk/i/software/dermofit-image-library.html) host images of skin lesions, labeled according to their diagnoses. For the activity, we use images from the dataset that has been recently made available for the training of methods competing for the ISIC 2019 challenge (https://challenge2019.isic-archive.com), a competition aimed at supporting research toward automated melanoma detection. The full dataset contains 25,331 images of skin lesions associated to 8 different diagnostic categories (melanoma, melanocytic nevus, basal cell carcinoma, actinic keratosis, benign keratosis, dermatofibroma, vascular lesion, and squamous cell carcinoma) and can be accessed by registering to the ISIC website.

DESCRIPTION OF THE HANDS-ON ACTIVITY

The files to perform the activity are stored on the GitHub public repository https://github.com/qubilab/CNN-for-skin-lesion-classification. The two links, associated to examples of a binary (benign/malignant) and a multiclass (melanoma/melanocytic

nevus/basal cell carcinoma/actinic keratosis/benign keratosis/dermatofibroma/vascular lesion/squamous cell carcinoma) classification of images of skin lesions, automatically redirect to the respective Colab notebooks.

For the basic use of the notebook, no configuration is needed. For applications requiring hardware accelerators (e.g., training or fine-tuning), GPU or TPU can be enabled by picking the required accelerator from the menu that appears by selecting Runtime/Change runtime type.

For a better pedagogical support, the notebook is organized in consecutive sections, each with a brief explanation of the task performed, that guide the user steps-by-step along the activity. To execute the code in a cell, it is sufficient to select it with a click and then either press the play button within the cell box or use the keyboard shortcut "Command/Ctrl+Enter." For more advanced applications, the visualization of input form fields or code is achieved by unfolding the cell content, by clicking on the little arrowhead at the left of the cell, thus enabling the necessary editing.

Image Pre-processing and CNN Basics

The first cell "0. Imports" gives access to the code provided in other modules and libraries and defines some basic functions. Once this operation has been performed, we enter into the core of the activity. In fact, since most of the deep learning approaches are data-driven, a major focus must be set on the dataset and its organization. The cell "1. Loading and organizing the dataset" loads the labeled images on the Colab cloud space and arrange them into folders (**Figure 1A**). The first block of this section requires the input of user credential to login on the ISIC archive and the selection of the number of images per category. The photographs will then be organized into folders according to their category and further randomly split into training, validation, and test sets. A variable percentage of images (10–30%) can be used for the final testing, whereas the others are split between training (70–80%) and validation. The folder tree can be visualized in the left frame of Colab, by selecting "Files." In the example, we use percentages of 65, 20, and 15% of the total number of images for training, validation and test, respectively. These percentages can be changed by the user through the form fields of block 1.3.

The cell "2. Understanding images and convolution" allows the user to visualize an image from a selected folder, together with its decomposition into layers according to RGB color model and the representation of the pixel intensity value. To provide an intuitive understanding of the principle of CNN, the activity shows different convolution kernels and their pixel values. The convolution of the image with these kernels is further provided. An introductory description of the convolution and of the hyperparameters of a convolutional layer can be found in our previous article (5).

Often, the limited amount of data available for training might produce the memorization of specific details of the training images, leading to overfitting and the inability of the model to generalize. In this case, it is recommendable to perform a procedure called data augmentation. The augmentation generates modified images by applying random transformations, such as rotation, shift, scaling, and reflection, to existing data (**Figure 1B**). Typically, the computer function used for augmentation also takes care of resizing the images to the input size required by the network. These steps can be visualized on a random image by executing the cell "3. Data augmentation."

CNN Selection

Once the data have been obtained and properly organized, the following step entails the choice of the classification network. In principle, users could build their own network by assembling it layer-by-layer. Application program interfaces allow one to create a CNN from scratch relatively easily. However, this is generally not recommended for beginners, since it requires some background knowledge, a good dose of intuition, and some trial and error. Moreover, unless one is facing a new and very specific image classification task, a personalized CNN is often not needed: many popular deep learning architectures are released under a permissive license for reuse. Even in the case that it is essential to build a custom model, classic networks might still serve as an inspiration, a scaffold, or as a block of the new model. Nowadays, several networks offering outstanding performance for image classification are available, therefore choosing the most suitable CNN for one's application is not straightforward. Since these CNNs have been originally built for applications on different datasets, the selection should be based on their performance on the target dataset and thus requires their evaluation and comparison (6).

ResNet-50

We use the CNN ResNet-50 (7). ResNet architectures were developed by the Microsoft Research team (7) and are available in several versions with different number of layers, such as 50, 101, 152 (https://github.com/KaimingHe/deep-residual-networks). Notably, the ResNet-152 won the 1st places in all the sections of the ILSVRC and COCO (http://cocodataset.org/#detection-2015) competitions in 2015. Pre-trained ResNet architectures have been frequently used for the classification of skin lesions, even by several participants to ISIC challenges (8–12).

A schematic representation of the architecture and functions of ResNet-50 is shown in **Figure 2**. **Figure 2A** shows examples of feature maps obtained at specific layers. Moreover, the code of the hands-on activity displays the feature map for any selected layer of the CNN (cell "8.5 Visualize features generated at a specific layer"). **Figure 2B** contains a scheme of the layers and the connections of the network. **Figure 2C** shows the effect of the application of specific operations (convolution, batch normalization, activation and maxpooling) on an image.

As shown in **Figure 2A** and in cell "2. Understanding images and convolution," an image is a collection of two-dimensional matrices (channels) which elements (pixels) have numeric values representing the brightness in each channel. Color images are composed of multiple channels (e.g., 3 for the RGB representation) whereas grayscale images only have one. The application of the network over an input image, produces its progressive transformation into a larger number of features with smaller lateral dimensions. Eventually, the features are combined to obtain a set of scalar values with the same dimension of the

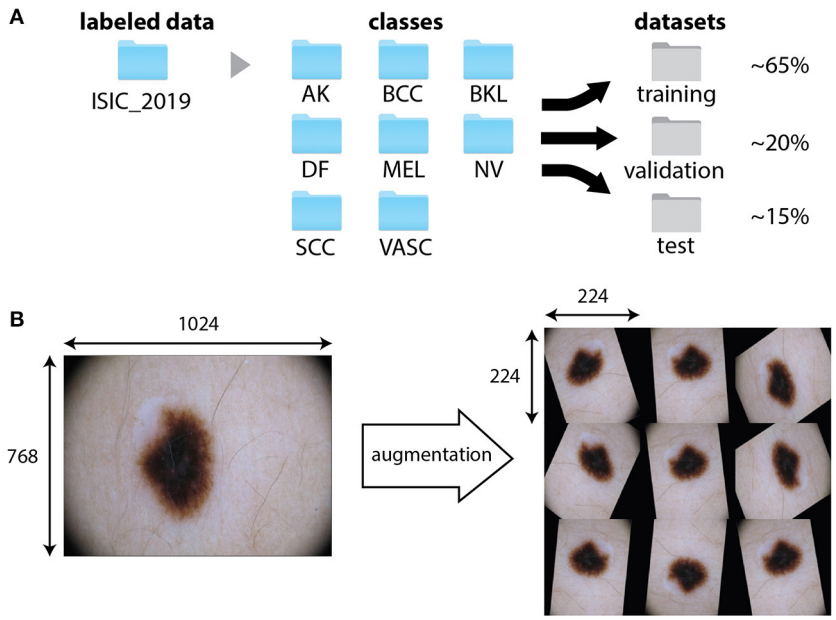

FIGURE 1 | Data pre-processing and augmentation. **(A)** Example of the organization of the training dataset ISIC 2019. Images are first divided into folders associated to the different categories. A specific function split them randomly into training, validation and test datasets. **(B)** An original image from the training dataset ISIC 2019 (class NV) and possible outputs of the application of the augmentation procedure, consisting in combinations of random shift, rotation, and reflection. The data augmentation function resizes the images to fit the input size of the network (224 × 224 × 3).

output categories. This is achieved through the repetition of mathematical operations performed by the layers and depending on a large number of learnable parameters.

The input is first processed by a convolutional layer. Convolution is a mathematical operation involving the input image and a kernel, typically a matrix with smaller lateral dimensions with respect to the input. During CNN training, kernels are randomly generated and each kernel produces a different feature. Convolution is performed by sequentially shifting the kernel along the input image by a fixed number of pixels, called stride. At each step, the sum of the element-by-element multiplication between overlapping pixels returns the pixel value of the convolutional feature. In cell "2. Understanding images and convolution" the output provided by different kernels can be interactively explored. It must be pointed out that a stride larger than one can be used to obtain features with reduced lateral size with respect to the input.

The first convolutional layer of the ResNet-50 uses 64 kernels of 7 × 7 pixels^2 with a stride of 2 pixels and thus produces 64 features with half the lateral size of the input image (**Figure 2**). The features are regularized through a batch normalization layer (**Figure 2C**), that performs the standardization of the input, corresponding to the subtraction of the mean of the batch and the division by the standard deviation. The convolutional and batch normalization layers are generally followed by an activation function that performs a non-linear transformation of the feature map, providing the input for the next convolutional layer. Non-linear functions (like sigmoid or hyperbolic tangent) are used as activation functions for their similarity to the behavior of real neurons, i.e., the transformation of a continuous input into a digital output. The most widely used function is the rectified linear unit (ReLU). The ReLU performs a simple calculation: it returns the same value provided by the input if the input is positive. However, if the input value is negative or null, it returns zero. Inputs that are converted to zero constitute non-activated neurons. In this way, not all neurons are firing simultaneously. The sparse activation and the simpler mathematical operation guarantee a higher computational efficiency for ReLU as compared with other non-linear functions.

The batch normalization and the activation layers preserve the lateral size of features obtained at the output of the convolution layer. However, it is often recommendable to create a lower resolution version (downsampling) of the output image to reduce the number of parameters and account for variations in the position of features in the input image. A common approach is to use a pooling layer, which substitutes adjacent subregions of specific size with the sum, average or maximum values of the corresponding pixels. The ResNet-50 uses a maxpooling layer (**Figure 2C**) to downsample images by taking the maximum of the input over 3 × 3 regions.

Combinations of these layers are applied along the network, progressively reducing the lateral size from 224 × 224 to 7 × 7 and increasing the depth of the feature map from 3 (the RGB layers of the input image) to 2048. At this point, a group of three layers flattens the feature map, i.e., transforms it into a score vector with the same length as the number of categories. The values of elements of this vector correspond to the probability that the input image belongs to each category (**Figure 2B**) and

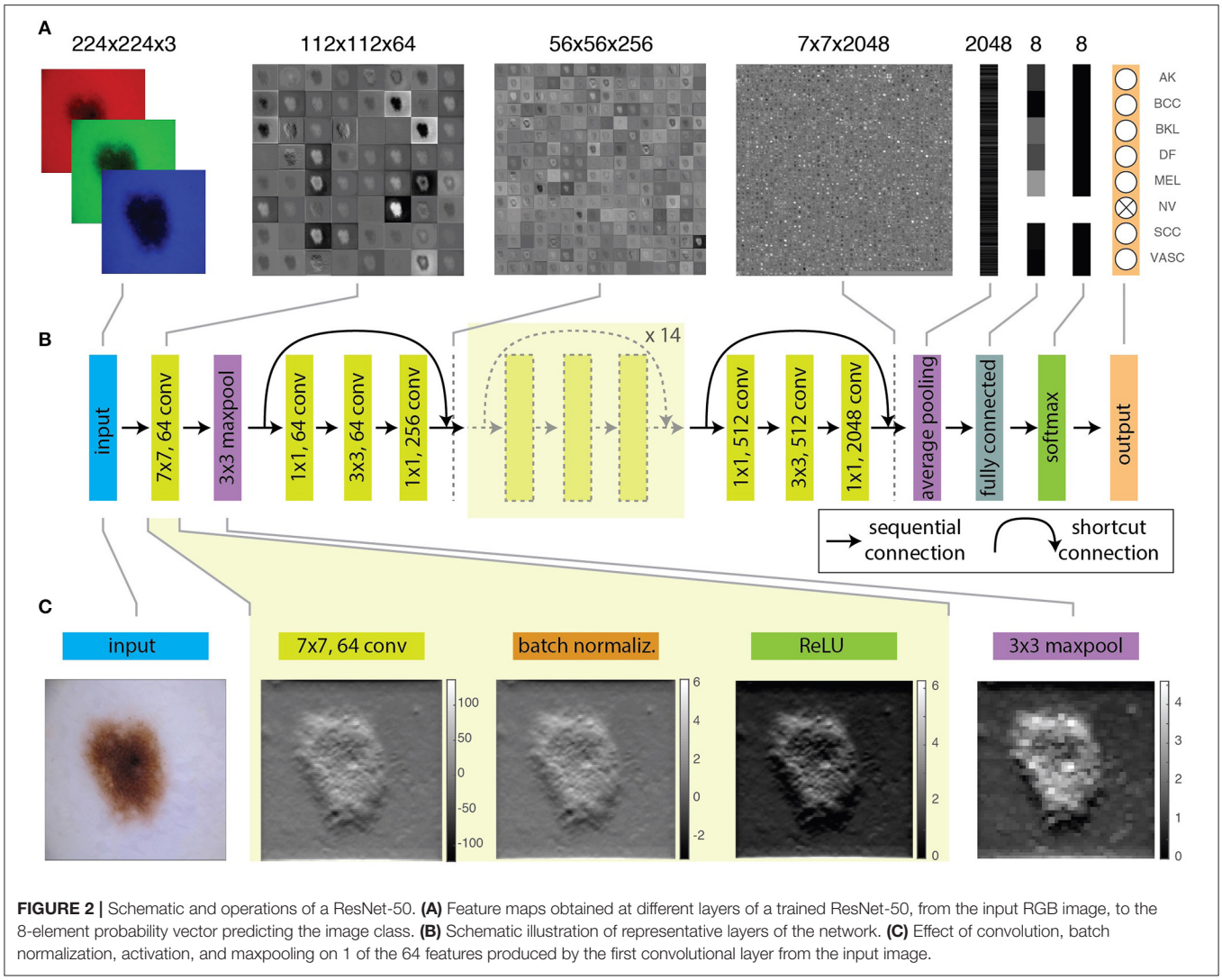

FIGURE 2 | Schematic and operations of a ResNet-50. **(A)** Feature maps obtained at different layers of a trained ResNet-50, from the input RGB image, to the 8-element probability vector predicting the image class. **(B)** Schematic illustration of representative layers of the network. **(C)** Effect of convolution, batch normalization, activation, and maxpooling on 1 of the 64 features produced by the first convolutional layer from the input image.

the maximum of this vector will correspond to the category assigned to the input image by the CNN. The first layer of the group performs a downsampling through average pooling, a pooling operation returning the mean of the region of the image considered. By using an average pooling over 7×7 regions, each of the 2048 features is thus reduced to a single value given by the average of all the pixels in the 7×7 map (**Figure 2A**).

The further reduction of the number of elements of the vector to a size equal to the number of categories is obtained through the fully connected layer. Each output value of this layer has a complete connection with all the 2048 inputs, as it is obtained as their weighted sum. The very last layer normalizes these values into the probabilities to belong to each labeled category. Usually, this task is performed through a softmax function that generalizes binary logistic regression to the case of a multiclass problem.

Training

Once the dataset is ready and the CNN has been chosen, it is possible to start the actual training of the network. During this procedure, values of the learnable parameters are randomly changed, and the corresponding features are calculated to provide a tentative classification of the images in the training set. The performance of the network is evaluated by the calculation of a metric (loss function) that quantifies the similarity between the prediction and the ground-truth. Parameters are iteratively adjusted to optimize the loss function and thus increase correct predictions.

However, as mentioned earlier, we need to distinguish between two different situations. The first refers to the case in which the network needs to be fully trained. In this case, the values of all the parameters of the network need to be learned from scratch. This procedure requires very large datasets, often not available for medical applications. However, the use of a classical network further enables the possibility of performing transfer learning: besides using the same architecture as a classical network, one can also take advantage of parameters learned by the previous training of the CNN on a different, larger dataset. In transfer learning, the parameters obtained from the training

of the model over a large dataset are only fine-tuned to adapt the network for the classification of a different target dataset. In this way, one can skip the time-consuming training steps but still take advantage of the features learned from the training over many photographs. As reported in (6), the top-performing methods submitted for ISIC challenges 2016, 2017, and 2018 used CNNs pre-trained on the ImageNet database. In cells 4–6, we perform these steps using the ResNet-50 pre-trained on the ImageNet dataset.

The ResNet-50 is designed for the ImageNet challenge and thus its output is composed of 1,000 categories. To use the ResNet-50 to classify skin lesion images among a different number of classes, it is first necessary to replace the last layers by ones providing an output over the desired number (2 or 8) of categories (**Figure 2B**). This procedure is performed in the section "4. The CNN: ResNet-50."

Hyperparameters

The CNN will learn weights and biases by minimizing the loss function over the training set using a method called stochastic gradient descent. However, due to the large size of the dataset and the limited memory, it is not possible to feed all the images simultaneously to the CNN. Therefore, training images are generally passed to the CNN in smaller groups called batches (cell 4.1). The optimum batch size must be set by trial and error in order to provide the fastest convergence. As a rule of thumb, small but not too small batch sizes (e.g., 32, 64, 128) are preferred, since they show higher accuracy than very large batches (13). The number of iterations necessary for the network to "see" the entire training dataset constitutes an epoch.

Another relevant hyperparameter is the global learning rate (cell 5.1), a number between 0 and 1 determining the step size used to update the weights at each iteration. The learning rate sets the speed at which the model is adjusted to the data. A low learning rate applies small changes to the weights at each update, thus requires more epochs of training. Although a high learning rate produces faster changes, if too high it might not converge to an optimal model. The correct learning rate should be empirically chosen to obtain convergence in a reasonable amount of time. Typically, the learning rate is not fixed but is progressively reduced during the optimization. Large rates are first used to quickly obtain values of the weights corresponding to a loss function close to its minimum. At that point, smaller rates further adjust the weights to better approximate the exact minimum of the loss function (cell 5.2). In addition, since in CNN the features provided by the early layers are more generic, whereas those belonging to the last layers are dataset specific, one can introduce non-uniform learning rates and either "freeze" the early layers or train the new layers at a faster rate with respect to the others (cell 5.1 and 5.3). Besides, several other hyperparameters need to be set in relation to the optimization procedure. In the activity, we adopt a procedure and use hyperparameters similar as those described in (11).

Optimization

The algorithm is now ready to start the optimization process, a procedure involving the minimization of a loss function that measure the distance between the predicted and the ground-truth classification. For classification tasks, the cross-entropy function is the usual choice (cell 5.4). The optimization will run until some convergence condition is met. This condition is set by the user based either on the value of accuracy/error calculated on the validation set, or on a maximum number of validations without improving the loss value (cell 5.2).

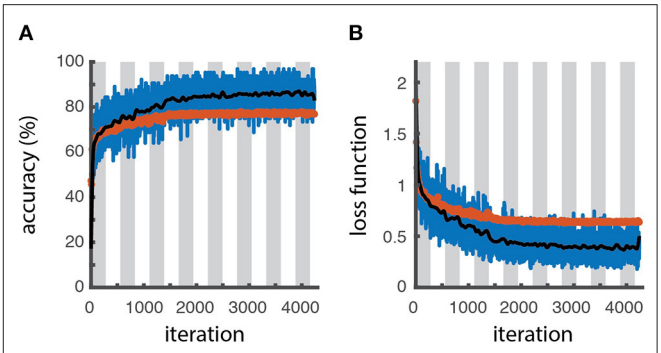

FIGURE 3 | Learning curves. Accuracy **(A)** and loss function **(B)** as a function of the number of iterations for the training batch (blue line for raw data, black line for filtered data) and validation sets (red symbols), as obtained through the optimization procedure. The white and gray areas delimit different epochs. The slightly higher accuracy and lower loss values obtained for the training dataset respect to the validation one reveals a slight overfitting.

The actual training is performed in section "6. Fine-tuning the model." The learning process can be visually monitored by displaying the trend of learning curves calculated from both the training and validation datasets as a function of algorithm iterations, to have an idea about how well the model is, respectively, learning and generalizing (defined in cell 5.5). Typically, plots of learning curves associated to optimization (e.g., cross-entropy loss) and performance (e.g., accuracy) are simultaneously created for both datasets (**Figures 3A,B**). The comparison of learning curves obtained for training and validation datasets is a valuable diagnostic method for the model behavior. A training loss showing a continuous decrease with a validation loss showing a minimum, in general correspond to an overfitting model. A good fit is usually associated with training and validation losses decreasing simultaneously toward closely spaced horizontal asymptotes (4). However, a higher accuracy (lower loss) of the training set with respect to the validation can still indicate some degree of overfitting, as obtained for the example shown in **Figures 3A,B**.

Since the training can sometimes run for quite a long time, in section "7. Load a trained network" we also provide a previously-trained model with weights. By loading this model, the user can perform the remaining part of the activity without having to wait for the completion of the training procedure.

Performance Evaluation

Once the learning phase is complete, the network can be finally applied to predict the class of the images contained in the test dataset, that were not used for the training. Since the ground-truth of these images is known, they can be used to calculate

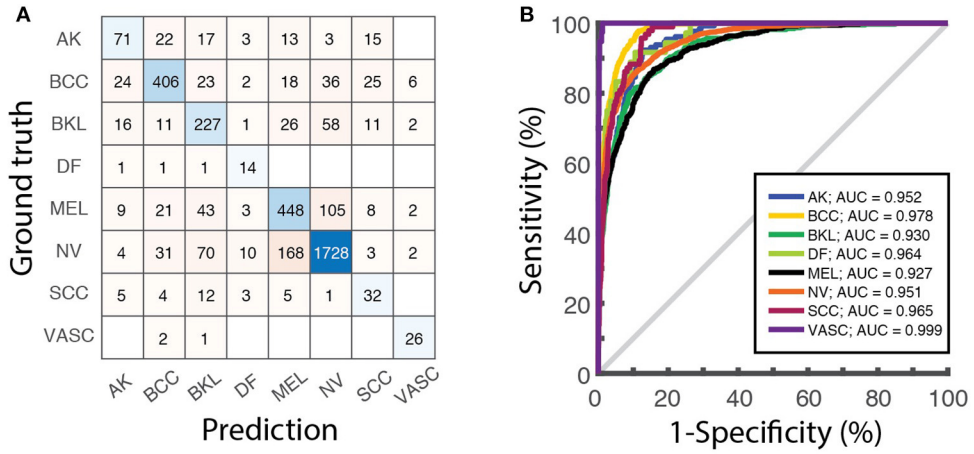

FIGURE 4 | Model evaluation over the test dataset. **(A)** Confusion matrix displaying the number of images of the test dataset associated to each category by the ResNet-50 network. **(B)** ROC curves obtained on the same dataset and the corresponding values of the AUC for each class.

metrics to assess the performance of the classifier (section "8. Performance assessment"). Besides the overall accuracy, the confusion matrix, reporting the number of correct and incorrect predictions over all the classes, (**Figure 4A**) visually summarize classification and mis-classification performance of the model. The evaluation of the model performance further includes the plot of the receiver operating characteristic (ROC) curves and the calculation of the area under the curve (AUC) for each category (**Figure 4B**), obtained as detailed in (5).

DISCUSSION AND CONCLUSIONS

We have developed a hands-on activity based on the interactive computer code and a detailed description of the steps needed to implement and fine-tune a CNN to perform the classification of dermatological images, together with an intuitive explanation, suitable for non-experts, of the functions performed by the main blocks of the network. The description is based on two practical examples, consisting of the fine-tuning of a pre-trained ResNet-50 network on a public dataset, containing images of skin lesions corresponding to different diagnoses. The use of *ad hoc* toolboxes and libraries largely simplifies the coding and makes it accessible to beginners.

In our opinion, the hands-on example, together with the description provided in this article, can act as a tool for students interested in obtaining a first understanding of the inner working of a CNN. However, the same activity can also be offered to provide a tutorial for beginners' initiation to computer programming for building and optimizing CNNs. In the first case, the code can be simply executed with the default parameters to visualize the output of each cell. The visualization of the results provides an intuitive understanding of CNN principles. As an example, plotting the feature maps obtained at consecutive layers allows comparing the changes introduced on the features by pooling, batch normalization and activation layers. In the second case, the user can further explore how modifications of the dataset and the change of hyperparameters affect the network's performance. Examples in this sense might involve the comparison of performance upon the change of learning rates (or even the freezing) of specific layers.

The use of an interactive hands-on activity reproducing a novel approach in its complexity might be a powerful strategy to approach the development of problem-solving and analytical skills, possibly through group work in the classroom. In addition, we believe that making this technology more accessible for non-expert will contribute to further strengthen the collaboration between dermatologists and computer scientists, toward the joint effort of improving image-based medical diagnosis.

AUTHOR CONTRIBUTIONS

CM and MC-D contributed to conception and design of the study. SN, IM, and CM wrote the code and performed analyses. MC-D wrote the first draft of the manuscript. CM wrote the final version of the manuscript. CM and MO-V supervised the research. All authors contributed to manuscript revision, read, and approved the submitted version.

FUNDING

CM gratefully acknowledges funding from FEDER/Ministerio de Ciencia, Innovación y Universidades – Agencia Estatal de Investigación through the Ramón y Cajal program 2015 (Grant No. RYC-2015-17896), and the Programa Estatal de I+D+i Orientada a los Retos de la Sociedad (Grant No. BFU2017-85693-R); from the Generalitat de Catalunya (AGAUR Grant No. 2017SGR940). CM also acknowledges the support of NVIDIA Corporation with the donation of the Titan Xp GPU. MO-V gratefully acknowledges funding from the PO FEDER of Catalonia 2014-2020 (project PECT Osona Transformació Social, Ref. 001-P-000382) and the Spanish Ministry of Science, Innovation, and Universities through the Instituto de Salud Carlos III-FEDER program (FIS PI19/01379). IM acknowledges the support of the Erasmus+ program of the European Union.

REFERENCES

1. LeCun Y, Haffner P, Bottou L, Bengio Y. Object recognition with gradient-based learning. In: *Shape, Contour and Grouping in Computer Vision Lecture Notes in Computer Science, vol 1681*. Berlin; Heidelberg: Springer (1999). p. 319–45. doi: 10.1007/3-540-46805-6_19
2. Litjens G, Kooi T, Bejnordi BE, Setio AAA, Ciompi F, Ghafoorian M, et al. A survey on deep learning in medical image analysis. *Med Image Anal*. (2017) 42:60–88. doi: 10.1016/j.media.2017.07.005
3. Erickson BJ. Magician's corner: how to start learning about deep learning. *Radiol Artif Intell*. (2019) 1:e190072. doi: 10.1148/ryai.2019190072
4. Chollet F. *Deep Learning with Python*. Shelter Island: Manning Publications Company (2018).
5. Cullell-Dalmau M, Otero-Viñas M, Manzo C. Research techniques made simple: deep learning for the classification of dermatological images. *J Invest Dermatol*. (2020) 140:507–14.e1. doi: 10.1016/j.jid.2019.12.029
6. Perez F, Avila S, Valle E. Solo or ensemble? Choosing a CNN architecture for melanoma classification. In: *Proceedings of the IEEE Conference on Computer Vision and Pattern Recognition Workshops*. Long Beach, CA (2019).
7. He K, Zhang X, Ren S, Sun J. Deep residual learning for image recognition. *Proc IEEE Comput Soc Conf Comput Vis Pattern Recognit*. (2016) 2016-Decem:770–8. doi: 10.1109/CVPR.2016.90
8. Gutman D, Codella NCF, Celebi E, Helba B, Marchetti M, Mishra N, et al. Skin lesion analysis toward melanoma detection. *In: A Challenge at the International Symposium on Biomedical Imaging (ISBI) 2016, hosted by the International Skin Imaging Collaboration (ISIC)* (2016). Available online at: https://arxiv.org/abs/1605.01397
9. Marchetti MA, Codella NCF, Dusza SW, Gutman DA, Helba B, Kalloo A, et al. Results of the 2016 international skin imaging collaboration international symposium on biomedical imaging challenge: comparison of the accuracy of computer algorithms to dermatologists for the diagnosis of melanoma from dermoscopic images. *J Am Acad Dermatol*. (2018) 78:270–7.e1. doi: 10.1016/j.jaad.2017.08.016
10. Codella NCF, Gutman D, Celebi ME, Helba B, Marchetti MA, Dusza SW, et al. Skin lesion analysis toward melanoma detection: a challenge at the 2017 International symposium on biomedical imaging (ISBI), hosted by the international skin imaging collaboration (ISIC). In: *2018 IEEE 15th International Symposium on Biomedical Imaging (ISBI 2018)*. New York, NY: IEEE (2018). p. 168–72.
11. Han SS, Kim MS, Lim W, Park GH, Park I, Chang SE. Classification of the clinical images for benign and malignant cutaneous tumors using a deep learning algorithm. *J Invest Dermatol*. (2018) 138:1529–38. doi: 10.1016/j.jid.2018.01.028
12. Codella N, Rotemberg V, Tschandl P, Celebi ME, Dusza S, Gutman D, et al. Skin lesion analysis toward melanoma detection 2018. In: *A Challenge Hosted by the International Skin Imaging Collaboration (ISIC)*. Washington, DC (2019).
13. Mishkin D, Sergievskiy N, Matas J. Systematic evaluation of convolution neural network advances on the Imagenet. *Comput Vis Image Underst*. (2017) 161:11–9. doi: 10.1016/j.cviu.2017.05.007

Conflict of Interest: The authors declare that the research was conducted in the absence of any commercial or financial relationships that could be construed as a potential conflict of interest.

frontiers in Medicine

ORIGINAL RESEARCH
published: 26 March 2021
doi: 10.3389/fmed.2021.649392

Female Pattern Hair Loss in Female and Male: A Quantitative Trichoscopic Analysis in Chinese Han Patients

Xi Chen[1,2], *Xiangqian Li*[1], *Baifu Chen*[1], *Yue Yin*[2], *Jianzhong Zhang*[1] *and Cheng Zhou*[1]*

[1] *Department of Dermatology, Peking University People's Hospital, Beijing, China,* [2] *Department of Dermatology, Beijing Tongren Hospital, Capital Medical University, Beijing, China*

Objectives: To investigate the trichoscopic features of female pattern hair loss (FPHL) in Chinese Han patients and analyze the difference between male and female patients with FPHL.

Materials and Methods: Trichoscopic images were taken in four different scalp areas, including right frontal hairline, vertex, right parietal and occipital areas. Hair density, hair shaft diameter, vellus hair ratio and single hair follicle unit ratio were counted manually and analyzed.

Results: Seventy-three subjects were enrolled in this study, including 38 patients with FPHL (28 females and 10 males) and 35 normal controls without hair loss. The hair density and hair shaft diameter of FPHL patients reduced in the whole scalp. Vellus hair ratio and single hair follicle unit ratio were both increased in FPHL compared to normal controls. The vertex was the most affected area and the hair shaft diameter showed the most significant difference. Parietal and occipital area were also affected in FPHL. The reduction or increase was correlated with the severity of Ludwig staging. Very few gender differences were detected in male and female FPHL patients.

Conclusion: FPHL patients showed decreased hair density and hair shaft diameter, accompanied by increased vellus hair ratio and single hair follicle unit ratio. Parietal and occipital area can be also affected in FPHL, though not as severe as in vertex area. FPHL in male basically has the same characteristic as those in female patients.

Limitation: The main limitation of the study is the small sample size which only enrolled 10 male FPHL patients, in comparison to the female cases. The findings could not be representative of the normal population with the limited sample size.

Keywords: hair, trichoscopy, female pattern hair loss, Chinese, gender

OPEN ACCESS

Edited by:
Yong Cui,
China-Japan Friendship Hospital, China

Reviewed by:
ZhiQiang Yin,
Nanjing Medical University, China
Simone Garcovich,
Catholic University of the Sacred Heart, Italy
Poonkiat Suchonwanit,
Mahidol University, Thailand

***Correspondence:**
Cheng Zhou
chengzhou@live.cn

Specialty section:
This article was submitted to Dermatology, a section of the journal Frontiers in Medicine

Received: *04 January 2021*
Accepted: *01 March 2021*
Published: *26 March 2021*

Citation:
Chen X, Li X, Chen B, Yin Y, Zhang J and Zhou C (2021) Female Pattern Hair Loss in Female and Male: A Quantitative Trichoscopic Analysis in Chinese Han Patients. Front. Med. 8:649392. doi: 10.3389/fmed.2021.649392

INTRODUCTION

Hair is one of the essential skin appendages in human. Thinning, damaging, or abnormal shedding of hair can not only impair the physical protection of scalp, but also affects mental health, and can even lead to severe social dysfunction. Androgenic alopecia (AGA) is the most common hair loss disease in the world, affecting both male and female. Rather than hair shedding, the process

of hair loss in AGA is related to the gradual miniaturization of hair follicles, and eventually, lead to progressive, symmetric baldness (1). Two major hair loss patterns have been widely described in AGA. Male pattern hair loss (MPHL) or named male pattern baldness (MPB) usually manifests as a recession of the frontal hairline, with or without baldness of the vertex area (2). In contrast, female pattern hair loss (FPHL) presents with diffuse hair loss over the middle scalp and show no recession of frontal hairline, mainly affecting women (3).

The nomenclature of male and female pattern hair loss still cause confusion nowadays. Since the pathological changes of hair follicles are similar, most researchers regarded MPHL and FPHL as two variants of the same entity with different clinical presentation and treatment response (3, 4). It is hypothesized that FPHL and MPHL share common susceptibility genes, but genetic studies have not identified any susceptibility locus/gene for FPHL and suggested the etiology differs substantially from that of MPHL (5, 6).

Dermoscopy can magnify the skin lesions while eliminating the reflected light on the skin surface, helping clinicians to fully grasp the characteristics of disease skin lesions. As a branch of dermatoscopy, trichoscopy is cost-efficient, quick, and non-invasive, now is of great significance to evaluate hair and scalp disorders (7). When using a digital dermoscope (trichoscope), dermatologists can easily collect images with higher magnification, then use computer software to analyze the image data, such as hair density and hair shaft diameter. Previous studies have shown that one of the main trichoscopic features of AGA is the increased heterogeneity of hair shaft diameter, which can be quantified by hair shaft diameter and the ratio of vellus hair (8). The increase of single hair follicle units is also a manifestation of hair follicle microminiaturization in AGA patients (9). Besides, yellow dots, brown/white peripilar sign, honeycomb pigmentation, and pinpoint white dots are other important trichoscopic features of AGA, which are potentially related to the severity of the disease (10–12).

In quantitative trichoscpic evaluation, previous studies have analyzed several hair parameters of FPHL in female patients and have come to the consistent conclusion that miniaturization of hair follicles is the characteristics of FPHL in female, which is shown as reduced hair density and hair shaft diameter under trichoscopy (7, 13–15). Hair density and hair shaft diameter are the most used indicators in quantitation evaluation, and the percentage of vellus hair ($< 30\,\mu m$) has also been involved in the studies mentioned above. However, few researches have evaluated the percentage of single-hair follicle units, which is also of significance in FPHL diagnoses (7). In contrast to MPHL, in which occipital and parietal (side of the head) areas are usually not involved, parietal and occipital sites can also be affected in FPHL (14). At present, there still lacks a comprehensive evaluation of all four main hair parameters involving multiple scalp areas (frontal, vertex, parietal, and occipital areas) in FPHL.

Although FPHL is usually used to describe AGA in women, it can also be observed in a proportion of men (16, 17). With an overall AGA prevalence of 21.3% in Chinese male, 3.7% of the male patients showed FPHL type of hair loss (18). However, the trichoscopic feature of FPHL in male patients have not been well-studied yet (4). It is unclear whether the trichoscopic features of FPHL in male and female are the same or not.

In this study, we investigated the quantitative features of FPHL with digital trichoscope, and compared to the normal controls without hair loss. The differences between male and female FPHL patients were also analyzed.

MATERIALS AND METHODS

Subjects

Both male and female Chinese Han subjects aged 18–59 years old who visited the dermatology department of Peking University People's hospital from January to August in 2020 were recruited into the study. The participants were screened by two experienced trichologists and categorized in two groups. The FPHL cases were diagnosed according to the Ludwig classification, with diffuse balding process and retention of the frontal hairline (3). The group of normal scalp subjects comprised volunteers who visited the dermatology clinic with complaints except for hair and scalp related diseases. The exclusion criteria included (1) presence of male pattern hair loss, alopecia areata, telogen effluvium, or other hair/scalp disorders; (2) positive results of hair-pull test; (3) history of anemia, thyroid disease, nutritional deficiency, autoimmune disease, or other systemic disease; (4) history of hair-loss treatment within 6 months; (5) hair coloring or perming within 3 months prior to the study; and (6) history of hair restoration surgery or scalp micropigmentation. All participants are agreed to participate in the study and provided written informed consent. The study was approved by the ethics committee of Peking University People's Hospital.

Trichoscopy and Analysis

Due to the symmetrical hair loss feature of FPHL, trichoscopy was performed in four regions, i.e., right frontal hairline, vertex, right parietal and occipital area, using a polarized contact dermoscope (Fotofinder body studio ATBM, FotoFinder Systems GmbH, Bad Birnbach, Germany). The measurement point of each area is shown in **Figures 1a–d**: (1) the top of right frontotemporal angle (marked as "frontal"); (2) the mid-point of the connection of the left and right external auditory ear canals ("vertex"); (3) 6 cm from the external ear canal on the right side of the participants ("parietal"); (4) the occipital carina ("occipital"). The lateral scalp is divided into three parts by hair transplant surgeons: temporal (anterior one-third), parietal (middle one-third), and occipital (posterior one-third). The measurement area of the lateral scalp used in this study may be called "temporal" or "temporoparietal" in some other previous researches; however, we named this point as "parietal" due to its anatomical location above the parietal bone.

In each area, one 20-fold and four 50-fold figures were taken. All the parameters were all manually measured in Trichoscale 3.0 software Smart Count (Fotofinder Universe 2019, Bad Birnbach, Germany). Hairs and hair follicle units in each 50-fold trichoscopic figure were noted and counted by clicking the mouse, which was conducted by two experienced trichologists. Hair shaft diameter was measured by mouse pointing and

FIGURE 1 | Measuring points of trichoscopy in frontal **(a)**, vertex **(b)**, parietal **(c)** and occipital **(d)** area.

dragging vertically from one edge of the hair shaft to the other edge, and the average value was calculated.

Statistical Analysis

Statistical analysis was done using SPSS software (IBM, 25.0, CA, USA). Narrative statistics described the basic characteristics of the population. Independent-sample *t*-tests and Chi-square tests were performed to test the significance between the FPHL patients and the normal subjects. Kruskal-Wallis *H*-tests, Mann-Whitney *U*-tests and Fisher's exact tests were performed to compare results between groups whose data did not subject to normal distribution. The results of the analysis were presented as mean ± standard deviation (SD), and a $p < 0.05$ was considered significant.

PASS 2019 software (NCSS LLC., Kaysville, U.T., USA) was used to calculate the sample size. The primary outcomes of this study are vertex hair density, hair-shaft diameter, vellus hair ratio and single hair follicle unit ratio of normal and FPHL patients. To detect the lowest mean difference of 15 with standard deviations of 19.0 and 11.0 between the two groups with a two-sided 0.0125% significance level (adjusted for multiple comparisons using Bonferroni method) and a power of 90%, a sample size of 33 for each group is needed, at last, 35 normal people and 38 FPHL people were enrolled in this study.

RESULTS

The participants were subdivided into two groups of 35 normal subjects and 38 FPHL patients based on the clinical diagnosis. The FPHL patients are graded following the Ludwig classification, from L1 to L3. The particular distribution of participants is shown in **Table 1**. The mean age of normal subjects and FPHL patients were 31.40 ± 10.38 and 31.08 ± 8.82 years old, respectively. No significant difference has been detected between normal and FPHL subjects. The typical clinical images of FPHL patients and trichoscopic images in vertex area of both FPHL and normal subjects are shown in **Figure 2**. The values of mean hair density, hair shaft diameter, vellus hair ratio and single hair follicle unit ratio at different scalp sites of FPHL patients are summarized in **Tables 2**, **3**, and the parameters of normal male and female are shown in **Table 4**.

Hair Density

The mean hair density at different scalp areas of our participants is shown in the first part of **Tables 2**–**4**. The hair density in parietal area was the lowest in both FPHL and normal participants, and in vertex area, all groups show the highest hair density (**Tables 2**, **3**). When compared to the normal subjects, the hair density in FPHL patients tended to reduce and statistically significant differences were detected in all scalp areas, especially in vertex area ($p < 0.0001$). However, no gender difference of hair density was detected in FPHL patients (**Table 3**), though the hair density in parietal area of male normal subjects was significantly lower than female (**Table 4**).

Hair Shaft Diameter

The second part of **Tables 2**–**4** has shown the mean hair shaft diameter of male and female participants. In normal participants, the hair of the frontal area was the thinnest, while in the FPHL patients the vertex area showed the lowest hair shaft diameter (**Table 2**). The hair shaft diameter of FPHL patients decreased in the whole scalp with statistically significant differences compared to normal. The highest reduction of hair shaft diameter of FPHL patients was detected in the vertex area ($p < 0.0001$). No gender difference was detected whether in patients or normal (**Tables 3**, **4**).

Vellus Hair Ratio

The vellus hair ratio is shown in the third part of **Tables 2**–**4**. The frontal area had the highest vellus hair ratio and the lowest ratio was found in occipital area in both FPHL and normal participants. The vellus hair ratio showed a tendency of increase in FPHL patients when compared to normal, and significant differences were detected in all scalp areas (**Table 2**). In vertex area, the vellus hair ratio also showed the highest increase ($p < 0.0001$). In FPHL patients, minor gender difference in vellus hair ratio were detected in parietal area, though no difference was shown between normal male and female participants (**Tables 3**, **4**).

Single Hair Follicle Unit Ratio

The single hair follicle ratio is shown in the last part of **Tables 2**–**4**. Similar to the vellus hair ratio, the frontal area had the highest single hair follicle ratio and the lowest ratio was found in occipital area in both FPHL and normal participants (**Table 2**). All four areas in FPHL patients showed statistical significance compared to the normal subjects, and the vertex area still had the top decrease among other scalp areas ($p < 0.0001$). There

TABLE 1 | Distribution of participants by hair loss status.

Classification		Male		Female		Total	
		n	Age (year)	*n*	Age (year)	*n*	Age (year)
FPHL	Ludwig L1	4	24.75 (± 3.43)	15	30.13 (± 7.96)	19	29.00 (± 7.51)
	Ludwig L2	4	29.75 (± 7.14)	9	35.78 (± 12.81)	13	33.92 (± 11.43)
	Ludwig L3	2	34.00 (± 1.41)	4	30.25 (± 5.44)	6	31.50 (± 4.68)
	Total	10	28.60 (± 5.89)	28	31.96 (± 9.59)	38	31.08 (± 8.21)
Normal		17	29.76 (± 11.02)	18	32.94 (± 9.79)	35	30.40 (± 10.38)
p-value		/	0.786	/	0.752	/	0.769

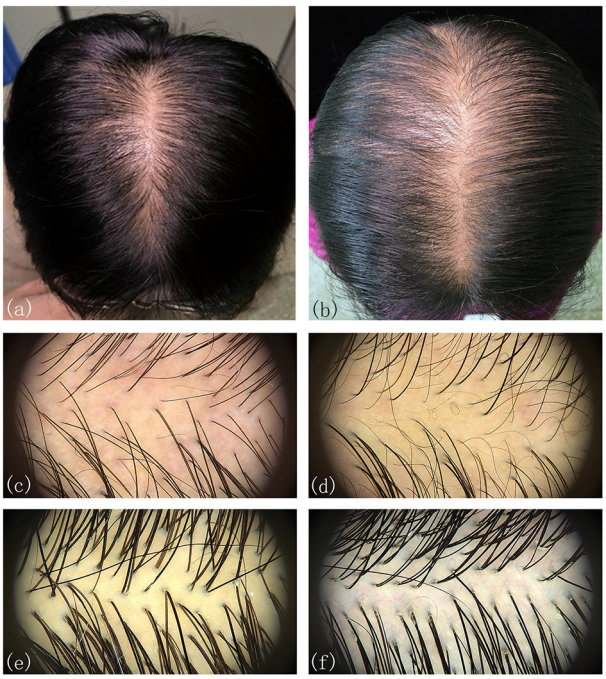

FIGURE 2 | Typical clinical and trichoscopic feature (vertex) of male FPHL **(a,c)** and female FPHL **(b,d)** patients, compared with normal male **(e)**, and female **(f)**.

was no gender difference in both normal and FPHL participants (**Tables 3**, **4**).

Hair Parameters From Grade L1 to L3 in FPHL Patients

We then analyzed the hair parameters of different severity in FPHL patients. According to the FPHL disease severity, patients were stratified into three groups (Ludwig L1-L3). In all scalp areas, the hair density and hair shaft diameter showed a decreasing tendency with the aggravation of the disease, and the ratio of vellus hair in and single hair follicle unit all raised as the disease got worse. Compared with normal group, the significant difference of the parameters was mainly found in vertex area (**Figure 3**) and in L2 and L3 groups. In L1 group, only the hair shaft diameter and vellus hair ratio of vertex area were significantly different with normal subjects.

DISCUSSION

According to our quantitative trichoscopic analysis, FPHL involved the whole scalp, especially at the vertex area, and primarily manifested as a decrease in hair shaft diameter. All of the four hair parameters including hair density, hair shaft diameter and the ratio of vellus hair and single hair follicle unit, have changed in our FPHL patients when compared to normal, confirmed that the miniaturization of hair follicle is the characteristics of FPHL. Similar to previous research, our study also showed that the involvement of parietal and occipital area is an additional important feature of FPHL (7, 13–15). This pattern of hair involvement is quite different from MPHL. The parietal and occipital parts are usually not involved in MPHL patients, and therefore occipital and even parietal parts are appropriate donor sites for hair transplantation (19). Thus, when consulting hair transplantation with FPHL patients, it should be fully considered that the hair may be abnormal in the whole scalp, and a comprehensive examination should be carried out. Medical treatment of parietal or occipital area is also necessary if the region has been involved. Besides, the frontal area was also involved slightly even though no receding of hairline was observed clinically.

The changes of the hair parameters were correlated with the severity of the disease, from Ludwig grade 1 to 3 (**Figure 3**), and the vertex area was the most severely affected area. In the early stage of disease (L1), significant decreases in hair shaft diameter had been detected and the vellus hair ratio also increased significantly. Although not as severe as the vertex area, all the parameters of parietal and occipital area also showed significant difference in the advanced stages of the disease (L2 and L3).

Though FPHL in male has been described previously (20), studies on the clinical features are extremely limited, especially on trichoscopic features. During a retrospective study of 2,140 male AGA patients, only 84 (3.9%) patients were diagnosed as FPHL (17).

FPHL in male has similar clinical manifestations as FPHL in female, showing diffuse scalp hair loss with no obvious

TABLE 2 | Hair parameters of FPHL patients and normal subjects.

Scalp area	Hair density (/cm^2)			Hair shaft diameter (μm)			Vellus hair ratio (%)			Single hair follicle unit ratio (%)		
	FPHL	Normal	*p*-value	FPHL	Normal	*p*-value	FPHL	Normal	*p*-value	FPHL	Normal	*p*-value
Frontal	102.89 (± 20.19)	117.07 (± 21.49)	0.010*	55.71 (± 8.83)	61.73 (± 6.92)	0.001*	22.00 (± 7.88)	16.89 (± 6.43)	0.003*	47.43 (± 16.82	35.78 (± 15.53)	0.005*
Vertex	112.05 (± 25.56)	140.21 (± 23.91)	<0.001*	54.23 (± 9.08)	67.38 (± 7.59)	<0.001*	20.92 (± 9.74)	9.26 (± 4.59)	<0.001*	39.69 (± 18.38	18.86 (± 11.37)	<0.001*
Parietal	85.18 (± 27.48)	96.19 (± 21.63)	0.028*	59.91 (± 10.02)	67.62 (± 8.30)	0.001*	16.68 (± 10.71)	10.72 (± 5.68)	0.001*	34.66 (± 18.26	17.89 (± 11.60)	<0.004*
Occipital	106.66 (± 22.94)	127.18 (± 22.7)	<0.001*	60.78 (± 10.31)	68.34 (± 7.70)	<0.001*	15.04 (± 8.2)	8.88 (± 4.23)	0.004*	28.32 (± 16.6)	13.47 (± 8.74)	<0.001*

*$p < 0.05$.

TABLE 3 | Comparisons of hair parameters in FPHL patients between male and female.

Scalp area	Hair density (/cm^2)			Hair shaft diameter (μm)			Vellus hair ratio (%)			Single hair follicle unit ratio (%)		
	Male	Female	*p*-value	Male	Female	*p*-value	Male	Female	*p*-value	Male	Female	*p*-value
Frontal	92.79 (± 21.29)	106.5 (± 18.87)	0.060	52.05 (± 8.29)	57.02 (± 8.79)	0.088	22.49 (± 5.74)	21.82 (± 8.6)	0.782	49.89 (± 24.29)	46.54 (± 13.71)	0.935
Vertex	113.1 (± 28.84)	111.68 (± 24.85)	0.883	53.23 (± 9.49)	54.59 (± 9.08)	0.636	18.15 (± 7.76)	21.91 (± 10.29)	0.302	38.3 (± 20.87)	40.18 (± 17.81)	0.807
Parietal	77.28 (± 10.14)	88.00 (± 31.14)	0.142	64.72 (± 9.63)	58.19 (± 9.74)	0.194	11.89 (± 8.35)	18.39 (± 11.07)	0.044*	34.32 (± 17.36)	34.78 (± 18.88)	0.568
Occipital	95.78 (± 16.38)	110.55 (± 23.92)	0.101	61.08 (± 11.32)	60.68 (± 10.14)	0.732	14.32 (± 8.39)	15.29 (± 8.27)	0.568	33.45 (± 20.65)	26.48 (± 14.9)	0.368

*$p < 0.05$.

TABLE 4 | Hair parameter of normal male and female subjects.

Scalp area	Hair density (/cm^2)			Hair shaft diameter (μm)			Vellus hair ratio (%)			Single hair follicle unit ratio (%)		
	Male	Female	*p*-value	Male	Female	*p*-value	Male	Female	*p*-value	Male	Female	*p*-value
Frontal	114.34 (± 24.12)	119.63 (± 19.01)	0.546	62.68 (± 5.04)	60.82 (± 8.37)	0.318	16.75 (± 5.98)	17.01 (± 6.99)	0.910	39.32 (± 16.40)	14.31 (± 8.37)	0.258
Vertex	137.63 (± 25.44)	142.63 (± 22.82)	0.503	68.03 (± 8.37)	66.74 (± 7.30)	0.590	9.00 (± 3.38)	9.49 (± 5.58)	0.752	18.86 (± 10.90)	18.87 (± 12.10)	0.909
Parietal	85.82 (± 17.23)*	105.98 (± 21.14)	0.004*	69.81 (± 7.51)	65.54 (± 8.67)	0.195	11.79 (± 5.18)	9.71 (± 6.09)	0.286	21.02 (± 13.64)	14.94 (± 8.68)	0.130
Occipital	127.51 (± 27.53)	126.87 (± 17.79)	0.883	68.96 (± 8.61)	67.75 (± 6.91)	0.443	10.07 (± 4.83)	7.72 (± 3.30)	0.105	15.83 (± 9.78)	7.20 (± 6.91)	0.163

*$p < 0.05$.

recession of the frontal hairline (21). Compared with female patients in the present study, we found the hair parameters changed in male FPHL patients are similar to that in female FPHL patients. Importantly, in male FPHL patients, parietal and occipital area can also be involved, which pattern is totally different from MPHL. Therefore, in our experience, diagnosing these male FPHL patients as MPHL or MPB is not appropriate. We suggested that FPHL in male or female should be diagnosed based on different hair loss patterns and trichoscopic alterations, rather than on the basis of gender alone. It is important to establish a classification for assessment and grading of parietal and occipital involvement, which could overcome the limitations in the Ludwig classification, the Sinclair scale and the basic and specific (BASP) classification (3, 22, 23). Oral finasteride 1 mg/day is effective in the majority of male patients with AGA, while in female FPHL patients it could not significantly slow hair thinning, increase hair growth or improve the appearance of the hair unless increasing the dose to 2.5–5 mg/day (24, 25). Whether available treatments for male FPHL patients could be as efficacy as in MPHL is unclear, and further treatment studies on male FPHL patients are needed. This study provides some evidence for clarifying the term of FPHL in male and is of great value for further study on its pathogenesis, treatment, and the similarities and differences with MPHL.

The two parameters, hair density and hair shaft diameter, are trichoscopic features that need precisely quantitative measurement, which might not be practical for daily diagnostics purposes. In our experience, vellus hair ratio and single hair follicle unit ratio are more likely to be perceived and estimated under trichoscopy without quantitative measurements, which are more valuable in clinical practice.

During the progressive and unsynchronized miniaturization of hair follicles in AGA, terminal hairs are gradually replaced by intermediate hair and vellus hairs. Although the relevant quantitative research is relatively limited, researchers have long agreed that hair shaft thickness heterogeneity of more than 20% is a hallmark of AGA, which means that vellus hair percentage for more than 20% of all the hairs in the same view (10, 12). In our study, the vellus hair ratio of FPHL in frontal and vertex areas were both over 20%. In the parietal and occipital area of the FPHL scalp, vellus hair ratio also increased, but not as much as 20%. The present values appear to be similar to the previous study of Caucasian women (9). Mai et al. has also used "terminal/vellus hair ratio" to describe the vellus hair percentage in their study, and we found our results were basically consistent with each other after conversion (15). According to the hair involvement characteristics of FPHL, evaluation of vellus hair ratio should be established on different parts of the scalp.

Hair exists in the form of follicular units on the scalp. The hair follicle unit, also known as the pilosebaceous gland unit, is composed of 1–5 hairs, erect hair muscles, sebaceous glands, and peripheral nerves and blood vessels. Guo et al. indicated that the hair follicle unit types found in healthy Han Chinese are dominated by 2-hair follicle

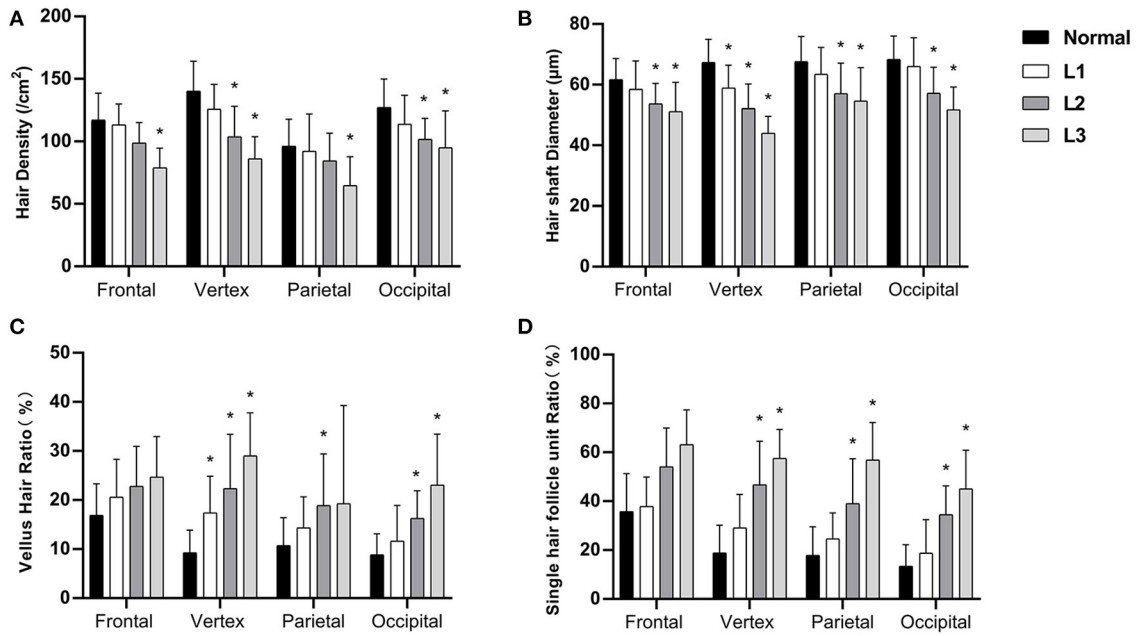

FIGURE 3 | Hair density **(A)**, hair shaft diameter **(B)**, vellus hair ratio **(C)**, and single hair follicle unit ratio **(D)** of FPHL patients from Ludwig L1 to L3. *$p < 0.05$ compared with normal subjects.

units, followed by single hair follicle units and 3-hair follicle units (26). The increase of single hair follicle units is also a trichoscopic manifestation of the miniaturization of hair follicles in AGA patients. Rakowska et al. included the increase of single hair follicle units as one of the secondary indicators of the trichoscopy criteria for diagnosing female androgenic alopecia (9). In our study, single hair follicle unit ratio elevated in FPHL patients as expected, however, it was not as high as in Caucasians. Interestingly, the single hair follicle unit ratio in Chinese normal controls was higher than Caucasians (9).

Hair density in this study showed a similar value to the previous study in Southern Chinese women (15). However, when comparing with other studies on Asian women including Korean and Thai women, the hair density of Chinese normal participants was a little bit lower and much lower than Caucasians, Hispanics and Africans (13, 27–29). In terms of hair shaft diameter, our results also seemed to be much "lower" than other similar studies except for the study of Caucasians women conducted by Rakowska et al. (9). The variation of the results in different studies may be caused by different devices and manners for the studies. Most of the previous study included about five randomly selected terminal hairs for hair shaft diameter measurement under 100-fold magnification, using trichoscopy system Folliscope® (LeedM Corporation) (13, 28). While in our study and Rakowska et al. (9) study, vellus hair was also included in the diameter measurement.

Gender factors showed a limited influence on hair parameters. Birnbaum et al. found that the differences in hair density of frontal, vertex and occipital area between men and women were not statistically significant in health Americans (including Hispanic, Caucasian, and African American) (27). A similar study of healthy Thai people also showed the same results (29). The only significant difference we noticed in this study is that the hair density of parietal region of men is lower than that of women, which was blank in the study of American people and not consistent with the data of Thai People. This gender difference in parietal hair density remains to be confirmed by more extensive studies.

LIMITATION

Compared with other trichoscopic studies on FPHL, the sample size of this study was relatively small. The main limitation of the study cohort is the presence of only 10 male subjects with FPHL, in comparison to the female cases. Though the study could be able to detect the difference of trichoscopic features between FPHL and normal controls, the findings could not be representative of the normal population.

CONCLUSION

In this study, the hair involvement in FPHL of Chinese Han patients was summarized with quantitative trichoscopic analysis. The miniaturization of hair follicles is the main characteristic of FPHL, which is shown as decreased hair density and hair shaft diameter, accompanied by increased vellus hair ratio and single hair follicle unit ratio. The hair in parietal and occipital area can be also affected, though not as severe as in vertex area. Although the incidence is exceptionally low, FPHL can occur in man, and its characteristics are basically the same as those in female patients.

DATA AVAILABILITY STATEMENT

The raw data supporting the conclusions of this article will be made available by the authors, without undue reservation.

ETHICS STATEMENT

The studies involving human participants were reviewed and approved by Ethics Committee of Peking University People's Hospital. The patients/participants provided their written informed consent to participate in this study.

AUTHOR CONTRIBUTIONS

All authors listed have made a substantial, direct and intellectual contribution to the work, and approved it for publication.

FUNDING

This study was supported by the National Natural Science Foundation of China (No. 81773311).

REFERENCES

1. Drake LA, Dinehart S, Farmer E, Goltz R, Graham G, Hordinsky M, et al. Guidelines of care for androgenetic alopecia. American academy of dermatology. *J Am Acad Dermatol.* (1996) 35:465–9. doi: 10.1016/S0190-9622(96)90627-1
2. Hamilton JB. Patterned loss of hair in man: types and incidence. *Ann N Y Acad Sci.* (1951) 53:708–28. doi: 10.1111/j.1749-6632.1951.tb31971.x
3. Ludwig E. Classification of the types of androgenetic alopecia (common baldness) occurring in the female sex. *Brit J Dermatol.* (1977) 97:247–54. doi: 10.1111/j.1365-2133.1977.tb15179.x
4. Ramos PM, Miot HA. Female pattern hair loss: a clinical and pathophysiological review. *An Bras Dermatol.* (2015) 90:529–43. doi: 10.1590/abd1806-4841.20153370
5. Nuwaihyd R, Redler S, Heilmann S, Drichel D, Wolf S, Birch P, et al. Investigation of four novel male androgenetic alopecia susceptibility loci: no association with female pattern hair loss. *Arch Dermatol Res.* (2014) 306:413–8. doi: 10.1007/s00403-013-1436-4
6. Redler S, Messenger AG, Betz RC. Genetics and other factors in the aetiology of female pattern hair loss. *Exp Dermatol.* (2017) 26:510–7. doi: 10.1111/exd.13373
7. Rudnicka L, Olszewska M, Rakowska A, Kowalska-Oledzka E, Slowinska M. Trichoscopy: a new method for diagnosing hair loss. *J Drugs Dermatol.* (2008) 7:651. doi: 10.1001/archderm.144.8.1007
8. De Lacharrière O, Deloche C, Misciali C, Piraccini BM, Vincenzi C, Bastien P, et al. Hair diameter diversity: a clinical sign reflecting the follicle miniaturization. *Arch Dermatol.* (2001) 137:641–6. doi: 10.1001/pubs.ArchDermatol.-ISSN-0003-987x-137-5-dob10023
9. Rakowska A, Slowinska M, Kowalska-Oledzka E, Olszewska M, Rudnicka L. Dermoscopy in female androgenic alopecia: method standardization and diagnostic criteria. *Int J Trichology.* (2009) 1:123. doi: 10.4103/0974-7753.58555
10. Inui S, Nakajima T, Itami S. Scalp dermoscopy of androgenetic alopecia in Asian people. *J Dermatol.* (2009) 36:82–5. doi: 10.1111/j.1346-8138.2009.00593.x
11. Zhang X, Caulloo S, Zhao Y, Zhang B, Cai Z, Yang J. Female pattern hair loss: clinico-laboratory findings and trichoscopy depending on disease severity. *Int J Trichol.* (2012) 4:23. doi: 10.4103/0974-7753.96082
12. Hu R, Xu F, Han Y, Sheng Y, Qi S, Miao Y, et al. Trichoscopic findings of androgenetic alopecia and their association with disease severity. *J Dermatol.* (2015) 42:602–7. doi: 10.1111/1346-8138.12857
13. Kang H, Kang TW, Lee SD, Park YM, Kim HO, Kim SY. The changing patterns of hair density and thickness in South Korean women with hair loss: clinical office-based phototrichogram analysis. *Int J Dermatol.* (2009) 48:14–21. doi: 10.1111/j.1365-4632.2009.03795.x
14. Rojhirunsakool S, Suchonwanit P. Parietal scalp is another affected area in female pattern hair loss: an analysis of hair density and hair diameter. *Clin Cosmet Investig Dermatol.* (2018) 11:7. doi: 10.2147/CCID.S153768
15. Mai W, Sun Y, Liu X, Lin D, Lu D. Characteristic findings by phototrichogram in southern Chinese women with female pattern hair loss. *Skin Res Technol.* (2019) 25:447–55. doi: 10.1111/srt.12672
16. Norwood OT. Male pattern baldness: classification and incidence. *South Med J.* (1975) 68:1359–65. doi: 10.1097/00007611-197511000-00009
17. Kerkemeyer KL, de Carvalho LT, Jerjen R, John J, Sinclair RD, Pinczewski J, et al. Female pattern hair loss in men: a distinct clinical variant of androgenetic alopecia. *J Am Acad Dermatol.* (in press). doi: 10.1016/j.jaad.2020.09.042. Available online at: https://www.jaad.org/article/S0190-9622(20)32632-3/pdf
18. Wang T, Zhou C, Shen Y, Wang X, Ding X, Tian S, et al. Prevalence of androgenetic alopecia in China: a community-based study in six cities. *Brit J Dermatol.* (2010) 162:843–7. doi: 10.1111/j.1365-2133.2010.09640.x
19. Rousso DE, Kim SW. A review of medical and surgical treatment options for androgenetic alopecia. *JAMA Facial Plast. Surg.* (2014) 16:444–50. doi: 10.1001/jamafacial.2014.316
20. Banihashemi M, Nahidi Y, Meibodi NT, Jarahi L, Dolatkhah M. Serum vitamin D3 level in patients with female pattern hair loss. *Int J Trichol.* (2016) 8:116–20. doi: 10.4103/0974-7753.188965
21. Trüeb RM. Female pattern baldness in men. *J Am Acad Dermatol.* (1993) 29:782–3. doi: 10.1016/S0190-9622(08)81702-1
22. Lee WS, Ro BI, Hong SP, Bak H, Sim Y, Park JK, et al. A new classification of pattern hair loss that is universal for men and women: basic and specific (BASP) classification. *J Am Acad Dermatol.* (2007) 57:37–46. doi: 10.1016/j.jaad.2006.12.029
23. Sinclair R, Torkamani N, Jones L. Androgenetic alopecia: new insights into the pathogenesis and mechanism of hair loss. *F1000Research.* (2015) 4:F1000. doi: 10.12688/f1000research.6401.1
24. Price VH, Roberts JL, Hordinsky M, Olsen EA, Savin R, Bergfeld W, et al. Lack of efficacy of finasteride in postmenopausal women with androgenetic alopecia. *J Am Acad Dermatol.* (2000) 43:768–76. doi: 10.1067/mjd.2000.107953
25. Iamsumang W, Leerunyakul K, Suchonwanit P. Finasteride and its potential for the treatment of female pattern hair loss: evidence to date. *Drug Des Devel Ther.* (2020) 14:951. doi: 10.2147/DDDT.S240615
26. Guo ZH, Wang G, Miao Y, Fan ZX, Liu XM, Qu Q, et al. The distribution of hair in Han Chinese. *Plastic Aesthetic Res.* (2017) 4:150. doi: 10.20517/2347-9264.2017.52
27. Birnbaum MR, McLellan BN, Shapiro J, Ye K, Reid SD. Evaluation of hair density in different ethnicities in a healthy American population using quantitative trichoscopic analysis. *Skin Append Disord.* (2018) 4:304–7. doi: 10.1159/000485522
28. Heo JH, Yeom SD, Byun JW, Shin J, Choi GS. Significant relationship between temporal hair loss and other scalp areas in female pattern hair loss. *J Dermatol.* (2020) 47:334–41. doi: 10.1111/1346-8138.15220
29. Leerunyakul K, Suchonwanit P. Evaluation of hair density and hair diameter in the adult thai population using quantitative trichoscopic analysis. *Biomed Res Int.* (2020) 2020:2476890. doi: 10.1155/2020/2476890

Conflict of Interest: The authors declare that the research was conducted in the absence of any commercial or financial relationships that could be construed as a potential conflict of interest.

frontiers in Medicine

BRIEF RESEARCH REPORT
published: 08 April 2021
doi: 10.3389/fmed.2021.631642

Dermoscopy Features of Acquired Perforating Dermatosis Among 39 Patients

Wenju Wang[1†], *Yansen Liao*[2†], *Lixin Fu*[1], *Bei Kan*[1], *Xiaodong Peng*[2*] and *Yonghong Lu*[1*]

[1] Department of Dermatovenereology, Chengdu Second People's Hospital, Chengdu, China, [2] Department of Oncology, Chengdu Second People's Hospital, Chengdu, China

In this report, we concluded there are four dermoscopic features of APD including a yellow-brown homogeneous structureless area in the center of the lesion, dotted and linear vessels distribution radially and a dam shape uplift at the periphery, as well as a white irregular ring surrounding the lesion. There are three features, including the yellow-brown homogeneous structureless area in the center of the lesion, the dotted and linear vessels distribution radially and the white irregular ring surrounding the lesion were correspond to the report of Emma Ormerod et al.These features are also similar to those previously discribed in three separated reports of seven cases with APD. In our report, we found a new dermoscopic features: the dam shape uplift at the periphery. These finding may be contributed to improve the rate of clinical diagnosis of APD.

Keywords: dermoscopy, acquired perforating dermatosis, characteristic, new dermoscopic features, clinical diagnosis

OPEN ACCESS

Edited by:
H. Peter Soyer, The University of Queensland, Australia

Reviewed by:
Elena Netchiporouk, McGill University, Canada
Unni Krishna SRL Samavedam, University of Cincinnati, United States

***Correspondence:**
Xiaodong Peng
3260172243@qq.com
Yonghong Lu
1255395583@qq.com

[†] These authors have contributed equally to this work

Specialty section:
This article was submitted to Dermatology, a section of the journal Frontiers in Medicine

Received: *20 November 2020*
Accepted: *10 March 2021*
Published: *08 April 2021*

Citation:
Wang W, Liao Y, Fu L, Kan B, Peng X and Lu Y (2021) Dermoscopy Features of Acquired Perforating Dermatosis Among 39 Patients. Front. Med. 8:631642. doi: 10.3389/fmed.2021.631642

Acquired perforating dermatosis (APD) is a penetrating skin disease characterized by the excretion of denatured collagen from the epidermis. The most common clinical symptom of APD is pruritus. The lesions are distributed widely and characterized by umbilicated papules and plaques with central crusted ulceration (1). The histopathological presentation of APD often shows local epidermal erosion and loss, homogenized denaturation of dermal superficial fibers, and denaturated fiber bundles penetrating the epidermis (2, 3).MASSON's trichrome and elastic fiber stain showed collagen fibers penetrating the epidermis in the dermis. APD is a rare disorder and the clinical presentation can vary from patient to patient, and it is difficult to differentiate clinically from prurigo nodularis, solar dermatitis, or other diseases. The real diagnosis is often missed or delayed.

Dermoscopy is a non-invasive technique that is used to aid the diagnosis of skin tumors and other inflammatory dermatoses (4, 5) In our clinical work, we found the APD is characteristic under dermoscopy. To the best of our knowledge, the dermoscopic features of APD have been described in three previous case reports (6–8). Here we analyze and report the dermoscopic feature in a series of 39 patients with APD.

We identified 39 patients (19 male and 20 female) with a diagnosis of APD in our department over the past 4 years. The age of these patients ranged from 18 to 65 years, the average age was 48.5 years. All of the patients were diagnosed by clinical (**Figure 1**) and histopathological examination (**Figure 2**).

FIGURE 1 | The clinical presentation of an APD patient. Skin lesions were widely distributed all over the trunk and limbs, the main manifestations were keratinized purplish-red papules or ulcers, about rice to bean size. The center of most papules was navel concave, the surface was a yellow adhesive exfoliated scab shell surrounded by a purplish-red halo. The edge of the ulcer was levee shaped and palpated with moderate hardness.

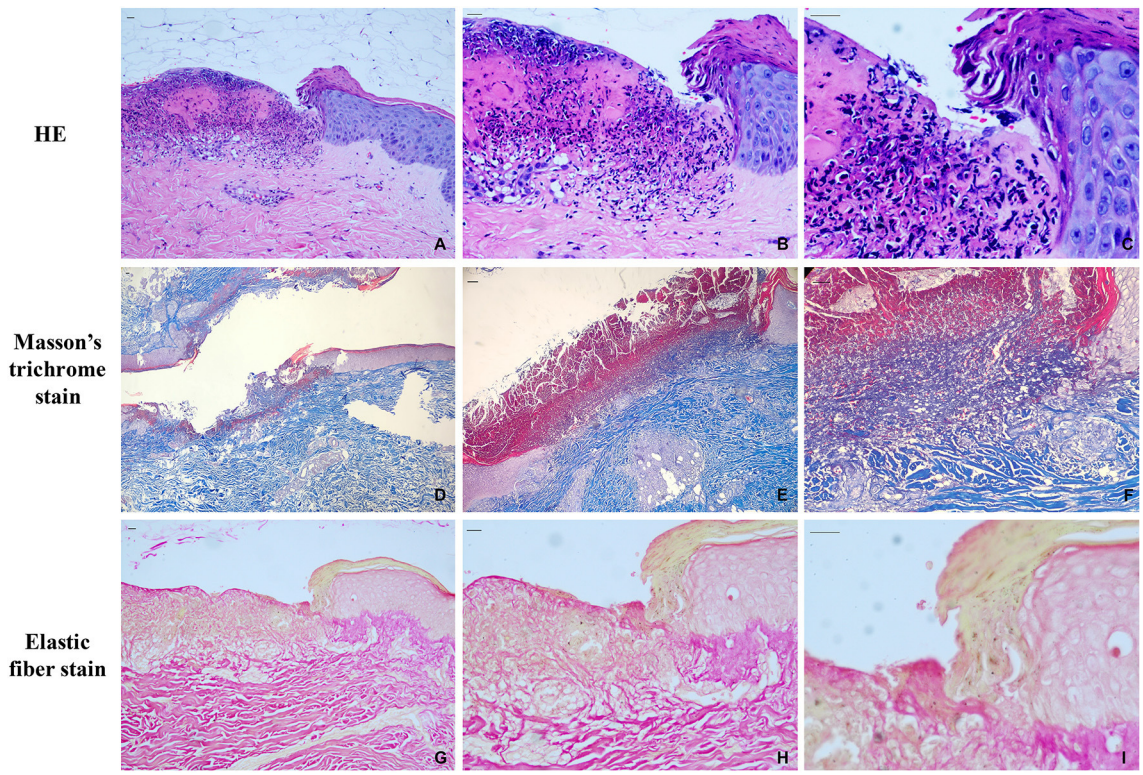

FIGURE 2 | Histopathological features at initial presentation. **(A)** the HE staining of APD patients (10x); **(B)** the HE staining of APD patients (200x); **(C)** the HE staining of APD patients (400x); **(D)** Masson trichrome staining (40x); **(E)** Masson trichrome staining (100x); **(F)** Masson trichrome staining (200x); **(G)** elastic fiber staining (100x); **(H)** elastic fiber staining (200x); **(I)** elastic fiber staining (400x). Scale bars, 200 μm.

We analyzed the dermoscopy pictures of all 39 patients (**Table 1**). Dermoscopic images revealed that there are nine features: (1) a yellow-brown homogeneous structureless area in the center of the lesion were found in 38 of the 39 cases, the accrue rate was about 97.43% (**Figure 3A**); (2) dotted and linear vessel distribution radially were found in 38 of the 39 cases, the accrue rate was about 97.43% (**Figure 3B**); (3) a dam shape uplift at the periphery of the lesion was found in 37 of the 39 cases, the accrue rate was about 94.87% (**Figure 3C**); (4) a white irregular halo surrounding the lesion was found in 34 of the

39 cases, the accrue rate was about 87.18% (**Figure 3D**); (5) a thin scale ring surrounding the lesion was found in 21 of the 39 cases, the accrue rate was about 53.84% (**Figure 3E**); (6) a pink background in the lesion were found in 16 of the 39 cases, the accrue rate was about 41.02% (**Figure 3F**); (7) we found an an orange background in the lesion in 12 of the 39 cases, the accrue rate was about 30.77% (**Figure 3G**); (8) we found a red background in the lesion in 11 of the 39 cases, the accrue rate is about 28.20% (**Figure 3H**); (9) a pigment structure surrounding the lesion were found in 3 of the 39 cases, the accrue rate is about 7.69% (**Figure 3I**).

TABLE 1 | Dermoscopic features observed in 39 ARPC patients with relative frequencies.

Dermoscopic features	*N* (Total 39)	Rate (%)
yellow-brown homogeneous structureless area in the center	38	97.43
dotted and linear vessels distribution radially	38	97.43
adam shape uplift at the periphery	37	94.87
white irregular halo surrounding the lesion	34	87.18
thin scale ring surrounding the lesion	21	53.84
pink background	16	41.02
orange background	12	30.77
red background	11	28.20
pigment structure surrounding the lesion	3	7.69

Dermatoscopic images reveal that the first four clear and consistent features corresponded to the histopathology changes of APD. The yellow-brown homogeneous structureless area in the center of the lesion was found to correspond to the collagen bundle that penetrates the epidermis vertically. The dotted and linear vessel distribution radially in the lesion was found to correspond to the perivascular inflammatory cells. The dam shape uplift at the periphery was found to correspond to the thickening of stratum spinosum and the form of cup-shaped depression of the epidermis by extruded collagen. This white irregular ring surrounding the lesion indicates pigment loss. The first three features also corresponded to a report of Emma Ormerod et al. (6). As described above, the dermoscopic features may be an aid in diagnosing APD and improve the rate of clinical diagnosis.

At present, there is no special treatment method for APD. Common treatment methods are to treat the primary disease to eliminate inducement. In this report, all patients were treated with oral antihistamines, topical glucocorticoid, and retinoic acid ointment combined with NB-UVB irradiation, and the efficacy was satisfactory. In conclusion, we found there are four common dermoscopic features of APD including a yellow-brown homogeneous structureless area in the center of the lesion, dotted

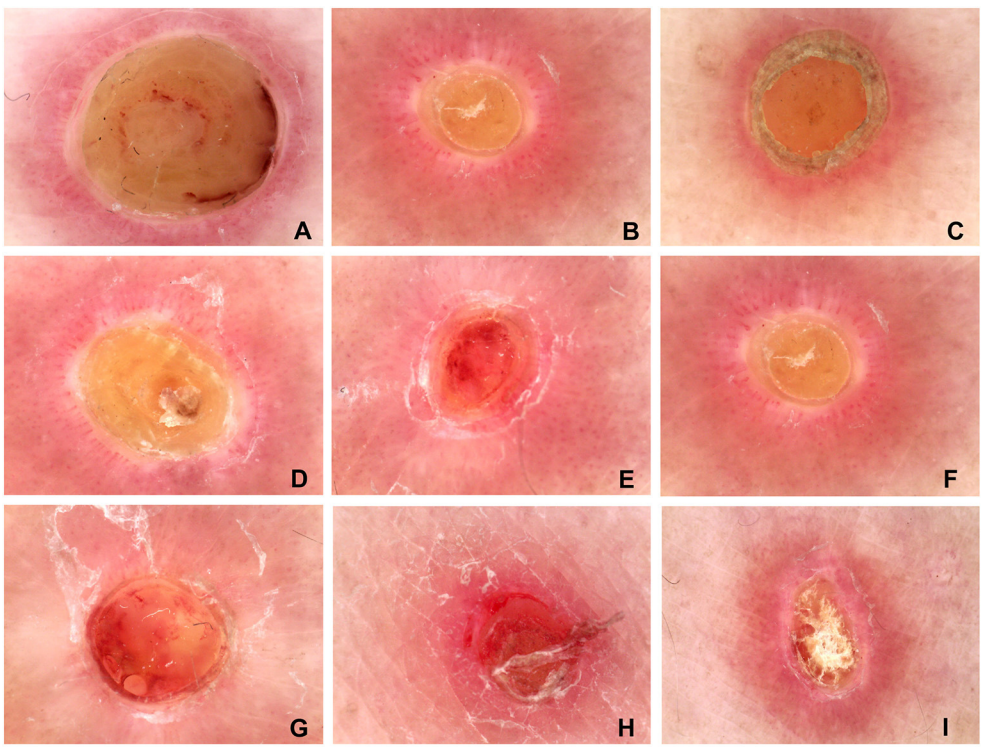

FIGURE 3 | The common dermatoscopic features of the typical lesions from the 39 patients. **(A)** the yellow-brown homogeneous structureless area in the center of the lesion; **(B)** dotted and linear vessels distribution radially; **(C)** a dam shape uplift at the periphery of the lesion; **(D)** the white irregular halo surrounding the lesion; **(E)** a thin scale ring surrounding the lesion; **(F)** pink background; **(G)** orange background; **(H)** red background; **(I)** pigment structure surrounding the lesion. **(A–D)** the four common dermoscopic features of APD.

and linear vessel distribution radially, and a dam shape uplift at the periphery, as well as a white irregular ring surrounding the lesion. There are three features, including the yellow-brown homogeneous structureless area in the center of the lesion, the dotted and linear vessel distribution radially, and a white irregular ring surrounding the lesion, which corresponds with the findings of Emma Ormerod et al. (6). These features are also similar to those previously described in three separate reports relating to seven cases of APD. In our report, we found a new dermoscopic feature: the dam shape uplift at the periphery. These findings could improve the rate of clinical diagnosis of APD.

According to our understanding, the kind of penetrating dermatosis, such as penetrating folliculitis, Kyrle disease, and elastosis perforans, have common features under the pathology, including parakeratosis keratotic plug or elastic fiber through the epidermis. We also summarized the differences in dermoscopic features between prurigo and APD. The dermoscopic features of prurigo show pale brown solitary raised papules with sticky white scabs, irregular white unstructured areas, and spotty, linear vascular foci. Different from the dermoscopic features of APD, there is no yellow-brown homogeneous structureless area in the center, no dam shape uplift at the periphery of the lesion, a white irregular halo surrounding the lesion, and the vascular arrangement is irregular. Therefore, hypothesize that the four dermoscopic features of APD described above are common dermoscopic features of penetrating collagen disease. The question of whether these four features can be defined simply as APD, requires further confirmation and study.

DATA AVAILABILITY STATEMENT

The original contributions generated for this study are included in the article/Supplementary Material, further inquiries can be directed to the corresponding author/s.

ETHICS STATEMENT

Human research was approved by the Ethics Committee of Chengdu Second People's Hospital. The authors certify that they have obtained all appropriate patient consent forms and patients provided consent, confirming that their clinical information could be reported in journal articles.

AUTHOR CONTRIBUTIONS

All authors listed have made a substantial, direct and intellectual contribution to the work, and approved it for publication.

REFERENCES

1. Millard PR, Young E, Harrison DE, Wojnarowska F. Reactive perforating collagenosis: light, ultrastructural and immunohisto-logical studies. *Histopathology*. (1986) 10:1047–56. doi: 10.1111/j.1365-2559.1986.tb02541.x
2. Kim SW, Kim MS, Lee JH, Son SJ, Park KY, Li K, et al. A clinicopathologic study of thirty cases of acquired perforating dermatosis in Korea. *Ann Dermatol*. (2014) 26:162–71. doi: 10.5021/ad.2014.26.2.162
3. Cerio R, Calnan CD, Wilson-Jones E. A clinic-pathological study of reactive perforating collagenosis: report of 10 cases. *Br J Dermatol*. (1987) 117:16–7. doi: 10.1111/j.1365-2133.1987.tb11997.x
4. Argenziano G, Soyer HP, Chimenti S, Talamini R, Corona R, Sera F, et al. Dermoscopy of pigmented skin lesions: results of a consensus meeting via the internet. *J Am Acad Dermatol*. (2003) 48:679–93. doi: 10.1067/mjd.2003.281
5. Goncharova Y, Attia EA, Souid K, Protzenko O, Koktishev I. Dermoscopic features of clinically inflammatory dermatoses and their correlation with histopathologic reaction patterns. *Arch Dermatol Res*. (2015) 307:23–30. doi: 10.1007/s00403-014-1513-3
6. Ormerod E, Atwan A, Intzedy L, Stone N. Dermoscopy features of acquired reactive perforating collagenosis: a case series. *Dermatol Pract Concept*. (2018) 8:303–5. doi: 10.5826/dpc.0804a11
7. Kittisak P, Tanaka M. Dermoscopic findings in a case of reactive perforating collagenosis. *Dermatol Pract Concept*. (2015) 5:75–7. doi: 10.5826/dpc.0502a13
8. Ramirez-Fort MK, Khan F, Rosendahl CO, Mercer SE, Shin-Chang H, Levitt JO. Acquired perforating dermatosis: a clinical and der-matoscopic correlation. *Dermatol Online J*. (2013) 19:18958.

Conflict of Interest: The authors declare that the research was conducted in the absence of any commercial or financial relationships that could be construed as a potential conflict of interest.

frontiers in Medicine

MINI REVIEW
published: 15 April 2021
doi: 10.3389/fmed.2021.637216

Diagnosis of Onychomycosis: From Conventional Techniques and Dermoscopy to Artificial Intelligence

Sophie Soyeon Lim[1], *Jungyoon Ohn*[2,3] *and Je-Ho Mun*[2,3]*

[1] Alfred Health, Melbourne, VIC, Australia, [2] Department of Dermatology, Seoul National University College of Medicine, Seoul, South Korea, [3] Institute of Human-Environment Interface Biology, Seoul National University, Seoul, South Korea

Onychomycosis is a common fungal nail infection. Accurate diagnosis is critical as onychomycosis is transmissible between humans and impacts patients' quality of life. Combining clinical examination with mycological testing ensures accurate diagnosis. Conventional diagnostic techniques, including potassium hydroxide testing, fungal culture and histopathology of nail clippings, detect fungal species within nails. New diagnostic tools have been developed recently which either improve detection of onychomycosis clinically, including dermoscopy, reflectance confocal microscopy and artificial intelligence, or mycologically, such as molecular assays. Dermoscopy is cost-effective and non-invasive, allowing clinicians to discern microscopic features of onychomycosis and fungal melanonychia. Reflectance confocal microscopy enables clinicians to observe bright filamentous septate hyphae at near histologic resolution by the bedside. Artificial intelligence may prompt patients to seek further assessment for nails that are suspicious for onychomycosis. This review evaluates the current landscape of diagnostic techniques for onychomycosis.

Keywords: diagnosis, diagnostic imaging, onychomycosis, fungi, pathology, dermoscopy, reflectance confocal microscopy, artificial intelligence

OPEN ACCESS

Edited by:
Robert Gniadecki,
University of Alberta, Canada

Reviewed by:
Sepideh Emam,
University of Alberta, Canada
William Faber,
Academic Medical Center, Netherlands

***Correspondence:**
Je-Ho Mun
jehomun@gmail.com

Specialty section:
This article was submitted to Dermatology, a section of the journal Frontiers in Medicine

Received: *03 December 2020*
Accepted: *19 March 2021*
Published: *15 April 2021*

Citation:
Lim SS, Ohn J and Mun J-H (2021) Diagnosis of Onychomycosis: From Conventional Techniques and Dermoscopy to Artificial Intelligence. Front. Med. 8:637216. doi: 10.3389/fmed.2021.637216

INTRODUCTION

Onychomycosis is a fungal nail infection caused by dermatophytes (60–70%), non-dermatophyte molds (NDMs) (20%) and yeast (10–20%) (1–3). It is the most common nail disorder encountered in clinical practice worldwide (4–6). It is a significant public health issue, as human to human transmission occurs *via* direct or indirect contact of surfaces contaminated with scales or keratin from infected patients. Risk of developing onychomycosis increases with advancing age. Thus, onychomycosis is likely to become an even more pertinent issue given the aging population (7, 8). Its other risk factors include diabetes, obesity, trauma, history of tinea pedis, and immunosuppression (9, 10). Onychomycosis is detrimental to patients' quality of life, as its physical appearance can cause significant psychological distress, and the localized pain in severely dystrophic nails can impede everyday living (11).

Onychomycosis is important to diagnose as it is curable with antifungal agents such as oral terbinafine, itraconazole, albaconazole, posaconazole, and fluconazole (12, 13). Topical antifungal solutions including ciclopirox 8%, amorolfine 5%, efinaconazole 10%, and tavaborole 5%, are used as adjuncts to oral agents in severe cases or as alternatives when oral agents are contraindicated or in mild cases (12). Due to costs and long treatment course lasting at least 3 months, patients often find difficulty adhering to therapy (12, 14–16). Ensuring that patients

who do not have onychomycosis do not receive antifungal treatment is also important because oral antifungals have adverse systemic effects, including gastrointestinal disturbance and hepatotoxicity (13).

To diagnose onychomycosis, clinical suspicion needs to be confirmed with mycologic testing. This review highlights key characteristics of conventional diagnostic tools, including potassium hydroxide (KOH) testing, fungal culture and histopathology of nail clippings, and newly developed techniques, including dermoscopy, reflectance confocal microscopy, molecular assays and artificial intelligence.

CLINICAL FEATURES AND DIFFERENTIAL DIAGNOSES

Onychomycosis is typically characterized by a yellow or brown, brittle nail plate with subungual hyperkeratosis causing onycholysis (17–19). It is classified according to the site and involvement of disease: distal and lateral subungual, superficial, endonyx, proximal subungual, and total dystrophic onychomycosis (20). Distal and lateral subungual onychomycosis is the most common, thus the commonly described features of onychomycosis are those observed in this subtype (19, 20). Superficial onychomycosis presents with nail plate discoloration, superficial patches and transverse striae, and endonyx onychomycosis presents with lamellar splitting, discoloration and indentations (19, 20). Proximal subungual onychomycosis predominantly presents with a whitish area in the proximal nail plate (19, 20). This subtype is often seen in immunosuppressed patients, such as those with the human immunodeficiency virus, systemic lupus erythematosus or on immunosuppressants (**Figure 1A**) (10).

According to a prospective cross-sectional diagnosis study in seven dermatology outpatient clinics, features that increase the likelihood of clinically diagnosing onychomycosis are previous diagnosis of fungal disease in feet [likelihood ratio (LR+) for a positive result = 1.84], abnormal plantar desquamation involving > 25% of the sole (LR+ = 3.61), interdigital tinea pedis (LR+ = 1.46) and onychomycosis being considered the most probable diagnosis by dermatologists (LR+ = 1.46) (9). When abnormal plantar desquamation is coupled with onychomycosis being considered the most likely diagnosis, probability of diagnosing onychomycosis is 81% (**Figure 1B**). Onychomycosis can present alongside green nail syndrome. A retrospective analysis of green nail syndrome patients at referral centers revealed fungal co-infection in 65.2% of patients (21). Onychomycosis can present with a dermatophytoma, a compact ball of fungal filaments and large spores which appears as a white/yellow or orange/brown longitudinal streak in the nail plate (22, 23). Features of severe or long-standing disease include dermatophytoma, worsening subungual hyperkeratosis, expanding area of disease involvement and closer proximity of disease to the nail matrix (24). Severe disease can cause pain secondary to onychocryptosis (ingrown nail), nail bed infection and partial or complete nail plate loss (18).

Abbreviations: AI, artificial intelligence; AUC, area under curve; GMS, Grocott-Gomori methanamine silver; KOH, potassium hydroxide; LR+, likelihood ratio for a positive result; NDM, non-dermatophyte mold; PAS, periodic acid-Schiff; PCR, polymerase chain reaction; RCM, reflectance confocal microscopy; R-CNN, region-based convolutional neural network; SCC, squamous cell carcinoma; SDA, Sabouraoud dextrose agar.

Differential Diagnoses

Trachyonychia

Trachyonychia is an inflammatory nail disease which is commonly idiopathic but can be secondary to systemic inflammatory conditions such as alopecia areata and nail psoriasis (25, 26). It is characterized by a rough and brittle nail plate (opaque trachyonychia) or, less frequently, an opalescent nail plate lined with small geometric pits (shiny trachyonychia) (27). Trachyonychia is diagnosed clinically and dermoscopy is a useful diagnostic aid. Key dermoscopic features of trachyonychia that differentiate it from onychomycosis include red coloration, longitudinal ridging, involvement of the proximal nail plate (at >50% of the nail plate width), splinter hemorrhages, pitting, and onychoschizia (nail plate splitting) (28).

Onycholysis

Onycholysis involves separation of the nail plate from the nail bed due to repetitive trauma, phototoxicity, contact dermatitis, underlying tumor or infection, nail psoriasis, or nail lichen planus (29). Onycholysis secondary to trauma can be differentiated from that resulting from onychomycosis on dermoscopic examination. The proximal border of onycholysis is linear with trauma, but jagged with spiked edges in onychomycosis (30).

Onychomadesis

Onychomadesis is characterized by complete separation and shedding of the nail plate from the proximal nail bed due to temporary nail matrix arrest (31, 32). Conditions that cause nail matrix arrest include infections such as hand-foot-and-mouth disease and varicella, trauma, chemotherapy, anticonvulsants, lichen planus, and Kawasaki disease (32). Nails affected by onychomadesis are at risk of developing onychomycosis (33).

Onychocryptosis

Onychocryptosis (ingrowing nail) involves the nail plate burying within the periungual skin, causing painful inflammation, infection and granulation (34). Although it is observed secondary to severe onychomycosis, it is primarily associated with genetic disposition, trauma, poorly-fitted shoes, and incorrect nail trimming (31, 34).

Nail Squamous Cell Carcinoma

Nail SCC is the most common malignant nail disorder and can clinically resemble onychomycosis (35, 36). Like onychomycosis, immunosuppression increases the risk of developing nail SCC. Other risk factors include chronic sun exposure, human papillomavirus infection and trauma (37). Diagnosis delays occur frequently as nail SCC presents with non-specific clinical features, including subungual tumor, lateral onycholysis, subungual hyperkeratosis, painless nail bed erosion, ulceration, purulent discharge, serous ooze, bleeding and nail loss (37, 38).

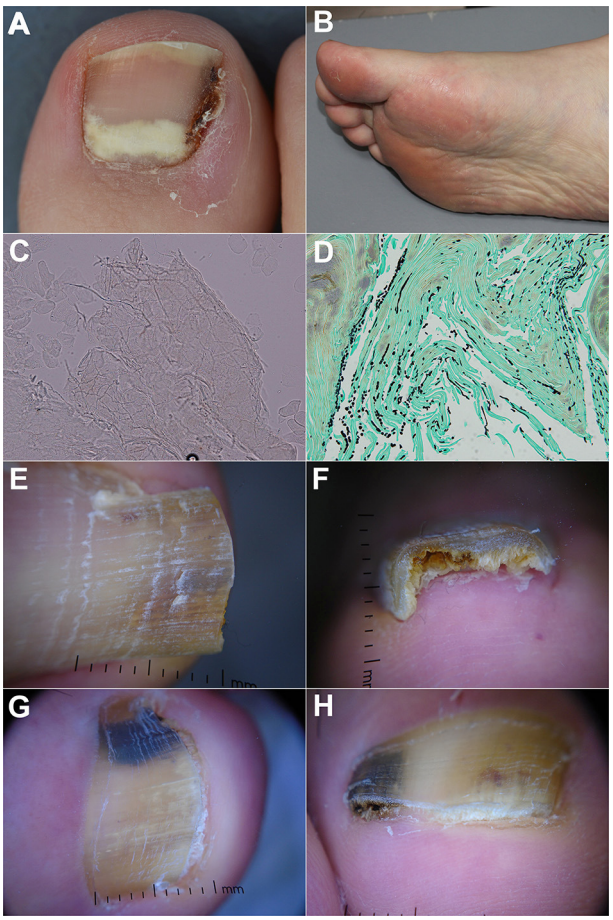

FIGURE 1 | (A) Proximal subungual onychomycosis in a patient with systemic lupus erythematosus. **(B)** Abnormal plantar desquamation increases the likelihood of clinically diagnosing onychomycosis. Thus, the sole should also be examined while assessing onychomycosis. **(C)** KOH-test highlighting presence of fungal hyphae (×200 magnification). **(D)** Histopathology (nail clipping) with GMS staining showing numerous fungal hyphae in the nail plate (×400). The fungi are highlighted in black with GMS staining. **(E,F)** Dermoscopic examination of onychomycosis showing yellowish discoloration with spikes pattern and surface scales. Distal edge dermoscopy demonstrating subungual hyperkeratosis. **(G,H)** Dermoscopic examination of fungal melanonychia showing reverse triangular pattern, yellow streaks, black and yellow coloration, scales, and subungual hyperkeratosis.

Therefore, nail dystrophies refractory to treatment need to be carefully investigated.

Nail Apparatus Melanoma

Nail apparatus melanoma is another malignant nail disorder that warrants prompt diagnosis (39). Its prognosis is poorer than other melanomas due to diagnosis delays resulting from non-specific clinical features and high incidence of amelanosis (40, 41). Nail apparatus melanoma commonly presents with a ≥3 mm-thick brown or black band with variegated borders, nail dystrophy and Hutchinson's sign, where the proximal and/or lateral nail fold is pigmented (41–44). Nail apparatus melanoma can be mistaken for onychomycosis and they may be co-exist with onychomycosis, thus detailed investigation is warranted in onychomycosis with malignant features (45, 46).

CONVENTIONAL DIAGNOSTIC TOOLS

To diagnose onychomycosis, confirmatory mycologic testing is essential. The potential harm caused by misdiagnosis and inappropriate use of empiric antifungal therapy outweigh the cost benefit of bypassing mycologic testing (18, 47, 48).

Potassium Hydroxide Testing

Direct potassium hydroxide (KOH) testing is a simple, quick and inexpensive technique integral to dermatological practice for identifying fungal organisms (**Figure 1C**) (49, 50). It involves retrieving the specimen from the nail bed and underneath the nail plate then dissolving it in KOH (51). KOH dissolves the keratin, allowing microscopic visualization of the fungal septate hyphae (51). Specimens can be further treated with stains such as Calcofluor White, Evans Blue, Gram, Giemsa, and India ink (52, 53).

KOH testing has 61% sensitivity and 95% specificity (51). It is cost-effective and can determine the presence of fungal organisms within an hour. However, it cannot specify the exact type of pathogenic organism (19). Retrieving adequate amount of specimen is critical in ensuring the success of KOH testing. To optimize accuracy, specimens should not be interpreted immediately after applying KOH, as it takes at least 15–30 min for the KOH to adequately dissolve the keratin (19). Overall, KOH testing is a quick and inexpensive diagnostic tool for confirming presence of fungi in nails, enabling clinicians to commence treatment for onychomycosis (**Table 1**).

Fungal Culture

Fungal culture can identify the specific pathogen subtype (53, 64). After removing debris from the nail plate, the subungual specimen is cultured in Sabouraoud dextrose agar (SDA) at 26–30°C for up to a month (18, 52). The media is treated with chloramphenicol and gentamicin to prevent bacteria from interfering with fungal growth (52). Laboratories often culture the subungual specimen in SDA with and without cycloheximide which prevents growth of NDMs. Repeat cultures are required to diagnose NDM onychomycosis, as NDMs are common contaminants of skin surfaces (18).

Fungal culture has 99% specificity, its pooled sensitivity is 56% (range 29–82%) according to a recent meta-analysis (51, 53). Sensitivity of fungal culture is largely dependent on the expertise of the testing center (65). Although specialized mycology centers may report fewer false negatives, most tertiary centers and general clinics observe low sensitivity rates. Clinical utility of fungal culture is further limited by delays in retrieving results (several weeks to months). Therefore, fungal culture is recommended when identifying the fungal organism is necessary (53).

Histopathology (Nail Clipping)

Histopathological assessment involves examining the microscopic features of nail clipping specimens embedded

TABLE 1 | Summary of diagnostic techniques for onychomycosis.

	Sensitivity	Specificity	Advantages	Disadvantages
KOH testing (51)	61% (44–100%)	95% (75–100%)	Easy to conduct	Diagnostic accuracy dependent on examiner's expertise
			Inexpensive	Cannot identify pathogen subtype
			Quick results (15–60 min)	
Fungal culture (51)	56% (29–82%)	99% (83–100%)	Can identify pathogen subtype	Low sensitivity
				Delay in results (up to 1 month)
Histopathology (51)	84% (61–93%)	89% (44–100%)	Most sensitive conventional mycological test	Expensive
				Cannot specify pathogen subtypes
Nail dermoscopy	Jagged onycholytic edge with spikes: 86.4% (54), 100% (30)	Jagged onycholytic edge with spikes: 58.3% (54), 100% (30)	Bedside tool, non-invasive	Cannot demonstrate presence of fungi
	Longitudinal striae: 25% (54), 86.5% (30)	Longitudinal striae: 83.3% (54), 100% (30)	Quick results	
	Ruins aspect: 59.1% (54)	Ruins aspect: 91.7% (54)	Inexpensive	
	Homogenous opacity: 34.1% (54)	Homogenous opacity: 83.3% (54)		
Reflectance confocal microscopy	52.9% (55), 79.5% (56), 91.67% (57)	57.58% (57), 81% (56), 90.2% (55)	Bedside tool, non-invasive	Moderate sensitivity and specificity
				Cannot assess thick nails
Polymerase chain reaction	85% (58)	94% (58)	Can identify pathogen subtype	Assays still under development
	87.3% (59)	94.3% (59)	High sensitivity	Risk of false positives
	100% (60)	100% (60)	Can deliver results with small amount of sample	
	Pandermatophyte assay: 90% (61)	Pandermatophyte and panfungal assays: NR		
	Panfungal assay: 47% (61)			
Flow cytometry and mass spectrometry	NR	NR	Can theoretically identify pathogen subtype	Experimental
Artificial intelligence	70.2% (62)	72.7% (62)	Inexpensive	Still under development: require improving dataset and considering method of distribution to clinicians
	82.7–96% (63)	69.3–96.7% (63)	Can be used by patients to screen for highly suspicious nails	Not confirmatory technique

NR, not reported.

in paraffin blocks (18, 52). To acquire an adequate nail sample for examination, at least 4 mm of the free edge of the nail plate should be retrieved using a dual-action or heavy-duty nail nipper (66). Samples can be transported to the laboratory in a dry container or in formaldehyde (67). Softening nail samples before routine processing with solutions such as chitin-softening agent, 4% phenol or 10% Tween 40, facilitates sectioning and thus optimizes the quality of sections (66, 67). After paraffin embedding and sectioning, stains highlight presence of fungi (**Figure 1D**). Using the periodic acid-Schiff (PAS) staining method, periodic acid oxidizes hydroxyl groups of the cell wall in spores, hyphae, pseudohyphae and yeasts into aldehydes (52, 53). These then react with Schiff to produce a red color (52, 53). Using the Grocott-Gomori methanamine silver (GMS) staining method, the chromic acid oxidizes the cell wall then reduces the methanamine silver nitrate into metallic silver to produce a dark brown color (53).

Histopathology of nail clippings is highly sensitive (84%) and specific (89%) (51). It can also be stored and retrospectively reviewed in refractory cases, as the paraffin embedding allows for long-term storage. Histopathology is however rather costly than KOH testing and unable to specify the exact subtype or viability of the causative organism (18, 19, 53, 68).

NEW DIAGNOSTIC TOOLS

Nail Dermoscopy (Onychoscopy)

Nail dermoscopy (onychoscopy) is a non-invasive bedside tool that allows clinicians to visualize microscopic features of abnormal nails. Key dermoscopic features of distal and

lateral subungual onychomycosis include a jagged proximal edge of the onycholytic area with spikes and longitudinal striae (**Figures 1E,F**) (30, 54). These features and a ruins aspect are associated with total dystrophic onychomycosis (54). Homogenous opacity is found in superficial onychomycosis (54).

Onychomycosis can also present with longitudinal melanonychia (fungal melanonychia). In such cases, white or yellow streaks, non-longitudinal homogenous pattern, yellow coloration, reverse triangular pattern, subungual hyperkeratosis, multicolor pattern and nail scaling are positive predictors of fungal melanonychia (**Figures 1G,H**) compared to nail matrix naevi or subungual melanomas (69). As nail dermoscopy is quick, non-invasive and inexpensive, it has the potential to help physicians identify onychomycosis by the bedside and decide whether to proceed to mycological assessment (70).

Reflectance Confocal Microscopy

Reflectance confocal microscopy (RCM) is a real-time imaging tool that allows clinicians to observe features of abnormal nails at near-histologic resolution by the bedside. It uses a 830 nm laser in reflectance mode which divides the nail unit into thin horizontal sections for examination (56). Reflectance confocal microscopy of onychomycosis reveals networks of bright filamentous septate hyphae (56, 71, 72). It has 52.9–91.67% sensitivity and 57.58–90.2% specificity for detecting onychomycosis (55–57). Reflectance confocal microscopy is expensive and not subsidized in many countries, and further studies are needed to support its utility in the clinical setting (72). Therefore, it is yet to be integrated into clinical practice in many countries. In addition, it is difficult to assess thick nails with RCM as its depth of imaging is limited to $\sim$200 μm.

Molecular Assays

Molecular assays including polymerase chain reactions (PCR), flow cytometry and mass spectrometry are advanced diagnostic tools that involve analysis of the fungal DNA causing onychomycosis.

Polymerase chain reactions involves amplifying the fungal DNA then detecting this with specialized fluorescent primers (73). Therefore, it can detect small amounts of pathogenic organisms within nails (74). Real-time PCR is the most frequently used form of PCR as it is relatively simple to conduct, can detect multiple organisms and has a low risk of contamination (73, 74). Various assays have been developed to facilitate commercial use of PCR technology when detecting dermatophytes, but these are not widely available (74). They report sensitivity of 85–100% and specificity of 94–100% (58–60).

Hafirassou et al. investigated usefulness of panfungal and pandermatophyte assays for real-time PCR compared to fungal culture in detecting onychomycosis (61). The pandermatophyte assay was 90% sensitive relative to culture. The panfungal assay showed a low sensitivity of 47% relative to culture due to multiple fungal species residing within diseased and healthy nails, as demonstrated by the candida and aspergillus assays. Further studies are warranted to examine PCR use in a real-world setting and reduce the risk of false positives.

Other molecular assay techniques include flow cytometry and mass spectrometry. Flow cytometry separates cells according to size, granulosity and presence of DNA and protein markers (18). Mass spectrometry involves charging chemical species and separating ions according to their mass-to-charge ratio (18, 53, 75). These techniques are experimental, requiring further research and development prior to integration into clinical practice.

Artificial Intelligence

Artificial intelligence (AI) has caused a recent paradigm shift in clinical medicine (76, 77). Its diagnostic performance has been shown to be comparable to that of specialist clinicians in identifying diabetic retinopathy and skin cancer (78, 79). Many dermatologists recognize that AI has great potential to improve dermatologic care (80, 81). Currently, it is mainly explored in the setting of skin cancer, ulcers, psoriasis and other inflammatory skin diseases, predicting skin-sensitizing substances, histopathological assessment, and gene expression profiling (82).

Developing a large database of photographs capturing a wide range of disease presentations is critical in AI training (82). Onychomycosis is an ideal candidate for AI as it is a common condition with minimal racial differences (63). Clinics worldwide can contribute to the database, and the AI technology would not be limited to specific populations.

In 2018, Han et al. developed AI for diagnosing onychomycosis (63). Two datasets, A1 (n = 49,567) and A2 (n = 3,741), were generated. A2 consisted of images of clinically diagnosed onychomycosis (63). For A1, standardized clinical images were generated by a hand and foot image selecting convolutional neural network (CNN), followed by a nail part extracting regional CNN (R-CNN) then a fine image CNN. Two CNN algorithms, ResNet-152 and VGG-19, were then trained to classify nails as onychomycosis or one their differential diagnoses using the two datasets. These algorithms were then validated against datasets (B1, B2, C, and D) of mycologically confirmed onychomycosis cases.

Algorithms trained with A1 were more accurate in diagnosing onychomycosis than those trained with A2. Moreover, the AI (two-layered feedforward neural networks computing the combined output of ResNet-152 and VGG-19) achieved test sensitivity/specificity/area under the curve values of (96.0/94.7/0.98), (82.7/96.7/0.95), (92.3/79.3/0.93), and (87.7/69.3/0.82) for the B1, B2, C, and D datasets, respectively. AI performed better than most of the 42 dermatologists. The Youden index (sensitivity + specificity−1) of AI which reflects its diagnostic accuracy was significantly higher than that of the dermatologists (p = 0.01) when evaluating the B1 and C datasets.

More recently, the group reported that the deep neural network at operating point achieved 70.2% sensitivity, 72.7% specificity and AUC of 0.75 in diagnosing onychomycosis in a prospective cohort of 90 patients (62). This was comparable to the performance of dermoscopy (sensitivity 72.7%, specificity 72.9%,

AUC 0.755; $p = 0.952$) and experienced dermatologists (mean Youden index 0.230 ± 0.176; $p = 0.667$).

Although there is limited literature on this topic, these results showed that AI has the potential to assist clinicians decide whether they should test nails for onychomycosis. AI can also help improve telemedicine, as it can act as an accessible resource for patients to evaluate their own nails and, if needed, promptly initiate a formal clinician review. To further develop AI, the database should be optimized to include rigorously confirmed onychomycosis and various non-onychomycosis onychopathies that are evaluated with relevant mycological examinations. Finding a suitable means of distributing this technology to the public is also necessary. Finally, whilst integrating AI into clinical practice is important, dermatologists should use their clinical judgment to prevent overdiagnosis and excessive testing which would increase the burden on health care costs.

CONCLUSION

A wide range of conventional and newly developed tools help diagnose onychomycosis. Each tool has its advantages and disadvantages, and combining these tools improves the sensitivity and specificity of testing (51). KOH testing is best for prompt initial diagnosis. In ambiguous cases, histopathologic assessment of affected nail plates can identify presence of fungi. Fungal culture can be used when the pathogen subtype needs to be specified. Dermoscopy can assist clinicians identify nails that are highly suspicious for onychomycosis. Reflectance confocal microscopy allows visualization of hyphae by the bedside but is not widely

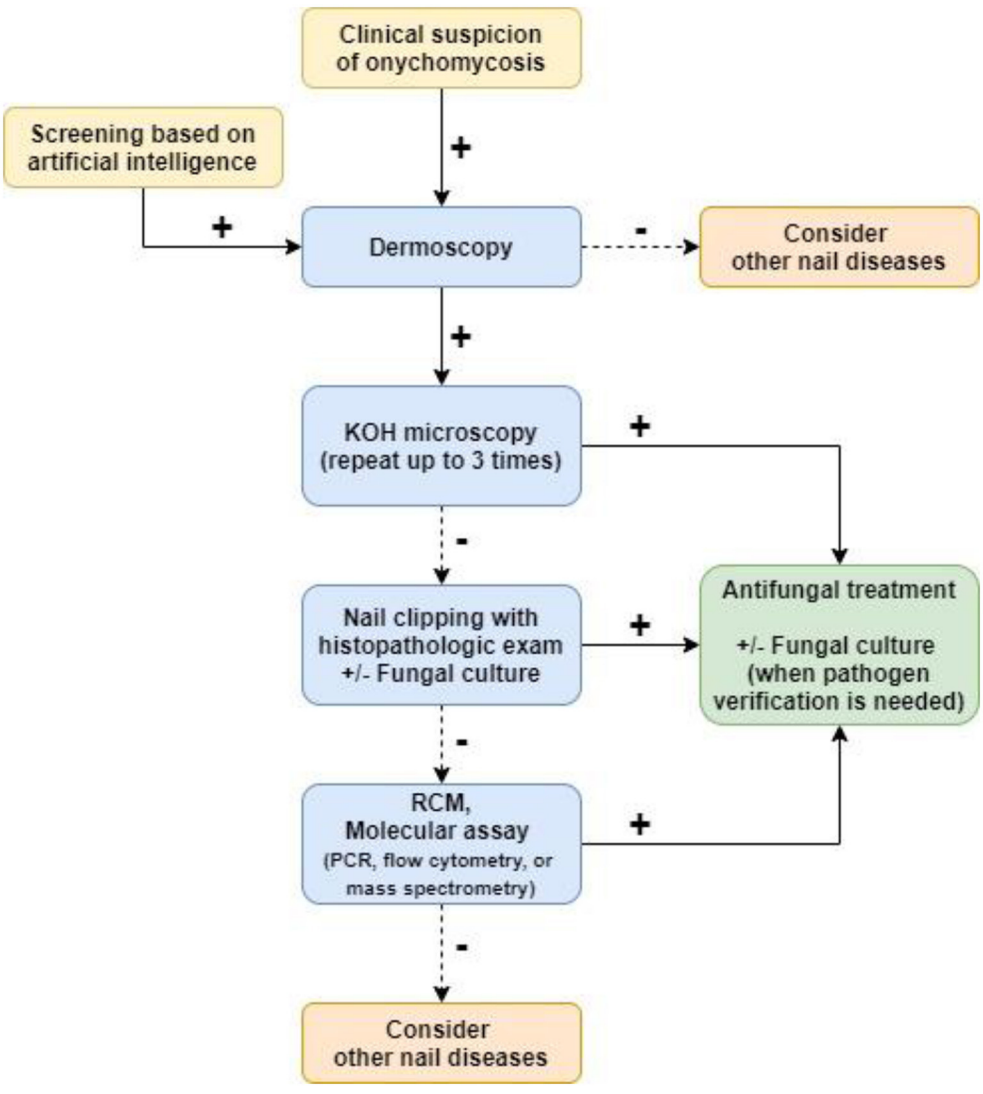

FIGURE 2 | A flowchart for diagnosing onychomycosis.

available, and molecular assays may act as supplementary diagnostic tests but require more research. AI has the potential to help patients identify affected nails and seek further medical assessment. A diagnostic algorithm integrating these tools can help maximize clinicians' accuracy of diagnosing onychomycosis (**Figure 2**).

AUTHOR CONTRIBUTIONS

SL: data acquisition, analysis, and manuscript drafting. JO: manuscript critical revision. J-HM: conception of work, manuscript critical revision, and final approval. All authors: contributed to the article and approved the submitted version.

REFERENCES

1. Ghannoum MA, Hajjeh RA, Scher R, Konnikov N, Gupta AK, Summerbell R, et al. A large-scale North American study of fungal isolates from nails: the frequency of onychomycosis, fungal distribution, and antifungal susceptibility patterns. *J Am Acad Dermatol*. (2000) 43:641–8. doi: 10.1067/mjd.2000.107754
2. Gupta AK, Gupta G, Jain HC, Lynde CW, Foley KA, Daigle D, et al. The prevalence of unsuspected onychomycosis and its causative organisms in a multicentre Canadian sample of 30 000 patients visiting physicians' offices. *J Eur Acad Dermatol Venereol*. (2016) 30:1567–72. doi: 10.1111/jdv.13677
3. Svejgaard EL, Nilsson J. Onychomycosis in Denmark: prevalence of fungal nail infection in general practice. *Mycoses*. (2004) 47:131–5. doi: 10.1111/j.1439-0507.2004.00968.x
4. Faergemann J, Baran R. Epidemiology, clinical presentation and diagnosis of onychomycosis. *Br J Dermatol*. (2003) 149(Suppl. 65):1–4. doi: 10.1046/j.1365-2133.149.s65.4.x
5. Gupta AK, Mays RR, Versteeg SG, Piraccini BM, Takwale A, Shemer A, et al. Global perspectives for the management of onychomycosis. *Int J Dermatol*. (2019) 58:1118–29. doi: 10.1111/ijd.14346
6. Sigurgeirsson B, Baran R. The prevalence of onychomycosis in the global population: a literature study. *J Eur Acad Dermatol Venereol*. (2014) 28:1480–91. doi: 10.1111/jdv.12323
7. Papini M, Piraccini BM, Difonzo E, Brunoro A. Epidemiology of onychomycosis in Italy: prevalence data and risk factor identification. *Mycoses*. (2015) 58:659–64. doi: 10.1111/myc.12396
8. Hwang S, Kim D, Suh M, Kwon K, Kim H, Ro B, et al. Epidemiologic survey of onychomycosis in Koreas: multicenter study. *Korean J Med Mycol*. (2011) 16:35–43. doi: 10.17966/kjmm.2011.16.2.35
9. Garcia-Doval I, Cabo F, Monteagudo B, Alvarez J, Ginarte M, Rodríguez-Alvarez MX, et al. Clinical diagnosis of toenail onychomycosis is possible in some patients: cross-sectional diagnostic study and development of a diagnostic rule. *Br J Dermatol*. (2010) 163:743–51. doi: 10.1111/j.1365-2133.2010.09930.x
10. Tlacuilo-Parra A, Guevara-Gutierrez E, Mayorga J, Garcia-De La Torre I, Salazar-Paramo M. Onychomycosis in systemic lupus erythematosus: a case control study. *J Rheumatol*. (2003) 30:1491–4. Available online at: https://www.jrheum.org/content/30/7/1491
11. Stewart CR, Algu L, Kamran R, Leveille CF, Abid K, Rae C, et al. Effect of onychomycosis and treatment on patient reported quality of life outcomes: a systematic review. *J Am Acad Dermatol*. (2020). doi: 10.1016/j.jaad.2020.05.143
12. Lipner SR, Scher RK. Onychomycosis: treatment and prevention of recurrence. *J Am Acad Dermatol*. (2019) 80:853–67. doi: 10.1016/j.jaad.2018.05.1260
13. Fávero MLD, Bonetti AF, Domingos EL, Tonin FS, Pontarolo R. Oral antifungal therapies for toenail onychomycosis: a systematic review with network meta-analysis toenail mycosis: network meta-analysis. *J Dermatolog Treat*. (2020) 1–10. doi: 10.1080/09546634.2020.1729336. [Epub ahead of print].
14. Singh S, Shukla P. End of the road for terbinafine? Results of a pragmatic prospective cohort study of 500 patients. *Indian J Dermatol Venereol Leprol*. (2018) 84:554–7. doi: 10.4103/ijdvl.IJDVL_526_17
15. Roh D, Kim H, Nam J, Mun J, Park J, Park J, et al. Public awareness of onychosis in Korea: a survey of 621 participants. *J Mycol Infect*. (2018) 23:15–23. doi: 10.17966/jmi.2018.23.1.15
16. Wu AG, Geizhals S, Lipner SR. Retrospective study of factors affecting medication adherence in patients prescribed efinaconazole 10% solution for onychomycosis. *J Am Acad Dermatol*. (2020) 84:208–10. doi: 10.1016/j.jaad.2020.04.126
17. Zaias N. Onychomycosis. *Arch Dermatol*. (1972) 105:263–74. doi: 10.1001/archderm.1972.01620050069017
18. Gupta AK, Mays RR, Versteeg SG, Shear NH, Piguet V. Update on current approaches to diagnosis and treatment of onychomycosis. *Expert Rev Anti Infect Ther*. (2018) 16:929–38. doi: 10.1080/14787210.2018.1544891
19. Leung AKC, Lam JM, Leong KF, Hon KL, Barankin B, Leung AAM, et al. Onychomycosis: an updated review. *Recent Pat Inflamm Allergy Drug Discov*. (2020) 14:32–45. doi: 10.2174/1872213X13666191026090713
20. Hay RJ, Baran R. Onychomycosis: a proposed revision of the clinical classification. *J Am Acad Dermatol*. (2011) 65:1219–27. doi: 10.1016/j.jaad.2010.09.730
21. Ohn J, Yu DA, Park H, Cho S, Mun JH. Green nail syndrome: analysis of the association with onychomycosis. *J Am Acad Dermatol*. (2020) 83:940–2. doi: 10.1016/j.jaad.2020.01.040
22. Lipner SR, Scher RK. Evaluation of nail lines: color and shape hold clues. *Cleve Clin J Med*. (2016) 83:385–91. doi: 10.3949/ccjm.83a.14187
23. Martinez-Herrera E, Moreno-Coutiño G, Fernández-Martínez RF, Finch J, Arenas R. Dermatophytoma: description of 7 cases. *J Am Acad Dermatol*. (2012) 66:1014–6. doi: 10.1016/j.jaad.2010.06.034
24. Carney C, Tosti A, Daniel R, Scher R, Rich P, DeCoster J, et al. A new classification system for grading the severity of onychomycosis: onychomycosis severity index. *Arch Dermatol*. (2011) 147:1277–82. doi: 10.1001/archdermatol.2011.267
25. Jacobsen AA, Tosti A. Trachyonychia and twenty-nail dystrophy: a comprehensive review and discussion of diagnostic accuracy. *Skin Appendage Disord*. (2016) 2:7–13. doi: 10.1159/000445544
26. Starace M, Alessandrini A, Bruni F, Piraccini BM. Trachyonychia: a retrospective study of 122 patients in a period of 30 years. *J Eur Acad Dermatol Venereol*. (2020) 34:880–4. doi: 10.1111/jdv.16186
27. Haber JS, Chairatchaneeboon M, Rubin AI. Trachyonychia: review and update on clinical aspects, histology, and therapy. *Skin Appendage Disord*. (2017) 2:109–15. doi: 10.1159/000449063
28. Jo G, Park JS, Yu DA, Ohn J, Sheu SL, Mun JH. Onychoscopy of trachyonychia: an analysis of 30 patients and comparison with onychomycosis. *Br J Dermatol*. (2018) 179:491–3. doi: 10.1111/bjd.16431
29. Zaias N, Escovar SX, Zaiac MN. Finger and toenail onycholysis. *J Eur Acad Dermatol Venereol*. (2015) 29:848–53. doi: 10.1111/jdv.12862
30. Piraccini BM, Balestri R, Starace M, Rech G. Nail digital dermoscopy (onychoscopy) in the diagnosis of onychomycosis. *J Eur Acad Dermatol Venereol*. (2013) 27:509–13. doi: 10.1111/j.1468-3083.2011.04323.x
31. Smith RJ, Rubin AI. Pediatric nail disorders: a review. *Curr Opin Pediatr*. (2020) 32:506–15. doi: 10.1097/MOP.0000000000000921
32. Salgado F, Handler MZ, Schwartz RA. Shedding light on onychomadesis. *Cutis*. (2017) 99:33–6. Available online at: https://www.mdedge.com/dermatology/article/128565/pediatrics/shedding-light-onychomadesis?sso=true
33. Li M, Chen Z, Yin S, Xue R, Chen Z, Huang H, et al. Onychomycosis secondary to onychomadesis: an underdiagnosed manifestation. *Mycoses*. (2017) 60:161–5. doi: 10.1111/myc.12555
34. Gera SK, PG Zaini DKH, Wang S, Abdul Rahaman SHB, Chia RF, Lim KBL. Ingrowing toenails in children and adolescents: is nail avulsion

superior to nonoperative treatment? *Singapore Med J*. (2019) 60:94–6. doi: 10.11622/smedj.2018106
35. Lecerf P, Richert B, Theunis A, André J. A retrospective study of squamous cell carcinoma of the nail unit diagnosed in a Belgian general hospital over a 15-year period. *J Am Acad Dermatol*. (2013) 69:253–61. doi: 10.1016/j.jaad.2013.02.008
36. Park JH, Lee DY, Kim N. Nail neoplasms. *J Dermatol*. (2017) 44:279–87. doi: 10.1111/1346-8138.13702
37. Starace M, Alessandrini A, Dika E, Piraccini BM. Squamous cell carcinoma of the nail unit. *Dermatol Pract Concept*. (2018) 8:238–44. doi: 10.5826/dpc.0803a017
38. Lee TM, Jo G, Kim M, Lee SH, Cho SI, Jo SJ, et al. Squamous cell carcinoma of the nail unit: a retrospective review of 19 cases in Asia and comparative review of Western literature. *Int J Dermatol*. (2019) 58:428–32. doi: 10.1111/ijd.14306
39. Durbec F, Martin L, Derancourt C, Grange F. Melanoma of the hand and foot: epidemiological, prognostic and genetic features. A systematic review. *Br J Dermatol*. (2012) 166:727–39. doi: 10.1111/j.1365-2133.2011.10772.x
40. Csányi I, Houshmand N, Szucs M, Ócsai H, Kemény L, Oláh J, et al. Acral lentiginous melanoma: a single-centre retrospective review of four decades in East-Central Europe. *J Eur Acad Dermatol Venereol*. (2020) 34:2004–10. doi: 10.1111/jdv.16227
41. Levit EK, Kagen MH, Scher RK, Grossman M, Altman E. The ABC rule for clinical detection of subungual melanoma. *J Am Acad Dermatol*. (2000) 42:269–74. doi: 10.1016/S0190-9622(00)90137-3
42. Sohng C, Han MH, Park D, Park KD, Jang YH, Lee WJ, et al. Clinical features of subungual melanoma according to the extent of Hutchinson's nail sign: a retrospective single-centre study. *J Eur Acad Dermatol Venereol*. (2020) 35:380–6. doi: 10.1111/jdv.16762
43. Phan A, Dalle S, Touzet S, Ronger-Savlé S, Balme B, Thomas L. Dermoscopic features of acral lentiginous melanoma in a large series of 110 cases in a white population. *Br J Dermatol*. (2010) 162:765–71. doi: 10.1111/j.1365-2133.2009.09594.x
44. Ohn J, Jo G, Cho Y, Sheu SL, Cho KH, Mun JH. Assessment of a predictive scoring model for dermoscopy of subungual melanoma *in situ*. *JAMA Dermatol*. (2018) 154:890–6. doi: 10.1001/jamadermatol.2018.1372
45. Riahi RR, Cohen PR, Goldberg LH. Subungual nail bed melanoma masquerading as tinea ungium. *Dermatol Online J*. (2018) 24. Retrieved from: https://escholarship.org/uc/item/4z5191rj
46. Gatica-Torres M, Nelson CA, Lipoff JB, Miller CJ, Rubin AI. Nail clipping with onychomycosis and surprise clue to the diagnosis of nail unit melanoma. *J Cutan Pathol*. (2018) 45:803–6. doi: 10.1111/cup.13333
47. Lipner SR, Scher RK. Onychomycosis—a small step for quality of care. *Curr Med Res Opin*. (2016) 32:865–7. doi: 10.1185/03007995.2016.1147026
48. Lipner SR, Scher RK. Confirmatory testing for onychomycosis. *JAMA Dermatol*. (2016) 152:847. doi: 10.1001/jamadermatol.2016.0785
49. Dasgupta T, Sahu J. Origins of the KOH technique. *Clin Dermatol*. (2012) 30:238–41; discussion 41-2. doi: 10.1016/j.clindermatol.2011.11.020
50. Weinberg JM, Koestenblatt EK, Tutrone WD, Tishler HR, Najarian L. Comparison of diagnostic methods in the evaluation of onychomycosis. *J Am Acad Dermatol*. (2003) 49:193–7. doi: 10.1067/S0190-9622(03)01480-4
51. Velasquez-Agudelo V, Cardona-Arias JA. Meta-analysis of the utility of culture, biopsy, and direct KOH examination for the diagnosis of onychomycosis. *BMC Infect Dis*. (2017) 17:166. doi: 10.1186/s12879-017-2258-3
52. Gupta AK, Simpson FC. Diagnosing onychomycosis. *Clin Dermatol*. (2013) 31:540–3. doi: 10.1016/j.clindermatol.2013.06.009
53. Ghannoum M, Mukherjee P, Isham N, Markinson B, Rosso JD, Leal L. Examining the importance of laboratory and diagnostic testing when treating and diagnosing onychomycosis. *Int J Dermatol*. (2018) 57:131–8. doi: 10.1111/ijd.13690
54. Kayarkatte MN, Singal A, Pandhi D, Das S, Sharma S. Nail dermoscopy (onychoscopy) findings in the diagnosis of primary onychomycosis: a cross-sectional study. *Indian J Dermatol Venereol Leprol*. (2020) 86:341–9. doi: 10.4103/ijdvl.IJDVL_100_19
55. Pharaon M, Gari-Toussaint M, Khemis A, Zorzi K, Petit L, Martel P, et al. Diagnosis and treatment monitoring of toenail onychomycosis by reflectance confocal microscopy: prospective cohort study in 58 patients. *J Am Acad Dermatol*. (2014) 71:56–61. doi: 10.1016/j.jaad.2014.02.020
56. Rothmund G, Sattler EC, Kaestle R, Fischer C, Haas CJ, Starz H, et al. Confocal laser scanning microscopy as a new valuable tool in the diagnosis of onychomycosis—comparison of six diagnostic methods. *Mycoses*. (2013) 56:47–55. doi: 10.1111/j.1439-0507.2012.02198.x
57. Krammer S, Krammer C, Vladimirova G, Salzer S, Ruini C, Sattler E, et al. *Ex vivo* confocal laser scanning microscopy: a potential new diagnostic imaging tool in onychomycosis comparable with gold standard techniques. *Front Med (Lausanne)*. (2020) 7:586648. doi: 10.3389/fmed.2020.586648
58. Kondori N, Abrahamsson AL, Ataollahy N, Wennerås C. Comparison of a new commercial test, Dermatophyte-PCR kit, with conventional methods for rapid detection and identification of *Trichophyton rubrum* in nail specimens. *Med Mycol*. (2010) 48:1005–8. doi: 10.3109/13693781003743130
59. Mehlig L, Garve C, Ritschel A, Zeiler A, Brabetz W, Weber C, et al. Clinical evaluation of a novel commercial multiplex-based PCR diagnostic test for differential diagnosis of dermatomycoses. *Mycoses*. (2014) 57:27–34. doi: 10.1111/myc.12097
60. Petinataud D, Berger S, Ferdynus C, Debourgogne A, Contet-Audonneau N, Machouart M. Optimising the diagnostic strategy for onychomycosis from sample collection to FUNGAL identification evaluation of a diagnostic kit for real-time PCR. *Mycoses*. (2016) 59:304–11. doi: 10.1111/myc.12471
61. Hafirassou AZ, Valero C, Gassem N, Mihoubi I, Buitrago MJ. Usefulness of techniques based on real time PCR for the identification of onychomycosis-causing species. *Mycoses*. (2017) 60:638–44. doi: 10.1111/myc.12629
62. Kim YJ, Han SS, Yang HJ, Chang SE. Prospective, comparative evaluation of a deep neural network and dermoscopy in the diagnosis of onychomycosis. *PLoS ONE*. (2020) 15:e0234334. doi: 10.1371/journal.pone.0234334
63. Han SS, Park GH, Lim W, Kim MS, Na JI, Park I, et al. Deep neural networks show an equivalent and often superior performance to dermatologists in onychomycosis diagnosis: automatic construction of onychomycosis datasets by region-based convolutional deep neural network. *PLoS ONE*. (2018) 13:e0191493. doi: 10.1371/journal.pone.0191493
64. Jeelani S, Ahmed QM, Lanker AM, Hassan I, Jeelani N, Fazili T. Histopathological examination of nail clippings using PAS staining (HPE-PAS): gold standard in diagnosis of Onychomycosis. *Mycoses*. (2015) 58:27–32. doi: 10.1111/myc.12251
65. Feuilhade de Chauvin M. New diagnostic techniques. *J Eur Acad Dermatol Venereol*. (2005) 19(Suppl. 1):20–4. doi: 10.1111/j.1468-3083.2005.01287.x
66. Stephen S, Tosti A, Rubin AI. Diagnostic applications of nail clippings. *Dermatol Clin*. (2015) 33:289–301. doi: 10.1016/j.det.2014.12.011
67. Bertanha L, Chiacchio ND. Nail clipping in onychomycosis. *An Bras Dermatol*. (2016) 91:688–90. doi: 10.1590/abd1806-4841.20164968
68. Lilly KK, Koshnick RL, Grill JP, Khalil ZM, Nelson DB, Warshaw EM. Cost-effectiveness of diagnostic tests for toenail onychomycosis: a repeated-measure, single-blinded, cross-sectional evaluation of 7 diagnostic tests. *J Am Acad Dermatol*. (2006) 55:620–6. doi: 10.1016/j.jaad.2006.03.033
69. Ohn J, Choe YS, Park J, Mun JH. Dermoscopic patterns of fungal melanonychia: a comparative study with other causes of melanonychia. *J Am Acad Dermatol*. (2017) 76:488–93.e2. doi: 10.1016/j.jaad.2016.08.013
70. Jo G, Mun J. Dermoscopic findings in onychomycosis. *Korean J Med Mycol*. (2017) 22:50–1. doi: 10.17966/kjmm.2017.22.1.50
71. Hongcharu W, Dwyer P, Gonzalez S, Anderson RR. Confirmation of onychomycosis by *in vivo* confocal microscopy. *J Am Acad Dermatol*. (2000) 42:214–6. doi: 10.1016/S0190-9622(00)90128-2
72. Cinotti E, Fouilloux B, Perrot JL, Labeille B, Douchet C, Cambazard F. Confocal microscopy for healthy and pathological nail. *J Eur Acad Dermatol Venereol*. (2014) 28:853–8. doi: 10.1111/jdv.12330
73. Jensen RH, Arendrup MC. Molecular diagnosis of dermatophyte infections. *Curr Opin Infect Dis*. (2012) 25:126–34. doi: 10.1097/QCO.0b013e32834f5f6e
74. Watanabe S, Ishida K. Molecular diagnostic techniques for onychomycosis: validity and potential application. *Am J Clin Dermatol*. (2017) 18:281–6. doi: 10.1007/s40257-016-0248-7
75. Erhard M, Hipler UC, Burmester A, Brakhage AA, Wöstemeyer J. Identification of dermatophyte species causing onychomycosis and tinea pedis by MALDI-TOF mass spectrometry. *Exp Dermatol*. (2008) 17:356–61. doi: 10.1111/j.1600-0625.2007.00649.x
76. Briganti G, Le Moine O. Artificial intelligence in medicine: today and tomorrow. *Front Med (Lausanne)*. (2020) 7:27. doi: 10.3389/fmed.2020.00027

77. Cho SI, Han B, Hur K, Mun JH. Perceptions and attitudes of medical students regarding artificial intelligence in dermatology. *J Eur Acad Dermatol Venereol*. (2020) 35:e72–3. doi: 10.1111/jdv.16812
78. Esteva A, Kuprel B, Novoa RA, Ko J, Swetter SM, Blau HM, et al. Dermatologist-level classification of skin cancer with deep neural networks. *Nature*. (2017) 542:115–8. doi: 10.1038/nature21056
79. Gulshan V, Peng L, Coram M, Stumpe MC, Wu D, Narayanaswamy A, et al. Development and validation of a deep learning algorithm for detection of diabetic retinopathy in retinal fundus photographs. *JAMA*. (2016) 316:2402–10. doi: 10.1001/jama.2016.17216
80. Polesie S, Gillstedt M, Kittler H, Lallas A, Tschandl P, Zalaudek I, et al. Attitudes towards artificial intelligence within dermatology: an international online survey. *Br J Dermatol*. (2020) 183:159–61. doi: 10.1111/bjd.18875
81. Tschandl P, Rinner C, Apalla Z, Argenziano G, Codella N, Halpern A, et al. Human-computer collaboration for skin cancer recognition. *Nat Med*. (2020) 26:1229–34. doi: 10.1038/s41591-020-0942-0
82. Gomolin A, Netchiporouk E, Gniadecki R, Litvinov IV. Artificial intelligence applications in dermatology: where do we stand? *Front Med (Lausanne)*. (2020) 7:100. doi: 10.3389/fmed.2020.00100

Conflict of Interest: The authors declare that the research was conducted in the absence of any commercial or financial relationships that could be construed as a potential conflict of interest.

frontiers in Medicine

ORIGINAL RESEARCH
published: 16 April 2021
doi: 10.3389/fmed.2021.626369

A Deep Learning Based Framework for Diagnosing Multiple Skin Diseases in a Clinical Environment

Chen-Yu Zhu[1†], Yu-Kun Wang[1†], Hai-Peng Chen[2], Kun-Lun Gao[2], Chang Shu[1], Jun-Cheng Wang[1], Li-Feng Yan[2], Yi-Guang Yang[3], Feng-Ying Xie[3] and Jie Liu[1]*

[1] Department of Dermatology, State Key Laboratory of Complex Severe and Rare Diseases, Peking Union Medical College Hospital, Chinese Academy of Medical Sciences and Peking Union Medical College, Beijing, China, [2] DeepWise AI Lab, Beijing, China, [3] Image Processing Center, School of Astronautics, Beihang University, Beijing, China

OPEN ACCESS

Edited by:
H. Peter Soyer, The University of Queensland, Australia

Reviewed by:
Elisabeth Ammitzbøll, Private Practitioner, Hareskov Hudklinik, Værløse, Denmark
Philippe Lefrançois, McGill University, Canada

****Correspondence:***
Jie Liu
liujie04672@pumch.cn

[†] These authors have contributed equally to this work

Specialty section:
This article was submitted to This article was submitted to Dermatology, a specialty of Frontiers in Medicine, a section of the journal Frontiers in Medicine

Received: *05 November 2020*
Accepted: *25 March 2021*
Published: *16 April 2021*

Citation:
Zhu C-Y, Wang Y-K, Chen H-P, Gao K-L, Shu C, Wang J-C, Yan L-F, Yang Y-G, Xie F-Y and Liu J (2021) A Deep Learning Based Framework for Diagnosing Multiple Skin Diseases in a Clinical Environment. Front. Med. 8:626369. doi: 10.3389/fmed.2021.626369

Background: Numerous studies have attempted to apply artificial intelligence (AI) in the dermatological field, mainly on the classification and segmentation of various dermatoses. However, researches under real clinical settings are scarce.

Objectives: This study was aimed to construct a novel framework based on deep learning trained by a dataset that represented the real clinical environment in a tertiary class hospital in China, for better adaptation of the AI application in clinical practice among Asian patients.

Methods: Our dataset was composed of 13,603 dermatologist-labeled dermoscopic images, containing 14 categories of diseases, namely lichen planus (LP), rosacea (Rosa), viral warts (VW), acne vulgaris (AV), keloid and hypertrophic scar (KAHS), eczema and dermatitis (EAD), dermatofibroma (DF), seborrheic dermatitis (SD), seborrheic keratosis (SK), melanocytic nevus (MN), hemangioma (Hem), psoriasis (Pso), port wine stain (PWS), and basal cell carcinoma (BCC). In this study, we applied Google's EfficientNet-b4 with pre-trained weights on ImageNet as the backbone of our CNN architecture. The final fully-connected classification layer was replaced with 14 output neurons. We added seven auxiliary classifiers to each of the intermediate layer groups. The modified model was retrained with our dataset and implemented using Pytorch. We constructed saliency maps to visualize our network's attention area of input images for its prediction. To explore the visual characteristics of different clinical classes, we also examined the internal image features learned by the proposed framework using t-SNE (t-distributed Stochastic Neighbor Embedding).

Results: Test results showed that the proposed framework achieved a high level of classification performance with an overall accuracy of 0.948, a sensitivity of 0.934 and a specificity of 0.950. We also compared the performance of our algorithm with three most widely used CNN models which showed our model outperformed existing models with the highest area under curve (AUC) of 0.985. We further compared this model with 280 board-certificated dermatologists, and results showed a comparable performance level in an 8-class diagnostic task.

Conclusions: The proposed framework retrained by the dataset that represented the real clinical environment in our department could accurately classify most common dermatoses that we encountered during outpatient practice including infectious and inflammatory dermatoses, benign and malignant cutaneous tumors.

Keywords: artificial intelligence, deep learning, convolutional neural networks, dermatology, skin diseases, skin imaging, dermoscopy

INTRODUCTION

Dermatology is a branch of clinical medicine of which the diagnosis and treatment monitor greatly rely on the morphology of various cutaneous lesions. The traditional diagnostic process of dermatoses is thus based on the integration of patients' medical history, clinical manifestation, dermoscopic images and sometimes histopathological evaluation by the dermatologists. However, the training of becoming an experienced dermatologist is time-consuming. Furthermore, cutaneous diseases are vast in type and can be very similar in appearance under human eyes, leading to the difficulties in accurate and effective diagnosis. Recent advances on artificial intelligence (AI), particularly convolutional neural networks (CNN) based deep learning algorithms, have made it possible to learn the most predictive features of diseases directly from medical images given a large dataset of labeled examples (1, 2). Esteva et al. proposed a dermatologist level classification of skin cancer via fine-tuning a pre-trained Inception-v3 network (3). Menegola et al. also conducted experiments comparing training from scratch with fine-tuning of pre-trained networks on images with skin lesions (4). Their work showed that fine-tuning of pre-trained networks worked better than training from scratch. Numerous researches based on AI using dermoscopic and non-dermoscopic images have attempted to apply this technology in the dermatological field, including segmentation and classification of melanocytic tumors, keratinocyte tumors, ulcers, psoriasis and other inflammatory dermatoses (5–11). Some of the AI models showed astonishing diagnostic capacity that could reach or even surpass a dermatologist level (3, 7, 12, 13). Therefore, currently those computer-aided diagnostic model applications are tied with great hope and promise in screening and helping to diagnose cutaneous diseases.

Although these studies have achieved acceptable accuracy in specific diseases with different models trained by various databases, researches under real clinical settings are scarce. Additionally, previous studies applying AI models in real clinical settings showed relatively poorer performance outcomes comparing with that using their own experimental datasets (14, 15). In clinical practice, the most frequently encountered diseases are not limited to the kinds mentioned above, especially in Asian countries like China where the incidence of melanoma is relatively lower. Therefore, for better adaption of the AI application in dermatological field, we investigated the imaging database of the Department of Dermatology, Peking Union Medical College Hospital, and extracted the imaging data of the 14 most frequently encountered dermatoses to form a dataset that represented the real clinical environment of our clinics. The disease categories included melanocytic nevus (MN), seborrheic keratosis (SK), dermatofibroma (DF), keloid and hypertrophic scar (KAHS), basal cell carcinoma (BCC), hemangioma (Hem), port wine stain (PWS), eczema/dermatitis (EAD), psoriasis (Pso), seborrheic dermatitis (SD), rosacea (Rosa), acne vulgaris (AV), lichen planus (LP), and viral warts (VW). We used this dataset to construct a novel framework based on deep learning, aiming to verifying the classification performance of this proposed framework under a more practical and representative circumstance, and further compare its diagnostic accuracy with certificated dermatologists in China.

This novel CNN model we proposed here was on the basis of the EfficientNet-b4 CNN algorithm. We utilized multiple auxiliary prediction modules among different intermediate layers to accumulate discriminative information from different levels of features. The proposed CNN model was trained on 13,603 clinical images from 2,538 patient cases, and had been evaluated on expert-confirmed clinical images grouped into 14 different dermatologist-labeled diagnoses mentioned above. According to the experiment, it outperformed common convolutional networks and was competitive with dermatologists in real-world diagnosis.

MATERIALS AND METHODS

Ethical Approval

We conducted this research according to the ethical tenets of the *Declaration of Helsinki*. And this study was approved by the Medical Ethics Committee of Peking Union Medical College Hospital (NO. JS-2003). Informed written consents were obtained from all the included adult patients or the guardians of juvenile patients.

Datasets

Our dataset was collected and formed from the imaging database of the Department of Dermatology, Peking Union Medical College Hospital in China from October 2016 to April 2020. All the included patients were Asian with Fitzpatrick skin type III or IV, and their dermoscopic images were consecutively acquired using a digital dermoscopy system (MoleMax HD 1.0 dermoscope, Digital Image Systems, Vienna, Austria) by the same technician to ensure the quality and standardization of the images. Generally, multiple dermoscopic images were captured of a single lesion in different angles or in subsequent follow-up presentations. The annotation process was performed by 2 dermatologists with more than 5-years experience according

to the patients' medical history, clinical manifestations and dermoscopic features independently. All the patients with BCC and few ambiguous cases with benign conditions were confirmed by histopathological investigations. Whenever there was a disagreement between the annotators, consensus was reached through discussion or consultant with a third dermatological expert. Cases with unclear or incomplete medical history, whose images were poorly focused, and lesions located on the nail or mucosa areas were excluded. The final dataset for the development of the model and the demographic characteristics of the included patients were shown in **Table 1**.

CNN and Deep Learning Algorithm

Instead of training a new model from scratch, we applied a fine-tuning strategy directly on pre-trained models via a multi-step retraining strategy with our dataset. In this strategy, we gradually unfroze the layer weights in steps with the first few layers being unfrozen last. In these steps, we reduced learning rates progressively from 1e-3 to 1e-5 and kept other parameters unchanged. As shown in **Figure 1**, we applied Google's EfficientNet-b4 (16) with pre-trained weights on the 2015 ImageNet dataset (17) with 1,000 object categories as the backbone of the proposed deep learning framework. The final fully-connected classification layer was replaced with 14 output neurons of our classifier. We also add seven auxiliary classifiers at the end of each intermediate layer (18) to make the model learn classification information from different level of features as shown in **Figure 2**.

Our deep learning network was implemented using Pytorch. Initially, a global learning rate 0.001 was used and it decayed to 0.0001 at epoch 25. We used a mini-batch gradient descent with a momentum 0.9 as the model parameters optimizer. In training, each image was resized to 380*380 pixels in RGB channels, the optimized input size of EfficientNet-b4. For each epoch, each image would be rotated from -30° to 30° randomly, together with 50% probabilities for vertical and horizontal flipping. Color constancy method was also applied to eliminate the color deviation.

The raw output of our classifiers (seven auxiliary classifiers plus 1 final classifier) was summarized by 14 classification neurons. And then an argmax operation was used to find the most likely classification of the input image. The formula is as follows:

$$\text{classification} = \text{argmax}\left(\sum_{i=1}^{\text{Classifiers\_number}} \text{output}_i\right)$$

where output_i is the classification vector with dimension (1, 14) and the sum of eight classification vectors is an element-wise summation.

Saliency Maps

As illustrated in **Figure 3**, to facilitate triaging referrals and focusing one's clinical examination, we also created a heatmap via gradient-weighted class activation mapping (Grad-CAM) algorithm (20), which can produce visual explanations for CNN based deep learning models. Grad-CAM uses the gradient information flowing into the last convolutional layer to understand the importance of each neuron for a decision of interest thereby highlighting the important regions in the image for prediction. In our case, we used gradients of 14 classification neurons which flowed into the final convolutional layer to produce a coarse localization map highlighting the important regions in the image for predicting the label. It can be noticed that our network has the capability of focusing on the skin area affected by the disease and neglecting the background pixels and healthy skin around the lesions.

Comparison Between the Proposed CNN Model and Previous Reported Methods

To both quantitatively and qualitatively demonstrate the effectiveness of the proposed deep learning framework, we compared the performance of our algorithm with previous reported methods, namely Inception-v3 (19), ResNet-101 (21), and the original EfficientNet-b4 (16) using our test set.

Comparison Between our CNN Model and Dermatologists

We also compared the proposed framework with 280 board-certified dermatologists who previously participated in at least 72-h systemic dermoscopic training on diagnosing clinical cases, using an independent test set that consisted of 200 cases with a clinical image and a dermoscopic image. These cases were composed by eight categories of diseases, namely MN, SK, BCC, EAD, SD, Pso, VW and Rosa, with 25 cases each (also demonstrated in **Table 1**). For this reader study, every dermatologist was asked for the most likely diagnosis of each case from eight choices of included diseases. This questionnaire reflects the actual in-clinic task that dermatologists will decide whether or not to request further examinations or biopsies. For a fair comparison, the proposed deep learning framework also output the top-1 diagnosis with probabilities/confidence scores of the same 8 categories. However, clinical images were not provided to our CNN model. The outcome was considered "Correct" when the diagnosis made by the proposed deep learning framework or a dermatologist was the real diagnosis for the corresponding case.

Statistical Analysis

In the reader study, Kappa coefficients were used to assess the consistency between dermatologists (or CNN) and the reference standard on the classification of each disease. Kappa coefficient >0.75 indicates good consistency, 0.40–0.75 indicates moderate consistency, and <0.40 indicates poor consistency. Adjusted Z-tests were used to assess differences in Kappa coefficients between dermatologists and CNN. We also calculated the Kappa coefficients of the dermatologists (as standard) and included CNNs. Results were considered statistically significant at the $P < 0.05$ level. All analyses were carried out using Scikit-learn 0.22.2 and Numpy 1.16.4.

TABLE 1 | Dataset overview.

Characteristics	Development set		Test set of the reader study	
	Images	Patients	Images	Patients
Numbers included in study (*n*)	13,603	2,538	200	200
Mean age (years), mean ± SD (range)	-	57.38 ± 16.81	-	43.55 ± 19.68
Female, *n* (%)	-	1,532 (60.36)	-	123 (61.50)
Lichen planus, *n* (%)	804 (5.91)	126 (4.96)	-	-
Rosacea, *n* (%)	597 (4.39)	80 (3.15)	25 (12.5)	25 (12.5)
Viral warts, *n* (%)	1,110(8.16)	298 (11.74)	25 (12.5)	25 (12.5)
Acne vulgaris, *n* (%)	2,023(14.87)	277 (10.91)	-	-
Keloid and hypertrophic scar, *n* (%)	438 (3.22)	96 (3.78)	-	-
Eczema/dermatitis, *n* (%)	2,440 (17.94)	419 (16.51)	25 (12.5)	25 (12.5)
Dermatofibroma, *n* (%)	343 (2.52)	116 (4.57)	-	-
Seborrheic dermatitis, *n* (%)	767 (5.64)	124 (4.89)	25 (12.5)	25 (12.5)
Seborrheic keratosis, *n* (%)	553 (4.07)	143 (5.63)	25 (12.5)	25 (12.5)
Melanocytic nevus, *n* (%)	1,214 (8.92)	345 (13.59)	25 (12.5)	25 (12.5)
Hemangioma, *n* (%)	200 (14.70)	61 (2.40)	-	-
Psoriasis, *n* (%)	1,707 (12.55)	234 (9.22)	25 (12.5)	25 (12.5)
Port wine stain, *n* (%)	920 (6.76)	112 (4.41)	-	-
Basal cell carcinoma, *n* (%)	487 (3.58)	107 (4.22)	25 (12.5)	25 (12.5)

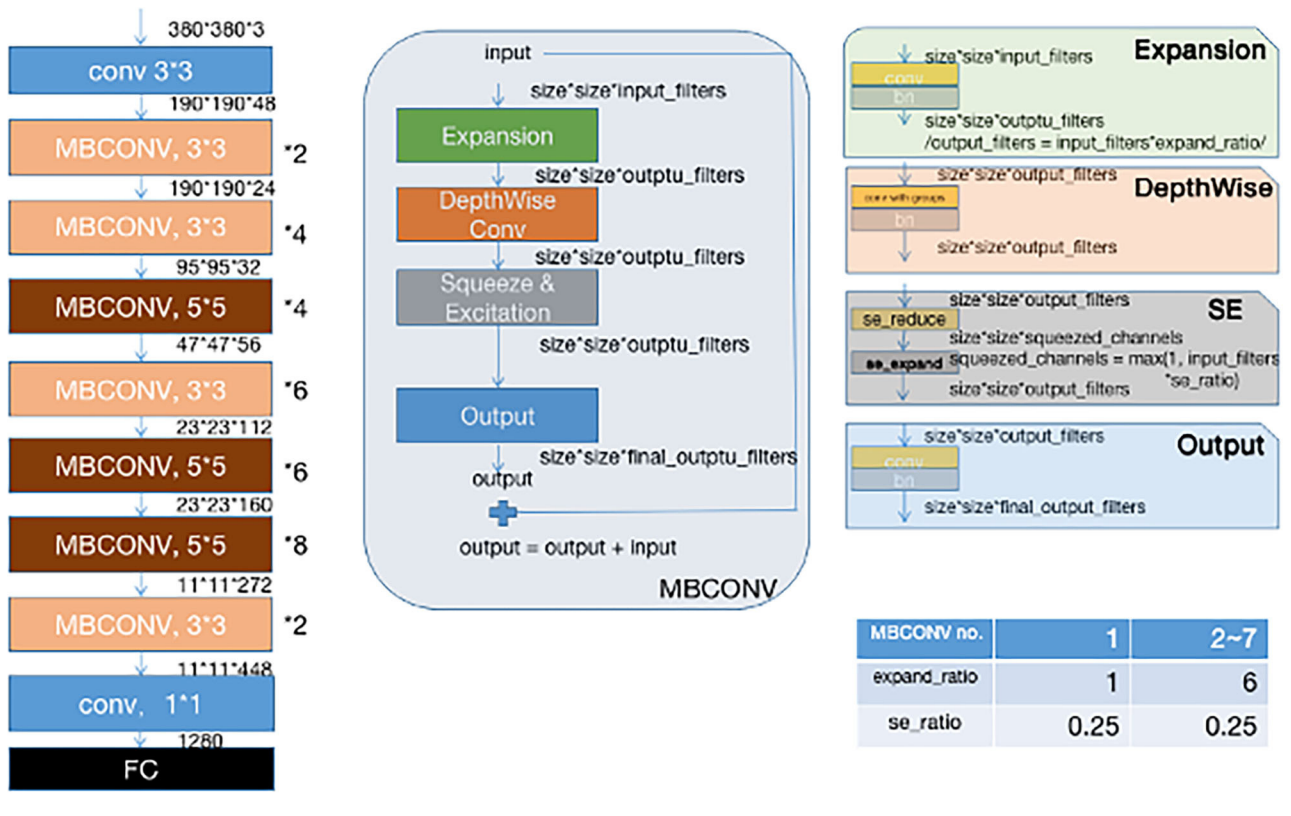

FIGURE 1 | Original efficientnet-b4 architecture.

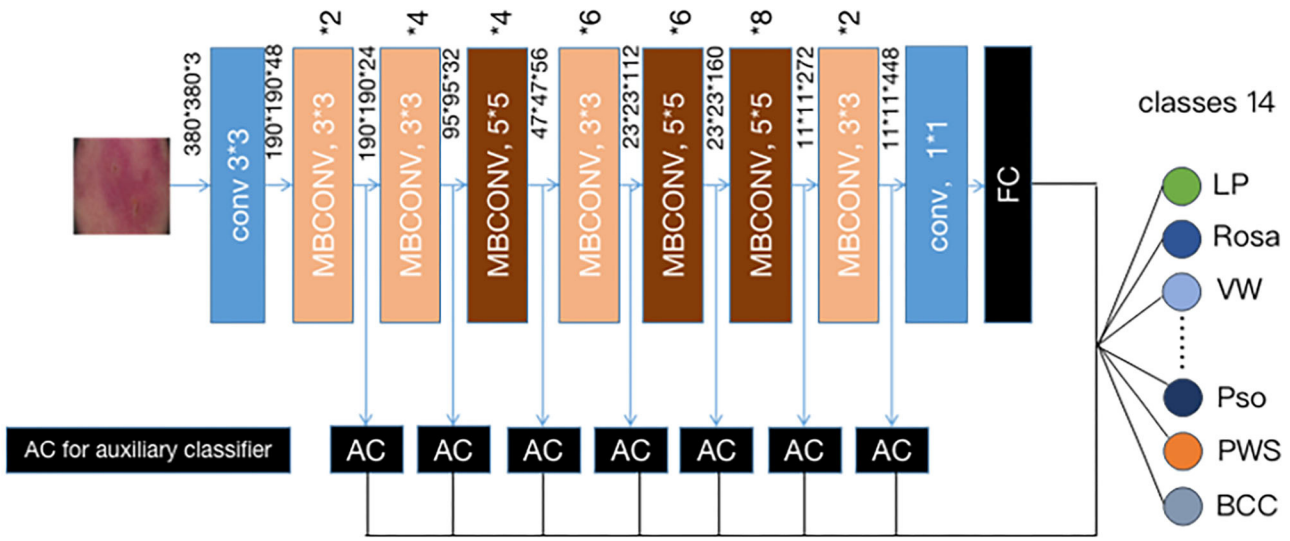

FIGURE 2 | Our modified (19) EFFICIENTNET-b4 architecture. Data flow is from left to right: a dermoscopic image is put into the network and finally transformed into a probability distribution over clinical classes of skin disease using our modified EfficientNet-b4 architecture pretrained on the ImageNet dataset and fine-tuned on our own dataset of 13,603 dermoscopic images in 14 categories.

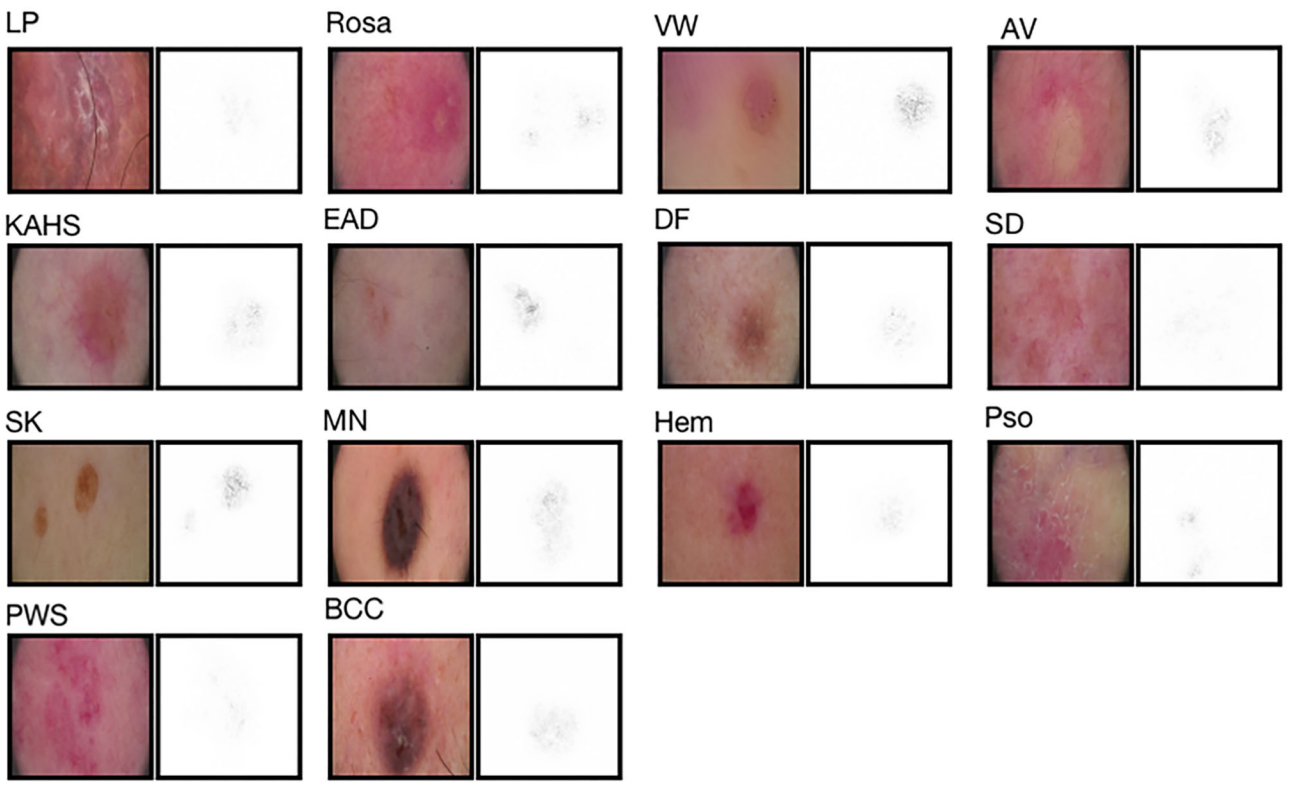

FIGURE 3 | Saliency maps for 14 example images from validation set. Saliency maps for example images from each of the 14 disease classes of the validation set reveal the pixels that most influence a CNN's prediction. Saliency maps show the pixel gradients with respect to the CNN's loss function.

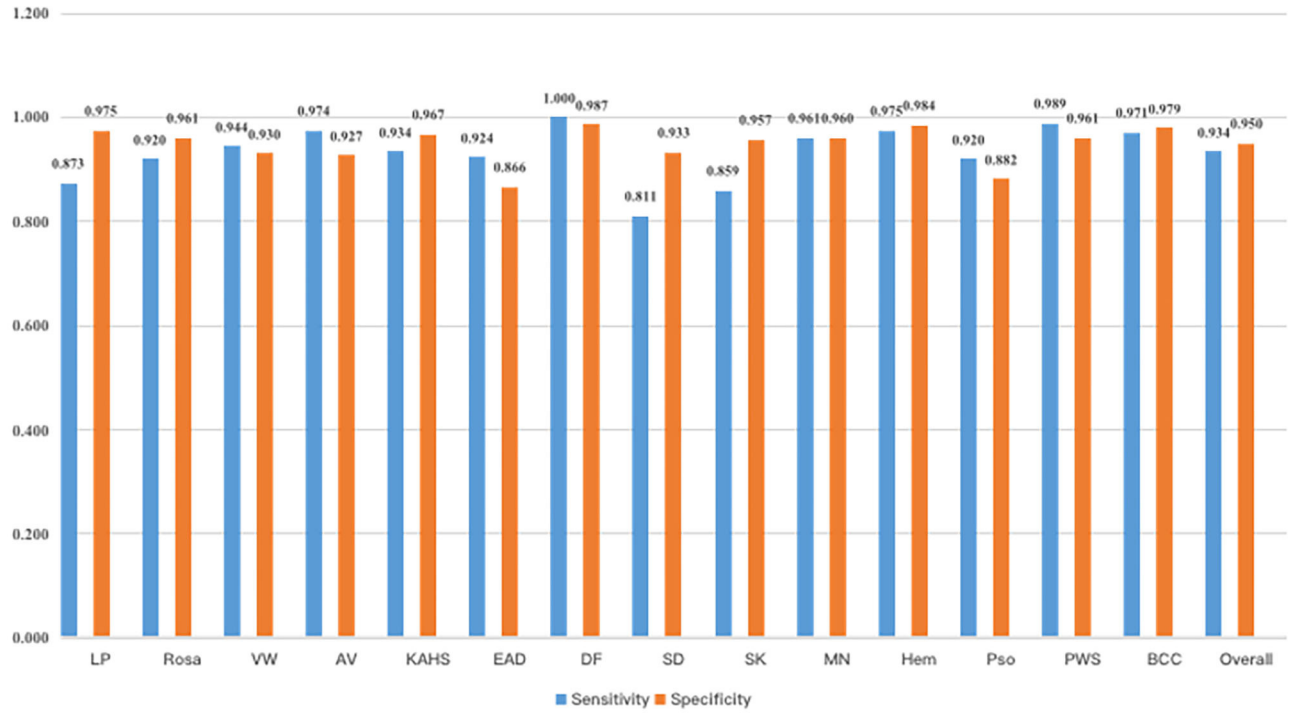

FIGURE 4 | Sensitivity and specificity of our model. As a result, our model had an overall sensitivity of 93.38 ± 0.08% and specificity 94.85 ± 0.05%.

RESULTS

Performance Evaluation

To evaluate the performance of the proposed framework, we applied our method on a dataset of 13,603 dermatologist-labeled images with 14 categories of skin diseases. Sensitivity and specificity defined below are applied as the performance evaluation metrics:

$$\text{Sensitivity} = \frac{\text{true positive}}{\text{positive}}$$

$$\text{Specificity} = \frac{\text{true negative}}{\text{negative}}$$

Figure 4 demonstrated that the proposed framework achieved a rather high overall accuracy of 0.948 ± 0.001 (mean ± SD), with a sensitivity of 0.934 ± 0.001 (mean ± SD), a specificity of 0.950 ± 0.001 (mean ± SD). The specific diagnostic values according to disease categories were summarized in **Table 2**. Receiver operating characteristic (ROC) curve in **Figure 5** also showed that the proposed model achieved 0.985 of area under curve (AUC) value in 14-way classification. **Figure 6** illustrated the corresponding confusion matrices for the 14 predefined diseases. The diagonal of the matrix showed the overlap of true positives and ground truth for each label, while the other cells of the matrix were misclassification of images with their true labels.

TABLE 2 | The classification accuracy, sensitivity and specificity of the proposed CNN model according to disease category.

Disease category	Accuracy	Sensitivity	Specificity
Overall	0.948	0.934	0.950
Lichen planus	0.969	0.873	0.975
Rosacea	0.959	0.920	0.961
Viral warts	0.932	0.944	0.930
Acne vulgaris	0.935	0.974	0.927
Keloid and hypertrophic scar	0.969	0.934	0.970
Eczema/dermatitis	0.877	0.924	0.866
Dermatofibroma	0.987	1.000	0.987
Seborrheic dermatitis	0.926	0.811	0.933
Seborrheic keratosis	0.953	0.858	0.957
Melanocytic nevus	0.960	0.961	0.960
Hemangioma	0.984	0.975	0.984
Psoriasis	0.886	0.920	0.882
Port wine stain	0.963	0.989	0.961
Basal cell carcinoma	0.979	0.971	0.979

Comparative Outcomes Between the Proposed CNN Model and Previous Reported Methods

Figure 7 demonstrated the comparative results among our model, Inception-v3, ResNet-101 and the original EfficientNet-b4 with respect to the ROC curves and the AUC value. The AUC

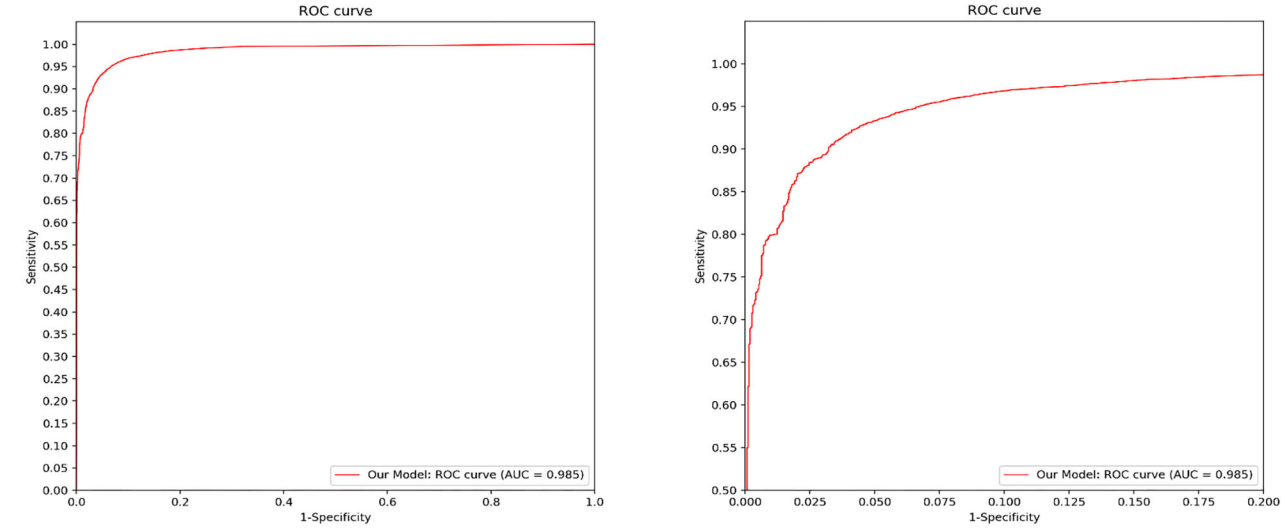

FIGURE 5 | Disease classification performance of the proposed model. We fix a threshold probability t such that the prediction y for any image is y = P ≥ t, and the curve is drawn by sweeping t in the interval 0–1. The AUC is the CNN's measure of performance, with a maximum value of 1. Our model achieves 0.985 AUC in 14-way classification. **(A)** The full view of the ROC curve of the proposed model. **(B)** The local enlarged image of the ROC curve between abscissa 0∼0.2.

value can reflect the overall accuracy of each model. As shown in **Figure 7**, our model has the best diagnosis performance over all other models. To be specific, our model outperformed existing models with the highest AUC of 0.985 whereas the Inception-v3 had an AUC of 0.953; the ResNet-101 had an AUC of 0.976; and the original EfficientNet-b4 had an AUC of 0.948, respectively, and the ROC curve of our CNN model was always situated higher than the ROC curves of other 3 models. **Table 3** revealed the detailed overall sensitivity, specificity and accuracy of our and other 3 CNN models.

Comparative Outcomes Between our CNN Model and Dermatologists

The general information of patients included in an independent dataset is also shown **Table 1**. The performance of our CNN model and that of the dermatologists using the reader study test set is revealed in **Table 4**. The proposed CNN model achieved 92.75% average accuracy for all 200 cases, with a sensitivity of 83.50% and a specificity of 94.07%. While the average accuracy of board-certificated dermatologists is 92.13%, with an average sensitivity of 68.51% and an average specificity of 95.50%. Furthermore, according to the Kappa coefficients and adjusted Z test (summarized in **Table 5**), except for EAD and SD, the CNN model reached better consistency (moderate to good) with the reference standard than the average level of 280 dermatologists, and the difference is statistically significant. It needs to be mentioned that the CNNs is extremely fast, yielding its ranked diagnosis selections within 0.04 s. We also analyzed the diagnostic consistency of dermatologists (as standard) and 4 included CNN models on the 8-class task. Results showed that when taking dermatologists' performance as standard, statistical significance of differences between our model and dermatologists lay merely in psoriasis, and the Kappa coefficient of our model was higher than dermatologists (0.795 vs. 0.675). Furthermore, dermatologists' performance was significantly better than Origin EfficientNet in diagnosing Rosa (0.683 vs. 0.304) and worse in VW (0.533 vs. 0.759). Differences of other classifications between dermatologists and CNNs did not show statistical significance.

Visualization of Internal Features

To explore the visual characteristics of different clinical classes, we examined the internal features learned by the proposed framework using t-SNE (t-distributed Stochastic Neighbor Embedding) (22). As demonstrated in **Figure 8**, each point represents a skin image projected from the 1792-dimensional output of the last hidden layer of the proposed network into 2-dimensions. We can notice clusters of points from same clinical classes. This visualization represents that our method is capable of separating various skin diseases objectively for referral.

DISCUSSION

In China, the board-certificated dermatologists are sparse, with the dermatologist to patient ratio as low as 1:60,000. Furthermore, the majority of well-trained dermatologists are practicing in large cities which worsens the reality that the demand for dermatological consultant is increasingly difficult to satisfy in remote and rural areas of China (23). Moreover, the capacity of giving correct diagnosis and management plans of Chinese dermatologists vary tremendously due to the imbalanced training and learning opportunities of

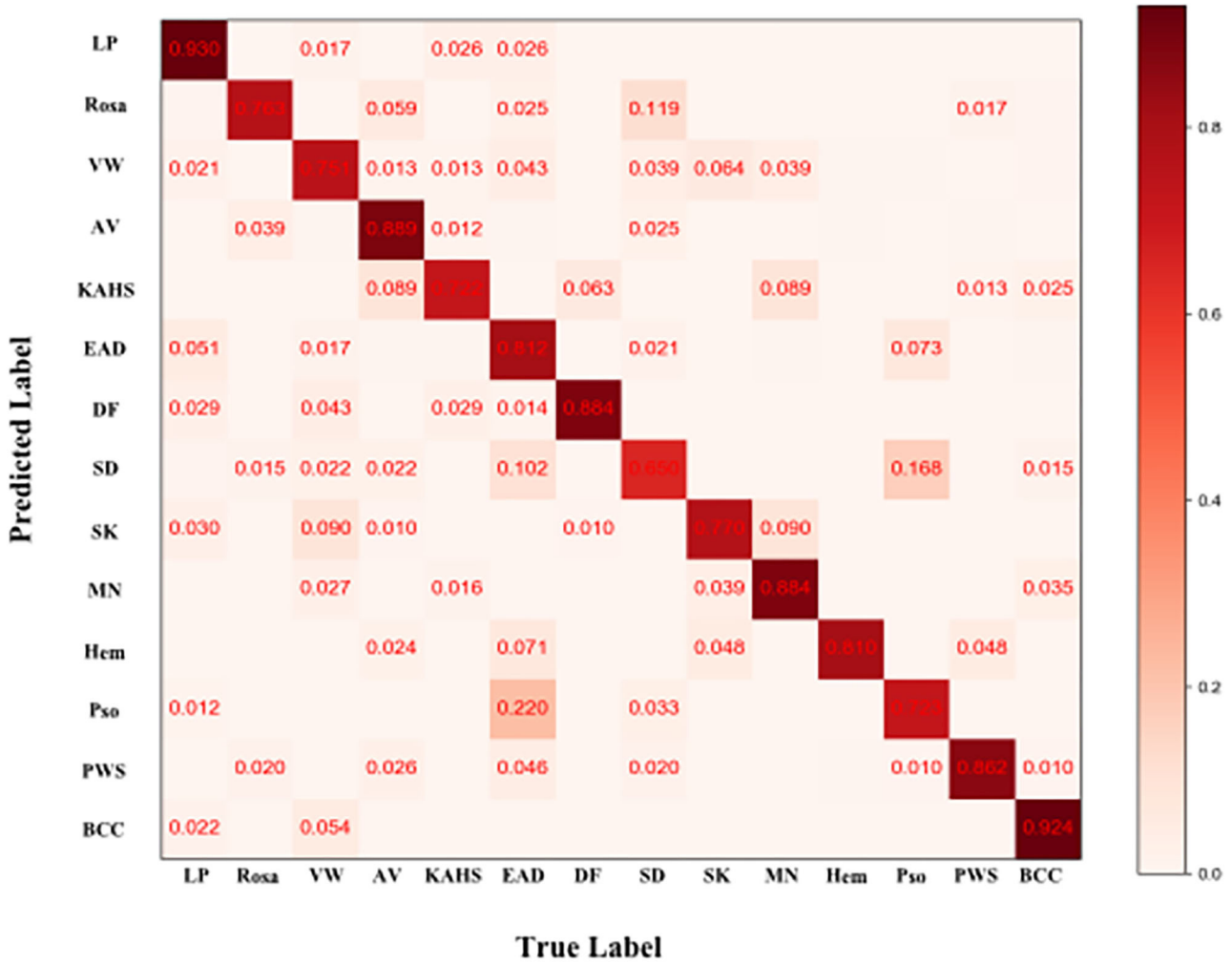

FIGURE 6 | Confusion matrix of the classification result. Element (i, j) of each confusion matrix represents the empirical probability of predicting class i given that the ground truth was class j, with i and j referencing classes from **Table 1**. Light red means low percentage and deep red represents high percentage.

medical education system in China. Although the growing application of multiple non-invasive skin imaging techniques such as dermoscopy, high-frequency ultrasonography and reflectance confocal microscopy has to some extent improved the diagnostic accuracy of Chinese dermatologists, the reality is still not optimistic according to a recent study shown that the imaging diagnostic ability for cutaneous tumors of Chinese dermatologists is relatively poor, and the results of dermatologists in different regions are uneven (24). The insufficiency of well-trained dermatologists and the high incidence of misdiagnosis are calling for a more efficient and accurate way of screening and triaging the Chinese patients suffered from cutaneous diseases.

Ever since Esteva et al. (3) reported that their CNN model, utilizing a GoogleNet Inception v3 CNN architecture trained by a large datasets (>120,000 dermoscopic images), could outperform board-certified dermatologists in classification of skin cancer, the number of researches on AI application in dermatology is constantly increasing and many of them could achieve a dermatologist-level accuracy, giving the hope of improving the primary screening process of patients because it is impossible for all the patients to be referred to the skin cancer professionals before a suspicious diagnosis of malignancy. However, the majority of these researches are based on different imaging datasets that mainly include Caucasian patients with cutaneous tumors, especially malignant melanoma because of its relatively high incidences and risks in Western countries. But in Asia, the prevalence of cutaneous diseases is very distinct from that of Western countries, for example, the average annual age-adjusted incidence rate of melanoma in Asian population was reported as <1/100,000 (25, 26). Therefore, the existing CNN models constructed using a large portion of Caucasian patients' images with a preference of those specific skin diseases can hardly meet the real-world clinical needs in Asian countries like China. In fact, recently, Minagawa et al. (27) confirmed that the diagnostic performance of CNN model in diagnosing skin

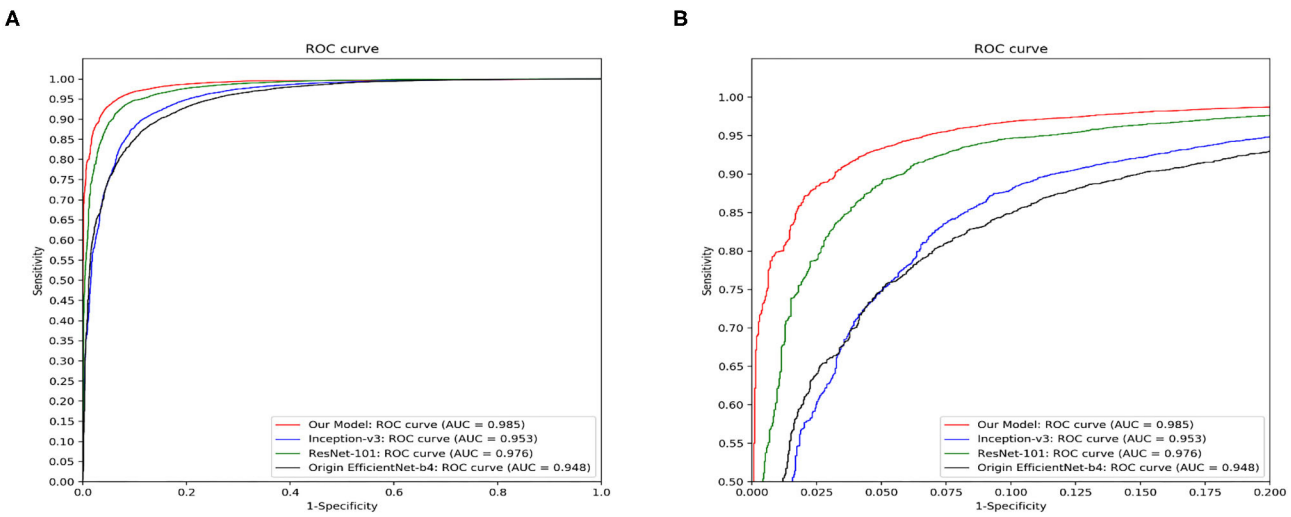

FIGURE 7 | The ROC curves and the AUC value of our model, Inception-v3, ResNet-101 and the original EfficientNet-b4. Our model outperforms other reported methods for this skin disease diagnosis problem. **(A)** The full view of the ROC curve of the proposed model. **(B)** The local enlarged image of the ROC curve between abscissa 0∼0.2.

tumors in Japanese patients would be improved if retrained by a dataset composed of cases with darker skin type.

We developed this CNN model based on pre-trained Google's EfficinetNet-b4 using a unique dataset that consisted of 14 most common skin diseases encountered and examined with dermoscopy in Chinese hospital dermatological clinics, including benign cutaneous neoplasms (MN, SK, DF, and KAHS), cutaneous malignancy (BCC), vascular neoplasm and malformation (Hem and PWS), inflammatory diseases with predilection sites of trunk and extremities (EAD, Pso, and LP) and with predilection sites of facial areas (SD, AV, and Rosa) and infectious diseases (VW). To the best of our knowledge, the construction of this dataset, including 14 categories of diseases, 2,538 cases and 13,603 dermoscopic images, is innovative, with many of the diseases firstly involved in a CNN model training, such as PWS, KAHS, and VW, aiming to propose a CNN model with better adaption of the real, complicated clinical environment in China. We initially chose dermoscopic images to construct the dataset because dermoscopic images usually reveal more valuable information of the lesion morphology than clinical images, and the process of taking a dermoscopic image is easier to standardize, and furthermore the background noises are much more prominent in clinical images which can affect the accuracy of the CNN model. Besides, since each skin diseases included in our research had unique and valuable dermoscopic features for differential diagnosis in clinical practice, we speculated our model would also benefit more from dermoscopic images than clinical images. However, we still tried to perform the 14-classification task using clinical images in the preliminary experiment as well. Results showed that the overall accuracies of clinical-image based CNN was 0.883, while the result our model based on dermoscopic images was 0.948. We thought the modest performance of clinical-image based CNN was relevant to the limited clinical dataset (for each patient, only 1 or 2 clinical images were recorded in our imaging database) and the relatively poor standardization of the clinical images (e.g., complex background interferes, different luminous intensity and camera angles). Therefore, we persisted in presenting our research based on the dermoscopy-based CNN. Yet, we would also attempt to construct CNN models based on the combination of clinical and dermoscopic image data since the former would certainly complement the information such as lesion distributions, skin textures and sites of involvement, potentially contributing to an even more satisfying diagnostic accuracy. The detailed performance results of the clinical-image based CNN in our preliminary experiment on the 14-classification task is also provided within the **Supplementary Material**.

TABLE 3 | The detailed overall sensitivity, specificity and accuracy of our and other 3 CNN models.

Performance \ Model	Our model	Original EfficientNet	ResNet-101	Inception-v3
Sensitivity	0.934	0.882	0.919	0.890
Specificity	0.950	0.875	0.935	0.895
Accuracy	0.948	0.875	0.934	0.895

In a recent article, Liu et al. (28) developed and validated a deep learning system for differential diagnosis of 26 types of skin diseases using clinical-only images from telemedicine, of which the top-1 diagnostic accuracy was non-inferior to dermatologists and higher than primary care physicians and nurse practitioners. Dermoscopy has been increasingly promoted and used in both dermatologists in the metropolises and general practitioners in the rural areas for its convenience and low costs, while the pace of the qualified telemedicine center construction is relatively

TABLE 4 | Comparison between doctors and our CNN model in an 8-class task, the better outcomes of our CNN model are colored orange.

Dermatologists	Rosa (%)	VW (%)	EAD (%)	SD(%)	SK (%)	MN(%)	Pso (%)	BCC(%)
Sensitivity	79.70	62.04	74.96	46.53	59.43	77.23	67.66	80.54
Specificity	96.39	98.48	92.42	93.70	94.28	94.68	97.32	96.73
Accuracy	94.31	93.93	90.24	87.81	89.92	92.50	93.61	94.71
OUR MODEL								
Sensitivity	92.00	92.00	84.00	48.00	76.00	96.00	92.00	88.00
Specificity	92.57	95.43	88.57	91.43	96.00	94.86	94.29	99.43
Accuracy	92.50	95.00	88.00	86.00	93.50	95.00	94.00	98.00

TABLE 5 | Kappa coefficients (95% confidence interval) of the included four CNN models and dermatologists (as standard) on the eight-class task.

Disease category	Dermatologists	Our model	Original EFFICIENTNET	ResNet101	Inception-v3
Rosacea	0.683 (0.609∼0.757)	0.712 (0.640∼0.783) *P*-value: 0.080	0.304 (0.194∼0.414) *P*-value: 0.010	0.646 (0.567∼0.726) *P*-value: 0.358	0.691 (0.616∼0.765) *P*-value: 0.349
Viral warts	0.533 (0.445∼0.621)	0.793 (0.731∼0.854) *P*-value: 0.057	0.759 (0.693∼0.825) *P*-value: 0.017	0.684 (0.609∼0.759) *P*-value: 0.065	0.761 (0.695∼0.827) *P*-value: 0.095
Eczema/dermatitis	0.757 (0.694∼0.820)	0.570 (0.484∼0.655) *P*-value: 0.104	0.507 (0.416∼0.598) *P*-value: 0.310	0.558 (0.471∼0.645) *P*-value: 0.313	0.585 (0.500∼0.670) *P*-value: 0.347
Seborrheic dermatitis	0.607 (0.526∼0.689)	0.381 (0.280∼0.483) *P*-value: 0.379	0.337 (0.233∼0.440) *P*-value: 0.137	0.352 (0.247∼0.457) *P*-value: 0.198	0.380 (0.277∼0.484) *P*-value: 0.227
Seborrheic keratosis	0.410 (0.311∼0.509)	0.708 (0.635∼0.780) *P*-value: 0.249	0.576 (0.489∼0.663) *P*-value: 0.239	0.576 (0.489∼0.663) *P*-value: 0.237	0.682 (0.606∼0.758) *P*-value: 0.350
Melanocytic nevus	0.683 (0.609∼0.758)	0.799 (0.738∼0.860) *P*-value: 0.224	0.786 (0.723∼0.849) *P*-value: 0.263	0.759 (0.693∼0.825) *P*-value: 0.234	0.719 (0.648∼0.790) *P*-value: 0.237
Psoriasis	0.675 (0.600∼0.749)	0.759 (0.693∼0.825) *P*-value: 0.043	0.744 (0.676∼0.813) *P*-value: 0.357	0.621 (0.539∼0.703) *P*-value: 0.387	0.701 (0.627∼0.774) *P*-value:0.194
Basal cell carcinoma	0.738 (0.671∼0.805)	0.905 (0.863∼0.948) *P*-value: 0.220	0.875 (0.826∼0.924) *P*-value: 0.204	0.725 (0.654∼0.796) *P*-value: 0.235	0.853 (0.800∼0.905) *P*-value: 0.229

slower. Therefore, the accessibility of dermoscopy could be better than teledermatology consult in many countries. Furthermore, for inflammatory dermatoses included in our research, each of them has meaningful dermoscopic features for differential diagnosis in clinical practice, well-established and summarized in dermoscopy textbooks, reviews and expert consensuses (29, 30). For example, although clinically similar, Rosa typically appears as multiple polygonal vessels while SD appears as erythema, scattered linear vessels and yellowish scales. According to our experience, CNN might capture those subtle features and make classification more accurate based on dermoscopy images. Moreover, a recent research proposed by Brinker et al. (31) revealed that CNN trained by dermoscopic images could also accurately classify clinical melanoma images, showing that training CNN using images with higher resolution and more details might be able to differentiate images with lower resolution and less information.

Fujisawa et al. (12) previously proposed a CNN model trained by a small dataset of 4,867 clinical images but harvested a satisfactory diagnostic accuracy in classifying 14 skin tumors with an overall accuracy in differentiating benign and malignant conditions of 93.4%. Wang et al. (13) used pre-trained GoogLeNet Inception v3 CNN network trained by 7,192 dermoscopic images also achieved an overall classification accuracy of 81.49% in multiclass model and 77.02% in two-class model. Similarly, considering the classifications are up to 14 categories, the number of images in our dataset is relatively modest, but our CNN model achieved even better results, with an overall sensitivity of 93.38 ± 0.08% and specificity of 94.85 ± 0.05% in this 14-class task, emphasizing that utilizing specific training methods, the CNN model trained by relatively limited imaging data can reach a satisfying performance level as well.

As mentioned above, the proposed CNN model achieved rather high overall classification accuracy, sensitivity and specificity, and was considered capable of aiding the patient screening in real dermatological clinics of China, especially for the remote and rural areas where the medical resources were extremely limited. We also compared our CNN model with previous reported methods including Inception-v3, ResNet-101, and the original EfficientNet-b4. Results showed that our model outperformed all of them in ROC curve and AUC value evaluation using our test set images.

For further verifying the effectiveness of this proposed CNN model, we compared it with 280 board-certificated

FIGURE 8 | t-SNE visualization of the last hidden layer representations in the CNN for four disease classes. Here we show the CNN's internal representation of eight disease classes by applying t-SNE, a method for visualizing high-dimensional data, to the last hidden layer representation (1792-D vector) in the CNN. Colored point clouds represent the different disease categories, showing how the algorithm clusters the diseases.

dermatologists who undergone at least 72-h systemic dermoscopic training, using an independent test dataset different from that for the routine performance evaluation process. To the best of our knowledge, this was the largest group of dermatologists included to compare with AI performance (10, 12, 13, 32–34). Results demonstrate that our CNN model has higher sensitivity in all the tested eight categories of skin diseases compared with dermatologists, and higher accuracy in five of them (namely VW, SK, MN, Pso, and BCC), higher specificity in 3 of them (namely, SK, MN and BCC). And statistical analysis revealed that the proposed CNN model reached better consistency (moderate to good) with the reference standard than the average level of 280 dermatologists in 6 of the 8 categories (namely Rosa, VW, SK, MN, Pso, and BCC), and the difference is statistically significant. However, the dermatologists had better outcomes in EAD and SD. According to the confusion matrix of the classification result (**Figure 6**), the proposed CNN model misclassified EAD mostly into Pso and SD, and misclassified SD mostly into Rosa. In our training set, the numbers of Pso images (1707) and EAD images (2440) are much larger than SD images (767) and Rosa images (597), which could lead to an imbalance of data and brought a risk of this inconsistency. Furthermore, in real clinical practice, the diagnosis of EAD is quite straightforward, based on the clinical lesion morphology and symptoms like pruritus in China, including the cases of our dataset, so the morphological diagnosis might include various EAD subtypes (e.g., dyshidrotic, disseminated and nummular) and disease durations (acute, subacute, and chronic), which would at last largely affect the feature extraction of EAD for the CNN. Moreover, it is often quite difficult to differentiate these inflammatory dermatoses in real clinical practice and the conditions of coexistence are not rare. Of note, the dermatologists were even provided with extra clinical images because this process would be more like the real clinical environment. This is critical because for inflammatory dermatoses like EAD, Pso, SD, and Rosa, the lesion distribution and sites of involvement that only shown in clinical images are of vital importance for differential diagnosis, which could also contribute for the relatively worse performance of our CNN in classifying EAD and SD. The outcomes reveal that our CNN model is dependable in classifying theses common cutaneous conditions, and might

have a fewer chance to miss the correct diagnosis compared with dermatologists.

However, our study has several limitations. First, our dataset completely came from the imaging database of the Department of Dermatology, Peking Union Medical College Hospital, using the same dermoscopy system. Therefore, it is possible that the accuracy of our CNN model might be lower when the dataset involves cases and images from other hospital or devices because the standardization would be affected. Second, as for the real clinical practice, the diagnosis of cutaneous diseases is not only based on the morphology of the skin lesions but also impacted by the general information and complicated medical history of the present patients, but we still do not know whether the accuracy would increase or decrease if such additional information is provided to the CNN model. Third, the disease spectrum in dermatology is rather wide. Although our dataset could to the best extent mimic the overall clinical conditions in our daily practice, there still lack a vast range of cutaneous diseases, such as skin cancers (e.g., squamous cell carcinoma and melanoma) uncommon in China. For further study, a CNN model should be refined by utilizing data from multiple centers or devices to improve the universality, and including more constantly encountered disease types in clinical practice, and possibly adding the information other than dermoscopic images such as sex, age, disease duration and clinical or high-frequency ultrasonic images. Finally, as forwarded by Tschandl et al. (35), CNN-support diagnosis gains are relative to the clinicians' experience, confidence in diagnosis and specific tasks. Human–computer collaboration will make full use of CNN assistance. The future studies ought to emphasize the cooperation instead of competence between clinicians and CNN. However, our study lacked the validation of the influences of CNN assistance on dermatologists as mentioned above.

In conclusion, we proposed a CNN model based on Google's EfficientNet-b4 with pre-trained weights on ImageNet trained by a novel dermoscopic dataset represented the real dermatological clinics environment of a tertiary class hospital in China with 14 categories of common cutaneous diseases. Our CNN model achieved a rather high level of performance, with an overall accuracy of 0.948 ± 0.001 (mean ± SD), a sensitivity of 0.934 ± 0.001 (mean ± SD), and a specificity of 0.950 ± 0.001 (mean ± SD). Furthermore, we compared this framework with previously reported methods and it outperformed all of them. Also, the performance of this CNN model was comparable to 280 board-certified dermatologists in an eight-class diagnostic task, with higher sensitivity in all of the included diseases.

DATA AVAILABILITY STATEMENT

The datasets for this study are not available because they contain the dermoscopic images of patients with cutaneous diseases according to the regulations of our informed written consents. Requests to access the datasets should be directed to Jie Liu, liujie04672@pumch.cn.

ETHICS STATEMENT

The studies involving human participants were reviewed and approved by the Medical Ethics Committee of Peking Union Medical College Hospital. Written informed consent to participate in this study was provided by the participants' legal guardian/next of kin.

AUTHOR CONTRIBUTIONS

C-YZ, Y-KW, H-PC, K-LG, and JL made the concept and design of this study. C-YZ, Y-KW, and JL were responsible for the literature search, patient enrolment, dermoscopic evaluation, and dataset formation. H-PC, L-FY, and K-LG developed, refined, and validated the proposed CNN model using the dataset mentioned above. C-YZ, Y-KW, CS, J-CW, and JL organized the comparative reader study of 280 board-certificated dermatologists in a formal dermoscopy conference in China. Y-GY and F-YX collected and analysed the classification results of dermatologists. H-PC and Y-GY made the statistical analysis. The manuscript was prepared by Y-KW and H-PC, edited and reviewed by L-FY, JL, and F-YX. All authors contributed to the article and approved the submitted version.

FUNDING

This work was supported by The Non-profit Central Research Institute Fund of Chinese Academy of Medical Sciences (2019XK320024), The National Natural Science Foundation of China (No. 61871011), The Beijing Natural Science Foundation (No. 7182127), and The National Key Research and Development Program of China (No.2016YFC0901500).

SUPPLEMENTARY MATERIAL

The Supplementary Material for this article can be found online at: https://www.frontiersin.org/articles/10.3389/fmed.2021.626369/full#supplementary-material

REFERENCES

1. Litjens G, Kooi T, Bejnordi BE, Setio AAA, Ciompi F, Ghafoorian M, et al. A survey on deep learning in medical image analysis. *Med Image Anal.* (2017) 42:60–88. doi: 10.1016/j.media.2017.07.005
2. Kermany DS, Goldbaum M, Cai W, Valentim CCS, Liang H, Baxter SL, et al. Identifying medical diagnoses and treatable diseases by image-based deep learning. *Cell.* (2018) 172:1122–31.e9. doi: 10.1016/j.cell.2018.02.010
3. Esteva A, Kuprel B, Novoa RA, Ko J, Swetter SM, Blau HM, et al. Dermatologist-level classification of skin cancer with deep neural networks. *Nature.* (2017) 542:115–8. doi: 10.1038/nature21056
4. Menegola A, Fornaciali M, Pires R, Avila S, Valle E. *Towards automated melanoma screening: exploring transfer learning schemes. arXiv [Preprint].* (2016).
5. Huang ML, Hung YH, Lee WM, Li RK, Jiang BR. SVM-RFE based feature selection and Taguchi parameters optimization for multiclass SVM classifier. *Scient World J.* (2014) 2014:795624. doi: 10.1155/2014/795624

6. Jafari MH, Nasr-Esfahani E, Karimi N, Soroushmehr SMR, Samavi S, Najarian K. Extraction of skin lesions from non-dermoscopic images for surgical excision of melanoma. *Int J Comput Assist Radiol Surg.* (2017) 12:1021–30. doi: 10.1007/s11548-017-1567-8
7. Spyridonos P, Gaitanis G, Likas A, Bassukas ID. Automatic discrimination of actinic keratoses from clinical photographs. *Comput Biol Med.* (2017) 88:50–9. doi: 10.1016/j.compbiomed.2017.07.001
8. Xie F, Fan H, Li Y, Jiang Z, Meng R, Bovik A. Melanoma classification on dermoscopy images using a neural network ensemble model. *IEEE Trans Med Imaging.* (2017) 36:849–58. doi: 10.1109/TMI.2016.2633551
9. Garcia-Zapirain B, Elmogy M, El-Baz A, Elmaghraby AS. Classification of pressure ulcer tissues with 3D convolutional neural network. *Med Biol Eng Comput.* (2018) 56:2245–58. doi: 10.1007/s11517-018-1835-y
10. Han SS, Kim MS, Lim W, Park GH, Park I, Chang SE. Classification of the clinical images for benign and malignant cutaneous tumors using a deep learning algorithm. *J Invest Dermatol.* (2018) 138:1529–38. doi: 10.1016/j.jid.2018.01.028
11. Emam S, Du AX, Surmanowicz P, Thomsen SF, Greiner R, Gniadecki R. Predicting the long-term outcomes of biologics in patients with psoriasis using machine learning. *Br J Dermatol.* (2020) 182:1305–7. doi: 10.1111/bjd.18741
12. Fujisawa Y, Otomo Y, Ogata Y, Nakamura Y, Fujita R, Ishitsuka Y, et al. Deep-learning-based, computer-aided classifier developed with a small dataset of clinical images surpasses board-certified dermatologists in skin tumour diagnosis. *Br J Dermatol.* (2019) 180:373–81. doi: 10.1111/bjd.16924
13. Wang S-Q, Zhang X-Y, Liu J, Tao C, Zhu C-Y, Shu C, et al. Deep learning-based, computer-aided classifier developed with dermoscopic images shows comparable performance to 164 dermatologists in cutaneous disease diagnosis in the Chinese population. *Chin Med J.* (2020) 133:2027–36. doi: 10.1097/CM9.0000000000001023
14. Dreiseitl S, Binder M, Vinterbo S, Kittler H. Applying a decision support system in clinical practice: results from melanoma diagnosis. *AMIA Annu Symp Proc.* (2007) 2007:191–5.
15. Dreiseitl S, Binder M, Hable K, Kittler H. Computer versus human diagnosis of melanoma: evaluation of the feasibility of an automated diagnostic system in a prospective clinical trial. *Melanoma Res.* (2009) 19:180–4. doi: 10.1097/CMR.0b013e32832a1e41
16. Tan M, Le QV. *EfficientNet: rethinking model scaling for convolutional neural networks. arXiv:1905.11946* (2019).
17. Russakovsky O, Deng J, Su H, Krause J, Satheesh S, Ma S, et al. ImageNet large scale visual recognition challenge. *Int J Comp Vision.* (2015) 115:211–52. doi: 10.1007/s11263-015-0816-y
18. Hu J, Shen L, Albanie S, Sun G, Wu E. Squeeze-and-Excitation Networks. *IEEE Trans Pattern Anal Mach Intell.* (2020) 42:2011–23. doi: 10.1109/TPAMI.2019.2913372
19. Szegedy C, Vanhoucke V, Ioffe S, Shlens J, Wojna Z. *Rethinking the inception architecture for computer vision*. In: *2016 IEEE Conference on Computer Vision and Pattern Recognition (CVPR)*. Las Vegas, NV: IEEE (2015). p. 2818–26. doi: 10.1109/CVPR.2016.308
20. Selvaraju RR, Cogswell M, Das A, Vedantam R, Batra D. Grad-CAM: visual explanations from deep networks via gradient-based localization. *Int J Comp Vision.* (2019) 128:336–59. doi: 10.1007/s11263-019-01228-7
21. He K, Zhang X, Ren S, Sun J, editors. Deep residual learning for image recognition. In: *2016 IEEE Conference on Computer Vision and Pattern Recognition (CVPR)*. p. 27–30. doi: 10.1109/CVPR.2016.90
22. Hinton GE. Visualizing high-dimensional data using t-SNE. *J Mach Learn Res.* (2008) 9:2579–605.
23. Zhao S, Xie B, Li Y, Zhao X, Kuang Y, Su J, et al. Smart identification of psoriasis by images using convolutional neural networks: a case study in China. *J Eur Acad Dermatol Venereol.* (2020) 34:518–24. doi: 10.1111/jdv.15965
24. Shen CB, Shen X, Li CX, Meng RS, Cui Y. Assessment of imaging diagnosis ability of skin tumors in Chinese dermatologists. *Chin Med J (Engl).* (2019) 132:2119–20. doi: 10.1097/CM9.0000000000000389
25. Cress RD, Holly EA. Incidence of cutaneous melanoma among non-Hispanic whites, Hispanics, Asians, and blacks: an analysis of california cancer registry data, 1988-93. *Cancer Causes Control.* (1997) 8:246–52.
26. MacKie RM, Hauschild A, Eggermont AMM. Epidemiology of invasive cutaneous melanoma. *Ann Oncol.* (2009) 20 (Suppl 6):vi1-vi7. doi: 10.1093/annonc/mdp252
27. Minagawa A, Koga H, Sano T, Matsunaga K, Teshima Y, Hamada A, et al. Dermoscopic diagnostic performance of Japanese dermatologists for skin tumors differs by patient origin: a deep learning convolutional neural network closes the gap. *J Dermatol.* (2020) 48:232–6. doi: 10.1111/1346-8138.15640
28. Liu Y, Jain A, Eng C, Way DH, Lee K, Bui P, et al. A deep learning system for differential diagnosis of skin diseases. *Nat Med.* (2020) 26:900–8. doi: 10.1038/s41591-020-0842-3
29. Errichetti E. Dermoscopy of inflammatory dermatoses (Inflammoscopy): an up-to-date overview. *Dermatol Pract Concept.* (2019) 9:169–80. doi: 10.5826/dpc.0903a01
30. Errichetti E, Zalaudek I, Kittler H, Apalla Z, Argenziano G, Bakos R, et al. Standardization of dermoscopic terminology and basic dermoscopic parameters to evaluate in general dermatology (non-neoplastic dermatoses): an expert consensus on behalf of the International Dermoscopy Society. *Br J Dermatol.* (2020) 182:454−67. doi: 10.1111/bjd.18125
31. Brinker TJ, Hekler A, Enk AH, Klode J, Hauschild A, Berking C, et al. A convolutional neural network trained with dermoscopic images performed on par with 145 dermatologists in a clinical melanoma image classification task. *Eur J Cancer.* (2019) 111:148–54. doi: 10.1016/j.ejca.2019.02.005
32. Haenssle HA, Fink C, Schneiderbauer R, Toberer F, Buhl T, Blum A, et al. Man against machine: diagnostic performance of a deep learning convolutional neural network for dermoscopic melanoma recognition in comparison to 58 dermatologists. *Ann Oncol.* (2018) 29:1836–42. doi: 10.1093/annonc/mdy520
33. Brinker TJ, Hekler A, Enk AH, Klode J, Hauschild A, Berking C, et al. Deep learning outperformed 136 of 157 dermatologists in a head-to-head dermoscopic melanoma image classification task. *Eur J Cancer.* (2019) 113:47–54. doi: 10.1016/j.ejca.2019.04.001
34. Maron RC, Weichenthal M, Utikal JS, Hekler A, Berking C, Hauschild A, et al. Systematic outperformance of 112 dermatologists in multiclass skin cancer image classification by convolutional neural networks. *Eur J Cancer.* (2019) 119:57–65. doi: 10.1016/j.ejca.2019.06.013
35. Tschandl P, Rinner C, Apalla Z, Argenziano G, Codella N, Halpern A, et al. Human-computer collaboration for skin cancer recognition. *Nat Med.* (2020) 26:1229–34. doi: 10.1038/s41591-020-0942-0

Conflict of Interest: The authors declare that the research was conducted in the absence of any commercial or financial relationships that could be construed as a potential conflict of interest.

frontiers in Medicine

ORIGINAL RESEARCH
published: 26 April 2021
doi: 10.3389/fmed.2021.673861

Ultra-High-Frequency Ultrasound in the Evaluation of Paediatric Pilomatricoma Based on the Histopathologic Classification

Li Li[1†], *Jiaosheng Xu*[2*†], *Siwei Wang*[3] *and Jun Yang*[4]

[1] *Department of Dermatology, Plastic Surgery Hospital, Chinese Academy of Medical Sciences and Peking Union Medical College, Beijing, China,* [2] *Department of Dermatology, Beijing Children's Hospital, National Center for Children's Health, Capital Medical University, Beijing, China,* [3] *Department of Radiology, Beijing Children's Hospital, National Center for Children's Health, Capital Medical University, Beijing, China,* [4] *Institute of Biomedical Engineering, Chinese Academy of Medical Sciences, Tianjin, China*

Background: Pilomatricoma (PM) is one of the most common benign tumours in children. However, the inaccuracy of preoperative diagnosis and evaluation is high. Non-invasive examinations, including dermoscopy and ultrasound are helpful for diagnosing and evaluating PM. To date, ultra-high-frequency ultrasonographic features of PM have been rarely studied.

Objective: We aimed to investigate the ultra-high frequency ultrasonographic features of PM in a large paediatric cohort and to determine the associations of these features with the clinical features of different histological subtypes of PM.

Methods: This was a retrospective study. Patients who had both preoperative ultra-high-frequency ultrasonographic evaluation and pathological diagnosis of PM were enrolled. A series of infantile haemangiomas and cutaneous cysts during the same period were included as controls. Histological findings, including the stage, calcifying type, and ultrasonographic features of each lesion, were described.

Results: A total of 133 patients with PM were included, and 147 PM lesions were analysed. The male-to-female ratio was 1:1.58, and the median age of onset was 91 (range: 10–188) months. On ultra-high-frequency ultrasonography, PM presented as heterogeneous (144/147, 98.0%), well-demarcated (143/147, 97.3%), and hypoechoic (126/147, 85.7%) tumours located between the deep dermis and subcutaneous tissue (139/147, 94.6%). The most common features were internal echogenic foci (135/147, 91.8%), hypoechoic rim (133/147, 90.5%), and posterior acoustic shadowing (94/147, 63.9%). Fourteen (9.5%) lesions were histologically categorized in the early stage, 58 (39.5%) in the fully developed stage, 65 (44.2%) in the early regressive stage and 10 (6.8%) in the late regressive stage. Three calcifying types, including scattered dots, clumps and arcs, were observed on histologic examination, which corresponded well with grey-scale imaging on ultra-high-frequency ultrasonography. Each calcifying type was significantly different in various histological stages ($P = 0.001$), among which scattered dots were mainly present in the early and fully developed stage and

OPEN ACCESS

Edited by:
H. Peter Soyer, The University of Queensland, Australia

Reviewed by:
Adriana Polanska, Poznan University of Medical Sciences, Poland
Steven Kaddu, Medical University of Graz, Austria

***Correspondence:**
Jiaosheng Xu
xujiaosheng@sina.com

†These authors have contributed equally to this work

Specialty section:
This article was submitted to Dermatology, a section of the journal Frontiers in Medicine

Received: *28 February 2021*
Accepted: *29 March 2021*
Published: *26 April 2021*

Citation:
Li L, Xu J, Wang S and Yang J (2021) Ultra-High-Frequency Ultrasound in the Evaluation of Paediatric Pilomatricoma Based on the Histopathologic Classification. Front. Med. 8:673861. doi: 10.3389/fmed.2021.673861

arc-shaped calcifying were present in the regressive stages. Calcification was observed in skin cysts, while there was more frequent posterior enhancement, less frequent posterior shadowing, and hypoechoic rim than PM. Haemangioma also presented as a hypoechoic tumour on grey-scale imaging. However, haemangioma was homogeneous and rarely calcifying.

Conclusions: PM is a heterogeneous, well-demarcated, hypoechoic tumour located between the deep dermis and the subcutis on ultra-high-frequency ultrasonography. The most common features are internal echogenic foci (calcifying) and hypoechoic rim. Calcifying types can help in the staging of PM. Ultra-high-frequency ultrasound is a useful tool for the diagnosis and evaluation of PM.

Keywords: pilomatricoma, ultrasound, ultra-high-frequency, diagnosis, paediatric, histopathologic

INTRODUCTION

Pilomatricoma (PM) is a benign, deep dermal or subcutaneous tumour that is derived from the hair cortex cell (1). It is also known as calcifying epithelioma of Malherbe (2). PM has a bimodal peak, first presenting in the first two decades and second in the sixth decade. It has a female predominance. Lesions mainly occur on the head, neck, and extremities, which range from 0.5 to 3 cm in size. On palpation, PM is characteristically hard and nodular or multinodular. The overlying skin can be bluish or reddish, which can mimic infantile haemangioma (3).

The typical histopathology of PM shows sheets of basaloid cells and masses of eosinophilic cornified material containing ghost cells. Calcification is mostly observed in the ghost cell regions. Based on morphological features, PM is classified into four stages (4). The first is the early stage and is typified by small cystic structures lined by squamoid and basaloid epithelium, and shadow cell formation. The second is the fully developed stage characterized by large neoplasms lined by basaloid epithelium at their periphery; within, it comprises clusters of shadow cells. The third is the early regressive stage with no apparent epithelial lining but has basaloid cell foci at the periphery; within, it comprises shadow cells surrounded by granulation tissue. The fourth is the late regressive stage, demonstrating no obvious parenchymal cells but irregularly shaped, partially confluent masses of faulty hair material, and calcification or ossification, with little or no inflammatory infiltrate.

The clinical diagnosis rate of PM is usually very low. Prior reviews have shown that preoperative diagnostic accuracy for PMs ranges from 21 to 32% (1, 5). The most common differential diagnoses are haemangiomas and several types of skin cysts (3, 6). Non-invasive techniques such as dermoscopy and ultrasonography have been increasingly used to aid in the diagnosis of skin tumours (7, 8). They are popular in paediatric patients because they are simple, quick, and non-invasive. Hughes et al. reported on the sonographic diagnosis of PM in childhood with a diagnostic accuracy of 80% (9). On ultrasound, PM is a heterogeneous tumour with inner echogenic foci and a hypoechoic rim or a completely echogenic mass with strong posterior acoustic shadowing in the subcutis (10). The reliable diagnostic features for PM are hypoechogenicity, heterogenicity, internal echogenic foci, hypoechoic rim, and posterior shadowing (11).

However, another study has demonstrated PM as a well-defined hyperechoic or calcific nodule in subcutaneous fat (12), probably because of the different frequencies of the transducer. Therefore, we used ultra-high-frequency ultrasound to explore the ultrasonographic features and determine the histopathological correlations of PM.

MATERIALS AND METHODS

This was a retrospective study. From April 2016 to December 2020, paediatric patients with histopathologically proven PM after surgery at the Plastic Surgery Hospital, Chinese Academy of Medical Sciences and Peking Union Medical College and Beijing Children's Hospital, Capital Medical University, were included in this study with Institutional Review Board approval. Written informed consent for the procedure was obtained from all the patients' parents. A series of 91 infantile haemangiomas and 28 cutaneous cysts (including dermal and epidermal cysts) during the same period were included as controls.

Ultra-High-Frequency Ultrasonography

Ultrasonographic examination was performed using an ultrasound skin scanner (MD-300S, MEDA, Co., Ltd., Tianjin, China) equipped with 50 MHz linear array transducers. The grey-scale images were captured by the bioscope (MD-300SII, MEDA, Co., Ltd., Tianjin, China) attached to the ultrasonograph. Each image was reviewed by an experienced radiologist and dermatologist. The analysis of ultrasonographic features included tumour location, margin, shape, size, echo texture, and echogenicity. The tumour echo texture was recorded as homogeneous or heterogeneous, and echogenicity as hyperechoic if the tumour echogenicity was higher than that of dermal connective tissues. The following ultrasonographic features were observed in the study: inner echogenic foci, posterior shadowing, hypoechoic rim, and peritumoral hyperechogenicity. Inner echogenic foci were defined as calcification regardless of posterior shadowing. The calcification mode was described as an arc, scattered dots, or clumps.

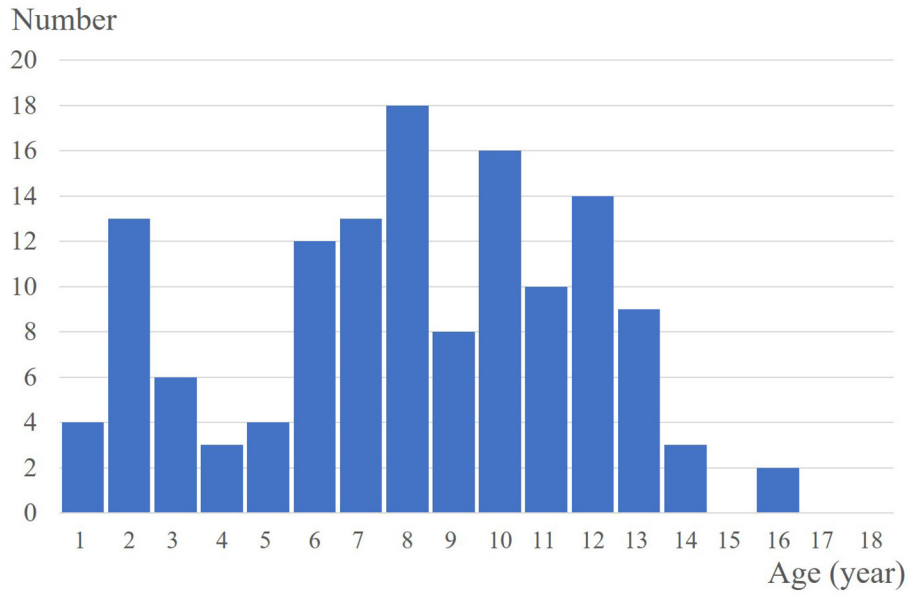

FIGURE 1 | Population distribution with age in pediatric PM.

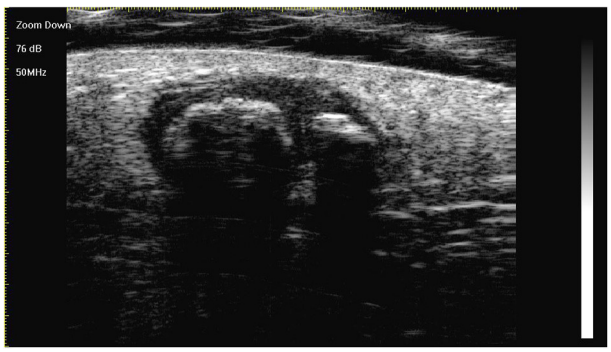

FIGURE 2 | The lesion is a heterogeneous, well-demarcated, hypoechoic tumour located between the deep dermis and the subcutis with typical ultra-high-frequency ultrasonographic features, including internal echogenic foci, hypoechoic rim, and posterior acoustic shadowing.

Histopathology

After ultrasonographic examination, the tumours were arranged for complete resection and routine histological examination. Each lesion was examined by the experienced pathologist and dermatologist. Based on the morphology of tumour and infiltrating cells, the histopathological stages were categorized into four stages as in a previous report (4): early, fully developed, early regressive, or late regressive stage. The calcification shape at low magnification was described as scattered dots, an arc, or clumps.

Statistical Analyses

Descriptive statistics for categorical variables are presented as numbers. The differences between two independent categorical variables were evaluated using the chi-square test (Fisher exact test when necessary) and Kruskal-Wallis rank sum tests were performed for grouped data. SPSS Windows version 26.0 (SPSS Inc., Chicago, IL, USA) was used for the statistical analyses and $P < 0.05$ was considered statistically significant.

RESULTS

All patients underwent preoperative ultra-high-frequency ultrasound examination and were histologically diagnosed with PM post-operatively.

Clinical and Histopathological Findings of PM

A total of 133 patients with PM were included, and 147 PM lesions were analysed. The male-to-female ratio was 1:1.58. The median age of onset was 91 (range: 10–188) months, and two peaks were observed (ages 2 and 8) (**Figure 1**). The meantime from onset to diagnosis was 14.8 months (range: 0.5–132 months). One hundred and twenty-two patients had a solitary lesion, eight patients had two lesions, and three patients had three lesions (113 in the head and neck, 11 in the trunk and 23 in the extremities). The mean length of the largest tumour diameter was 0.8 (range: 0.3–7) cm. Fourteen (9.5%) lesions were histologically categorized in the early stage (**Figure 3A**), 58 (39.5%) in the fully developed stage (**Figure 4A**), 65 (44.2%) in the early regressive stage (**Figure 5A**), and 10 (6.8%) in the late regressive stage (**Figure 6A** and **Table 1**). Three calcifying types, including scattered dots, clumps and arcs, were observed on low power histologically. On high power, bone formation was noted in the arc-shaped calcification but not in the other two types.

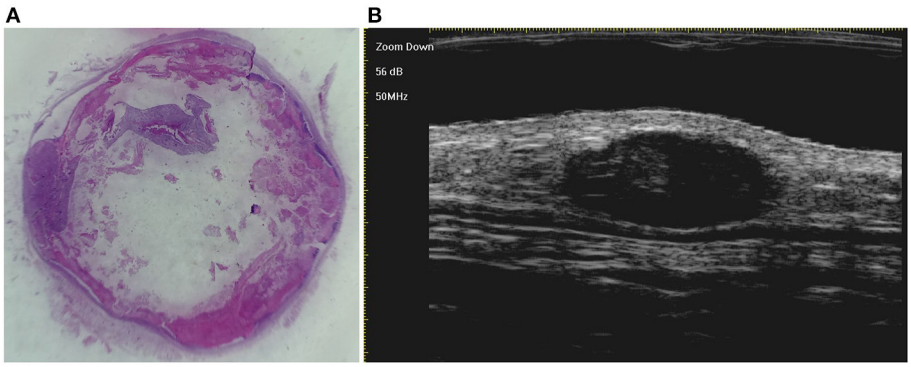

FIGURE 3 | The histological presentation [**(A)** HE, original magnification × 10] and ultra-high frequency ultrasound **(B)** of PM in the early stage, indicating no obvious calcification and cystic formation.

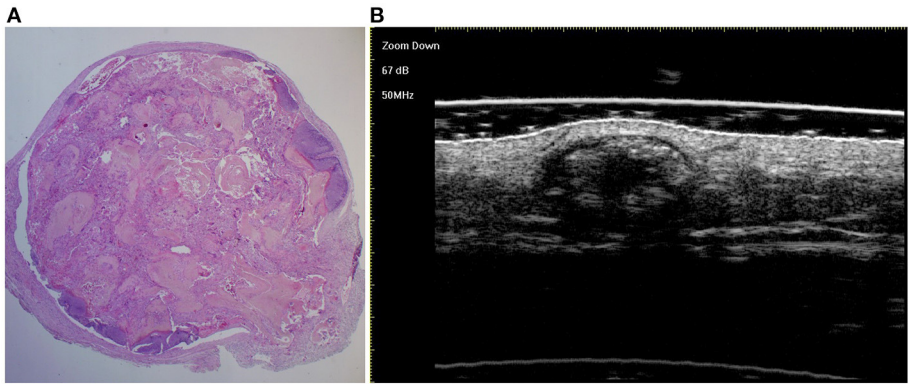

FIGURE 4 | The histological presentation [**(A)** HE, original magnification × 25] and ultra-high frequency ultrasound **(B)** of PM in the fully developed stage, indicating scattered dot calcification.

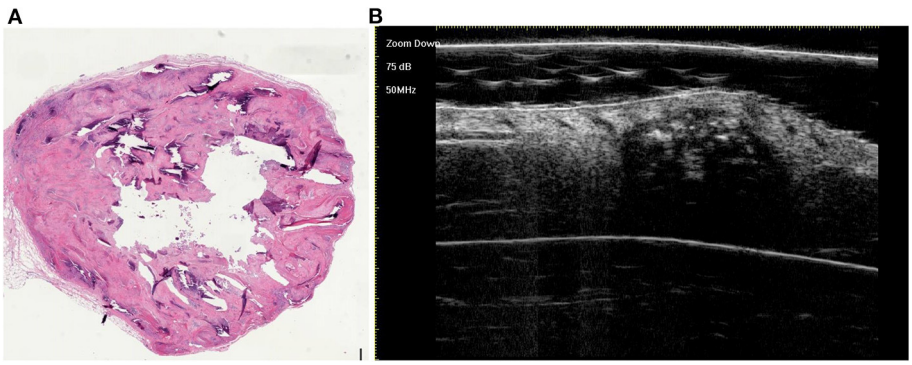

FIGURE 5 | The histological presentation [**(A)** HE, original magnification × 10] and ultra-high frequency ultrasound **(B)** of PM in the early regressive stage, indicating clump calcification.

Ultrasonographic Features of PM and Its Clinical and Histological Correlations

On ultra-high frequency ultrasonography, PM manifested as heterogeneous (144/147, 98.0%), well-demarcated (143/147, 97.3%), and hypoechoic (126/147, 85.7%) tumours located between the deep dermis and subcutaneous tissue (139/147, 94.6%) (**Table 2**). The lesions were mostly arranged in a regular shape (oval or round), while a few were irregular in shape. The most common features were internal echogenic foci (135/147, 91.8%), hypoechoic rim (133/147, 90.5%), posterior shadowing (94/147, 63.9%), and peritumoral hyperechogenicity (45/147, 30.6%) (**Figure 2**). Three calcifying types, including

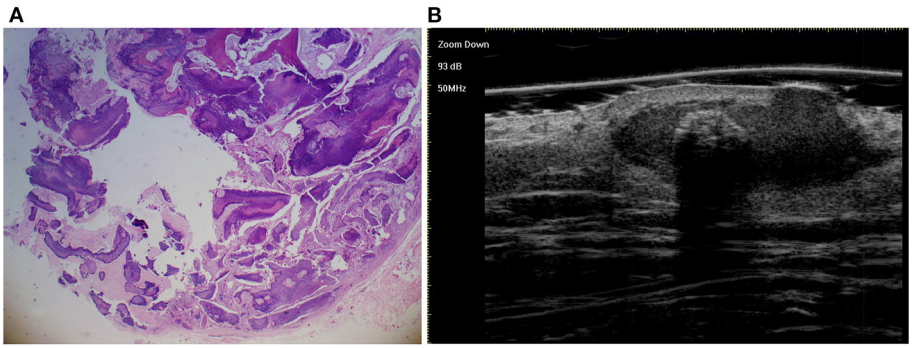

FIGURE 6 | The histological presentation [**(A)** HE, original magnification × 25] and ultra-high frequency ultrasound **(B)** of PM in the early regressive stage, indicating arc calcification.

TABLE 1 | Ultra-high-frequency ultrasonographic features in various histological stages.

Ultrasound features	Histological staging				*P**
	Early ($n = 14$)	Fully developed ($n = 58$)	Early regressive ($n = 65$)	Late regressive ($n = 10$)	
Echogenicity					
Hyperechoic	2	8	11	0	
Hypoechoic	12	50	54	10	
Echotexture					
Homogeneous	2	1	0	0	
Heterogeneous	12	57	65	10	
Margin					0.001
Well	13	57	63	10	
Ill	1	1	2	0	
Calcification	8	53	60	10	
Scattered dots	5	34	20	0	
Clumps	3	17	28	4	
An arc	0	2	12	6	
Hypoechoic rim	13	57	63	10	
Posterior shadowing	1	30	55	8	
Posterior enhancement	3	6	0	0	
Peritumoral hyperechogenicity	2	23	18	2	

**Kruskal-Wallis rank-sum test.*

scattered dots, clumps, and arcs, were observed on ultra-high frequency ultrasonography corresponding well with the histological manifestations (**Figures 3B**, **4B**, **5B**, **6B**). Each calcifying type was significantly different in the various histological stages ($P < 0.05$), among which scattered dots were mainly presented in the early and developed stages, while arc-shaped calcifications were present in the regressive stages. The different stages were observed in one lesion (**Figure 7**). Posterior enhancement was observed only in the early (3/14) and fully developed (6/58) stages, when cystic architecture formation was detected histologically (**Table 2**).

Comparison With PM From Infantile Haemangioma and Skin Cysts

A total of 91 patients with infantile haemangioma and 28 patients with skin cysts were enrolled as controls. The male–to–female ratio was 1:2.6 and 1:0.87, respectively. The mean age of onset was 3 (range: 1–20) months and 41 (range: 3–204) months, respectively. Infantile haemangioma also presented as a well-defined (81/91, 89.0%), and hypoechoic tumour (90/91, 98.9%) on grey-scale imaging. However, infantile haemangiomas were irregular (81/91, 89.0%) in shape and homogenous (88/91, 96.7%), rarely with calcification (2/91, 2.2%), and mostly located in the dermis (79/91, 86.8%). In addition, hypoechoic rim, posterior shadowing, posterior enhancement, and peritumoral hyperechogenicity were rarely observed in infantile haemangiomas. Calcification was observed in skin cysts (5/28, 17.9%), while there was more frequent posterior enhancement (24/28, 85.7%), less frequent posterior shadowing (3/28, 10.7%), and less hypoechoic rim (2/28, 7.1%) than in PM (**Table 2**).

DISCUSSION

In our study of the paediatric population, PM had a predilection for girls and the lesions mostly presented as solitary nodules,

TABLE 2 | Comparison of PM with hemangioma and skin cysts on ultrasound.

Ultrasonographic features	PM	Hemangioma	*P**	PM	Cysts	*P**
Shape			0.001			NS
Round/oval	143	10		143	26	
Irregular	4	81		4	2	
Location			0.001			0.001
Dermis	8	79		8	19	
Dermis to subcutaneous layer	139	12		139	9	
Largest diameter (mean, mm)	0.8 (0.3–7)	0.7 (0.6–8)	NS	0.8 (0.3–7)	0.6 (0.5–1.2)	NS
Echogenicity			0.001			NS
Hyperechoic	21	1		21	11	
Hypoechoic	122	90		122	17	
Echotexture			0.001			0.001
Homogeneous	3	88		3	19	
Heterogeneous	140	3		140	9	
Margin			0.01			0.001
Well	143	81		143	20	
Ill	4	10		4	6	
Internal echogenic foci		0.001			0.001	
Scattered dots	59	1		59	4	
Clumps	52	1		52	1	
An arc	20	0		20	0	
Hypoechoic rim	140	1	0.001	143	2	0.001
Posterior shadowing	94	0	0.001	94	3	0.001
Posterior enhancement	9	1	NS	9	24	0.001
Peritumoral hyperechogenicity	45	1	0.001	45	2	0.001

NS, not significant; PM, pilomatricoma.
**Chi-square test.*

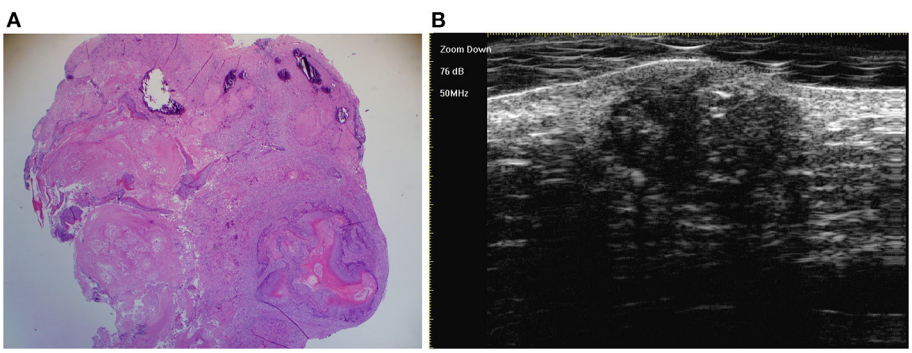

FIGURE 7 | The last three stages overlap in one lesion, which is detected by histology [**(A)** original magnification × 25] and ultra-high frequency ultrasound **(B)**.

mainly occurring in the head and neck area, as previously reported (12). However, two peaks of onset in paediatric population were observed in our study. PMs in children present a great challenge in clinical diagnosis and treatment, especially regarding the first peak onset age. Although PM is one of the most common skin tumours in children, its clinical diagnosis is very low (1, 6). The accurate diagnosis rate in accordance with post-operative histopathology is <35% (1). Ultrasonographic assessment can improve the diagnosis of PM (11, 13, 14).

The ultrasonographic features of PM have been described in several studies (9–13), and include calcification in the heterogeneous background of the hypoechoic area, posterior acoustic shadowing, hypoechoic rim, and peritumoral hyperechogenicity. The background of the hyperechoic areas was also described (12). These ultrasonographic features of PM were observed in the present study. According to our data, most of the cases were hypoechoic on ultra-high frequency ultrasonography. On histopathology, this hypoechoic area demonstrated infiltrates

of basaloid, ghost cells, and reactive inflammation accordingly. The high ratio of hypoechogenicity was detected mainly due to the use of ultra-high-frequency transducers in our study, which improved the lesion tissue resolution (7).

The most common ultrasonographic features of PM are calcification and a hypoechoic rim compared with infantile haemangiomas and skin cysts. The ultra-high-frequency ultrasound is sensitive to display minimal calcification. Calcification on ultrasound mainly presented as scattered dots, clumps, and arcs, which is consistent with the previous reports (15). The morphology of the calcification is well-demonstrated on histopathology. Moreover, various histological stages notably displayed distinct calcifying types in our study. In the early and fully developed stages, scattered dots were the main type of calcification, whereas in the regressive stages, arc-shaped calcifications were the main type. Clumps can manifest in all the histological stages. Histopathologic examination reveals that the hypoechoic rim represents a connective tissue capsule surrounding the tumour. Unlike various types of skin cysts, there is no cystic wall in PM, which is lined with compact epithelial tissues. This annular connective loose connective tissue in PM was well-demonstrated characteristically on high frequency ultrasonography as a hypoechoic rim. The overall analysis of calcification and the hypoechoic rim can help in the diagnosis of PM. Moreover, the evolution of calcification reflects the PM process (4). The analysis of calcifying type on preoperative ultrasound may aid in the staging of PM.

Clinically, the overlying skin of some PMs may manifest as bruises or reddish hues. On ultrasound, infantile haemangioma also presents as a hypoechoic tumour, as in PM. Occasionally, PM may manifest as a confluent colour Doppler flow, mimicking haemangioma. However, infantile haemangioma often manifests in a homogeneous manner compared to PM and rarely displays calcification on grey-scale imaging. Calcification can be present in skin cysts on ultrasound. However, the calcifying type mainly present as scattered dots in the skin cysts. In addition, a hypoechoic rim is rarely present, while posterior acoustic enhancement is common in skin cysts.

The main method for PM management is surgical resection. However, surgery is usually not accepted for PM in young children because of the risk associated with surgery and systemic anaesthesia. Thus, ultra-high-frequency ultrasonography can be used to detect PM progression according to the calcifying type when a follow-up strategy is adopted. PM evolves into a regressive stage with age and can be resected with more safety at an older age. Moreover, preoperative evaluation of location, size, margin, and shape can be obtained by ultra-high-frequency ultrasonography.

In summary, PM is a heterogeneous, well-demarcated, hypoechoic tumour located between the deep dermis and subcutis on ultra-high-frequency ultrasonography. The most common features are calcification and a hypoechoic rim. Calcifying types can help in the staging of PM. Ultra-high-frequency ultrasound seems a useful tool for the diagnosis and evaluation of PM.

To our knowledge, this is the largest sample of PM used to explore ultra-high-frequency ultrasonographic characteristics based on histopathological stages. However, this study was limited by its retrospective nature and lack of vascularity analysis on colour Doppler ultrasonography. Further prospective studies with larger samples should be initiated to expatiate the results described herein.

DATA AVAILABILITY STATEMENT

The original contributions generated for the study are included in the article/supplementary material, further inquiries can be directed to the corresponding author/s.

ETHICS STATEMENT

The studies involving human participants were reviewed and approved by Plastic Surgery Hospital, Chinese Academy of Medical Sciences and Beijing Children's Hospital, Capital Medical University. Written informed consent to participate in this study was provided by the participants' legal guardian/next of kin. Written informed consent was obtained from the individual(s), and minor(s)' legal guardian/next of kin, for the publication of any potentially identifiable images or data included in this article.

AUTHOR CONTRIBUTIONS

LL and JX conceptualized and designed the study, drafted the initial manuscript, and reviewed and revised the manuscript. JX conceptualized and designed the study, coordinated and supervised data collection, conducted the initial analyses, drafted the initial manuscript, and critically reviewed the manuscript for important intellectual content. SW and JY designed the data collection instruments, collected data, conducted the initial analyses, and reviewed and revised the manuscript. All authors approved the final manuscript as submitted and agree to be accountable for all aspects of the work.

FUNDING

This work was supported by CAMS Initiative for Innovative Medicine (No. 2017-12M-3-020); Institute of Biomedical Engineering, Chinese Academy of Medical Sciences and Peking Union Medical College.

REFERENCES

1. Julian CG, Bowers PW. A clinical review of 209 pilomatricomas. *J Am Acad Dermatol.* (1998) 39(2 Pt 1):191–5. doi: 10.1016/S0190-9622(98)70073-8
2. Malherbe A, Chenantis J. Note sur l'epitheliome calcifie des glandes sebacees. *Prog Med.* (1880) 8:826–8.
3. Hassanein AH, Alomari AI, Schmidt BA, Greene AK. Pilomatrixoma imitating infantile hemangioma. *J Craniofac Surg.* (2011) 22:734–6. doi: 10.1097/SCS.0b013e318207f29f

4. Kaddu S, Soyer HP, Hodl S, Kerl H. Morphological stages of pilomatricoma. *Am J Dermatopathol.* (1996) 18:333–8. doi: 10.1097/00000372-199608000-00001
5. Cevik HB, Erkan M, Kayahan S, Bulut G, Gumustas SA. A skin tumor from an orthopedic oncology perspective: Pilomatrixoma in extremities (11 years experience with 108 cases). *Dermatol Ther.* (2019) 32:e13004. doi: 10.1111/dth.13004
6. Jones CD, Ho W, Robertson BF, Gunn E, Morley S. Pilomatrixoma: a comprehensive review of the literature. *Am J Dermatopathol.* (2018) 40:631–41. doi: 10.1097/DAD.0000000000001118
7. Izzetti R, Vitali S, Aringhieri G, Nisi M, Oranges T, Dini V, et al. Ultra-high frequency ultrasound, a promising diagnostic technique: review of the literature and single-center experience. *Can Assoc Radiol J.* (2020). doi: 10.1177/0846537120940684. [Epub ahead of print].
8. Zaballos P, Llambrich A, Puig S, Malvehy J. Dermoscopic findings of pilomatricomas. *Dermatology.* (2008) 217:225–30. doi: 10.1159/000148248
9. Hughes J, Lam A, Rogers M. Use of ultrasonography in the diagnosis of childhood pilomatrixoma. *Pediatr Dermatol.* (1999) 16:341–4. doi: 10.1046/j.1525-1470.1999.00090.x
10. Lin SF, Xu SH, Xie ZL. Calcifying epithelioma of malherbe (Pilomatrixoma): clinical and sonographic features. *J Clin Ultrasound.* (2018) 46:3–7. doi: 10.1002/jcu.22517
11. Choo HJ, Lee SJ, Lee YH, Lee JH, Oh M, Kim MH, et al. Pilomatricomas: the diagnostic value of ultrasound. *Skeletal Radiol.* (2010) 39:243–50. doi: 10.1007/s00256-009-0678-x
12. Lim HW, Im SA, Lim GY, Park HJ, Lee H, Sung MS, et al. Pilomatricomas in children: imaging characteristics with pathologic correlation. *Pediatr Radiol.* (2007) 37:549–55. doi: 10.1007/s00247-007-0461-x
13. Marino MA, Ascenti G, Cardia R, Ieni A, Colonna MR. Pilomatrixoma of the right thigh: sonographic-pathologic correlation in a young man. *Radiol Case Rep.* (2020) 15:230–3. doi: 10.1016/j.radcr.2019.11.007
14. Ubals M, Castany A, Bassas P, Mollet J, Aparicio G, Garcia-Patos V. Utility of ultrasound in a rapidly growing cutaneous nodule in an infant. *J Pediatr.* (2017) 180:290–290e1. doi: 10.1016/j.jpeds.2016.09.038
15. Hwang JY, Lee SW, Lee SM. The common ultrasonographic features of pilomatricoma. *J Ultrasound Med.* (2005) 24:1397–402. doi: 10.7863/jum.2005.24.10.1397

Conflict of Interest: The authors declare that the research was conducted in the absence of any commercial or financial relationships that could be construed as a potential conflict of interest.

frontiers in Medicine

BRIEF RESEARCH REPORT
published: 26 May 2021
doi: 10.3389/fmed.2021.675383

Teledermatology Adaptations in the COVID-19 Era

Harrison A. Edwards[1,2,3]*, *Xiaohua Shen*[1] *and H. Peter Soyer*[1,3]

[1] *Princess Alexandra Hospital, Woolloongabba, QLD, Australia,* [2] *School of Public Health, University of Queensland, Herston, QLD, Australia,* [3] *Dermatology Research Centre, The University of Queensland Diamantina Institute, The University of Queensland, Brisbane, QLD, Australia*

The COVID-19 pandemic has required health services worldwide to adapt to dramatically changing healthcare needs and risks across all medical specialties. In the dermatology department at Princess Alexandra Hospital, Brisbane, Australia, we developed and implemented a teledermatology system with 1 week's notice to help reduce infection risk bidirectionally, while saving patients many hours of travel and waiting time with acceptable technological substitutes for the clinical encounters. In this study, we report the efficacy and tolerability of our telephone consultation and store and forward imaging system, including patient experience from validated survey data. Our design, implementation and usage of a remote-default system provides experience and lessons to draw upon in developing future telemedicine systems to address dermatology service maldistribution – an issue affecting large areas of Australia – as well as preparedness for future infection mitigation requirements.

Keywords: teledermatology, telemedicine, COVID-19 pandemic, infection control, clinical epidemiology, health services research [MeSH], clinical pathways, performance and evaluation

OPEN ACCESS

Edited by:
Andreas Recke,
University of Lübeck, Germany

Reviewed by:
Maurice Mars,
University of KwaZulu-Natal, South Africa
Joseph English,
University of Pittsburgh Medical Center, United States

***Correspondence:**
Harrison A. Edwards
harrison.edwards@health.qld.gov.au

Specialty section:
This article was submitted to Dermatology, a section of the journal Frontiers in Medicine

Received: *03 March 2021*
Accepted: *21 April 2021*
Published: *26 May 2021*

Citation:
Edwards HA, Shen X and Soyer HP (2021) Teledermatology Adaptations in the COVID-19 Era. Front. Med. 8:675383. doi: 10.3389/fmed.2021.675383

INTRODUCTION

The COVID-19 pandemic has required health services worldwide to adapt to dramatically changing healthcare needs and risks across all medical specialties.

In the dermatology department at Princess Alexandra Hospital, Brisbane, Australia we developed, and instituted a teledermatology system with 1 week's notice. This system comprised of appointments conducted by telephone, and the capacity to receive images by email. Here, we discuss the successes and lessons of implementing this simple system which helped reduce in-person patient numbers and infection risk bidirectionally, while saving patients many hours of travel and waiting time.

Our department has experience in managing a live interactive telehealth dermatology service to treat patients in remote locations (1), as well as a same-day store and forward emergency teledermatology service (2, 3). However, until the current pandemic, face-to-face assessment had been the modality for nearly all routine and urgent appointments and thus comprised the vast majority of patient care.

When the COVID-19 pandemic struck in March 2020 in Brisbane, Australia, and strict lockdown measures were enacted, our dermatology department faced the decision between closing entirely and leaving our catchment of over a million people without a dermatology service, or quickly developing a way that we could continue to serve our patients.

The pre-existing videoconferencing arrangement is limited in that it takes place in the hospital's telehealth center and can only be allocated limited space and time (one session per week), as it uses

dedicated hardware and requires a clinic-to-clinic format. Video calls using smartphones would have required either the doctors to use their personal mobile phones and phone numbers, or for the department to acquire and setup additional hardware. These options unfortunately were not feasible, especially in the short time frame and in the context of institutional IT rules.

This study reports on the clinical efficacy and patient experience of a new remote consultation system we devised.

METHOD

Clinic Process

The system devised consisted of administrative staff checking in the patients by phone and confirming their phone number and email address in the hour prior to their booked appointment, which saves doctors time. Additionally, because most patients are waiting comfortably at home rather than in the clinic waiting room, they are less inconvenienced by waiting to be seen.

Patient files are queued by nursing staff, and the medical staff call the patients by phone. An email address with shared staff access was approved and created to receive clinical photos from patients to support the phone consultations when indicated. The images were then incorporated into the usual electronic medical record, Millennium (Cerner Corporation; North Kansas City, Missouri, United States).

Prescriptions and investigation forms are physically mailed to the patient's home address, and urgent prescriptions are faxed directly to the patient's pharmacy for rapid preparation and dispensing (**Figure 1**).

System Implementation

This system was developed by nursing and administrative staff in the department with input and feedback from the doctors, and was instituted on 23rd March 2020 after a week of preparation.

At first, dermatology trainees were tasked with determining which upcoming appointments would be suitable for remote consultation. Factors evaluated included patient location, diagnosis, and current management if the appointment was for a review, and expected risk of deterioration and ability to evaluate without in-person examination.

Subsequently, we changed to a system whereby phone consultation was the default. If issues arose during the consultation that would require in-person review (such as an inability to adequately examine the patient using photos, a requirement for discussion of complex management decisions, or urgent physical treatments), a subsequent in-person appointment was made. Patients located nearby could sometimes attend the clinic in-person the same day; for other cases, an appointment would be arranged within a week.

This system of teledermatology by default and escalation when required increased the numbers of consultations conducted remotely and eliminated the time requirement of dermatology trainees assessing appropriateness for teledermatology prior to the appointment.

As the year progressed and government lockdown rules were reduced, more appointments were conducted in-person. In June to September, review appointments could be booked as in-person or teledermatology depending on doctors' clinical judgment and patient preference, whereas appointments for new patients were booked for teledermatology. During this period, appointments conducted in-person approached 50%.

By November, in-person appointments became the default, and subsequently ∼20% of appointments were conducted by teledermatology.

Evaluation

To assess the implementation of this system, clinic appointment counts were assessed and compared with the same period in the calendar year prior, appointments requiring a language interpreter were noted, and a count of cases in the email system was conducted.

For the patient perspective, a survey was conducted by phone of 100 patients of the ∼2,000 patients who had a phone appointment between 23rd March 2020 and 15th January 2021. To minimize recall bias and to elicit the most accurate and detailed responses, this sample of patients was taken from those who had a phone appointment within the recent time frame of 18th November 2020 to 15th January 2021.

A validated survey tool, the Telehealth Usability Questionnaire (TUQ), was used to comprehensively cover the domains of usefulness, ease of use and learnability, interface quality, interaction quality, reliability, satisfaction and

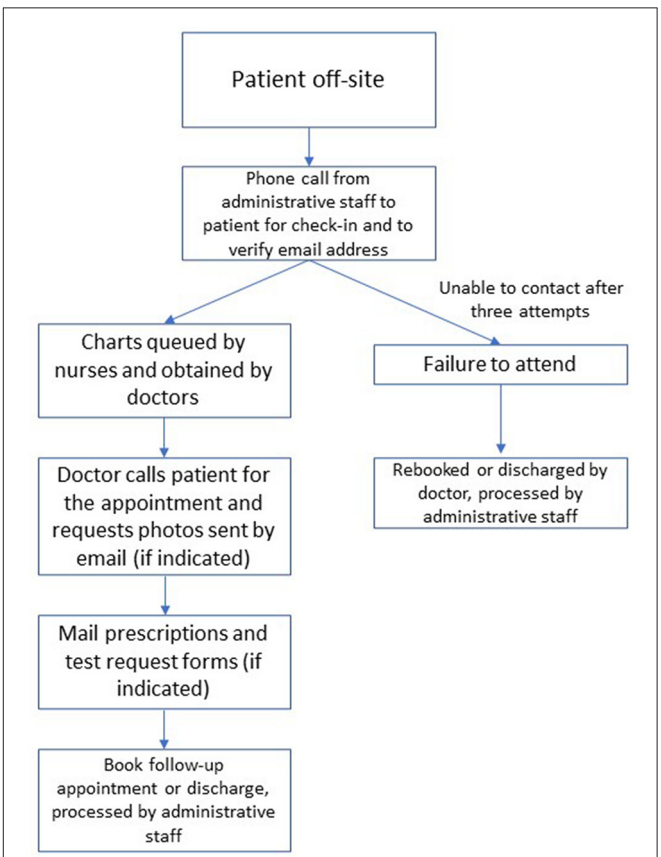

FIGURE 1 | Clinic workflow in the teledermatology system.

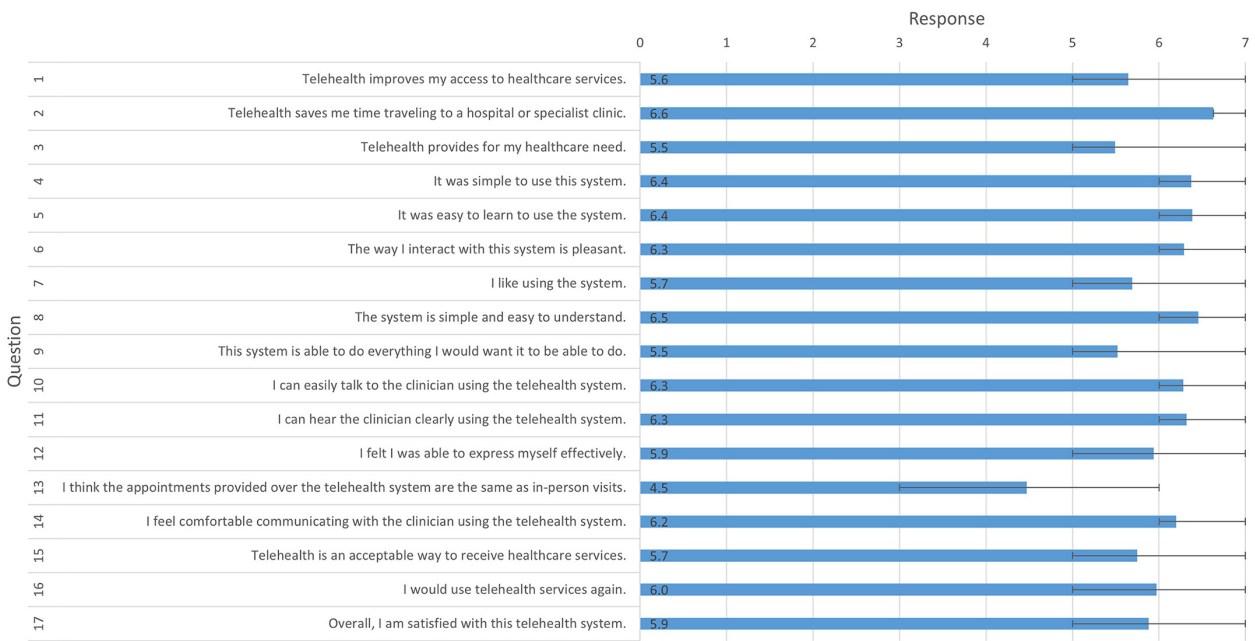

FIGURE 2 | Modified Telehealth Usability Questionnaire, responses to quantitative questions. Likert scale; 1 (disagree) to 7 (agree); mean and interquartile range.

future use. The TUQ has demonstrated strong validity and reliability across various telecommunication systems, whereas most other questionnaires apply primarily to special purpose videoconferencing hardware or other single modalities (4).

The TUQ was modified to exclude questions that were not applicable to our context. Consequently, a set of 17 questions (based on a 7-point Likert scale) and an open-ended feedback question were used.

RESULTS

Through this system, in-person clinic attendance was reduced by 95% at the initial peak of the pandemic while maintaining high clinical throughput: a sample of medical dermatology clinic sessions in the first 2 months of the teledermatology system showed higher patient numbers than the same period the year prior.

However, surgical clinic sessions were more negatively impacted by the pandemic: although appointment counts under the teledermatology system were only 11% lower than usual, these appointments served only as a safety check – urgent, complex lesions were subsequently booked for in-person management; patients were otherwise advised to see their general practitioner for other skin concerns.

A language interpreter was required in 5% of cases, and surprisingly, an evaluation of the email system in the first 3 weeks demonstrated that photos were required in only 36.5% (152/417) of appointments. When photos were required, patients could usually manage to send them by email to the shared inbox described above, and photos were generally of suitable quality. The proportion of consultations over the same period that required escalation to an in-person encounter was low, at 2.4% (10/417).

The major benefits identified from the survey (**Figure 2**) were saving travel time (Q2) and that it is simple and easy to understand and use (Q4, Q5, Q8).

Comparatively low scores were given for questions that asked about clinical equivalence to in-person appointments (Q3, Q9, Q13). However, most patients responded indicating that they were satisfied with the service and that they would use it again (Q16, Q17).

Based on 74 responses to the open-ended feedback question, certain benefits and drawbacks were identified. Some patients (5%), especially the elderly, identified difficulty with taking and emailing photos. Some patients (3%) whose phone appointment was not clinically adequate and required a subsequent in-person appointment were unhappy about the double handling and delay.

Many patients (20%) emphasized the benefit of eliminating travel time and reducing the interruption to their day, but many (27%) also felt that dermatology was particularly challenging for telemedicine due to the primacy of visual examination. Relatedly, a contingent of patients (7%), including some of those who reported overall satisfaction with the teledermatology system, stated a desire for periodic in-person appointments.

Despite the reduction in travel time, several patients (9%) expressed inconvenience regarding the unreliable appointment wait times on the day of their appointment. A surprisingly small number of patients (4%) commented on infection risk mitigation as a benefit of the teledermatology system.

DISCUSSION

Strengths

Our simple conventional phone-based teledermatology system has worked well, allowing patients to still receive clinical care while avoiding bidirectional infection risk. Although existing literature on teledermatology essentially always involves remote visual examination (either synchronously or asynchronously) (5, 6), our finding that images were required only in a minority of cases suggests that a large proportion of teledermatology, more feasibly follow-up appointments, could be conducted without visual examination. This may be due to the department's new:review ratio of 1:4; however, image requirement by appointment type could not be extracted to confirm this.

Administrative workload has been mostly unchanged in the new, remote system, and time-consuming steps such as patient and staff movement between waiting rooms and consultation rooms have been avoided.

This system is advantageous for reducing infection risk for the general patient population, but is especially protective for our many patients who are on immunosuppressive therapies. As well as reducing bidirectional infection risk, teledermatology reduces the need for personal protective equipment, helping to maintain supplies for clinical encounters where it is necessary.

As a department of a public hospital, we have the advantage that we do not rely on private health insurance or Medicare billing, and therefore issues related to those aspects can be avoided in our teledermatology process.

Weaknesses

Many patients were able to send clinical photos through the email system, but as described above, 33% of survey respondents either found the email system technically challenging (5%) or felt it was inferior compared to in-person visual examination (27%). Email was used to receive photos from patients, even though it is not an institutionally approved way of communicating with patients outside of emergency conditions such as the COVID-19 pandemic. The other store and forward methods requested by patients, Facebook Messenger and Multimedia Messaging Service (MMS), would have carried additional issues of privacy and difficulty of shared staff access.

Evaluation of patients for skin cancer is problematic in this teledermatology system, because of the difficulty of replicating examination electronically and the significant consequences of incorrect skin cancer diagnosis. Each lesion on a patient poses new diagnostic uncertainty, and biopsies cannot be done remotely. Consequently, skin cancer patients requiring urgent biopsy comprised many of the patients needing to be seen in-person. Generally, patients were advised that their skin cancer examination would be delayed and that they should see their GP in the meantime.

Appointments requiring a language interpreter were sometimes complicated. These were arranged either as a consultation with an interpreter co-located with the doctor and the patient on the phone, or as a three-way phone conversation with the doctor in the clinic and the interpreter and patient on the phone. If the dermatology consultant needed to be involved, the three-way call between the doctor, patient and interpreter would need to be ended and later reconnected to relay the consultant's input, which was cumbersome and time consuming.

CONCLUSION

This system was put in place after only 1 week of development, reduced the number of patients in the clinic by 95%, allowing us to greatly reduce the infection risk for both patients and staff, reduce PPE requirement, and also save patients travel time and waiting time.

The necessity of telemedicine systems to minimize infection risk during the current pandemic has been recognized in Australia and overseas. Health systems worldwide have responded by declaring that in-person medical care should be limited to only the most urgent patients. To facilitate this, they have reduced administrative and security requirements for telemedicine, allowing healthcare providers to serve patients through everyday communications technologies such as phone, email, instant messaging, and video chat software (7, 8).

Dermatology departments in the United States (9–11), China (12), and Europe (13–15) have accordingly restricted their in-person clinical encounters due to the recognized risk of SARS-CoV-2 transmission. Similarly, the Australian government has adapted administrative billing requirements for telemedicine by general practitioners and all medical specialists (16).

Our experience of urgently designing and implementing a teledermatology system was broadly positive, due to the benefits of infection risk reduction, reduced patient travel and waiting times, and acceptability to patients and doctors of in-person history and examination substitutes.

In the United States, The Society of Dermatology Hospitalists developed an algorithm to triage teledermatology consults. A high rate of teledermatology suitability was found, with only four out of the 35 patients sampled (11%) requiring escalation to in-person consultation (17), which accords with our result of 2.4%.

As before the COVID-19 pandemic, there is legitimate concern regarding technological security and patient privacy regarding teledermatology. Our imperfect but successful design, implementation and usage of a remote-default system using phone for consultations with supporting images sent by email provides experience and lessons to draw upon in developing future robust telemedicine systems to address dermatology service provision, taking into consideration specialist maldistribution in Australia as well as preparedness for future infection mitigation requirements.

DATA AVAILABILITY STATEMENT

The raw data supporting the conclusions of this article will be made available by the authors, without undue reservation.

ETHICS STATEMENT

The studies involving human participants were reviewed and approved by Metro South Health Human Research Ethics Committee. Written informed consent for participation was not

required for this study in accordance with the national legislation and the institutional requirements.

AUTHOR CONTRIBUTIONS

HE and XS contributed to data acquisition. HE and HS contributed to data analysis. All authors contributed equally to the concept, design, and contributed to the drafting and critical revision of the manuscript.

FUNDING

HS holds an NHMRC MRFF Next Generation Clinical Researchers Program Practitioner Fellowship (APP1137127).

REFERENCES

1. Miller BJ, Finnane A, Vun Y, Halloran S, Stapelberg A, Soyer HP, et al. Real-time teledermatology clinics in a tertiary public hospital: a clinical audit. *Australas J Dermatol.* (2020) 61:e383–7. doi: 10.1111/ajd.13322
2. Finnane AR, Siller G, Soyer HP. Teledermatologists' management of emergency skin conditions. *Med J Aust.* (2015) 203:286. doi: 10.5694/mja15.00362
3. Finnane A, Siller G, Mujcic R, Soyer HP. The growth of a skin emergency teledermatology service from 2008 to 2014. *Australas J Dermatol.* (2016) 57:14–8. doi: 10.1111/ajd.12411
4. Parmanto B, Lewis AN, Graham KM, Bertolet MH. Development of the Telehealth Usability Questionnaire (TUQ). *Int J Telerehabil.* (2016) 8:3–10. doi: 10.5195/ijt.2016.6196
5. Finnane A, Dallest K, Janda M, Soyer HP. Teledermatology for the diagnosis and management of skin cancer a systematic review. *JAMA Dermatol.* (2017) 153:319–27. doi: 10.1001/jamadermatol.2016.4361
6. Lee JJ, English JC. Teledermatology: a review and update. *Am J Clin Dermatol.* (2018) 19:253–60. doi: 10.1007/s40257-017-0317-6
7. United States Centers for Medicare & Medicaid Services. *President Trump Expands Telehealth Benefits for Medicare Beneficiaries During COVID-19 Outbreak*. Available online at: https://www.cms.gov/newsroom/press-releases/president-trump-expands-telehealth-benefits-medicare-beneficiaries-during-covid-19-outbreak/ (accessed April 9, 2020).
8. Lee I, Kovarik C, Tejasvi T, Pizarro M, Lipoff JB. Telehealth: helping your patients and practice survive and thrive during the COVID-19 crisis with rapid quality implementation. *J Am Acad Dermatol.* (2020) 82:1213–4. doi: 10.1016/j.jaad.2020.03.052
9. Pathoulas JT, Stoff BK, Lee KC, Farah RS. Ethical outpatient dermatology care during the coronavirus (COVID-19) pandemic. *J Am Acad Dermatol.* (2020) 82:1272–3. doi: 10.1016/j.jaad.2020.03.047
10. Kwatra SG, Sweren RJ, Grossberg AL. Dermatology practices as vectors for COVID-19 transmission: a call for immediate cessation of nonemergent dermatology visits. *J Am Acad Dermatol.* (2020) 82:e179–80. doi: 10.1016/j.jaad.2020.03.037
11. Price KN, Thiede R, Shi VY, Curiel-Lewandrowski C. Strategic dermatology clinical operations during COVID-19 pandemic. *J Am Acad Dermatol.* (2020) 82:e207–9. doi: 10.1016/j.jaad.2020.03.089
12. Chen Y, Pradhan S, Xue S. What are we doing in the dermatology outpatient department amidst the raging of the 2019 novel coronavirus? *J Am Acad Dermatol.* (2020) 82:1034. doi: 10.1016/j.jaad.2020.02.030
13. Wollina U. Challenges of COVID-19 pandemic for dermatology. *Dermatol Ther.* (2020) 33:e13430. doi: 10.1111/dth.13430
14. Radi G, Diotallevi F, Campanati A, Offidani A. Global coronavirus pandemic (2019-nCOV): implication for an Italian medium size dermatological clinic of a II level hospital. *J Eur Acad Dermatol Venereol.* (2020) 34:e213–4. doi: 10.1111/jdv.16386
15. Wang R, Helf C, Tizek L, Neuhauser R, Eyerich K, Zink A, et al. The impact and consequences of SARS-CoV-2 pandemic on a Single University Dermatology Outpatient Clinic in Germany. *Int J Environ Res Public Health.* (2020) 17:6182. doi: 10.3390/ijerph17176182
16. Medical Benefits Schedule. *COVID-19 Temporary MBS Telehealth Services*. Australian Government Department of Health. Available online at: http://www.mbsonline.gov.au/internet/mbsonline/publishing.nsf/Content/Factsheet-TempBB (accessed February 25, 2021).
17. Salamon M. *A Decade of Telemedicine Policy Has Advanced in Just 2 Weeks* [Internet]. Medscape (2020). Available online at: http://www.medscape.com/viewarticle/928038

Conflict of Interest: HS is a shareholder of MoleMap NZ Limited and e-derm consult GmbH, undertakes regular teledermatological reporting for both companies, and Medical Consultant for Canfield Scientific Inc., Revenio Research Oy and also a Medical Advisor for First Derm.

The remaining authors declare that the research was conducted in the absence of any commercial or financial relationships that could be construed as a potential conflict of interest.

frontiers in Medicine

ORIGINAL RESEARCH
published: 14 June 2021
doi: 10.3389/fmed.2021.686470

High-Frequency Ultrasonography and Evaporimetry in Non-invasive Evaluation of the Nail Unit

Marta Szymoniak-Lipska[1†], Adriana Polańska[2†], Dorota Jenerowicz[1], Adam Lipski[3], Ryszard Żaba[2], Zygmunt Adamski[1] and Aleksandra Dańczak-Pazdrowska[1]*

[1] Department of Dermatology, Poznan University of Medical Sciences, Poznan, Poland, [2] Department of Dermatology and Venereology, Poznan University of Medical Sciences, Poznan, Poland, [3] Department of Urology, Poznań University of Medical Sciences, Poznan, Poland

OPEN ACCESS

Edited by:
H. Peter Soyer, The University of Queensland, Australia

Reviewed by:
Je-Ho Mun, Seoul National University Hospital, South Korea
Irina Khamaganova, Pirogov Russian National Research Medical University, Russia

***Correspondence:**
Adriana Polańska
adriana-polanska@wp.pl

[†]These authors have contributed equally to this work and share first authorship

Specialty section:
This article was submitted to Dermatology, a section of the journal Frontiers in Medicine

Received: *26 March 2021*
Accepted: *12 May 2021*
Published: *14 June 2021*

Citation:
Szymoniak-Lipska M, Polańska A, Jenerowicz D, Lipski A, Żaba R, Adamski Z and Dańczak-Pazdrowska A (2021) High-Frequency Ultrasonography and Evaporimetry in Non-invasive Evaluation of the Nail Unit. Front. Med. 8:686470. doi: 10.3389/fmed.2021.686470

Background: The nail unit (NU) is a complex structure that performs a number of functions, including protection, defense, manipulation, and palpation. Non-invasive research methods can facilitate the recognition of NU structure and function. Evaporimetry and HF-USG due to their availability of equipment and low research costs seem to be particularly noteworthy, but so far have been assessed to a limited extent. The aim of the presented study was to check the usefulness of TOWL and HF-USG in examination of NU.

Materials and Methods: A total of 58 volunteers aged 25–65 years (mean age: 41 ± 10.16 years) were qualified for the study. The subjects did not present symptoms of clinically evident onychopathy and did not suffer from any dermatoses associated with lesions occurring within the NU. Additionally, the patients did not suffer from systemic diseases that could affect NU (including heart, lung, and endocrine diseases). In all volunteers, the measurement of TOWL and 20 MHz ultrasonography [high-frequency ultrasonography (HF-USG)] with the special emphasis on determination of nail plate thickness were performed.

Results: Analysis of 464 HF-USG images revealed that the nail plate presented as two hyperechoic, parallel streaks (railway sign) with a linear hypoechoic middle layer between them. Matrix was visualized as a hypoechoic structure with blurred boundaries, mostly within the fourth and fifth fingers and more often in women. We found statistically significant correlations between the type of a finger and the thickness of the nail plate both in the entire study group and taking into account gender. In the dominant hand, the results were $r = -0.341$; $p < 0.001$; $r = -0.417$, $p < 0.001$; and $r = 0.337$; $p = 0.001$ (for the whole group, for women, and for men, respectively). In the non-dominant hand, the results were $r = -0.465$; $p < 0.001$; $r = -0.493$, $p < 0.01$; and $r = -0.503$; $p < 0.01$ (for the whole group, for women, and for men, respectively). There were statistically significant differences in the thickness of the nail plates of the corresponding types of fingers between female and male NUs. Statistically significant correlations were found between the type of a finger and the TOWL value in the whole group and taking into account gender ($p < 0.05$), except for the non-dominant hand in men. There were no statistically significant differences in the

TOWL values of the corresponding types of fingers between male and female NUs ($p > 0.05$). There was no statistically significant correlation between the TOWL value and the nail plate thickness in any of the tested NUs, apart from the one statistically significant correlation in nd5 ($r = 0.390$, $p = 0.021$).

Conclusions: To sum up, non-invasive methods, such as HF-USG and TOWL, enable assessment of the NU and are useful in examination of its structure and function. HF-USG shows characteristic elements of NUs that can be distinguished because of differences in their echogenicity. The thickness of the nail plate and TOWL depend on the type of finger, and show a relationship with gender.

Keywords: HF-USG, High frequency ultrasonography, TOWL, transonychial water loss, nail plate thickness, nail, nail unit

INTRODUCTION

The nail unit (NU) is a complex structure that performs a number of functions, including protection, defense, manipulation, and palpation (1). Nowadays special attention is also paid to the aesthetic function of NU (2), and deterioration in its appearance may negatively affect the quality of life (3). For those reasons, diseases of NU seem to be hot topics for researchers around the world (4, 5). There is a significant tendency to look for non-invasive research methods that facilitate the recognition of NU structure and function. Among these methods, evaporimetry and HF-USG seem to be particularly noteworthy, due to the availability of equipment, and low research costs that so far have been assessed to a limited extent (6).

Transepidermal water loss (TEWL) measurement is used to indirectly assess the function of the epidermal barrier function and is applied mostly in studies conducted among patients with atopic dermatitis (AD) (7–9). The modification of this procedure adapted to NU is a transonychial water loss (TOWL). TOWL values have been reported in single studies and are many times higher than the TEWL values, which can be related to NU composition (10). The possibility of imaging NU in real time can be achieved using ultrasound examination (USG). With the application of frequencies dedicated for dermatological applications [high-frequency ultrasound (HF-USG)] (11), there is the possibility to visualize the NU structure. To date, in single reports, NU pathological processes like abscesses, hematomas (12), glomeruli, and mucous cysts were described with the use of HF-USG, and the utility of this method in differentiation of psoriasis (13) and onychomycosis (14) was presented. However, studies evaluating usefulness of HF-USG in examination of complete finger NU structure in regards to sex, age, and dominant hand are still lacking. The relationship between TOWL value and thickness of the nail plate was assessed only to a small extent in few reports (6, 15, 16), using a variety of research methodology. Thus, there is a need for detailed, global ultrasonographic assessment of NU, the knowledge of which could translate into a better understanding of the pathological processes occurring within this appendage.

The aim of the presented study was to explore the utility of TOWL and HF-USG in examination of NU as well as to obtain the ultrasonographic features of NU with special emphasis on non-invasive measurement of the nail plate thickness.

MATERIALS AND METHODS

Examined Group

A total of 58 volunteers aged 25–65 years (mean age: 41 ± 10.16 years) were qualified for the study. Thirty-five women (mean age: 41.49 ± 9.80 years) and 23 men were examined (mean age: 40.26 ± 10.86 years). All of the participants have given their written consent. The subjects did not present symptoms of clinically evident onychopathy and did not suffer from any dermatoses associated with lesions occurring within the NU. All subjects were right-handed and non-smokers. In two cases, two NU of the thumbs were excluded from the study due to the condition after mechanical trauma.

The tests were performed in standardized conditions at the temperature of 20–24°C. At least 30 days prior to examination, volunteers had to stop using any nail polish or varnish and performing manicure, except nail clipping. Subjects were asked not to use detergents and disinfectants for a minimum of 20 min before tests. First, TOWL measurement was performed, followed by HF-HSG. The above order was determined by necessity to use a medium in the form of an ultrasound gel for HF-USG examination. We were aware that its application to the nail plate could cause a change in NU hydration and make TOWL results unreliable.

The letter designation was adopted for the description of NU: "d" for the finger of the dominant hand and "nd" for the non-dominant one. The number describes the type of finger, and so the number (1), corresponded to the thumb; (2), the index finger; (3), the middle finger; (4), the ring finger; and (5), little finger.

HF-USG

The HF-USG examination was performed with the use of The Dermascan C device (version 3) by Cortex Technology (Hadsund, Denmark) equipped with a linear head 20 MHz (11). The probe was covered with a layer of ultrasound gel and then placed on the NU to obtain sagittal sections. The transducer was positioned in the midline to include the proximal nail fold and 1/2 proximal to the nail plate in the imaging. The axial

TABLE 1 | Percentage results of imaged matrixes.

Whole group								
Type of finger	d2	d3	d4	d5	nd2	nd3	nd4	nd5
% of visible matrixes (%)	12	9	19	22	21	22	28	24
Women								
Type of finger	d2	d3	d4	d5	nd2	nd3	nd4	nd5
% of visible matrixes (%)	14	11	29	29	29	31	37	20
Men								
Type of finger	d2	d3	d4	d5	nd2	nd3	nd4	nd5
% of visible matrixes (%)	9	4	4	13	9	9	13	30

nd, the finger of the non-dominant hand; d, the finger of the dominant hand; number, type of finger; i.e., 2, index finger.

resolution was 80 μm, and the lateral resolution was 200 μm. The ultrasonic wave propagated through the tissues at a speed of 2,480 m/s. The B-mode presentation was used to qualitatively evaluate the images. The A-mode presentation was used to carry out the measurements of the thickness of the nail plate, which was measured in each examined finger three times in the area between the proximal 1/3 and middle 1/3. Then, the arithmetic mean was calculated.

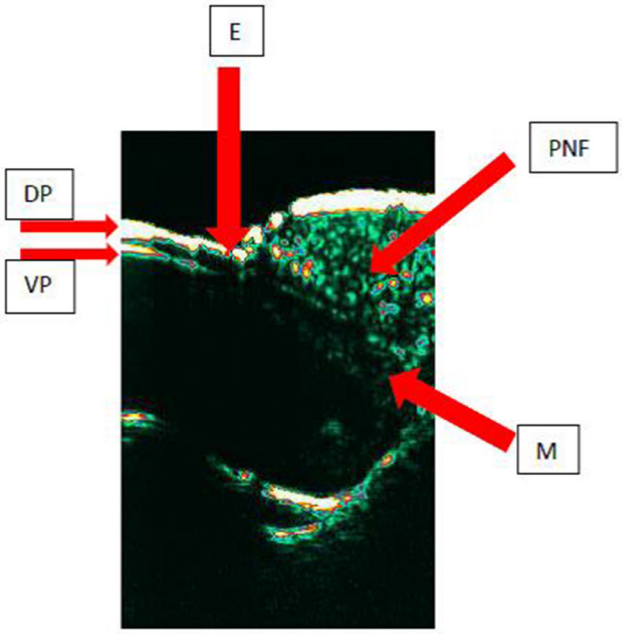

FIGURE 1 | The HF-USG image of the nail unit.

TOWL

TOWL measurements were conducted using a Tewameter® TM 300 Courage-Khazaka (Köln, Germany), with a reduction diaphragm recommended by the manufacturer (diameter 2 mm) for testing small areas (Z00812) according to the guidelines originally established for TEWL (17). The Tewameter® TM 300 was connected to the Cutometer® MPA 580. The device was placed in the middle on the nail plate within its proximal 1/3 and central part. An attempt was made to achieve the comparable pressure. In case of each examined NU, 20 measurements were performed at 1 s intervals. An arithmetic mean was then calculated. The results were presented in conventional units (c.u.).

Statistical Analysis

For the values of parameters such as plate thickness and TOWL, appropriate descriptive statistics were determined: arithmetic mean with the corresponding standard deviation, minimum, and maximum values. The differences between the groups were assessed using the non-parametric Mann–Whitney *U* test. The relationships between the parameters were investigated using Spearman's correlation. Values at $p < 0.05$ were considered statistically significant. The calculations were made with the use of the STATISTICA v 13.3 statistical package.

RESULTS

Analysis of HF-USG Results

Finally, HF-USG 464 images of NU were taken into consideration, which was related to the repeated unsuccessful attempts to visualize NU in the thumbs. The difficulties were associated with the inability to fit an ultrasound head for anatomical curvatures of NU within d1 and nd1 and the gained images had insufficient quality. Therefore, analysis of them was abandoned.

In all analyzed fingers, the nail plate presented as two hyperechoic, parallel streaks (railway sign). Between them, a linear hypoechoic middle layer was visible. The abovementioned hyperechoic bands were, respectively, the dorsal and ventral lamina of the nail plate. The cuticle was located proximally to the described structures and its echogenicity was similar to the echogenicity of the dorsal and ventral plates. Moving further, proximal nail fold, with an echogenicity lower than the mentioned dorsal and ventral plates, occurred. Matrix was visualized as a hypoechoic structure with blurred boundaries, adjacent to the nail fold and the proximal part of the abdominal plate. It was visible in a minority of respondents, and the number of visualized matrixes varied in different types of finger. The matrix was seen more often in the fourth and fifth fingers and more often in women. The detailed percentage results of imaged matrixes are presented in **Table 1**. **Figure 1** shows the sagittal section of HF-USG of the NU with its characteristic elements.

The average thickness of the nail plate in the whole group ranged from 0.36 mm in nd5 to 0.43 mm in nd2. The thinnest nail plate was observed in the group of women in nd5 (0.25 mm), and the thickest was observed in the group of men in nd2 (0.54 mm). The mean thickness of the nail plate in the group of women ranged from 0.35 mm in nd5 to 0.40 mm d2. The greatest thickness in this group was observed in nd2 (0.51 mm). The average thickness of the nail plate in the group of men ranged from 0.39 mm in nd5 to 0.45 mm in nd2. The lowest thickness in this group was noted in nd4 (0.30 mm). The thickness of nail plates is presented in **Table 2**.

TABLE 2 | The thickness of nail plates in the whole group and in the group of women and men.

Whole group				
Type of finger		**Mean ± SD [mm]**	**Min [mm]**	**Max [mm]**
2	D	0.42 ± 0.05	0.33	0.52
	Nd	0.43 ± 0.04	0.35	0.54
3	D	0.41 ± 0.05	0.30	0.51
	Nd	0.40 ± 0.05	0.29	0.50
4	D	0.39 ± 0.04	0.29	0.49
	Nd	0.38 ± 0.05	0.28	0.52
5	D	0.38 ± 0.05	0.27	0.48
	Nd	0.36 ± 0.04	0.25	0.45
WOMEN				
Type of finger		**Mean ± SD [mm]**	**Min [mm]**	**Max [mm]**
2	D	0.40 ± 0.04	0.33	0.49
	Nd	0.41 ± 0.04	0.35	0.51
3	D	0.39 ± 0.04	0.30	0.46
	Nd	0.39 ± 0.04	0.29	0.48
4	D	0.37 ± 0.04	0.29	0.44
	Nd	0.37 ± 0.04	0.28	0.43
5	D	0.36 ± 0.04	0.27	0.44
	Nd	0.35 ± 0.04	0.25	0.42
MEN				
Type of finger		**Mean ± SD [mm]**	**Min [mm]**	**Max [mm]**
2	D	0.45 ± 0.05	0.35	0.52
	Nd	0.45 ± 0.04	0.36	0.54
3	D	0.43 ± 0.05	0.34	0.51
	Nd	0.43 ± 0.04	0.36	0.50
4	D	0.41 ± 0.04	0.34	0.49
	Nd	0.41 ± 0.06	0.30	0.52
5	D	0.41 ± 0.04	0.33	0.48
	Nd	0.39 ± 0.03	0.33	0.45

nd, the finger of the non-dominant hand; d, the finger of the dominant hand; number, type of finger; i.e., 2, index finger.

We found statistically significant correlations between the type of a finger and the thickness of the nail plate both in the entire study group and taking into account gender. In the dominant hand, the results were as follows: $r = -0.3$; $p < 0.001$; $r = -0.4$, $p < 0.001$; and $r = 0.3$; $p = 0.001$ (for the whole group, for women, and for men, respectively). In the non-dominant hand, the results were $r = -0.5$; $p < 0.001$; $r = -0.5$, $p < 0.01$; and $r = -0.5$; $p < 0.01$ (for the whole group, for women, and for men, respectively). There were statistically significant differences in the thickness of the nail plates of the corresponding types of fingers between female and male NUs (**Table 3**).

There were no statistically significant differences in the thickness of the nail plates of the corresponding fingers of the dominant and non-dominant hand, both in the whole group and taking into account gender ($p > 0.05$).

The statistically significant correlation between the age and the thickness of the nail plate was observed only in the d5 fingers in the entire study group and in the group of men ($r = -0.3$, $p = 0.027$; $r = -0.4$, $p = 0.043$, respectively).

TABLE 3 | *p*-values for differences in the thickness of the nail plates of the corresponding types of fingers between female and male NUs.

Type of finger	**d2**	**d3**	**d4**	**d5**	**nd2**	**nd3**	**nd4**	**nd5**
P	<0.001	0.002	0.002	<0.001	<0.001	0.001	0.026	<0.001

nd, the finger of the non-dominant hand; d, the finger of the dominant hand; number, type of finger; i.e., 2, index finger.

Analysis of TOWL Values

The mean TOWL value in the entire group ranged from 5.02 c.u. in d1 to 7.41 c.u. in d5. The lowest measured TOWL value was recorded in the group of men in d1 (1.10 c.u.), and the highest value, also observed in the group of men, in nd3 (17.60 c.u.). The mean value of TOWL in the group of women ranged from 5.1 c.u. in d1 to 7.30 c.u. in d5. In this group, the minimal value of TOWL was observed in d1 (2.70 c.u.), and the highest value (12.80 c.u.) was obtained in d5. The mean value of TOWL in the group of men ranged from 4.90 c.u. in d1 to 7.58 c.u. in d5.

The TOWL value for each type of NU are presented in the **Table 4**

Statistically significant correlations were found between the type of a finger and the TOWL value in the whole group and taking into account gender ($p < 0.05$), except for the non-dominant hand in men ($r = 0.8$, $p = 0.068$) (**Table 5**).

There were no statistically significant differences in the TOWL values of the corresponding fingers of the dominant and non-dominant hand, both in the whole group and taking into account gender ($p > 0.05$). There were no statistically significant differences in the TOWL values of the corresponding types of fingers between male and female NUs ($p > 0.05$). The statistically significant correlation between the age and the TOWL value was observed only in the group of men in d3 finger ($r = -0.5$, $p = 0.031$).

Analysis of Correlations Between HF-USG Results and TOWL Values

There was no statistically significant correlation between the TOWL value and the nail plate thickness in any of the tested NUs, neither in the whole group and in the group of men. The significant correlations were not detected in the majority of fingers in women's group, the only statistically significant correlation was pointed in nd5 ($r = 0.4$, $p = 0.021$).

DISCUSSION

To our knowledge, our study presents for the first time a detailed characteristic of a NU achieved with the use of non-invasive tools in subjects with no evident onychopathy, taking into account all fingers of both hands in relation to volunteers' gender and age.

HF-USG

Similarly to previous studies (12), we found that the normal nail plate is a trilaminar structure with the first and third layer being hyperechoic, while the second layer is anechoic. The nail matrix is a hypoechoic area that is placed proximally within NU.

TABLE 4 | The values of TOWL measurements in the whole group, in the group of women, and in the group of men.

Whole group				
	Type of finger	**Mean ± SD [c.u.]**	**Min [c.u.]**	**Max [c.u.]**
1	D	5.02 ± 1.50	1.10	8.00
	Nd	5.33 ± 1.72	2.90	11.60
2	D	6.13 ± 1.80	3.30	10.90
	Nd	6.41 ± 2.27	2.10	12.80
3	D	6.64 ± 2.70	2.30	16.80
	Nd	6.43 ± 2.39	3.10	17.60
4	D	6.74 ± 2.00	2.90	12.50
	Nd	6.52 ± 2.24	3.30	16.30
5	D	7.41 ± 2.50	3.10	13.30
	Nd	6.53 ± 2.13	1.80	11.80
WOMEN				
	Type of finger	**Mean ± SD [c.u.]**	**Min [c.u.]**	**Max [c.u.]**
1	D	5.10 ± 1.20	2.70	8.00
	Nd	5.39 ± 1.55	2.90	9.90
2	D	5.92 ± 1.73	3.70	10.60
	Nd	6.40 ± 1.93	3.30	11.50
3	D	6.36 ± 1.64	3.90	12.00
	Nd	6.07 ± 1.40	3.50	8.50
4	D	7.03 ± 1.95	3.60	12.50
	Nd	6.50 ± 2.02	3.30	10.70
5	D	7.30 ± 2.41	3.50	12.80
	Nd	6.61 ± 1.87	3.90	11.10
MEN				
	Type of finger	**Mean ± SD [c.u.]**	**Min [c.u.]**	**Max [c.u.]**
1	D	4.90 ± 1.91	1.10	8.00
	Nd	5.24 ± 1.99	3.00	11.60
2	D	6.46 ± 1.90	3.30	10.90
	Nd	6.43 ± 2.75	2.10	12.80
3	D	7.08 ± 3.80	2.30	16.80
	Nd	6.97 ± 3.36	3.10	17.60
4	D	6.31 ± 2.03	2.90	10.40
	Nd	3.55 ± 2.58	3.40	16.30
5	D	7.58 ± 2.67	3.10	13.30
	Nd	6.41 ± 2.51	1.80	11.80

Nd, the finger of the non-dominant hand; d, the finger of the dominant hand; number, type of finger; i.e., 2, index finger; c.u., conventional units.

TABLE 5 | Values of *r* and *p* for correlations between the type of a finger and the TOWL value.

Dominant hand	***R***	***P***
Whole group	0.3	<0.001
Women	0.4	<0.001
Men	0.3	0.003
Non-dominant hand	*R*	*P*
Whole group	0.2	0.002
Women	0.2	0.012
Men	0.8	0.068

In our study, matrix was visible in a minority of respondents, and the number of visualized matrixes varied in different types of fingers. The matrix was seen more often in the fourth and fifth fingers and more often in women. It may be due to the fact that in these fingers, the nail plate is the thinnest and the visualization of deeper NU structures is easier. The other reason could be that the curvature of mentioned NUs is the slightest and USG probe adheres better, therefore giving higher chances to obtain good quality images. Unfortunately, in our study images gained from d1 and nd1 had insufficient quality, although repeated attempts to visualize these NU were performed. The difficulties were related to the limitations of our probe (inability to fit the ultrasound head for anatomical curvatures of thumbs). Finally, HF-USG 464 images of NU of fingers two to five were taken into consideration.

Literature data regarding NU USG in healthy volunteers are scarce and most researchers focus on NU pathologies (particularly psoriasis) (18–20). The pioneers of a nail plate thickness analysis using ultrasound transmission time were Finlay et al. (21). They compared acquired data with micrometer measurements and concluded that ultrasounds can be useful to determine nail thickness. In our study, we used A-mode to estimate the nail plate thickness. The average thickness of the nail plate in the whole group ranged from 0.36 mm in nd5 to 0.43 mm in nd2. Estimated borderline values suggest that the thinnest nail plate was observed in female volunteers in nd5 (0.25 mm), and the thickest was observed in males in nd2 (0.54 mm). Similar results were obtained by Wollina et al. (22)—according to their analysis, the thickness of the nail plate ranged between 0.481 mm (right hand thumb) and 0.397 mm (fifth finger of the left hand).

We observed statistically significant correlations between finger type and the thickness of the nail plate (in both the dominant and non-dominant hand) in the whole group and taking gender into account ($p < 0.05$). The average thickness of the nail plate was lower the further the finger was from the thumb. We assume that those observations arise from the more frequent use of the radially located fingers in everyday activities. The greater exposure to mechanical stimuli requires more effective protection of the fingertips and hence the appearance of thicker nail plates in index fingers than in the little fingers.

In our study, gender-related differences between nail thickness were observed—men presented with thicker nail plates. Wollina et al. (22) also showed differences in nail and matrix volume, also with higher levels in the male.

The results of our study showed that there is no significant difference between NU in the dominant and non-dominant hand. However, we would rather suspect that the dominant hand, as being more exposed to external factors, would have showed a higher thickness of NUs as an adaptation to more frequent exposure to destructive environmental factors and help in manipulation. Ruan et al. (23), however, also did not obtain data, suggesting differences between mentioned NU.

In our study, we found inverse statistically significant correlation between the age and the thickness of the nail plate only in the d5 in the whole study group and in the group of

men ($r = -0.3$, $p = 0.027$; $r = -0.4$, $p = 0.043$, respectively), whereas there were no such observations in case of other fingers. Those correlations are most likely random statistical results. In general, in examined subjects with no evident onychopathy, there were no significant changes in nail thickness, which is commonly described in the elderly (24, 25).

TOWL

Although the TEWL measurement is a well-recognized parameter reflecting the function of the stratum corneum (SC), this measurement in relation to the entirely keratinized structure of the nail plate, known as TOWL, is still not fully understood. There are just single reports regarding TOWL measurement within healthy NU, which present different methodology (6, 16, 26).

We have made an attempt to analyze the value of TOWL, taking into account various variables. We did not observe the relations of TOWL to age and sex, and the value of TOWL did not differ between the right and the left hand. We found that the lowest measured TOWL value was recorded in the group of men in d1 (1.10 c.u.), and the highest value was also observed in the group of men in nd3 (17.60 c.u.). Statistically significant correlations were found between finger type and TOWL value in the whole group and taking into account gender ($p < 0.05$) except of the non-dominant hand in men. In general, the further from the thumb the NU is, the higher TOWL values are obtained. We suspect that these findings may be linked to a better adaptation to preserve water in thumb and index, because of their utility in everyday activities. The results obtained in male non-dominant hand should be considered as random statistical discovery.

We observed moderate statistically significant correlation between the age and TOWL value only in the male group in the d3 finger ($r = -0.5$, $p = 0.031$) and we did not gain any statistically significant differences in the TOWL values of the corresponding types of fingers between male and female NUs. Jemec et al. (6) also showed no differences in case of TOWL—gender relation, but suggested that with aging TOWL, value decreases. However, they published data based on examination of thumbs' TOWL of 21 healthy volunteers (12 female, nine male; 22–71 years, median 32). We presume that differences between sexes may be related to the thicker nail plates in men; however, this observation was not confirmed by our research. Also, age may act as a factor deteriorating the function of water resistance within the NUs, although obtained data (TOWL value of only one type of NUs in men inversely correlated with age) suggest that it could be a random statistical finding.

We did not observe any significant statistical differences between NUs of the dominant and non-dominant hand. However, our suspicion was that the dominant hand (being highly exposed to external factors) would show a difference, with higher TOWL values. Murdan et al. measured TOWL values in only three volunteers using an evaporimeter with a closed condensation chamber with a dedicated adapter and showed that there are differences in the TOWL values in the same person in the corresponding fingers of the left and right hand and the left and right foot. However, the authors did not define if the extremities were dominant or non-dominant (16).

Also, the study of Sattler et al. (27) faces limitations considering the number of analyzed NUs—only a middle finger of the dominant and non-dominant hand was examined. The number of participants was higher than in previously mentioned studies; however, the group of 30 volunteers would benefit from broadening. In their study the authors used an open-chamber evaporimeter with holding ring. The researchers did not observe statistically significant differences in the TOWL values of the middle finger of the dominant and non-dominant hand, as it was presented in our study.

An equipment is definitely an important factor influencing acquired results. According to The European Group on Efficacy Measurement and Evaluation of Cosmetics and other Products (EEMCO) guidance for TEWL (17), three different measurement methods may be applied: open-chamber methods, semiopen methods (open-chamber method with wind shield incorporated in probe), and closed-chamber methods. Open-chamber evaporimeters are still the preferred techniques to measure TEWL. However, because of their susceptibility to environmental factors, they have been supplemented with semiopen- and closed-chamber probes, which are more convenient to use and more applicable to field studies. Closed-chamber methods interfere with evaporation and cannot be used for continuous monitoring. The authors suggest that validation of methods with respect to intra- and inter-instrument variation is still a challenge (17). Still, no guidelines related to TOWL measurement exist.

Correlation Between HF-USG Results and TOWL Values

The results of previous studies based on assessment of correlation between nail plate thickness and water loss (measured using various methods) are inconclusive and based on small groups (6, 15, 16).

We found that thickness of the nail plate is not correlated with TOWL value in most cases. There was no statistically significant correlation between the TOWL value and the thickness of the nail plate measured with HF-USG in any of the tested NUs. A similar observation was also made by Jemec et al. (6); however, they assessed only thumbs. Moreover, Spruit (15) investigated the specific permeability of the nail plate to water. The thickness of all NUs was measured with a caliper in only one volunteer. The author concluded that in a healthy volunteer, the loss of water is independent of the thickness of the nail plate. On the other hand, different results, partially obtained *in vitro*, were presented by Murdan et al. They showed a relationship between TOWL value and plate thickness assessed by measuring cut nails with a micrometer (16).

According to previous research, TEWL is not affected by skin thickness (28). It is worth considering if, similarly, the water permeability of nail plates, either does not depend on the thickness of the SC. However, the differences in chemical composition may be the factor influencing permeability of SC in the skin (29). Is it true for the NU? More research is required. Certainly, it would be necessary

to continue research in this area with a larger number of NU.

CONCLUSIONS

To sum up, non-invasive methods, such as high-frequency ultrasonography and TEWL, enable assessment of the NU and are useful in examination of its structure and function. High-frequency ultrasonography shows characteristic elements of NU that can be distinguished because of differences in their echogenicity. The thickness of the nail plate and TEWL depend on the type of finger, and show a relationship with gender.

DATA AVAILABILITY STATEMENT

The raw data supporting the conclusions of this article will be made available by the authors, without undue reservation.

ETHICS STATEMENT

The studies involving human participants were reviewed and approved by Bioethical Commission. The patients/participants provided their written informed consent to participate in this study.

AUTHOR CONTRIBUTIONS

RŻ and ZA assistance in writing article and performing research. AL statistical analysis. DJ supervision over writing thesis and English style analysis. AD-P assistance in conducting and interpreting research and supervision over writing thesis. AP originator of the research, assistance in conducting and interpreting research, author of the text on a par with the MS-L and AP. MS-L performer of research and analysis and author of the text on a par with the AP. All authors contributed to the article and approved the submitted version.

REFERENCES

1. de Berker DA, André J, Baran R. Nail biology and nail science. *Int J Cosmet Sci.* (2007) 29:241–75. doi: 10.1111/j.1467-2494.2007.00372.x
2. Rich P. Nail cosmetics and esthetics. *Skin Pharmacol Appl Skin Physiol.* (1999) 12:144–5. doi: 10.1159/000029869
3. Belyayeva E, Gregoriou S, Chalikias J, Kontochristopoulos G, Koumantaki E, Makris M, et al. The impact of nail disorders on quality of life. *Eur J Dermatol.* (2013) 23:366–71. doi: 10.1684/ejd.2013.2048
4. Ruben BS. Pathology of the nail unit. *Dermatol Clin.* (2021) 39:319–36. doi: 10.1016/j.det.2020.12.009
5. Rigopoulos D, Rompoti N, Gregoriou S. Management of nail psoriasis. *Dermatol Clin.* (2021) 39:211–20. doi: 10.1016/j.det.2020.12.014
6. Jemec GB, Agner T, Serup J. Transonychial water loss: relation to sex, age and nail-plate thickness. *Br J Dermatol.* (1989) 121:443–6. doi: 10.1111/j.1365-2133.1989.tb15511.x
7. Agner T. Noninvasive measuring methods for the investigation of irritant patch test reactions. A study of patients with hand eczema, atopic dermatitis and controls. *Acta Derm Venereol Suppl (Stockh).* (1992) 173:1–26.
8. Polańska A, Dańczak-Pazdrowska A, Silny W, Jenerowicz D, Osmola-Mańkowska A, Olek-Hrab K. Evaluation of selected skin barrier functions in atopic dermatitis in relation to the disease severity and pruritus. *Postep Derm Alergol.* (2012) 29:373–77. doi: 10.5114/pdia.2012.31492
9. Alexander H, Brown S, Danby S, Flohr C. Research techniques made simple: transepidermal water loss measurement as a research tool. *J Invest Dermatol.* (2018) 138:2295–300.e1. doi: 10.1016/j.jid.2018.09.001
10. Jacobi O. Die Nägel des lebenden Menschen und die Perspiration insensibilis. *Arch. klin. exp. Derm.* (1962) 214:559–72. doi.org/10.1007/BF00483524
11. Wortsman X, Alfageme F, Roustan G, Arias-Santiago S, Martorell A, Catalano O, et al. Guidelines for performing dermatologic ultrasound examinations by the DERMUS group. *J Ultrasound Med.* (2016) 35:577–80. doi: 10.7863/ultra.15.06046
12. Wortsman X, Jemec GB. Ultrasound imaging of nails. *Dermatol Clin.* (2006) 24:323–8. doi: 10.1016/j.det.2006.03.014
13. Gutierrez M, Wortsman X, Filippucci E, De Angelis R, Filosa G, Grassi W. High-frequency sonography in the evaluation of psoriasis: nail and skin involvement. *J Ultrasound Med.* (2009) 2:1569–74. doi: 10.7863/jum.2009.28.11.1569
14. Essayed SMA, Al-Shatouri MA, Allah YSN, Atwa MA. Ultrasonographic characterization of the nails in patients with psoriasis and onychomycosis. *Egypt J Radiol Nuc Med.* (2015) 46:733–39. doi: 10.1016/j.ejrnm.2015.04.009
15. Spruit D. Measurement of water vapor loss through human nail *in vivo*. *J Invest Dermatol.* (1971) 56:359–61. doi: 10.1111/1523-1747
16. Murdan S, Hinsu D, Guimier M. A few aspects of transonychial water loss (TOWL): inter-individual, and intra-individual inter-finger, inter-hand and inter-day variabilities, and the influence of nail plate hydration, filing and varnish. *Eur J Pharm Biopharm.* (2008) 70:684–9. doi: 10.1016/j.ejpb.2008.05.018
17. Berardesca E, Loden M, Serup J, Masson P, Rodrigues LM. The revised EEMCO guidance for the *in vivo* measurement of water in the skin. *Skin Res Technol.* (2018) 24:351–8. doi: 10.1111/srt.12599
18. Marina ME, Solomon C, Bolboaca SD, Bocsa C, Mihu CM, Tătaru AD. High-frequency sonography in the evaluation of nail psoriasis. *Med Ultrason.* (2016) 18:312–7. doi: 10.11152/mu.2013.2066.183.hgh
19. Idolazzi L, Gisondi P, Fassio A, Viapiana O, Giollo A, Rossini M, et al. Ultrasonography of the nail unit reveals quantitative and qualitative alterations in patients with psoriasis and psoriatic arthritis. *Med Ultrason.* (2018) 20:177–84. doi: 10.11152/mu-1327
20. Naredo E, Janta I, Baniandrés-Rodríguez O, Valor L, Hinojosa M, Bello N, et al. To what extend is nail ultrasound discriminative between psoriasis, psoriatic arthritis and healthy subjects? *Rheumatol Int.* (2019) 39:697–705. doi: 10.1007/s00296-018-4222-y
21. Finlay A, Moseley H, Duggan TC. Ultrasound transmission time: an *in vivo* guide to nail thickness. *Br J Dermatol.* (1987) 117:765–70. doi: 10.1111/j.1365-2133.1987.tb07358.x
22. Wollina U, Berger M, Karte K. Calculation of nail plate and nail matrix parameters by 20 MHz ultrasound in healthy volunteers and patients with skin disease. *Skin Res Technol.* (2001) 7:60–4. doi: 10.1034/j.1600-0846.2001.007001060.x
23. Ruan J, Wang XM, Xia MN. The evaluation of nail heath conditions with skin ultrasound. *Cutan Ocul Toxicol.* (2012) 31:318–22. doi: 10.3109/15569527.2011.645099
24. Abdullah L, Abbas O. Common nail changes and disorders in older people: diagnosis and management. *Can Fam Physician.* (2011) 57:173–81.
25. Baran R. The nail in the elderly. *Clin Dermatol.* (2011) 29:54–60. doi: 10.1016/j.clindermatol.2010.07.008
26. Krönauer C, Gfesser M, Ring J, Abeck D. Transonychial water loss in healthy and diseased nails. *Acta Derm Venereol.* (2001) 81:175–7. doi: 10.1080/000155501750376249
27. Sattler EC, Poloczek K, Kästle R, Welzel J. Confocal laser scanning microscopy and optical coherence tomography for the evaluation of the kinetics and quantification of wound healing after fractional laser therapy. *J Am Acad Dermatol.* (2013) 69:e165–73. doi: 10.1016/j.jaad.2013.04.052
28. Elias PM, Cooper ER, Korc A, Brown BE. Percutaneous transport in relation to stratum corneum structure and lipid composition. *J Invest Dermatol.* (1981) 76:297–301. doi: 10.1111/1523-1747.ep12526137

29. Hattingh J. The correlation between transepidermal water loss and the thickness of epidermal components. *Comp Biochem Physiol A Comp Physiol.* (1972) 43:719–22. doi: 10.1016/0300-9629(72)90140-5

Conflict of Interest: The authors declare that the research was conducted in the absence of any commercial or financial relationships that could be construed as a potential conflict of interest.

frontiers in Medicine

ORIGINAL RESEARCH
published: 22 June 2021
doi: 10.3389/fmed.2021.648233

IMPROVE 1.0: Individual Monitoring of Psoriasis Activity by Regular Online App Questionnaires and Outpatient Visits

Natalie Garzorz-Stark[1,2*†], *Sarah Beicht*[1†], *Veronika Baghin*[1], *Sebastian P. Stark*[1], *Tilo Biedermann*[1] *and Felix Lauffer*[1]

[1] *Department of Dermatology and Allergy, Technical University of Munich, Munich, Germany,* [2] *Division of Dermatology and Venereology, Department of Medicine Solna, Center for Molecular Medicine, Karolinska Institutet, Stockholm, Sweden*

Smartphone apps gain more and more importance in supporting management of chronic diseases. Psoriasis is a highly prevalent, lifelong chronic inflammatory skin disease with a high impact on patient's quality of life. Disease management includes regular topical and systemic treatment of skin lesions as well as co-treatment of metabolic and psychologic disorders. In this study, we investigated the potential of a new smartphone app (IMPROVE 1.0) for individual monitoring of disease activity and disease influencing factors. Twelve out of 50 psoriasis patients asked for study participation performed self-assessment of psoriasis severity, life quality, and stress scores using the app over a period of 1 year. Every 2 months, study participants were carefully examined by a dermatologist in order to control the quality of app-reported data. We found that psoriasis severity and life quality values as entered in the app closely correlate to physician's examination. Furthermore, we detected strong correlations of disease activity with life quality and psoriasis serum biomarker. Temporal relations between psoriasis aggravation and previous changes of lifestyle factors, such as increased stress levels, were observed in individual patients, indicating a high potential for preventive interventions in future psoriasis apps. The vast majority of study participants evaluated IMPROVE 1.0 app positively and wish to include the app into their daily life. Hence, we demonstrate that smartphone apps are a useful tool to raise self-awareness for the dimensions of complex diseases and fully integrate psoriasis patients into individual disease management. These data are important to develop more advanced digital tools supporting the management of chronic diseases in the future.

Keywords: smartphone, application, psoriasis, inflammatory skin disease, personalized medicine

OPEN ACCESS

Edited by:
Paola Pasquali,
Pius Hospital de Valls, Spain

Reviewed by:
Lara Ferrándiz,
Hospital Universitario Virgen Macarena, Spain
María-Elena De Las Heras-Alonso,
Ramón y Cajal University Hospital, Spain

****Correspondence:***
Natalie Garzorz-Stark
natalie.garzorz@tum.de

[†] These authors have contributed equally to this work

Specialty section:
This article was submitted to Dermatology, a section of the journal Frontiers in Medicine

Received: *31 December 2020*
Accepted: *29 March 2021*
Published: *22 June 2021*

Citation:
Garzorz-Stark N, Beicht S, Baghin V, Stark SP, Biedermann T and Lauffer F (2021) IMPROVE 1.0: Individual Monitoring of Psoriasis Activity by Regular Online App Questionnaires and Outpatient Visits. Front. Med. 8:648233. doi: 10.3389/fmed.2021.648233

INTRODUCTION

Smartphone apps play an increasingly important part in daily life. They are easily accessible, are handy, and facilitate access to information, communication, or management of routine tasks such as banking. As health care systems are limited by financial restrictions and personal capacities, smartphone apps might more and more support or take over routine physician's work. Several digital health tools have been developed over the last decade (1). While a plethora of smartphone

apps are created for patient education and mainly deliver information in a more convenient way (2, 3), the major restriction of more advanced apps is the lack of objective measurement tools to perform long-term disease monitoring. Therefore, many apps are linked to a conventional medical device in order to assess, for example, blood pressure, blood glucose, or overall healthy lifestyle in a prospective way (4, 5). However, to establish an app in a larger cohort of patients, all essential tools must be executable by the patients themselves without any further technical devices. For this purpose, inflammatory skin diseases (ISD) are an ideal disease model, as disease activity is usually assessed by morphological scores, such as the psoriasis area and severity index (PASI).

Psoriasis is one of the most common ISD, which affects up to 3% of the general population in western countries (6). Patient's life quality if critically diminished by visible and stigmatizing plaques of inflamed skin, itch, scaling, and comorbidities (7, 8). In the latter case, the metabolic syndrome, addictive diseases, and psychological disorders are the major causes of morbidity and mortality (7). However, obesity or distress can—vice versa—also impair psoriasis severity (9). Therefore, psoriasis patients need a disease management considering individual disease and lifestyle factors (10)—a comprehensive approach that might profit from digital support by a smartphone app. However, it is so far unknown if patients are capable to reliably judge psoriasis severity and reflect about comorbidities using an app and if they appreciate a digital tool for their individual disease management.

To test whether apps are useful to monitor psoriasis disease activity, we created a new app (IMPROVE 1.0) and asked psoriasis patients to regularly enter self-PASI, life quality, and stress questionnaires as well as lifestyle factors over a period of 12 months. In a prospective study, we compared data collected by the app with physician's examination, with disease scoring performed by dermatologists and biomarkers. Furthermore, we collected patients' feedback on utility and helpfulness of IMPROVE 1.0 in order to gain further insight into the potential of a psoriasis app in clinical practice.

METHODS

Study Cohort

Fifty adult patients (age $\geq$ 18 years) with histologically confirmed diagnosis of psoriasis regularly seen at our outpatient clinic who used a smartphone and had experience with smartphone apps were asked to participate in the study. Reasons for not participating were lack of time and/or no smartphone with Android system (app only programmed for Android system) at patient's disposal. Thirteen of these patients were enrolled, and 12 of the enrolled patients completed the 48-week study. One patient did not continue the study after the first outpatient visit for personal reasons. Patients were given an introduction of the app and every 2 weeks $\pm$ 1 week; they filled in the smartphone app questionnaire assessing disease severity and lifestyle factors (see below). Lifestyle factors and their potentially aggravating effect on psoriasis were explained at the beginning of the study to each patient but no intervention with regard to lifestyle factors was initiated. Every 8 $\pm$ 2 weeks, patients were examined by a physician during an outpatient visit. Moreover, blood samples were taken at each visit and analyzed for serum markers and blood count (see **Figure 1A**). At the end of the study, patients completed a final evaluation questionnaire on the app and the study. The study was approved by the Ethics Committee of the Faculty of Medicine of the Technical University of Munich (63/16S) and written informed consent was obtained from the patients.

Smartphone App Improve 1.0

The app was programmed using Eclipse for androids, an IDE for developers creating Android applications (http://www.eclipse.org). The app was sent to the patient *via* e-mail and downloaded by the patient. An introduction to the app was given by the study team. The app consisted of the DLQI questionnaire to measure the quality of life (11), the PSS questionnaire to measure the perception of stress (12), and of questions on their lifestyle (consumption of alcohol, cigarettes, and fast food; frequency of doing sports; body weight; and sleep), which were assessed on a verbal rating scale that was converted to a numeric rating scale for analysis (0–4, except for the amount of cigarettes 0–5). Besides, the patients assessed the severity of psoriasis according to the simplified PASI (SPASI) (13). The area of involvement (area score) was assessed on a 0–6 scale [0: no lesions, 1: $\leq$10 palms of the hand (PTH), 2: $\leq$30 PTH, 3: $\leq$50 PTH, 4: $\leq$70 PTH, 5: $\leq$90 PTH, and 6: complete body affected]. The average redness (R), thickness (T), and scaliness (S) of the lesions were assessed using a verbal rating scale that was converted to a numeric rating scale for analysis (0–4 scale). To facilitate this assessment, each scale point was visualized by a representative picture of the severity (see **Figure 1B**). SPASI was calculated as follows: SPASI = Area score $\times$ (R + T + S).

Blood Parameters

Blood counts (leukocytes, lymphocytes, neutrophils, eosinophils, basophils, and monocytes) and serum proteins (Cortisol, C3, C4, IgA, CRP, HbA1c, cholesterol, triglycerides, and LDL) were assessed by clinical routine laboratory. ELISA for human squamous cell carcinoma antigen 2 (SCCA2; PeproTech, Germany) and Beta-defensin-2 protein (HBD2; MyBioSource, CA, USA) were performed according to the manufacturer's instructions.

Statistical Analysis

Statistical analysis was performed using GraphPad Prism 7.00 Software (GraphPad Software, La Jolla, CA). Two-tailed paired sample test was used to compare variables of two different time points (beginning vs. end of the study) or of two different evaluators (mean PASI or DLQI as assessed by the physician vs. mean SPASI or DLQI as assessed by the patient *via* app) within individuals. Variables were correlated using Pearson correlation. Average Pearson coefficients across patients were obtained by transforming each correlation coefficient using Fisher's z, calculation of the mean of the z values, and back-transformation of the mean z value to the mean correlation coefficient. Parameters of outpatient visits were correlated with parameters assessed by the app if data of both visits and app were

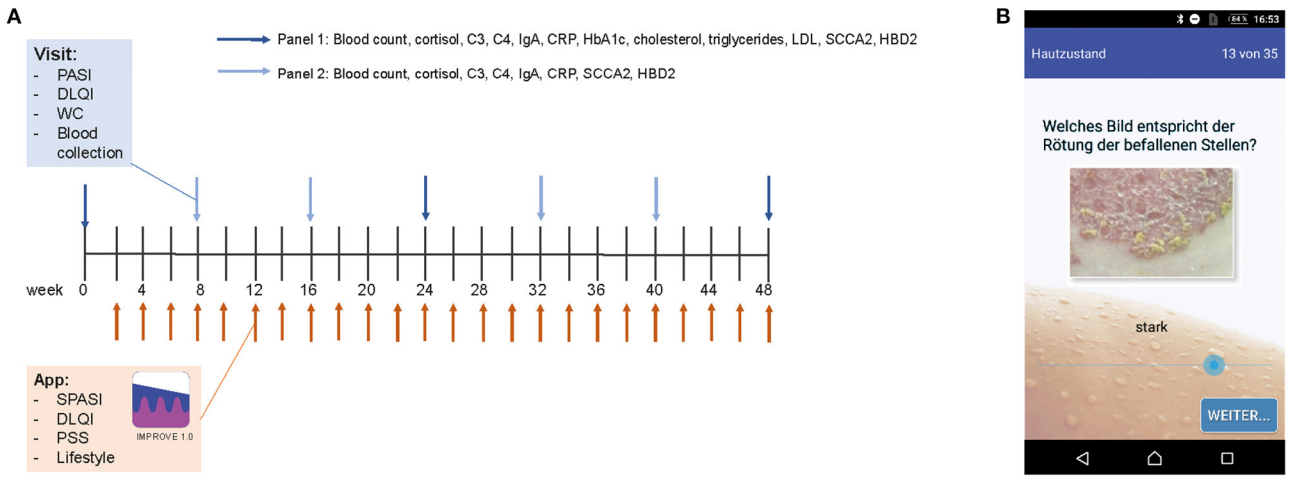

FIGURE 1 | Study design and app. PASI, DLQI, and waist circumference (WC) of psoriasis patients were assessed every 8 weeks. Besides, blood was taken and examined for blood counts and serum parameters (Panel 1 at visits 2, 3, 5, and 6 and Panel 2 at visits 1, 4, and 7) **(A)**. Biweekly, patients filled out an app questionnaire including SPASI, DLQI, PSS, and questions on lifestyle factors. Assessment of disease severity was supported visually by example pictures of psoriasis for redness, thickness, and scaling (here exemplarily shown for redness) **(B)**.

available from the same week. Correlation matrix was built using the agglomerative clustering tool within the scikit-learn package of Python 0.23.2 (https://scikit-learn.org/stable/). Mean values are shown with standard error of the mean (SEM).

RESULTS

Design of the Study and Characterization of the Study Cohort

Twelve psoriasis patients completed the 48-week study consisting of biweekly online smartphone app questionnaires and clinical outpatient visits every 8 weeks including clinical examination and blood tests (see **Figures 1A,B**). Details on the study cohort are listed in **Table 1**. Within the study cohort, the mean age of patients was 43.25 ± 4.11 years and 67.7% of the participants were male. Mean age of onset of psoriasis was 20.92 ± 3.77 years, and PASI at the time of the individual start with the study (week 0) was 7.37 ± 1.79. Fifty percent of participants were smoker, mean BMI at week 0 was 28.38 ± 1.68, and 8 out of 12 patients suffered from comorbidities such as type 2 diabetes and obesity.

App-Reported PASI and DLQI Correlate Closely to Physician's Objective Assessment

To assess if patients' reported disease activity would be in line with the physician's objective scoring of disease activity, curves for both SPASI as reported *via* app and PASI as determined by the physician during the outpatient visits were plotted together and are exemplarily shown for two patients (**Figures 2A,B**). Indeed, both curves showed a similar course (**Figures 2A,B**; other patients, **Supplementary Figure 1**) and mean PASI and SPASI did not significantly differ ($p = 0.2409$): Eight out of the 12 patients evaluated their PASI lower as the physician did, as shown by the mean over all PASI and SPASI values, respectively, over the course of the study (**Figure 2C**). However, SPASI and PASI values over all patients showed significant correlation ($r = 0.75$, $p < 0.0001$, **Figure 2D**). We next sought to compare DLQI as determined *via* app ($DLQI_{app}$) with DLQI values given by the patient during the outpatient visit ($DLQI_{visit}$). Also, here, both curves showed high accordance (**Figures E,F**; other patients, **Supplementary Figure 2**) and DLQI determined during visits and *via* app did not significantly differ ($p = 0.27$): 7 out of 12 patients reported lower quality of life *via* app than during outpatient visits as shown by the mean of all $DLQI_{app}$ and $DLQI_{visit}$ values, respectively, during the study (**Figure 2G**). Also, for DLQI, high correlation of $DLQI_{app}$ and $DLQI_{visit}$ over all patients could be found ($r = 0.997$, $p < 0.0001$, **Figure 2E**).

DLQI and HBD2 Correlate With Disease Activity, While Stress Shows Individual Temporal Correlation With PASI

To next assess factors correlating with PASI and SPASI on individual patient level but also across patients, we correlated PASI with serum parameters and $DLQI_{visit}$. Besides, SPASI was correlated with $DLQI_{app}$, BMI, stress, and lifestyle factors (see **Figures 3A,B**). Across all patients, PASI (SPASI) showed a mean correlation coefficient of 0.65 (0.64) with $DLQI_{visit}$ ($DLQI_{app}$). Moreover, human beta defensin 2 (HBD2), a previously described serum marker for psoriasis disease severity, showed the highest correlation coefficient among all measured blood parameters with disease activity ($r = 0.56$), which objectively confirmed correct assessment of PASI and SPASI in our cohort. Percentage of basophil granulocytes and levels of HbA1c showed a trend toward negative correlation with PASI.

TABLE 1 | Clinical characteristics of the patients included in the study.

Patient (no.)	Sex	Age	Psoriasis therapy (week of study: 0–48)	Comorbidities	Age of onset of psoriasis	Course of disease	Smoker	PASI at week 0	BMI at week 0
1	M	33	Secukinumab (0–56)	Overweight	20	Stable with no symptom-free intervals	No	0.5	28.4
2	F	54	Methotrexate (0–23), none (23–37), topical glucocorticosteroids (37–48)	Type 2 diabetes, obesity, COPD, hypothyroidism, myocardial infarction at age 49	20	Progression	No (until age 49)	18	38.3
3	M	26	Ustekinumab (0–47)		0	Progression	No	10.7	25.9
4	F	42	Secukinumab (0–42), ixekizumab (42–48)	Obesity	20	Stable with no symptom-free intervals	No	3.6	29.7
5	F	27	Methotrexate (36–48), topical glucocorticosteroids (0–48)	Atopic dermatitis, allergic rhinoconjunctivitis	9	Progression	Yes	0.9	23.9
6	M	36	Fumaric acid (0–31), methotrexate (31–48)	Allergic rhinoconjunctivitis, migraine, arterial hypertension, overweight	33	Progression	No	12.6	29.8
7	M	32	Fumaric acid (0–4), topical glucocorticosteroids (0–52)		31	Progression	Yes	10.2	22.8
8	F	56	Topical glucocorticosteroids (0–4)		4	No symptoms age 12–35, thereafter progression	No	16	20.9
9	M	57	Secukinumab (0–44)	Obesity, prediabetes	36	Stable with symptom-free interval at age 52–57 years	Yes	1	30.7
10	M	45	Methotrexate (0–18 and 31–48)	Obesity, prediabetes	43	Progression	Yes	6.8	38.5
11	M	73	Fumaric acid (0–4), apremilast (4–23), secukinumab (23–48)	Type 2 diabetes, obesity	21	Stable with symptom-free interval at age 21–56 years	Yes	1.2	30
12	M	38	Apremilast (0–48)		14	Stable with no symptom-free intervals	Yes	6.9	21.67

Interestingly, none of the lifestyle factors such as sleep, smoking, and consumption of fruits or vegetables correlated with SPASI across all patients. Instead, correlations on individual patient level between PASI and assessed parameters could be found (**Figures 3A,B** and **Supplementary Figures 3A,B**): For example, in patient 2, waist circumference (WC) and BMI significantly correlated with PASI and SPASI, respectively, whereas in patients 5 and 8, inflammatory activity is reflected on serum level by positive correlations between PASI and levels of leukocytes and neutrophils in the blood. In patient 3, e.g., amount of night sleep negatively correlated with SPASI. As stress has been discussed as a potential aggravator of psoriasis disease activity (14, 15), we next sought to investigate the influence of stress on PASI, SPASI, cortisol levels, and DLQI. Exemplarily shown for patient 12, a significant correlation between SPASI and $DLQI_{app}$ ($r = 0.91, p < 0.0001$) and also for PASI and $DLQI_{visit}$ ($r = 0.85, p < 0.015$) was found. No correlation of PASI with cortisol levels was observed; however, a trend for weak correlation with stress as measured by the PSS ($r = 0.39, p = 0.077$, **Figure 3C**) was observed, indicating that decrease of stress levels was timely accompanied by decrease in disease activity. In patient 10, however, one may come up with the hypothesis that rising cortisol and PSS levels preceded the increase of PASI (**Figure 3D**). Indeed, when shifting cortisol and PSS curves 20 weeks ahead, correlation values between SPASI and PSS increased from $r = 0.3$ and $p = 0.07$ to $r = 0.7$ and $p = 0.0004$ (**Figure 3E**). Increase in cortisol and PSS may also follow increasing PASI, as exemplified in patient 2 (**Figure 3F**): Indeed, when shifting both cortisol and PSS curves 10 weeks back, correlation values, though not at significant level, become positive for PSS and SPASI (PASI and cortisol) from $r = -0.34$ and $p = 0.23$ to $r = 0.23$ and $p = 0.6$ (from $r = -0.54, p = 0.2146$ to $r = 0.72, p = 0.1671$) (**Figure 3G**). Interestingly, PSS did not correlate with DLQI ($r = 0.12$) and cortisol levels ($r = -0.31$) across all patients (see **Supplementary Figure 3C**).

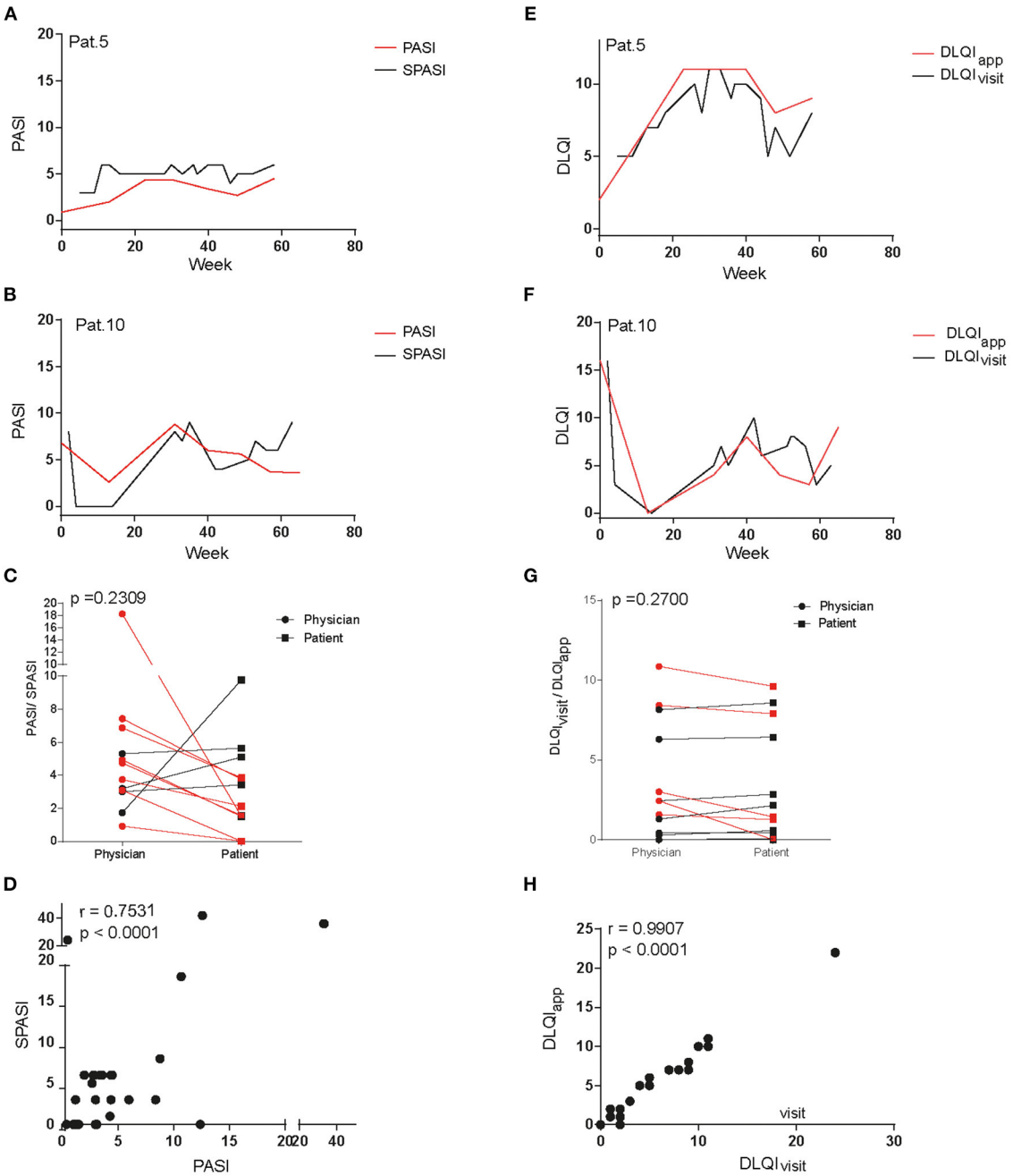

FIGURE 2 | Comparison of dermatology life quality index and disease severity assessed at outpatient visits and *via* app questionnaire. Curves of PASI and SPASI take a similar course as exemplarily shown for patients 5 **(A)** and 10 **(B)**. Comparison of mean PASI values as measured by physicians and mean SPASI values as measured by patients during the course of the study show no difference on patient level **(C)**. SPASI and PASI across patients show high correlation **(D)**. Also, curves of $DLQI_{app}$ and $DLQI_{visit}$ take a similar course in patients 5 **(E)** and 10 **(F)**. Mean $DLQI_{visit}$ values as stated during outpatient visits and mean $DLQI_{app}$ values as determined via app during the course of the study do not differ on patient level **(G)**. $DLQI_{app}$ and $DLQI_{visit}$ across patients show high correlation **(H)**.

Patients Reported Benefits of the Smartphone App

At the end of the study, patients were asked to evaluate the study regarding the skin condition, the study design and the app. More than 80% of the participants considered the study to have had a beneficial effect on their skin lesions (**Figure 4**); in particular, the individual care was highly appreciated. Indeed, PASI significantly decreased across all patients (7.37 ± 1.78 at the beginning of the study vs. 2.58 ± 0.45 at the end of the study, $p = 0.0249$, **Supplementary Figure 4A**). Only 3 out of 12 patients dealt more intensively with the disease by filling out the app questionnaire. This is reflected by the fact that none

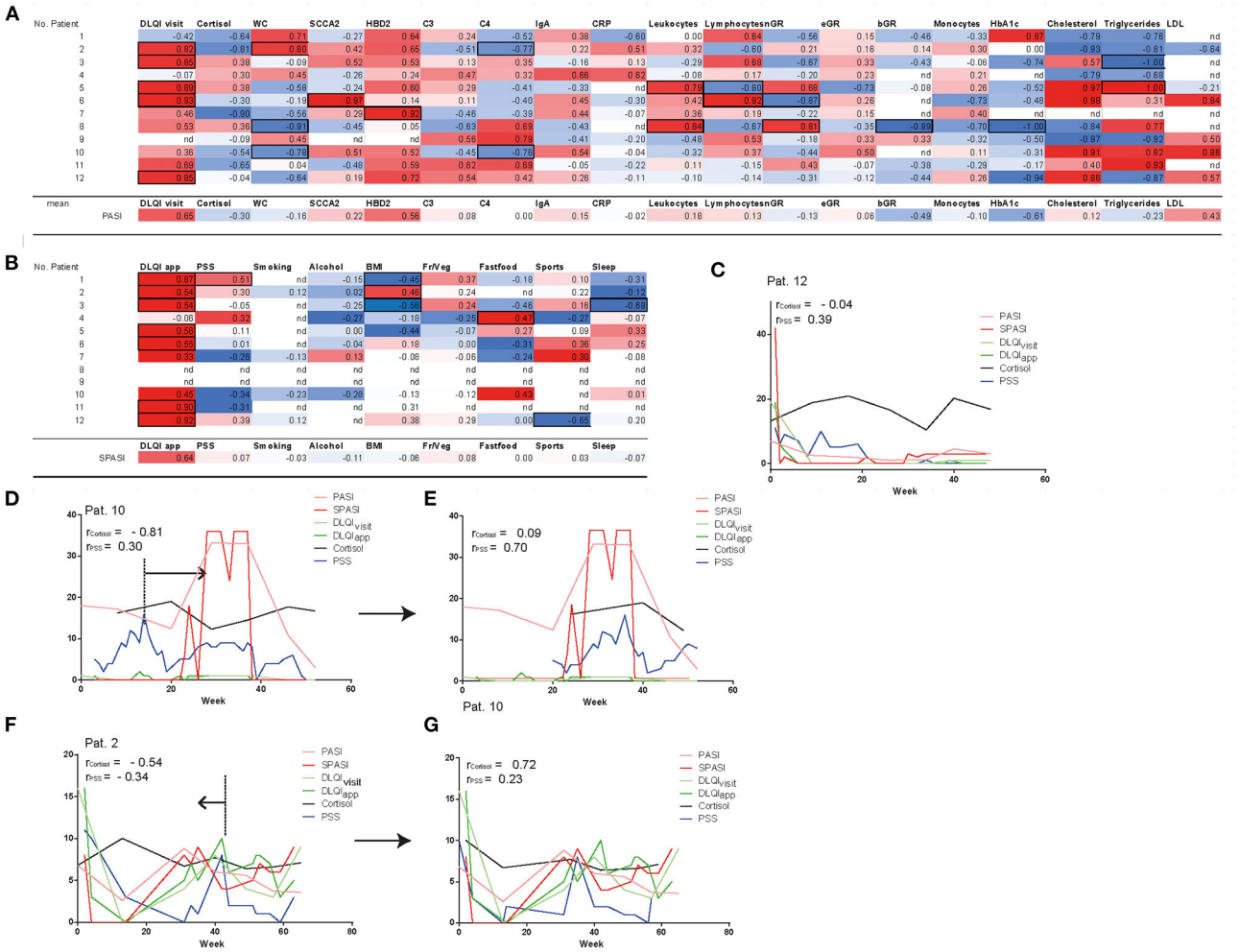

FIGURE 3 | Correlation of disease severity with parameters assessed at outpatient visits and *via* app. PASI shows correlation with $DLQI_{visit}$ and HBD2 **(A)**, SPASI with $DLQI_{app}$ **(B)**. Significance of parameters ($p < 0.01$) on patient level are shown in black frames. Besides, mean correlation coefficients of all patients are shown for each parameter with PASI/SPASI. Nd = no correlation could be calculated. Fr/Veg = consumption of fruits and vegetables. Curves of cortisol, PSS, $DLQI_{visit}$, $DLQI_{app}$, PASI, and SPASI are exemplarily shown in patient 12 **(C)**, patient 10 **(D,E)**, and patient 2 **(F,G)** and reveal temporal correlation of stress and PASI. In patients 10 and 2, curves of PSS and cortisol are timely shifted **(E,G)** to reveal PSS and cortisol as factors temporally preceding **(D)** or succeeding **(F)** increase of PASI. nGR, neutrophils, eGR, eosinophils; bGR, basophils; Fr/Veg, consumption of fruits and vegetables.

of the lifestyle factors (BMI, sports, consumption of fruits and vegetables, alcohol, and smoking) showed significant differences at the beginning of the study as compared to the end of the study (**Supplementary Figures 4B–F**). In contrast, consumption of fast food even increased ($p = 0.0281$). Fifty percent of patients would appreciate an updated version of the app supplemented with a lifestyle manager to achieve individual lifestyle goals.

DISCUSSION

In this study, we investigated the potential of a new smartphone app for assessment of psoriasis severity, life quality, and lifestyle factors. We found that patient reported disease severity (SPASI) using the app closely resembles PASI scoring performed by a dermatologist. Furthermore, we demonstrate that both PASI and SPASI significantly correlate to life quality (DLQI) and the well-established serum biomarker HBD2 (16). More than 80% of study participants gave a positive evaluation of the smartphone app, and mean PASI values significantly decreased during the entire course of the study.

Psoriasis is a lifelong inflammatory disease, which requires a comprehensive therapeutic concept. Patients need to be treated by several medical disciplines, for example, dermatologists primarily evaluating skin lesions or general physicians caring about metabolic disorders. Often, interdisciplinary communication, if any, relies on written reports and intuitively every physician involved mainly focuses on his own specialty, a situation that can be ineffective and time-consuming for both patients and physicians. Often, there is an active–passive relationship between health care professionals and patients, with patients being in a passive and inanimate role (17). Here, a smartphone app used by the patients would help to bring the patient back into the center of disease management as it was already shown for, e.g., neurological disorders (18). Regular

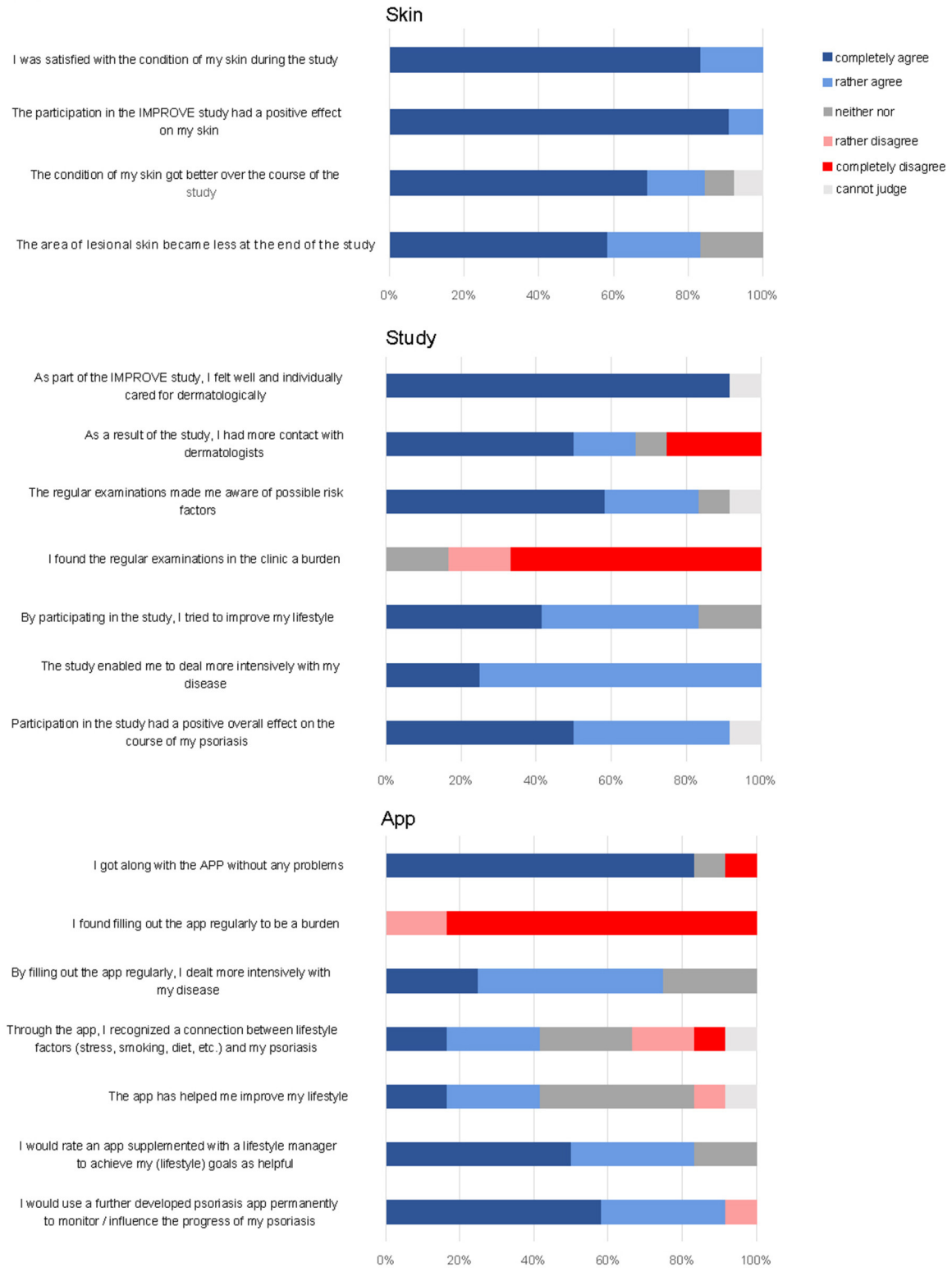

FIGURE 4 | Final questionnaire at the end of the study on skin, study design, and app. Shown are patients' responses in percent on a verbal rating scale.

assessment of the disease activity by the patients and easy display of disease course and disease-related factors *via* the app would clearly facilitate doctor–patient communication. Saving time of a detailed medical history allows more time for individual medical consultation. Furthermore, a structured evaluation of all disease-related factors in a smartphone app raises awareness and reflection about disease dimensions for health care professionals of different disciplines and patients.

Several apps supporting patients with chronic diseases or cancer have already been developed (19–21). In case of psoriasis in two randomized controlled trials, Sevendsen et al. demonstrated that a smartphone app improved patients' adherence to topical treatment and Spencer et al. showed that psoriasis patients learned more about their disease when using an app than a control group without digital support (22, 23). In contrast to these studies, IMPROVE 1.0 aims at not only facing one aspect of psoriasis, but on monitoring all disease-related factors. We did not choose a randomized, placebo-controlled study design, as the primary aim of the study was to compare data reliability between app and physician's examination in the same cohort of patients. Here, we could prove that data collected by the app, such as SPASI, correlate well to physician's scoring. Based on these findings, the next step of development will be to integrate more app functions. While PASI values decreased significantly during the study period, there was no change of lifestyle factors in our cohort, since no intervention for modulation of possibly aggravating lifestyle factors was initiated. However, we observed in individual patients that a change in BMI or stress level during the 12-month observation period was followed by an increase of PASI, indicating that our app can detect lifestyle changes preceding a shift in PASI. Thus, a valuable feature of an updated app version (IMPROVE 2.0) would be an implementation of an "alert system" drawing patient's attention to increasing stress levels or weight gain to optimize both psoriasis treatment and lifestyle to prevent an acute flare. Given that IMPROVE 2.0 is able to not only monitor psoriasis severity but also serve as an individualized feedback system for each patient, positive effects on psoriasis and overall healthy way of life can be expected and investigated by future randomized, controlled trials.

Our study has some limitations. First, we investigated only a limited cohort of patients in a proof-of-concept approach. Due to the small study cohort, a more advanced data analysis including robust statistical tests for significance of factors influencing future PASI changes was not possible. Second, IMPROVE 1.0 was only compatible to Android smartphones and many psoriasis patients were unwilling to participate due to technical difficulties in handling a smartphone app in general. Though both might lead to a selection bias, these observations are important to estimate psoriasis patients' willingness to use digital tools in real life and demonstrate that an app can only support a subgroup of patients with technical affinity. Furthermore, improvement of PASI scores during study participation must be interpreted with caution as they might be influenced by frequent physician consultation based on the study design. Despite these limitations, the strength of our study is that patients were followed up closely in a prospective manner over a period of 12 months. By comparing app performance to the current gold standard, namely, dermatologist's examination and collecting patient's feedback, this study proves that smartphone apps can be an important future component of a comprehensive therapeutic approach.

In summary, we demonstrated that a smartphone app is a valuable and reliable tool to assess disease activity, life quality, and potential influencing factors in psoriasis patients. This tool can markedly improve doctor–patient communication, facilitate interdisciplinary collaboration, and, most importantly, assign the patients an active role in disease management. Of note, we assessed temporal interrelations between PASI increase and lifestyle factors in individual patients. This points toward a high value of automated feedback loops—for example, by virtual disease managers helping patients to control individual risk factors—to improve disease activity in a future IMPROVE 2.0 app. These data are essential for the future implementation of digital tools in clinical routine care of complex, inflammatory diseases.

DATA AVAILABILITY STATEMENT

The original contributions presented in the study are included in the article/**Supplementary Material**, further inquiries can be directed to the corresponding author/s.

ETHICS STATEMENT

The studies involving human participants were reviewed and approved by the Ethics Committee of the Faculty of Medicine of the Technical University of Munich (63/16S). The patients/participants provided their written informed consent to participate in this study.

AUTHOR CONTRIBUTIONS

NG-S and FL designed the study and wrote the paper. NG-S, SB, VB, and FL generated the data. NG-S and SB analyzed the data. SS programmed the app. TB revised the manuscript. All authors contributed to the article and approved the submitted version.

FUNDING

The authors declare that this study received funding the Deutscher Psoriasis Bund e.V. Selbsthilfe bei Schuppenflechte, Hamburg, with funding of Biogen GmbH. Biogen GmbH was not involved in the study design, collection, analysis, interpretation of data, the writing of this article, or the decision to submit it for publication.

ACKNOWLEDGMENTS

The authors thank Jana Sänger for excellent technical assistance.

SUPPLEMENTARY MATERIAL

The Supplementary Material for this article can be found online at: https://www.frontiersin.org/articles/10.3389/fmed.2021.648233/full#supplementary-material

REFERENCES

1. King ALS, Padua MK, Goncalves LL, Santana de Souza Martins A, Nardi AE. Smartphone use by health professionals: a review. *Digit Health.* (2020) 6:2055207620966860. doi: 10.1177/2055207620966860
2. Wilson R, Cochrane D, Mihailidis A, Small J. Mobile apps to support caregiver-resident communication in long-term care: systematic search and content analysis. *JMIR Aging.* (2020) 3:e17136. doi: 10.2196/17136
3. Staiger PK, O'Donnell R, Liknaitzky P, Bush R, Milward J. Mobile apps to reduce tobacco, alcohol, and illicit drug use: systematic review of the first decade. *J Med Internet Res.* (2020) 22:e17156. doi: 10.2196/17156
4. Dörr M, Weber S, Birkemeyer R, Leonardi L, Winterhalder C, Raichle CJ, et al. iPhone app compared with standard blood pressure measurement -The iPARR trial: the iPARR trial. *Am Heart J.* (2021) 233:102–8. doi: 10.1016/j.ahj.2020.12.003
5. Kriventsov S, Lindsey A, Hayeri A. The diabits app for smartphone-assisted predictive monitoring of glycemia in patients with diabetes: retrospective observational study. *JMIR Diabetes.* (2020) 5:e18660. doi: 10.2196/18660
6. Boehncke WH, Schon MP. Psoriasis. *Lancet.* (2015) 386:983–94. doi: 10.1016/S0140-6736(14)61909-7
7. Dalgard FJ, Gieler U, Tomas-Aragones L, Lien L, Poot F, Jemec GB, et al. The psychological burden of skin diseases: a cross-sectional multicenter study among dermatological out-patients in 13 European countries. *J Invest Dermatol.* (2015) 135:984–91. doi: 10.1038/jid.2014.530
8. Zink A, Herrmann M, Fischer T, Lauffer F, Garzorz-Stark N, Bohner A, et al. Addiction: an underestimated problem in psoriasis health care. Journal of the European Academy of Dermatology and Venereology. *JEADV.* (2017) 31:1308-15. doi: 10.1111/jdv.14204
9. Kamiya K, Kishimoto M, Sugai J, Komine M, Ohtsuki M. Risk factors for the development of psoriasis. *Int J Mol Sci.* (2019) 20:4347. doi: 10.3390/ijms20184347
10. Nast A, Erdmann R, Pathirana D, Rzany B. Translating psoriasis treatment guidelines into clinical practice—the need for educational interventions and strategies for broad dissemination. *J Eval Clin Pract.* (2008) 14:803–6. doi: 10.1111/j.1365-2753.2008.00971.x
11. Finlay AY, Khan GK. Dermatology life quality index (DLQI)–a simple practical measure for routine clinical use. *Clin Exp Dermatol.* (1994) 19:210–6. doi: 10.1111/j.1365-2230.1994.tb01167.x
12. Cohen S, Kamarck T, Mermelstein R. A global measure of perceived stress. *J Health Soc Behav.* (1983) 24:385–96. doi: 10.2307/2136404
13. Louden BA, Pearce DJ, Lang W, Feldman SR. A simplified psoriasis area severity index (SPASI) for rating psoriasis severity in clinic patients. *Dermatol Online J.* (2004) 10:7.
14. Mueller SM, Itin PH, Navarini AA, Goldust M, Brandt O, Griffiths CEM, et al. The relationship between PASI and DLQI with itch, stress, and depression: do we need additional decision-making tools in psoriasis? *Dermatolo Ther.* (2020) 33:e13276. doi: 10.1111/dth.13276
15. Kwan Z, Bong YB, Tan LL, Lim SX, Yong ASW, Ch'ng CC, et al. Determinants of quality of life and psychological status in adults with psoriasis. *Arch Dermatol Res.* (2018) 310:443–51. doi: 10.1007/s00403-018-1832-x
16. Jansen PA, Rodijk-Olthuis D, Hollox EJ, Kamsteeg M, Tjabringa GS, de Jongh GJ, et al. Beta-defensin-2 protein is a serum biomarker for disease activity in psoriasis and reaches biologically relevant concentrations in lesional skin. *PLoS ONE.* (2009) 4:e4725. doi: 10.1371/journal.pone.0004725
17. Chipidza FE, Wallwork RS, Stern TA. Impact of the doctor-patient relationship. *Prim Care Companion CNS Disord.* (2015) 17. doi: 10.4088/PCC.15f01840
18. Winberg C, Kylberg M, Pettersson C, Harnett T, Hedvall PO, Mattsson T, et al. Feeling controlled or being in control? Apps for self-management among older people with neurological disability. *Disabil Rehabil Assist Technol.* (2019) 1–6. doi: 10.1080/17483107.2019.1685017. [Epub ahead of print].
19. Yin H, Wardenaar KJ, Wang Y, Wang N, Chen W, Zhang Y, et al. Mobile mental health apps in china: systematic app store search. *J Med Internet Res.* (2020) 22:e14915. doi: 10.2196/14915
20. Kong FW, Horsham C, Ngoo A, Soyer HP, Janda M. Review of smartphone mobile applications for skin cancer detection: what are the changes in availability, functionality, and costs to users over time? *Int J Dermatol.* (2020) 60:289–308. doi: 10.1111/ijd.15132
21. Harada N, Harada S, Ito J, Atsuta R, Hori S, Takahashi K. Mobile Health App for Japanese Adult Patients With Asthma: clinical Observational Study. *J Med Internet Res.* (2020) 22:e19006. doi: 10.2196/19006
22. Hawkins SD, Barilla S, Feldman SR. Web app based patient education in psoriasis—a randomized controlled trial. *Dermatol Online J.* (2017) 23:13030/qt26d525z5.
23. Svendsen MT, Andersen F, Andersen KH, Pottegard A, Johannessen H, Moller S, et al. A smartphone application supporting patients with psoriasis improves adherence to topical treatment: a randomized controlled trial. *Br J Dermatol.* (2018) 179:1062–71. doi: 10.1111/bjd.16667

Conflict of Interest: NG-S received speaker or consultant fees by LEO Pharma, Abbvie, Novartis and Lipidor AB. FL received speaker or consultant fees by Lilly, Amgen, Almirall, LEO Pharma, Abbvie, Roche, Sanofi, Janssen, Novartis not related to this manuscript.

The remaining authors declare that the research was conducted in the absence of any commercial or financial relationships that could be construed as a potential conflict of interest.

frontiers in Medicine

ORIGINAL RESEARCH
published: 28 June 2021
doi: 10.3389/fmed.2021.692060

Dermoscopic Features Summarization and Comparison of Four Types of Cutaneous Vascular Anomalies

Jing Gao[1†], Wenmin Fei[2,3,4†], Changbing Shen[5,6†], Xue Shen[7], Minghui Sun[1], Ning Xu[5,6], Qing Li[1], Cong Huang[5,6], Tingfang Zhang[1], Randy Ko[8], Yong Cui[2,3,4] and Chunjun Yang[1*]*

[1] Department of Dermatology, The Second Affiliated Hospital, Anhui Medical University, Hefei, China, [2] Department of Dermatology, China-Japan Friendship Hospital, Beijing, China, [3] Institute of Skin Health, China-Japan Friendship Hospital, Beijing, China, [4] Graduate School, Peking Union Medical College and Chinese Academy of Medical Sciences, Beijing, China, [5] Department of Dermatology, Peking University Shenzhen Hospital, Shenzhen, China, [6] Shenzhen Key Laboratory for Translational Medicine of Dermatology, Shenzhen Peking University–The Hong Kong University of Science and Technology Medical Center, Shenzhen, China, [7] Department of Dermatology, Chengdu Second People's Hospital, Chengdu, China, [8] Division of Molecular Medicine, Department of Internal Medicine, University of New Mexico Health Sciences Center, Albuquerque, NM, United States

OPEN ACCESS

Edited by:
Salvador Gonzalez,
University of Alcalá, Spain

Reviewed by:
Francesco Lacarrubba,
University of Catania, Italy
Irina Khamaganova,
Pirogov Russian National Research Medical University, Russia
Oriol Yelamos,
Hospital de la Santa Creu i Sant Pau, Spain

***Correspondence:**
Yong Cui
wuhucuiyong@vip.163.com
Chunjun Yang
yangchunjun9@163.com

[†] These authors have contributed equally to this work

Specialty section:
This article was submitted to Dermatology, a section of the journal Frontiers in Medicine

Received: 07 April 2021
Accepted: 02 June 2021
Published: 28 June 2021

Citation:
Gao J, Fei W, Shen C, Shen X, Sun M, Xu N, Li Q, Huang C, Zhang T, Ko R, Cui Y and Yang C (2021) Dermoscopic Features Summarization and Comparison of Four Types of Cutaneous Vascular Anomalies. Front. Med. 8:692060. doi: 10.3389/fmed.2021.692060

Objective: Dermoscopic features of cutaneous vascular anomalies have been reported, but the described features currently known are limited and not well-understood. The aim of this study is to comprehensively summarize and compare the dermoscopic features of the four different types of cutaneous vascular anomalies [infantile hemangiomas (IH), cherry angioma (CA), angiokeratomas (AK), and pyogenic granuloma (PG)] in the Chinese Han population.

Materials and Methods: Dermoscopic features of 31 IH, 172 CA, 31 AK, and 45 PG were collected based on the contact non-polarized mode of dermoscopy at 20-fold magnification. Dermoscopic features including background, lacunae, vessel morphology and distribution were collected and summarized. Additionally, we compared these features by age stage, gender, and anatomical locations in CA.

Results: The dermoscopic features of IH included the red lacunae, red/red-blue/red-white backgrounds, and vessel morphology such as linear curved vessels, serpiginous vessels, coiled vessels. For CA, the lacunae appeared reddish brown to reddish blue or only red. In terms of vascular morphology, serpentine vessels, coiled vessels, looped vessels, and curved vessels could be seen in the lesions. A few lesions were black or presented with a superficial white veil. There were statistical differences in red background ($P = 0.021$), unspecific vessel distribution ($P = 0.030$), black area ($P = 0.029$), and white surface ($P = 0.042$) among different age groups. Red-brown lacunae ($P = 0.039$), red-blue ($P = 0.013$), red-white background ($P = 0.015$), black area ($P = 0.016$), and white surface ($P = 0.046$) were of statistical difference in terms of the locations of lesions. Lacunae were also observed in AK, which presented with red, dark purple, dark blue, black. Global dermoscopic patterns that were characterized by a homogeneous area were obvious in all PG lesions, among which 30 (66.7%) were red-white and 15 (33.3%) were red. As for

local features, "white rail" lines were detected in 19 (42.2%) lesions and white collarette was seen in 34 (75.6%) lesions.

Conclusions: Dermoscopy is an applicable diagnostic tool for the diagnosis of cutaneous vascular anomalies. It is necessary to take into account the age stage and lesion location when we diagnose CA using dermoscopy.

Keywords: dermoscopy, features, cutaneous vascular anomalies, summarization, comparison

INTRODUCTION

Vascular anomalies account for a considerable number of patients in the dermatology and surgical outpatient departments, which can be grouped into vascular tumors and vascular malformations. Some vascular tumors are proliferative and have the potential to fade away spontaneously, while vascular malformations normally stay stagnant over a long period of time (1). Timely and accurate diagnosis of vascular anomalies are essential for treatment and management, but remains a challenge for clinicians (2). Infantile hemangioma (IH), pyogenic granuloma (PG), angiokeratoma (AK), and cherry angiomas (CA) are common cutaneous vascular anomalies. According to the latest classification for vascular anomalies by the International Society for Vascular Anomalies (ISSVA), IH and PG are classified into the benign vascular tumors, angiokeratoma (AK) is classified into provisionally unclassified vascular anomalies (3). However, CA are not included in the current classification by the latest ISSVA (4).

IH is one of the most common cutaneous vascular anomalies present in infants, with the affected population being approximately 2–4.5% (5). The majority of IHs can be identified by clinical features, but some cases may still be misdiagnosed. CA, also known as cherry hemangiomas, adult hemangiomas, or senile angiomas as their number tends to increase with age, are cherry-red papules on the skin containing abnormal growth of blood vessels. CA are the most common vascular anomalies in adults, and elderly patients are especially concerned about the possible progression to malignancy. AK is a rare vascular malformation of the upper dermis that tends to have a distinct clinical presentation without self-limiting behavior. Clinically, the presentation of AK is often a dark nodule or macule which may be easily confused with malignant tumors, such as malignant melanomas, or pigmented basal cell carcinomas. A previous study reported that 20% of AK lesions were clinically diagnosed as melanomas (6). PG is a common and benign vascular tumor that can be diagnosed correctly by medical history and appearance. However, a survey indicated that 38% of the clinical diagnosis of PG proved to be inaccurate (7).

Dermoscopy has been widely accepted as a useful non-invasive diagnostic tool for various pigmented and non-pigmented skin disorders for increasing the diagnostic accuracy and avoiding unnecessary biopsies (8–12). The dermoscopic features of the above four types of cutaneous vascular anomalies have been previously reported in a few cases (6, 7, 12–17). However, dermoscopic features described in these studies are limited and not well-understood. Hence, this study aimed to comprehensively summarize the dermoscopic features of the four types of cutaneous vascular anomalies in the Chinese Han population.

MATERIALS AND METHODS

Study Design

This study was a morphological study carried out at the Second Affiliated Hospital of Anhui Medical University and China-Japan Friendship Hospital from June 1st, 2017 to October 31st, 2020. Approval was granted by the two institutions' ethics committees and conformed to the Declaration of Helsinki. All patients or their guardians provided informed consents. All lesions were clinically diagnosed by two associate chief physicians or chief physicians. If there was a disagreement between the two experts, the lesion would be discussed by an additional chief physician. The exclusion criteria included the use of: topical beta blocker, or intra-lesion injection, or laser treatment in the past 2 weeks, or a history of hematological malignancy. One lesion of each patient was selected to undergo dermoscopic examination.

Imaging Procedure

Dermoscopic examinations were performed with a digital dermoscopy system (Medicam 800HD, FotoFinder Systems GmbH, Birbach, Germany) at a 20-fold magnification. The contact non-polarized mode of dermoscopy was utilized. In order to acquire better visualization, minimal pressure was applied and ultrasound gel was used to preserve vessels' morphology. Dermoscopic images were evaluated by two independent dermatologists (JG and WF). Any poor-quality images were excluded. We developed a list of features based from literature review and preliminary observation which included lacunae, background, vessel morphology and distribution. Two dermatologists (WF and XS) completed the list independently and also supplemented new items features beyond the list if necessary. If there was a disagreement between the two experts or any supplementary information, a consensus meeting with other experts was held to settle any discrepancies. The dermoscopic features described in this study refer to the standardized dermoscopic terminology from an expert consensus on behalf of the International Dermoscopy Society (18, 19).

Divisions of Body Locations and Age Stages

Previous studies showed that there were differences of dermoscopic features and patterns in different age stages, gender, body location of lesions (20, 21). General information such as age, gender, anatomical locations were collected in

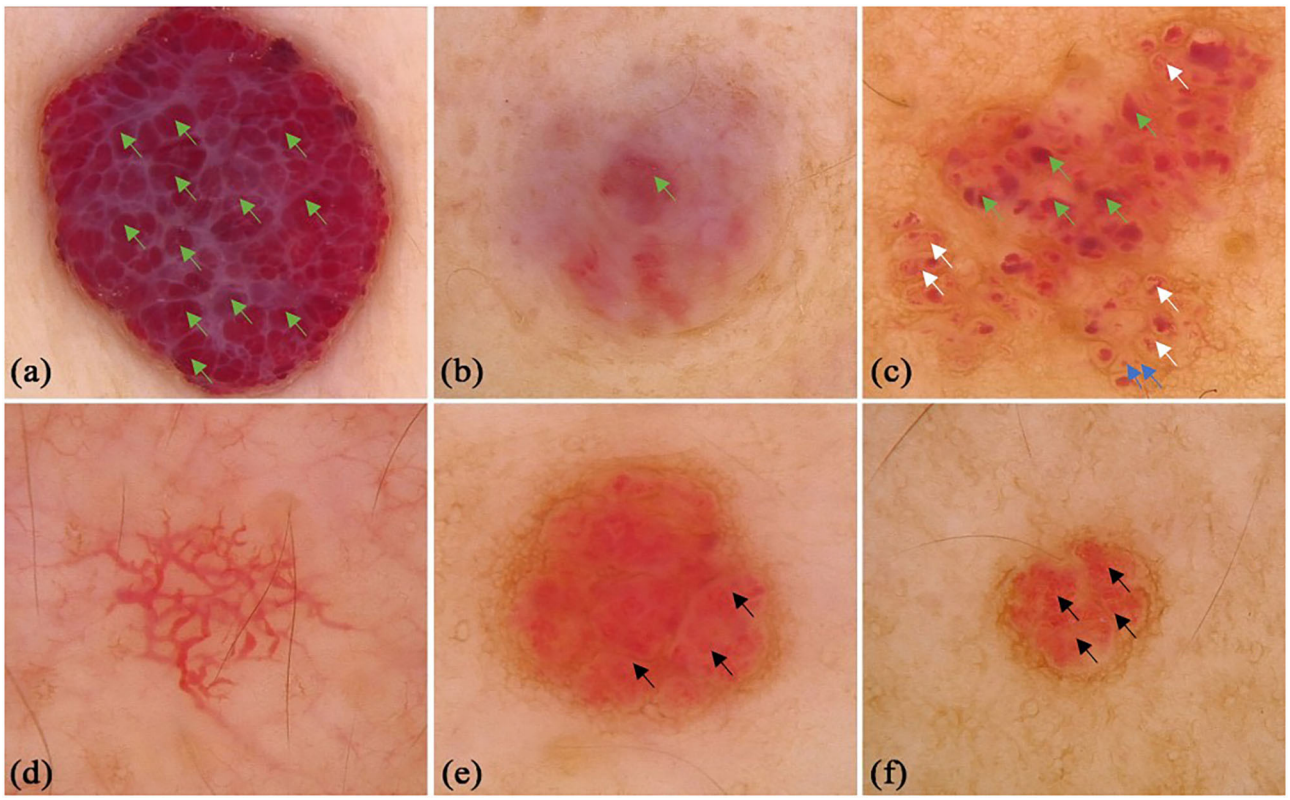

FIGURE 1 | Dermoscopic features of infant hemangiomas. **(a)** red-blue background, clustered red lacunae (green arrows); **(b)** red-white background, red lacunae (green arrows); **(c)** red background, red lacunae (green arrows), red globules (blue arrows) and helical vessels (white arrows); **(d)** reticular vessel distribution; **(e)** clustered serpentine vessels (black arrows); **(f)** serpentine vessels (black arrows).

this study. The body locations were divided into four groups, including upper limbs, lower limbs, head and neck, and trunk. The hips were classified into the lower limbs category, and the perineum was categorized into the lower trunk. Gender, age, and location difference were analyzed in CA. For the CA patients, we divided the patients' age into three stages: <18 years old group (children), 18–60 years old group (adults), and >60 years old group (elders).

Statistical Analysis

The continuous data are represented as mean (M) ± standard deviation (SD), and the categorical data are shown as number (N) and percentage (%). The categorical variables were compared by utilizing the Chi-square test. Regarding the Chi-square test in R x C contingency tables, if the expected count (T) of any grid in the R x C contingency tables were <1, or the number of grids with $1 \leq T < 5$ exceed 20% of the total number of grids, then Fisher's exact test was used to calculate the *P*-value. Statistical package for social science (SPSS), version 22.0 (IBM Corp., Armonk, NY, USA) was used for all analysis. A two-sided *P*-value < 0.05 was considered statistically significant in all analysis.

RESULTS

There were 31 patients with IH, including 8 male and 23 female infants. The lesions were located on the upper limbs ($n = 2$, 6.5%), lower limbs ($n = 4$, 12.9%), head and neck ($n = 12$, 38.7%), and trunk ($n = 13$, 41.9%). Red lacunae was seen in 10 (32.3%) lesions. Red, red-blue, and red-white backgrounds were seen in 19 (61.3%), 1 (3.2%), and 4 (12.9%) lesions, respectively. There were definitive vascular structures besides lacunae in some lesions. Linear curved vessels could be discovered in 2 (6.5%) lesions, serpiginous vessels in 9 (29.0%) lesions, and coiled vessels in 6 (19.4%) lesions. In the lesions that contained multiple structures, reticular vessel distribution was seen in 9 (29.0%) lesions, 12 (38.7%) lesions with unspecific vessel distribution, while 9 (29.0%) lesions with clustered vessel distribution. Some of the classical and specifical dermoscopic features were showed in **Figure 1**.

A total of 172 CA patients (92 males and 80 females, mean age was 39.38 ± 18.41 years old) were included in the study. There were 41 (23.8%) lesions located on the upper limbs, 28 (16.3%) lesions on the lower limbs, 52 (30.2%) lesions on the head and neck, and 51 (29.7%) lesions on the trunk. Typical lacunae existed in 127 (73.84%) lesions, among which red lacunae were seen in 78 (45.3%) lesions, red-brown lacunae in 24 (14.0%) lesions, and red-blue lacunae in 42 (24.4%) lesions. Different colored backgrounds were identified in 158 (91.86%) lesions. Among the lesions, 77 (44.8%) were red, 52 (30.2%) were red-blue, and 34 (19.8%) were red-white. Regarding the vessel morphology, linear curved vessels were found in 29 (16.9%) lesions, serpiginous vessels in 27 (15.7%)

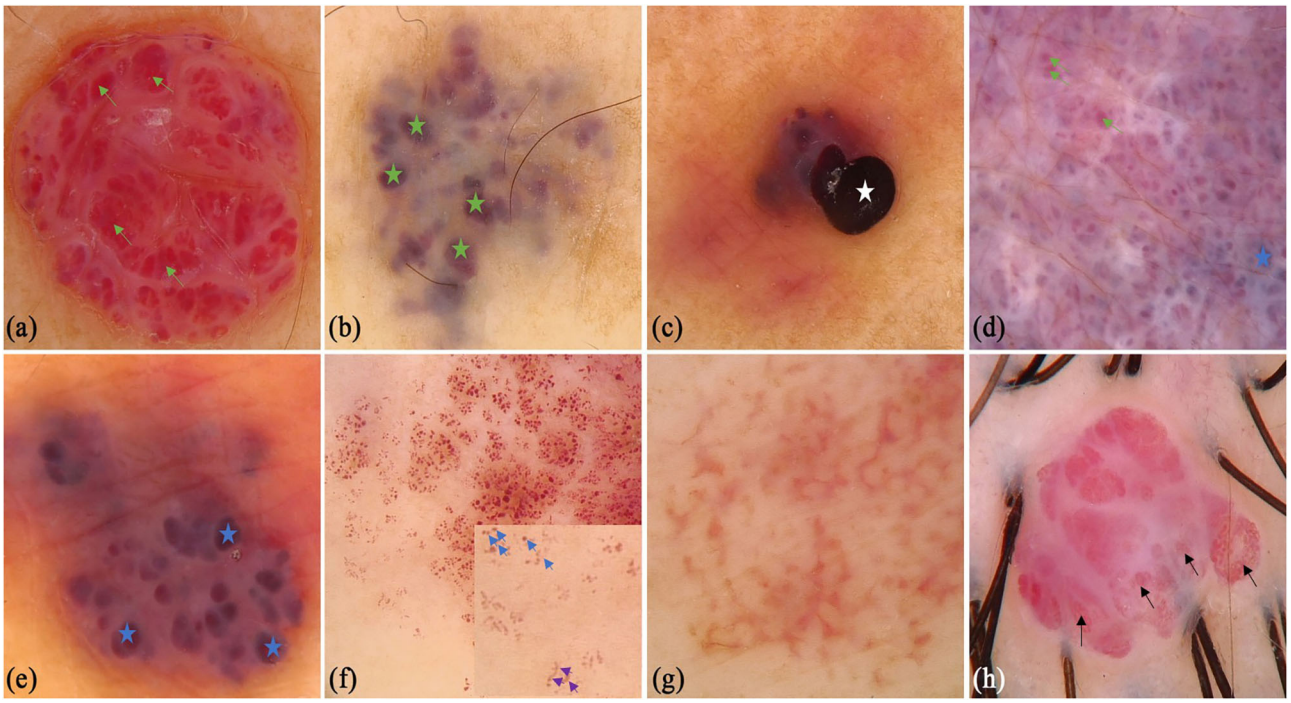

FIGURE 2 | Dermoscopic features of cherry angioma. **(a)** Typical dermoscopic appearance: red background, clustered red lacunae (green arrows), white surface; **(b)** red-white background, red-brown lacunae (green stars); **(c)** red background and black area (white star); **(d)** red-blue background, clustered red (green arrows) and red-blue lacunae (blue stars), white surface; **(e)** red-blue background, red-blue lacunae (blue stars), white surface; **(f)** red background, red globules (blue arrows) and curved vessels (purple arrows), clearer in the small box; **(g)** reticular vessel distribution; **(h)** clustered serpentine vessels (black arrows).

lesions, coiled vessels in 33 (19.2%) lesions, looped vessels in 7 (4.1%) lesions, and dotted vessels in 14 (8.1%) lesions. For the vessel distribution, reticular distribution in 12 (7.0%) lesions, 58 (33.7%) lesions with clustered vessel distribution, and 70 (40.7%) lesions with unspecific vessel distribution. A black area was seen in 24 (14.0%) lesions, and superficial white veil was seen in 63 (36.6%) lesions. Other infrequent vessel morphology in CA, included linear (n = 12, 6.98%), looped (n = 6, 3.49%), helical (n = 6, 3.49%), coiled (n = 7, 4.07%), serpiginous (n = 1, 0.58%), and branched (n = 1, 0.58%) vessels. Some classical and specifical dermoscopic features are shown in **Figure 2**.

We conducted comparisons of the dermoscopic features of CA (**Table 1**). There was no difference of dermoscopic features were observed between males and females. There were statistical differences in the red background (P = 0.021), clustered vessel distribution (P = 0.03), black area (P = 0.029), and white surface features (P = 0.042) among different age groups. Red-brown lacunae (P = 0.039), red-blue (P = 0.013), red-white background (P = 0.015), black area (P = 0.016), and white surface (P = 0.046) were of statistical difference in terms of the body locations of the lesions. Red lacunae were most common in head and neck, red background was most common in lower limbs, while a black area was most common in trunk.

We also collected 31 patients (16 males and 15 females) with AK, whereas the mean age was 33.29 (SD = 18.03) years old. Some of the classical and specifical dermoscopic features are shown in **Figure 3**. There were 5 (16.1%), 14 (45.2%), and 12 (38.7%) lesions that were located on the upper limbs, lower limbs, head and neck, respectively. Red lacunae could be seen in 13 (41.9%) lesions, dark purple lacunae in 25 (80.6%) lesions, dark blue in 3 (9.7%) lesions, and black lacunae in 4 (12.9%) lesions. A superficial white veil feature was found in 24 (77.4%) lesions, bleeding in 6 (19.4%) lesions, hemorrhagic crusts in 4 (12.9%) lesions, and scales in 7 (22.6%) lesions. Peripheral redness was seen in 7 (22.6%) lesions and peripheral pigment network in 2 (6.5%) lesions.

There were 45 patients (29 males and 16 females) with PG in this study, whereas the mean age was 44.11 (SD = 16.47) years old. Some of the classical and specifical dermoscopic features are shown in **Figure 4**. There were 26 (64.4%) lesions located on the upper limbs, 3 (6.7%) lesions on lower limbs, 15 (33.3%) lesions on head and neck, and only 1 (2.2%) lesion located on trunk. Global dermoscopic patterns that were characterized by a homogeneous area were obvious in all lesions, among which 30 (66.7%) were red-white and 15 (33.3%) were red. As for local features, "white rail" lines were detected in 19 (42.2%) lesions and white collarette in 34 (75.6%) lesions. Furthermore, vascular structures were observed in 19 (42.2%) lesions. Other atypical dermoscopic features included superficial ulcer (n = 2, 4.4%), thick crust (n = 10, 22.2%), bleeding (n = 4, 8.9%), scale (n = 13, 28.9%), and a central white veil (n = 2, 4.4%).

TABLE 1 | Summarization and comparison of dermoscopic features of cherry angioma.

Groups / Features	Sex			Age stage				Anatomical location				
	Male (*n* = 92)	**Female (*n* = 80)**	***P***	**<18 years old (*n* = 26)**	**18–60 years old (*n* = 120)**	**>60 years old (*n* = 26)**	***P***	**Upper limbs (*n* = 41)**	**Lower limbs (*n* = 28)**	**Head and neck (*n* = 52)**	**Trunk (*n* = 51)**	***P***
Lacunae												
Red	48 (52.2)	30 (37.5)	0.054	11 (42.3)	55 (45.8)	12 (46.2)	0.944	17 (41.5)	8 (28.6)	28 (53.8)	25 (49.0)	0.156
Red-brown	13 (14.1)	11 (13.8)	0.943	6 (23.1)	14 (11.7)	4 (15.4)	0.303	6 (14.6)	9 (32.1)	3 (5.8)	6 (11.8)	0.013
Red-blue	24 (26.1)	18 (22.5)	0.585	4 (15.4)	30 (25.0)	8 (30.8)	0.419	4 (9.8)	8 (28.6)	12 (23.1)	18 (35.3)	0.039
Background												
Red	41 (44.6)	36 (45.0)	0.954	7 (26.9)	62 (51.7)	8 (30.8)	0.021	21 (51.2)	13 (46.4)	20 (38.5)	23 (45.1)	0.668
Red-blue	26 (28.3)	26 (32.5)	0.546	10 (38.5)	31 (25.8)	11 (42.3)	0.155	11 (26.8)	14 (50.0)	12 (23.1)	15 (29.4)	0.082
Red-white	22 (23.9)	12 (15.0)	0.143	3 (11.5)	22 (18.3)	9 (34.6)	0.087	5 (12.2)	1 (3.6)	16 (30.8)	12 (23.5)	0.015
Vessel morphology												
Linear curved	18 (19.6)	11 (13.8)	0.310	5 (19.2)	21 (17.5)	3 (11.5)	0.739	9 (22.0)	1 (3.6)	10 (19.2)	9 (17.6)	0.211
Serpiginous	14 (15.2)	13 (16.3)	0.853	2 (7.7)	22 (18.3)	3 (11.5)	0.395	8 (19.5)	2 (7.1)	6 (11.5)	11 (21.6)	0.261
Globules	19 (20.7)	14 (17.5)	0.601	3 (11.5)	28 (23.3)	2 (7.7)	0.140	9 (22.0)	5 (17.9)	8 (15.4)	11 (21.6)	0.824
Looped	4 (4.3)	3 (3.8)	> 0.99*	0 (0.0)	6 (5.0)	1 (3.8)	0.835	3 (7.3)	0 (0.0)	2 (3.8)	2 (3.9)	0.583*
Dots	9 (9.8)	5 (6.3)	0.398	1 (3.8)	9 (7.5)	4 (15.4)	0.347	7 (17.1)	2 (7.1)	2 (3.8)	3 (5.9)	0.135*
Vessel distribution												
Reticular	4 (4.3)	8 (10.0)	0.147	4 (15.4)	5 (4.2)	3 (11.5)	0.058	4 (9.8)	3 (10.7)	2 (3.8)	3 (5.9)	0.567*
Clustered	33 (35.9)	25 (31.3)	0.523	4 (15.4)	41 (34.2)	13 (50.0)	0.030	10 (24.4)	8 (28.6)	16 (30.8)	24 (47.1)	0.103
Unspecific	36 (39.1)	34 (42.5)	0.654	11 (42.3)	49 (40.8)	10 (38.5)	0.959	23 (56.1)	7 (25.0)	21 (40.4)	19 (37.3)	0.068
Black area	16 (17.4)	8 (10.0)	0.163	6 (23.1)	18 (15.0)	0 (0.0)	0.029	4 (9.8)	7 (25.0)	2 (3.8)	11 (21.6)	0.016
White surface	34 (37.0)	29 (36.3)	0.924	7 (26.9)	41 (34.2)	15 (57.7)	0.042	9 (22.0)	8 (28.6)	25 (48.1)	21 (41.2)	0.046

**Fisher's exact test was used to calculate the P-values.*

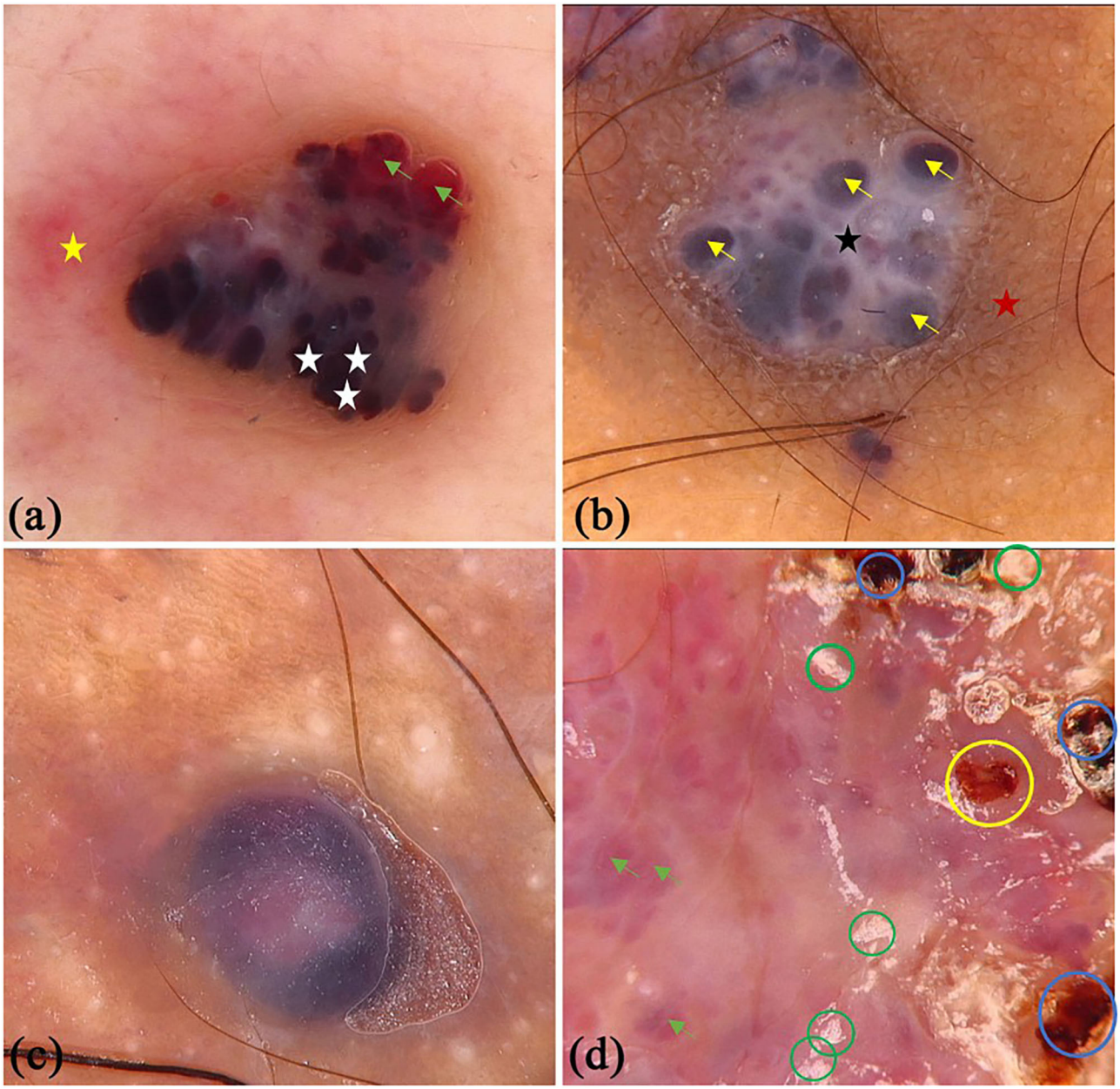

FIGURE 3 | Dermoscopic features of angiokeratoma. **(a)** clustered black area (white star) and red lacunae (green arrows), light white curtain, peripheral redness (yellow star); **(b)** dark purple lacunae (yellow arrows), light white curtain (black star), peripheral pigment network (red star); **(c)** dark blue lacuna; **(d)** red lacunae (green arrows), white scales (green circles), dark red scabs (blue circles) and bleeding (yellow circle).

DISCUSSION

Early and accurate diagnosis represents the safest strategy in the treatment of cutaneous vascular anomalies. This may reduce disease-related mortality, avoid unnecessary surgery, relieve the suffering of patients and ease potential financial burden. However, it can be difficult to manage as a result of the atypical clinical presentation and the progression being similar to malignancy. Dermoscopy is a non-invasive tool that has been applied clinically to support the diagnosis and differential diagnosis of skin tumors (22–25), here we present the dermoscopic differential diagnosis of four types of cutaneous vascular anomalies from other skin disorders (25–31) (**Table 2**). With dermoscopy, predominant vascular structures and other recognizable concomitant features can be observed. This may lead to improved accurate diagnosis of cutaneous vascular anomalies that originate from cutaneous vessels, if promptly recognized. This study describes the dermoscopic

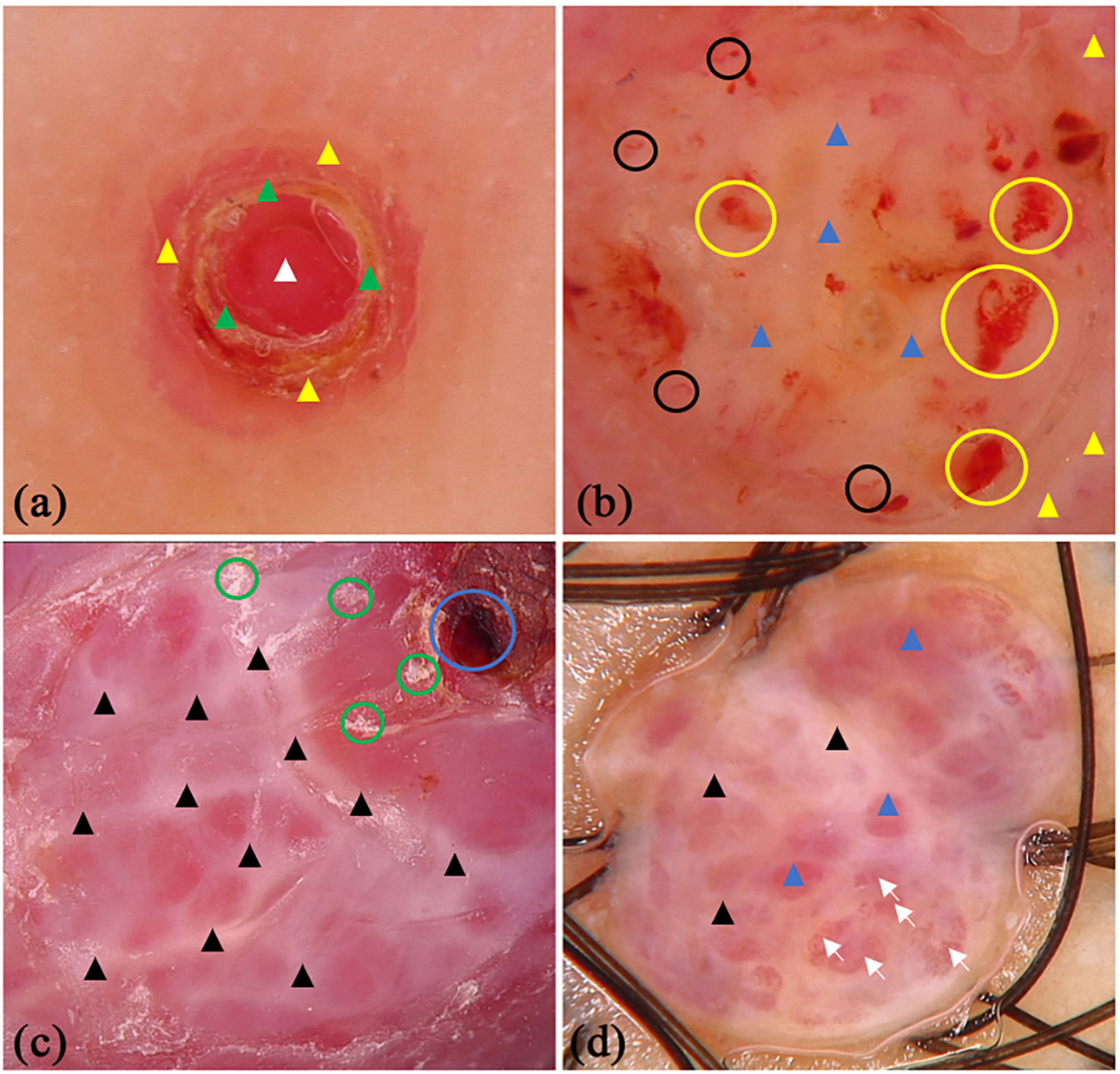

FIGURE 4 | Dermoscopic features of pyogenic granuloma. **(a)** red homogeneous area (white triangle), yellow scabs (green triangles), collar pattern (yellow triangles); **(b)** red-white homogeneous area (blue triangles), white collar pattern (yellow triangles), vascular structures (black circles) and bleeding (yellow circles); **(c)** "white rail" lines (black triangles), dark red scabs (blue circles) and white scales (green circles); **(d)** red-white homogeneous area (blue triangles) and "white rail" lines (black triangles), serpentine vessels (white arrows).

features of four types of cutaneous vascular anomalies in 279 patients.

Our study indicated that nearly three quarters of the lesions showed lacunae, which is regarded as a diagnostic clue for IH and CA (32). Lacunae corresponded to dilated vessels that are filled with red blood cells in the dermal papillae. Although lacunae appear in a variety of colors, their overall hue is red. The overall hue of backgrounds in IH and CA were red as well and the observed three colors in our study were consistent with a previous study (17). Besides lacunae, there are other vessels structures in IH and CA. The arrangement of vessels includes reticular, clustered, and unspecific vessel distributions, and the last one is the most common. It is worth noting that some lesions contain only one structure, and the possibilities of IH or CA should be taken into consideration when this is observed. In the vascular structures that have been reported before, we found that coiled vessel features were the most common. The appearance of a well-defined black area corresponds to thrombogenesis under histopathology (33). The superficial white veil feature, which were detected frequently, histopathologically resulted

TABLE 2 | Dermoscopic differential diagnosis of four types of cutaneous vascular anomalies from other skin disorders.

Category	Diseases	Common dermoscopic features
Four types of cutaneous vascular anomalies	IH	Red/red-blue/red-white background, clustered red lacunae; polymorphous vascular structures: red globular and helical vessels; clustered serpentine vessels (25).
	CA	Red/red-white/red-blue background, red/red-blue/dark lacunae, white surface; red globular and curved vessels, clustered serpentine, blue-whitish veil, ulceration, rainbow pattern.
	AK	Clustered black to dark red or purple-blue lacunae and whitish veil, peripheral redness; peripheral pigment network; white scales, dark red scabs and bleeding, blue whitish veil, ulceration, rainbow pattern (16).
	PG	Reddish homogeneous area, white collarette, "white rail" lines that intersect the lesion and ulceration (15). Red or white homogeneous area, surrounded by a white collar-like structure, thick tortuous blood vessels can be seen in the skin lesions. reddish homogeneous areas associated with "white rail" lines (17).
Other differential skin disorders	Foreign body granuloma	Orange background, white or blue-gray homogeneous areas; branched vessels (12).
	Verruca vulgaris	Multiple tightly packed papillae with red, brown dots, linear or looped vessels; white halos around looped vessels in some cases; irregular red, black, brown bleeding or scabs (12, 29, 30).
	Malignant melanoma	Negative or atypical pigment network; atypical streaks (radial streaming or pseudopods); blue-whitish veil; irregular dots or globules; irregular blotch; polychromatic; shiny white streaks; vascular pattern: pink areas, irregular dots or looped vessels (12).
	Spitz nevus	Starburst pattern, pink or pigment homogeneous pattern, globular pattern, atypical pattern, reticular pattern (12, 31).
	Bowenoid papulosis	Scattered dot, curved, looped, or coiled vessels; blue-gray or gray-brown homogeneous area (12, 27).
	Kaposi sarcoma	Bluish-reddish coloration including purple; multicolored areas showing various colors of the rainbow spectrum; scaly surface; small brown globule or blotch; reticular coarse vessels; shiny white streaks (12, 28).
	Dermatofi-brosarcoma protuberan	Topographic pattern background (pink, buff or tan); branched vessels (clustered or disseminated); shiny white streaks; delicate pigment network; structureless area or hypopigmented area (12).
	Proliferating trichilemmal tumor	Pink background, shiny white streaks, irregular and crown vessels, (sometimes) with hairs and ulceration (12, 26).

from the presence of an acanthotic epidermis with compact hyperkeratosis (34).

Typical dermoscopic features of AK include a well-demarcated, round lacunae and a whitish veil, whose histopathological basis are consistent with their equivalents in IH and CA (35). The overall hue of lacunae in AK is dark, with dark purple being the most common one in our study. Dark blue, purple, or a black color corresponds to vascular spaces that are partially or completely thrombosed. Peripheral redness, which likely represents inflammation of the lesion and erythrocyte extravasation in the papillary dermis, were seen in seven lesions. Two lesions presented a peripheral pigment network due to hyperpigmented rete ridges, which is akin to the network observed in dermatofibromas (36). Hemorrhagic crusts were detected in 12.9% lesions, which is far lower than the 53% reported in previous study (16). Scale features, which have been reported in previous study (6), were discovered in 22.6% lesions (7 of 31). Also, scale is a clinical manifestation of AK.

From our observation, a homogeneous area including reddish and red-whitish features, were the most frequent dermoscopic structure associated with PG, which is consistent with a previous study (7). The histopathological correlation of a homogeneous area may be attributed to the presence of numerous small capillaries or proliferating vessels which served as a foundation for various vascular structures. The white collarette, which was seen in 75.6% of lesions in our study, corresponds to the hyperplastic adnexal epithelium that partially or totally surrounds the lesion at the periphery of PG. This frequency of the white collarette is similar to previous study (7). The "white rail" lines may correspond to the fibrous septa that surround the capillary tufts or lobules (15), but it was not so common as white collarette features. The "white rail" lines can be observed in dermatofibromas and fully regressive melanomas when a polarized mode is used (37, 38). Erosion, bleeding, and scabbing are common clinical features of PG. These often lead to a misdiagnosis as malignant tumors which present as a dark-red or black homogeneous structure, hemorrhagic crusts, or ulceration revealed with dermoscopy. Serous exudation present explains the observation of orange-yellow crusts.

Other than the reported features in previous literatures, we observed some other dermoscopic findings in these cutaneous vascular anomalies. In IH and CA, some other morphology features include irregular linear, looped, helical, coiled, serpiginous, and branched vessels which were detected in our study. These features seem to be associated with dilated and proliferated vessels in the upper dermis and some of them had

diagnostic specificity for some malignant tumors. For example, coiled vessels in Bowen's disease (39). In our experience, scales and partial whitish veil features can also be seen in PG, which had never been described previously. These two features could appear in multiple diseases, for instance, scales may be present in inflammatory skin diseases and whitish veil in skin tumors.

We analyzed differences in gender, age stage, and location of the lesions. Red lacunae was more commonly observed in females. They may be linked to the higher levels of estrogen in female patients (40). Red-blue background and lacunae were more common in adults, which may be a signs of thrombi within the vascular spaces (17). This may also explain why black areas were more common in older patients. Additionally, dilated vessels in CA were veins, with the addition of some vessels in deeper dermis which may contribute to the color of red-blue in the adult. Another age-related dermoscopic feature was the presence of a superficial whitish veil, which may be explained as IH is self-limited while CA is not. In relation to anatomical areas, the feature of a black area, red-brown lacunae, and red-white background were the most prevalent in the trunk region.

It should be noted especially that there are some limitations of our study. One is that the diagnosis of four types of cutaneous vascular anomalies were based on clinical and dermoscopic features by two dermatologists and no histopathological examination was performed. The variations in anatomical sites and some newly discovered features have not been well-studied by histological analysis. Another one is the limited study sample size of IH, AK, and PG; many more numbers of these three cutaneous vascular anomalies patients should be recruited for a future study.

CONCLUSION

Dermoscopic evaluation is an easy, applicable, and ancillary diagnostic tool for the diagnosis of cutaneous vascular anomalies. In clinical practice, when dermatologists diagnose CA with dermoscopy, it is necessary to consider that dermoscopic features vary in age stages and different anatomical sites.

DATA AVAILABILITY STATEMENT

The original contributions generated for this study are included in the article, further inquiries can be directed to the corresponding authors.

ETHICS STATEMENT

The studies involving human participants were reviewed and approved by The Second Affiliated Hospital of Anhui Medical University and China-Japan Friendship Hospital. Written informed consent in this study was provided by participants or the participants' legal guardian/next of kin.

AUTHOR CONTRIBUTIONS

CY and YC designed this study. WF, XS, JG, CS, MS, NX, QL, and TZ collected the clinical and dermoscopic data. CS, JG, RK, and WF analyzed of data and interpreted the analysis results. JG, WF, CS, and XS prepared the manuscript. RK, CH, CS, CY, and YC revised this manuscript. All authors contributed to the article and approved the submitted version.

FUNDING

This study was supported by grants from Research Fund of Anhui Medical University (No. 2018xkj040), Milstein Medical Asian American Partnership Foundation Research Project (No. MMAAP2016023), Natural Science Foundation of Anhui Province (No. 2008085QH427), and Research Foundation of Peking University Shenzhen Hospital (No. JCYJ2020004).

REFERENCES

1. Johnson EF, Davis DM, Tollefson MM, Fritchie K, Gibson LE. Vascular tumors in infants: case report and review of clinical, histopathologic, and immunohistochemical characteristics of infantile hemangioma, pyogenic granuloma, noninvoluting congenital hemangioma, tufted angioma, and kaposiform hemangioendothelioma. *Am J Dermatopathol*. (2018) 40:231–9. doi: 10.1097/DAD.0000000000000983
2. Grazzini M, Stanganelli I, Rossari S, Gori A, Oranges T, Longo AS, et al. Dermoscopy, confocal laser microscopy, and hi-tech evaluation of vascular skin lesions: diagnostic and therapeutic perspectives. *Dermatol Ther*. (2012) 25:297–303. doi: 10.1111/j.1529-8019.2012.01547.x
3. International Society for the Study of Vascular Anomalies. *ISSVA classification for Vascular Anomalies [EB/OL]*. Available online at: http://www.issva.org/UserFiles/file/ISSVA-Classification-2018.pdf (accessed May 17, 2021).
4. Qadeer HA, Singal A, Patel BC. *Cherry Hemangioma, StatPearls, StatPearls Publishing Copyright © 2021*. (2021). Treasure Island (FL): StatPearls Publishing LLC.
5. Anderson KR, Schoch JJ, Lohse CM, Hand JL, Davis DM, Tollefson MM. Increasing incidence of infantile hemangiomas (IH) over the past 35 years: correlation with decreasing gestational age at birth and birth weight. *J Am Acad Dermatol*. (2016) 74:120–6. doi: 10.1016/j.jaad.2015.08.024
6. Kim JH, Kim MR, Lee SH, Lee SE, Lee SH. Dermoscopy: a useful tool for the diagnosis of angiokeratoma. *Ann Dermatol*. (2012) 24:468–71. doi: 10.5021/ad.2012.24.4.468
7. Zaballos P, Carulla M, Ozdemir F, Zalaudek I, Bañuls J, Llambrich A, et al. Dermoscopy of pyogenic granuloma: a morphological study. *Br J Dermatol*. (2010) 163:1229–37. doi: 10.1111/j.1365-2133.2010.10040.x
8. Braun RP, Rabinovitz HS, Oliviero M, Kopf AW, Saurat JH. Dermoscopy of pigmented skin lesions. *J Am Acad Dermatol*. (2005) 52:109–21. doi: 10.1016/j.jaad.2001.11.001
9. Fargnoli MC, Kostaki D, Piccioni A, Micantonio T, Peris K. Dermoscopy in the diagnosis and management of non-melanoma skin cancers. *Eur J Dermatol*. (2012) 22:456–63. doi: 10.1684/ejd.2012.1727
10. Shen X, Yu RX, Shen CB, Li CX, Jing Y, Zheng YJ, et al. Dermoscopy in China: current status and future prospective. *Chin Med J (Engl)*. (2019) 132:2096–104. doi: 10.1097/CM9.0000000000000396
11. Wang ZY, Shen CB, Fei WM, Shen X, Li CX, Jing Y, et al. Accuracy of dermoscopic and reflectance confocal microscopic criteria for diagnosis of psoriasis. *Chin Med J (Engl)*. (2020) 133:3010–2. doi: 10.1097/CM9.0000000000001198
12. Meng RS, Cui Y. *Multimodal Medical Imaging Atlas of Dermatology*. Beijing: People's Medical Publishing House (2021).

13. Lee JS, Mun JH. Dermoscopy of venous lake on the lips: a comparative study with labial melanotic macule. *PLoS ONE*. (2018) 13:e0206768. doi: 10.1371/journal.pone.0206768
14. Jassi R, Sanke S, Chander R. Dermoscopic evaluation of infantile hemangioma treated with topical timolol. *Dermatol Pract Concept*. (2020) 10:e2020073. doi: 10.5826/dpc.1004a73
15. Zaballos P, Llambrich A, Cuéllar F, Puig S, Malvehy J. Dermoscopic findings in pyogenic granuloma. *Br J Dermatol*. (2006) 154:1108–11. doi: 10.1111/j.1365-2133.2006.07193.x
16. Zaballos P, Daufí C, Puig S, Argenziano G, Moreno-Ramírez D, Cabo H, et al. Dermoscopy of solitary angiokeratomas: a morphological study. *Arch Dermatol*. (2007) 143:318–25. doi: 10.1001/archderm.143.3.318
17. Wolf IH. Dermoscopic diagnosis of vascular lesions. *Clin Dermatol*. (2002) 20:273–5. doi: 10.1016/S0738-081X(02)00222-5
18. Errichetti E, Zalaudek I, Kittler H, Apalla Z, Argenziano G, Bakos R, et al. Standardization of dermoscopic terminology and basic dermoscopic parameters to evaluate in general dermatology (non-neoplastic dermatoses): an expert consensus on behalf of the International Dermoscopy Society. *Br J Dermatol*. (2020) 182:454–67. doi: 10.1111/bjd.18125
19. Kittler H, Marghoob AA, Argenziano G, Carrera C, Curiel-Lewandrowski C, Hofmann-Wellenhof R, et al. Standardization of terminology in dermoscopy/dermatoscopy: results of the third consensus conference of the International Society of Dermoscopy. *J Am Acad Dermatol*. (2016) 74:1093–106. doi: 10.1016/j.jaad.2015.12.038
20. Piazza CD, Yamada S, Marcassi AP, Maciel MG, Seize MP, Cestari SCP. Dermoscopic patterns of melanocytic nevi in children and adolescents: a cross-sectional study. *An Bras Dermatol*. (2017) 92:340–4. doi: 10.1590/abd1806-4841.20175209
21. Cheng CY, Su HJ, Kuo TT. Dermoscopic features and differential diagnosis of sebaceous carcinoma. *J Dermatol*. (2020) 47:755–62. doi: 10.1111/1346-8138.15384
22. Darmawan CC, Jo G, Montenegro SE, Kwak Y, Cheol L, Cho KH, et al. Early detection of acral melanoma: a review of clinical, dermoscopic, histopathologic, and molecular characteristics. *J Am Acad Dermatol*. (2019) 81:805–12. doi: 10.1016/j.jaad.2019.01.081
23. Yélamos O, Braun RP, Liopyris K, Wolner ZJ, Kerl K, Gerami P, et al. Usefulness of dermoscopy to improve the clinical and histopathologic diagnosis of skin cancers. *J Am Acad Dermatol*. (2019) 80:365–77. doi: 10.1016/j.jaad.2018.07.072
24. Shen CB, Shen X, Li CX, Meng RS, Cui Y. Assessment of imaging diagnosis ability of skin tumors in Chinese dermatologists. *Chin Med J (Engl)*. (2019) 132:2119–20. doi: 10.1097/CM9.0000000000000389
25. Natsis NE, Gordon SC, Kaushik A, Seiverling EV. A practical review of dermoscopy for pediatric dermatology part II: vascular tumors, infections, and inflammatory dermatoses. *Pediatr Dermatol*. (2020) 37:798–803. doi: 10.1111/pde.14284
26. Miyachi H, Togawa Y, Yamamoto Y, Oguma R, Suehiro K, Matsue H. Proliferating trichilemmal tumour: a comparison of dermoscopic, ultrasonographic and histopathological features. *Eur J Dermatol*. (2016) 26:400–2. doi: 10.1684/ejd.2016.2795
27. Chan SL, Watchorn RE, Panagou E, Panou E, Ong EL, Heelan K, et al. Dermatoscopic findings of penile intraepithelial neoplasia: bowenoid papulosis, Bowen disease and erythroplasia of Queyrat. *Australas J Dermatol*. (2019) 60:e201–7. doi: 10.1111/ajd.12981
28. Hu SC, Ke CL, Lee CH, Wu CS, Chen GS, Cheng ST. Dermoscopy of Kaposi's sarcoma: areas exhibiting the multicoloured 'rainbow pattern'. *J Eur Acad Dermatol Venereol*. (2009) 23:1128–32. doi: 10.1111/j.1468-3083.2009.03239.x
29. Tognetti L, Cartocci A, Cinotti E, Moscarella E, Farnetani F, Carrera C, et al. Dermoscopy of early melanomas: variation according to the anatomic site. *Arch Dermatol Res*. (2021). doi: 10.1007/s00403-021-02226-x. [Epub ahead of print].
30. Kato J, Horimoto K, Sato S, Minowa T, Uhara H. Dermoscopy of melanoma and non-melanoma skin cancers. *Front Med (Lausanne)*. (2019) 6:180. doi: 10.3389/fmed.2019.00180
31. Lallas A, Apalla Z, Ioannides D, Lazaridou E, Kyrgidis A, Broganelli P, et al. Update on dermoscopy of Spitz/Reed naevi and management guidelines by the International Dermoscopy Society. *Br J Dermatol*. (2017) 177:645–55. doi: 10.1111/bjd.15339
32. Oiso N, Kawada A. The dermoscopic features in infantile hemangioma. *Pediatr Dermatol*. (2011) 28:591–3. doi: 10.1111/j.1525-1470.2011.01385.x
33. Moscarella E, Zalaudek I, Buccini P, Cota C, Catricalà C, Argenziano G. Dermoscopy and confocal microscopy of thrombosed hemangiomas. *Arch Dermatol*. (2012) 148:410. doi: 10.1001/archdermatol.2011.1027
34. Massi D, De Giorgi V, Carli P, Santucci M. Diagnostic significance of the blue hue in dermoscopy of melanocytic lesions: a dermoscopic-pathologic study. *Am J Dermatopathol*. (2001) 23:463–9. doi: 10.1097/00000372-200110000-00013
35. Jha AK, Sonthalia S, Jakhar D. Dermoscopy of angiokeratoma. *Indian Dermatol Online J*. (2018) 9:141–2. doi: 10.4103/idoj.IDOJ_278_17
36. Cuestas D, Perafan A, Forero Y, Bonilla J, Velandia A, Gutierrez A, et al. Angiokeratomas, not everything is Fabry disease. *Int J Dermatol*. (2019) 58:713–21. doi: 10.1111/ijd.14330
37. Bories N, Dalle S, Debarbieux S, Balme B, Ronger-Savlé S, Thomas L. Dermoscopy of fully regressive cutaneous melanoma. *Br J Dermatol*. (2008) 158:1224–9. doi: 10.1111/j.1365-2133.2008.08501.x
38. Zaballos P, Llambrich A, Ara M, Olazarán Z, Malvehy J, Puig S. Dermoscopic findings of haemosiderotic and aneurysmal dermatofibroma: report of six patients. *Br J Dermatol*. (2006) 154:244–50. doi: 10.1111/j.1365-2133.2005.06844.x
39. Yang Y, Lin J, Fang S, Han S, Song Z. What's new in dermoscopy of Bowen's disease: two new dermoscopic signs and its differential diagnosis. *Int J Dermatol*. (2017) 56:1022–5. doi: 10.1111/ijd.13734
40. Sun ZY, Yang L, Yi CG, Zhao H, Han DL, Yang T, et al. Possibilities and potential roles of estrogen in the pathogenesis of proliferation hemangiomas formation. *Med Hypotheses*. (2008) 71:286–92. doi: 10.1016/j.mehy.2008.02.015

Conflict of Interest: The authors declare that the research was conducted in the absence of any commercial or financial relationships that could be construed as a potential conflict of interest.

frontiers in Medicine

ORIGINAL RESEARCH
published: 06 August 2021
doi: 10.3389/fmed.2021.683900

Nailfold Capillaroscopy With USB Digital Microscopy in Connective Tissue Diseases: A Comparative Study of 245 Patients and Healthy Controls

Kumutnart Chanprapaph†, Wuttidej Fakprapai†, Preeyachat Limtong† and Poonkiat Suchonwanit†*

Division of Dermatology, Faculty of Medicine, Ramathibodi Hospital, Mahidol University, Bangkok, Thailand

OPEN ACCESS

Edited by:
Yong Cui,
China-Japan Friendship Hospital, China

Reviewed by:
Saeedeh Shenavandeh,
Shiraz University of Medical Sciences, Iran
Alireza Rajaei,
Shahid Beheshti University, Iran

***Correspondence:**
Poonkiat Suchonwanit
poonkiat@hotmail.com

†ORCID:
Kumutnart Chanprapaph
orcid.org/0000-0001-7931-3816
Wuttidej Fakprapai
orcid.org/0000-0002-2819-4287
Preeyachat Limtong
orcid.org/0000-0001-7258-5544
Poonkiat Suchonwanit
orcid.org/0000-0001-9723-0563

Specialty section:
This article was submitted to Dermatology, a section of the journal Frontiers in Medicine

Received: *22 March 2021*
Accepted: *25 June 2021*
Published: *06 August 2021*

Citation:
Chanprapaph K, Fakprapai W, Limtong P and Suchonwanit P (2021) Nailfold Capillaroscopy With USB Digital Microscopy in Connective Tissue Diseases: A Comparative Study of 245 Patients and Healthy Controls. Front. Med. 8:683900. doi: 10.3389/fmed.2021.683900

Background: Nailfold capillaroscopy (NFC) is a valuable tool to detect microcirculation abnormalities in connective tissue diseases (CTDs). However, whether the universal serial bus (USB) digital microscopy used as onychoscopy is as effective as the videocapillaroscopy in determining the diagnostic and prognostic values of CTDs remains to be determined.

Objective: This study aims to investigate NFC features of systemic lupus erythematosus (SLE), dermatomyositis (DM), and systemic sclerosis (SSc) patients and compare with normal controls as well as examine which feature could differentiate among CTDs. Furthermore, we aim to explore different capillaroscopic abnormalities and their association with disease activity.

Methods: Nailfold images were taken from patients and healthy controls using a USB digital microscopy. Patterns on the capillary morphology, diameter, architecture, and density were recorded and compared. We further determined the NFC findings in SLE, DM, and SSc and corresponded to their respective disease activity scoring system.

Results: A total of 245 participants, consisting of 54 SLE, 32 DM, and 51 SSc patients, as well as 108 controls, were enrolled. All capillaroscopic features, except for tortuous capillaries, were significantly more common in CTDs than healthy control (all $p < 0.05$). A multinomial logistic regression analysis revealed that bushy capillaries had significantly higher odds for both SLE and DM than SSc (OR: 4.10, 95% confidence interval (CI): 1.71–9.81, $p = 0.002$ and OR: 7.82, 95% CI, 2.86–21.38, $p < 0.001$, respectively). Elongated capillaries demonstrated significant odds for SLE compared with SSc (OR: 3.35, 95% CI: 1.005–11.20, $p = 0.049$), while prominent subpapillary plexus showed greater odds for SLE compared with both DM and SSc (OR: 2.75, 95% CI: 1.07–7.02, $p = 0.03$ and OR: 5.78, 95% CI: 2.29–14.58, $p < 0.001$, respectively). The presence of hemorrhage, enlarged capillaries, and the low-density index had significantly higher odds in favor of SSc than SLE. Bushy capillaries were the only pattern with a strong association for DM over SSc. The presence of enlarged capillaries indicated higher SLE severity, but no specific finding was related to DM or SSc skin scores.

Conclusions: Nailfold capillaroscopic examination using a digital microscope is a valuable method for the diagnosis of SLE, DM, and SSc. Several morphologic patterns can help differentiate among CTDs; however, the prognostic significance of this method requires further investigations.

Keywords: capillaroscopy, dermoscopy, nailfold, systemic lupus erythematosus, dermatomyositis, systemic sclerosis

INTRODUCTION

Nailfold capillaroscopy (NFC) represents the best method to analyze microvascular abnormalities among connective tissue diseases (CTDs) since capillaroscopic changes of the nailfold have been well established in many CTDs. It is commonly used for differentiating primary from secondary Raynaud's phenomenon and for the diagnosis of scleroderma-spectrum disorders, including systemic sclerosis (SSc), dermatomyositis (DM), undifferentiated CTD, and mixed CTD (1). NFC changes can also be detected in other chronic autoimmune rheumatic diseases, namely systemic lupus erythematosus (SLE), Sjogren's syndrome, rheumatoid arthritis, and antiphospholipid syndrome (2–5).

SSc is a prototype of scleroderma-spectrum disorders which exhibits the typical scleroderma pattern through NFC assessments. Characteristic capillaroscopic changes of scleroderma contain enlarged capillaries, bushy capillaries, capillary hemorrhage, disorganization of the normal distribution of capillaries, and avascular area (6). At present, nailfold microvascular abnormalities are of great importance both at the time of diagnosis and during follow-up and have been established as a part of the most recent classification criteria for the diagnosis of SSc, the American College of Rheumatology and European League Against Rheumatism (ACR/EULAR) 2013 for SSc criteria (7).

Capillaroscopic alterations were described in patients with inflammatory myopathies, typically exhibiting scleroderma-capillary patterns. DM patients appear to have more frequent nailfold capillary abnormality than polymyositis. Giant capillaries and bushy capillaries with other characteristics in the scleroderma pattern were found in 74% of cases (8). Conversely, NFC changes in SLE have been documented to be less specific (2, 9). The most frequent capillaroscopic features of SLE are tortuous capillaries, elongated capillaries, and prominent subpapillary plexus (10, 11).

Although NFC is extremely useful for detecting various nailfold abnormalities, being the gold standard to discover microvascular changes in the nailfold, it requires a special equipment, the videocapillaroscopy, which is relatively expensive, time consuming, and not widely available in most healthcare settings. Videocapillaroscopy is the current gold standard for NFC assessment (12). Dermoscopy is an easily applicable, low-cost, noninvasive diagnostic technique generally used among dermatologists to evaluate inflammatory and pigmentary skin conditions. There are broadly two types of dermoscopy: (i) hand-held dermoscopy, allowing 10–20 times magnification and (ii) videodermoscopy, providing higher magnification up to 1,000 times (13). Hair and scalp dermoscopy, also known as trichoscopy, has become a standard evaluation for alopecia and other scalp disorders (14). Currently, trichoscopic features among CTDs have been well described and may indicate their diagnostic and prognostic values (15–19). Onychoscopy refers to the examination of the nail unit using dermoscopy. It has been further adapted for the assessment of nailfold vascular abnormalities. There is growing evidence suggesting that microvascular nailfold changes reflect the presence of certain autoantibodies and the disease activity in patients with CTDs (8, 11, 20–29). However, whether the NFC changes possess prognostic values in rheumatic disorders remains to be determined.

Currently, reports on nailfold capillaroscopic features using a digital microscope as an onychoscopy in CTDs are limited, and direct comparison among the most common rheumatologic disorders, namely, SLE, DM, and SSc are sparse. This study aimed to explore the differences among onychoscopic microvascular features in SLE, DM, SSc, and healthy controls. The secondary objective was to determine NFC findings and their association to the disease activity.

MATERIALS AND METHODS

This cross-sectional, case-control study was approved by the Mahidol University Institutional Review Board (MURA 2019/263) and conducted at Ramathibodi Hospital, Bangkok, Thailand from February 2018 to February 2019. Informed consent to participate in the study was obtained from SLE, DM, and SSc patients, as well as healthy controls. SLE individuals who fulfilled the Systemic Lupus International Collaborating Clinics (SLICC) 2012 criteria and/or American College of Rheumatology (ACR) 1997 criteria (30), DM cases that met the Bohan and Peter criteria and/or the European League Against Rheumatism/American College of Rheumatology (EULAR/ACR) IIM criteria (31), and patients with SSc who satisfied the ACR/EULAR 2013 SSc criteria and/or the ACR 1980 criteria were recruited from the rheumatology and/or dermatology connective tissue disease clinics (7). The diagnosis and assessment of disease activity were made by a rheumatology-dermatology specialist. For healthy controls, healthcare personnel and patients who presented at the dermatology outpatient department for minor or cosmetic consultations, except for conditions involving the nails, and did not report signs and symptoms of CTD were recruited. Patients

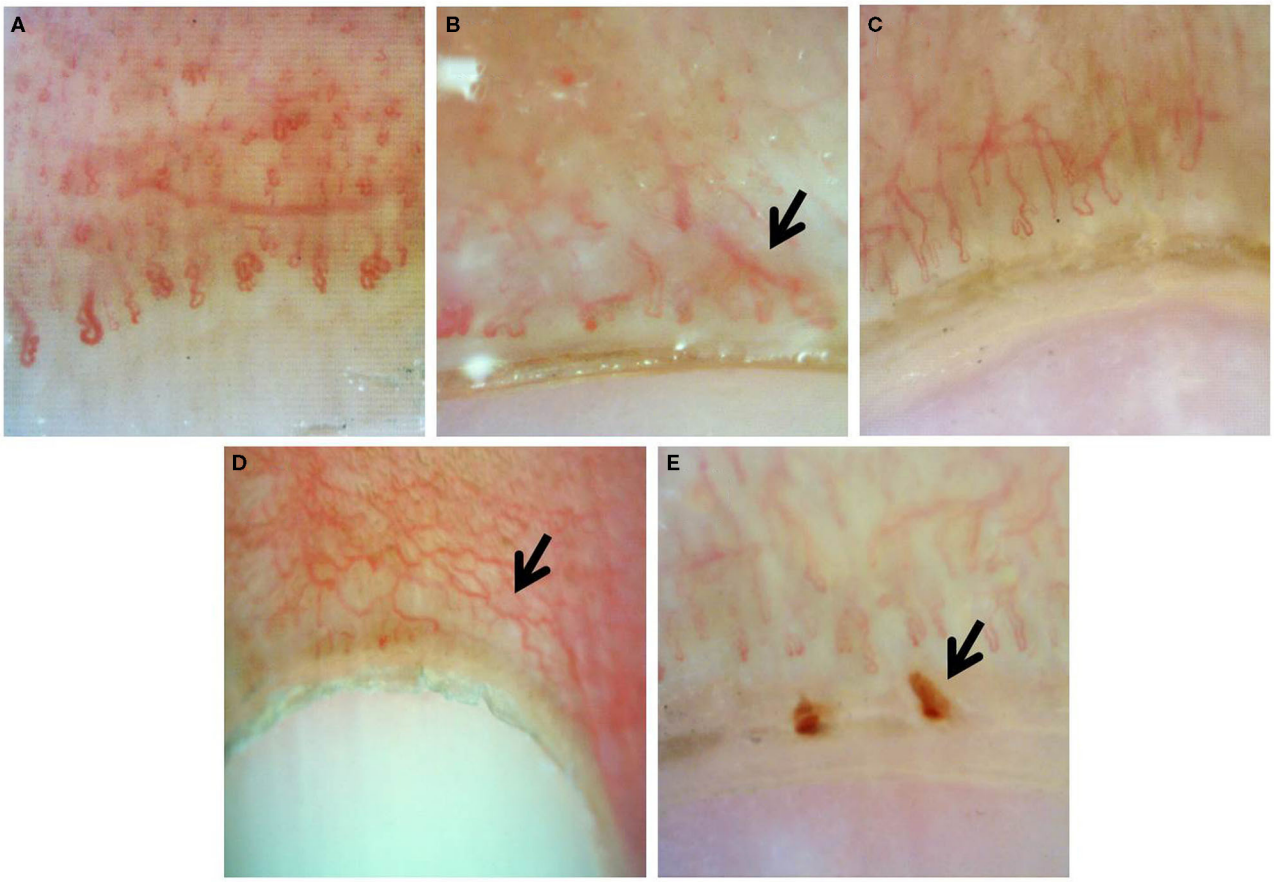

FIGURE 1 | Onychoscopic morphologic features: **(A)** tortuous capillaries, **(B)** bushy capillaries, **(C)** elongated capillaries, **(D)** prominent subpapillary plexus, and **(E)** capillary hemorrhage.

with other CTDs such as overlapping CTD, rheumatoid arthritis, Sjogren's syndrome, mixed CTD, and undifferentiated CTD were excluded from the study. Other exclusion criteria were patients who had traumatized finger and vascular occlusive diseases.

Nailfold examination was performed by a universal serial bus (USB) digital microscope with a polarizing light (Dinolite®; AnMo Electronics Corporation, Hsinchu, Taiwan) on both 4th and 5th fingers with × 200 magnification because their capillaries are the most visible. All examinations were operated by the same investigator. Patients were acclimatized for a minimum of 15–20 min before the examination at a room temperature (20–25°C). A drop of immersion oil was applied to the nailfold skin to improve resolution (32). Examination of the first distal row of capillaries was done to assess nailfold capillaroscopic features. Four consecutive images of each finger were captured. A blinded evaluation of images was conducted by an expert dermatologist.

Documented onychoscopic microvascular features consisted of morphology, diameter, architecture, and density of the nailfold capillaries. Morphologic parameters included tortuous capillaries (curled, crossed, or meandering capillaries; **Figure 1A**) (32), bushy capillaries (one capillary with three buddings; **Figure 1B**) (33), elongated capillaries (capillary loops longer than 300 μm; **Figure 1C**) (9, 34, 35), subpapillary plexus (vascular network at the base of the finger; **Figure 1D**) (34), and hemorrhages (extracapillary brown aggregations of erythrocytes and dived into punctate and confluent hemorrhages; **Figure 1E**) (9, 32, 35). The diameter index consisted of enlarged capillaries (capillaries with a diameter of arterial or venous limb wider than 20 μm; **Figure 2A**) (36), and giant capillaries (capillaries with a diameter wider than 50 μm; **Figure 2B**) (9, 32, 34). Architectural features included disorganized capillaries (irregular capillary pattern; **Figure 3A**) (34) and avascular area (distinct area in the nailfold where two or more adjacent capillaries are missing; **Figures 3B–D**) (34). Furthermore, the avascular area was quantitatively classified as grade 0 (no avascular area), grade 1 (mild or one or two avascular areas per millimeter), grade 2 (moderate or more than two avascular areas per millimeter), and grade 3 (severe or large and confluent avascular area) (35, 37). Capillary density was defined as the number of capillary loops in a 1-mm span of the distal row (9, 34, 37). We obtained capillary density by counting only the visible end row capillaries under a 90° angle. A capillary loop was considered a distal loop if the angle between the apex of that capillary and the apex of its two adjacent capillaries is >90° (**Figure 4**) (38). Any of the aforementioned

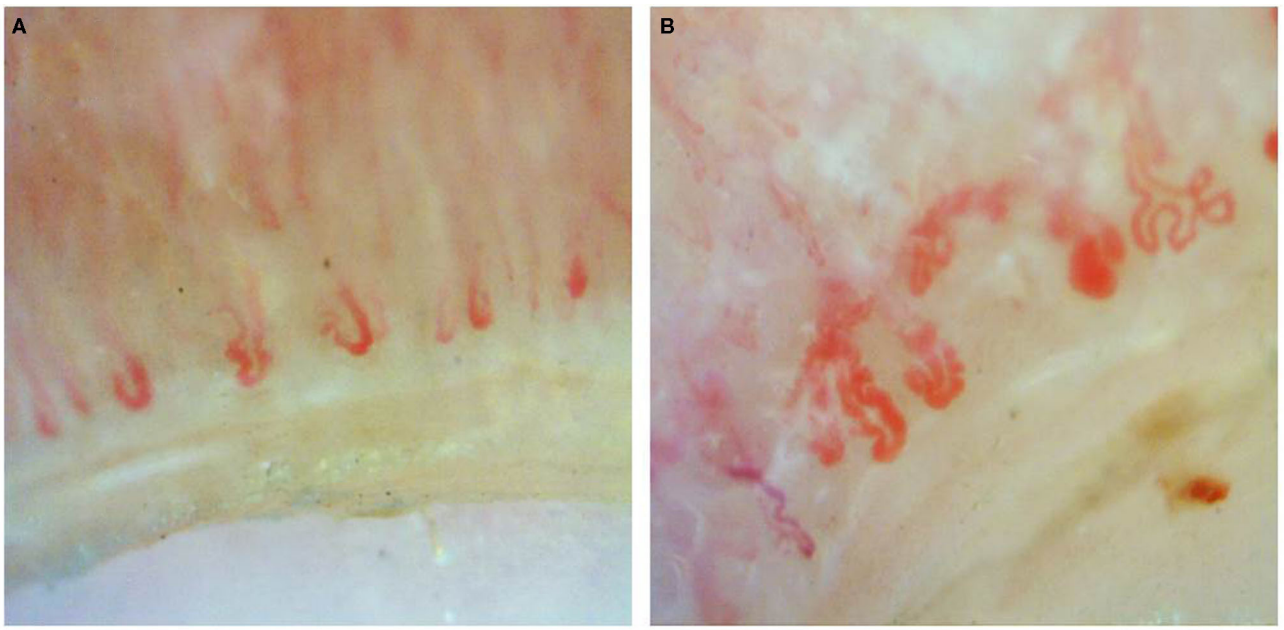

FIGURE 2 | Diameter index of onychoscopy: **(A)** enlarged capillaries and **(B)** giant capillaries.

features found at least in one finger was considered positive for capillary abnormality.

Nailfold capillaroscopic features among the three CTDs and controls were compared. Additionally, the correlation between onychoscopic microvascular changes and disease activity was additionally evaluated. The disease activity in SLE was assessed by using the Systemic Lupus Erythematosus Disease Activity Index 2000 (SLEDAI-2K) (39). We also evaluated the NFC changes in association to the skin scores of DM and SSC by using the Cutaneous Assessment tool for Myositis (CAT activity score) and modified Rodnan skin score, respectively (40, 41).

Data were analyzed using Stata 14.0 (Stata Corp LLC, College Station, TX). Results were expressed as mean ± standard deviation (SD) for continuous data and percentage for categorical data. Statistical analysis employed the chi-squared test or Fisher's exact test for categorical data and one-way ANOVA or Kruskal-Wallis test for continuous data. Multinomial logistic regression was used to determine the correlation among the three CTDs. A p-value of <0.05 was considered statistically significant. The magnitude of association was presented as odds ratio (OR) accounting for a 95% confidence interval (CI).

RESULTS

Of 255 subjects included in the study, 10 were excluded due to the diagnosis of overlapping CTD ($n = 5$), inadequate data to assess disease severity ($n = 3$), and having traumatized fingers ($n = 2$). The remaining patients for SLE, DM, and SSc groups were 54, 32, and 51, respectively. For healthy controls, 108 subjects were enrolled. **Table 1** demonstrates demographic data in patients with SLE, DM, SSc, and healthy controls. The mean age of the SLE cases was younger than DM and SSc patients (34.9, 52.2, and 56.8, respectively). Female predominance was observed in patients with CTDs. All patients and healthy controls had Fitzpatrick skin type III-V and were of Southeast Asian ethnicity. Raynaud's phenomenon was reported in 5 (9.3%), 4 (12.5%), and 29 (56.9%) of SLE, DM, and SSc patients, respectively. Anti U1-ribonucleoprotein (U1RNP) antibody was present in 14/35 (40%) of SLE, 0/22 (0%) of DM, and 3/30 (10%) of SSc cases. Patients manifesting Raynaud's phenomenon and/or anti-U1RNP antibody were found in 15 (40.5%), 4 (16.7%), and 29 (69%) of SLE, DM, and SSc groups, respectively.

The comparison between onychoscopic microvascular features in patients with CTDs versus healthy controls revealed that all features, except for tortuous capillaries, were found more in CTDs with statistical significance (all $p < 0.05$) (**Table 2**). A comparison of NFC changes in SLE, DM, and SSc demonstrated that morphologic patterns consisting of bushy capillaries, subpapillary plexus, hemorrhage, and enlarged capillaries were significantly different among the three conditions. Bushy capillary pattern favored SLE and DM over SSc ($p < 0.001$), whereas elongated capillaries and subpapillary plexus were prominent features of SLE ($p = 0.003$ and $p < 0.001$, respectively). Hemorrhage and enlarged capillaries were also predominant in SSc ($p < 0.001$). The dilated capillaries and avascular areas were seen more in SSc patients, which was statistically greater than SLE and DM cases ($p = 0.01$ and $p = 0.004$, respectively). A quantitative analysis on the degree of avascular areas revealed that the majority of SLE cases had no or mild (72.2%), DM patients had mild to moderate (78.2%), while SSc cases had moderate to severe (64.7%) avascular areas (**Supplementary Table 1**).

A multinomial logistic regression analysis comparing nailfold capillaroscopic findings among the three CTDs is demonstrated

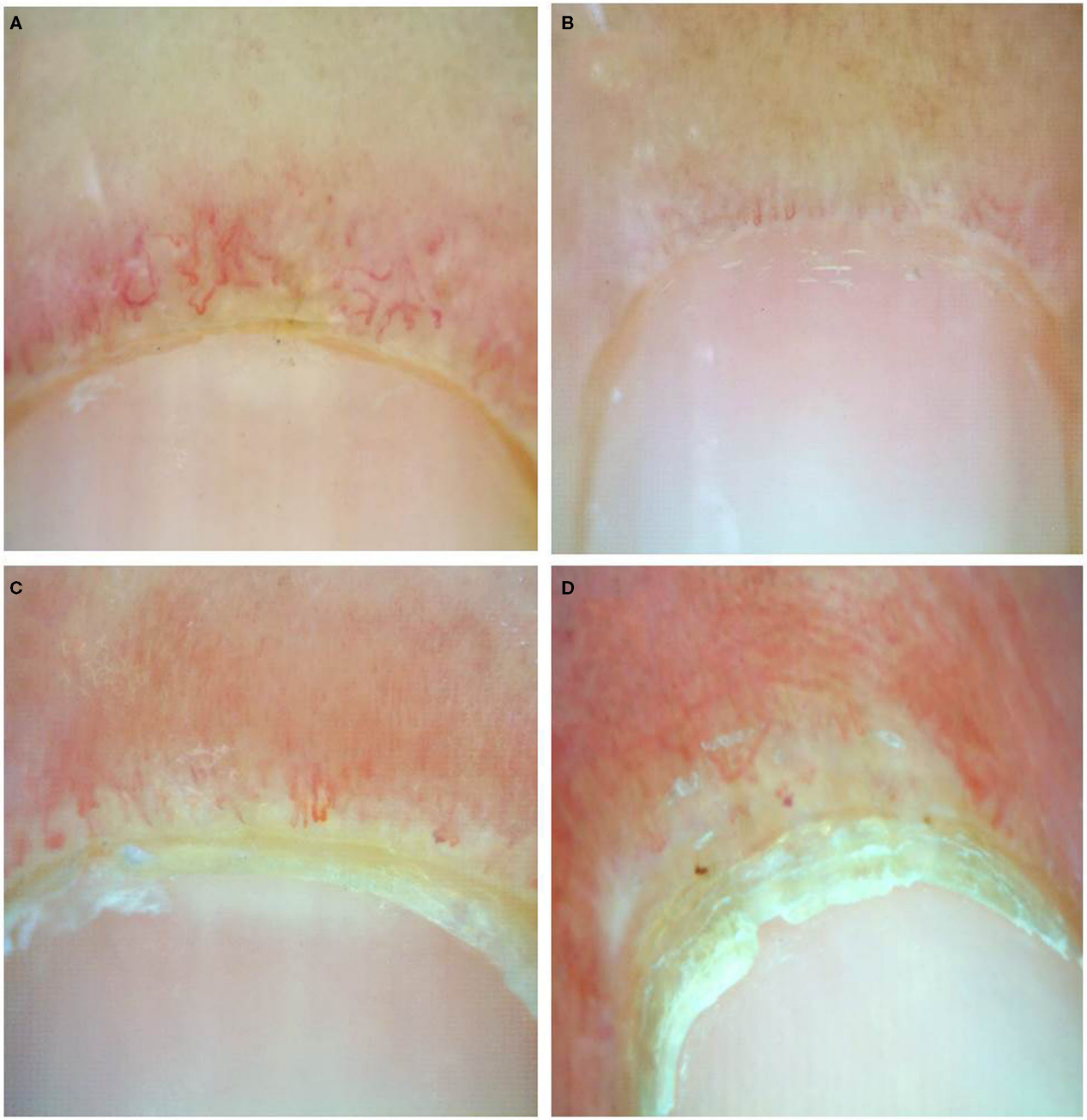

FIGURE 3 | Onychoscopic architectural features: **(A)** disorganized capillaries, **(B)** avascular area grade 1, **(C)** grade 2, and **(D)** grade 3.

in **Table 3**. The results on morphologic pattern revealed that the presence of bushy capillaries had significantly higher odds for having both SLE and DM than SSc (OR: 4.10, 95% CI: 1.71–9.81; $p = 0.002$ and OR: 7.82, 95% CI: 2.86–21.38; $p < 0.001$, respectively). Elongated capillaries demonstrated significant odds for SLE compared with SSc (OR: 3.35, 95% CI: 1.005–11.20; $p = 0.049$), while prominent subpapillary plexus showed greater odds for SLE compared with both DM and SSc (OR: 2.75, 95% CI: 1.07–7.02; $p = 0.03$ and OR: 5.78, 95% CI: 2.29–14.58; $p < 0.001$, respectively). For other morphological and architectural patterns (i.e., hemorrhage, enlarged capillaries, and avascular area) as well as the low-density index, significantly higher odds were in favor of SSc than SLE. Bushy capillaries were the only pattern that showed a strong association for DM over SSc (OR: 7.82, 95% CI: 2.86–21.38; $p < 0.001$). We further performed quantitative analysis on the degree of avascular areas. The absence of avascular

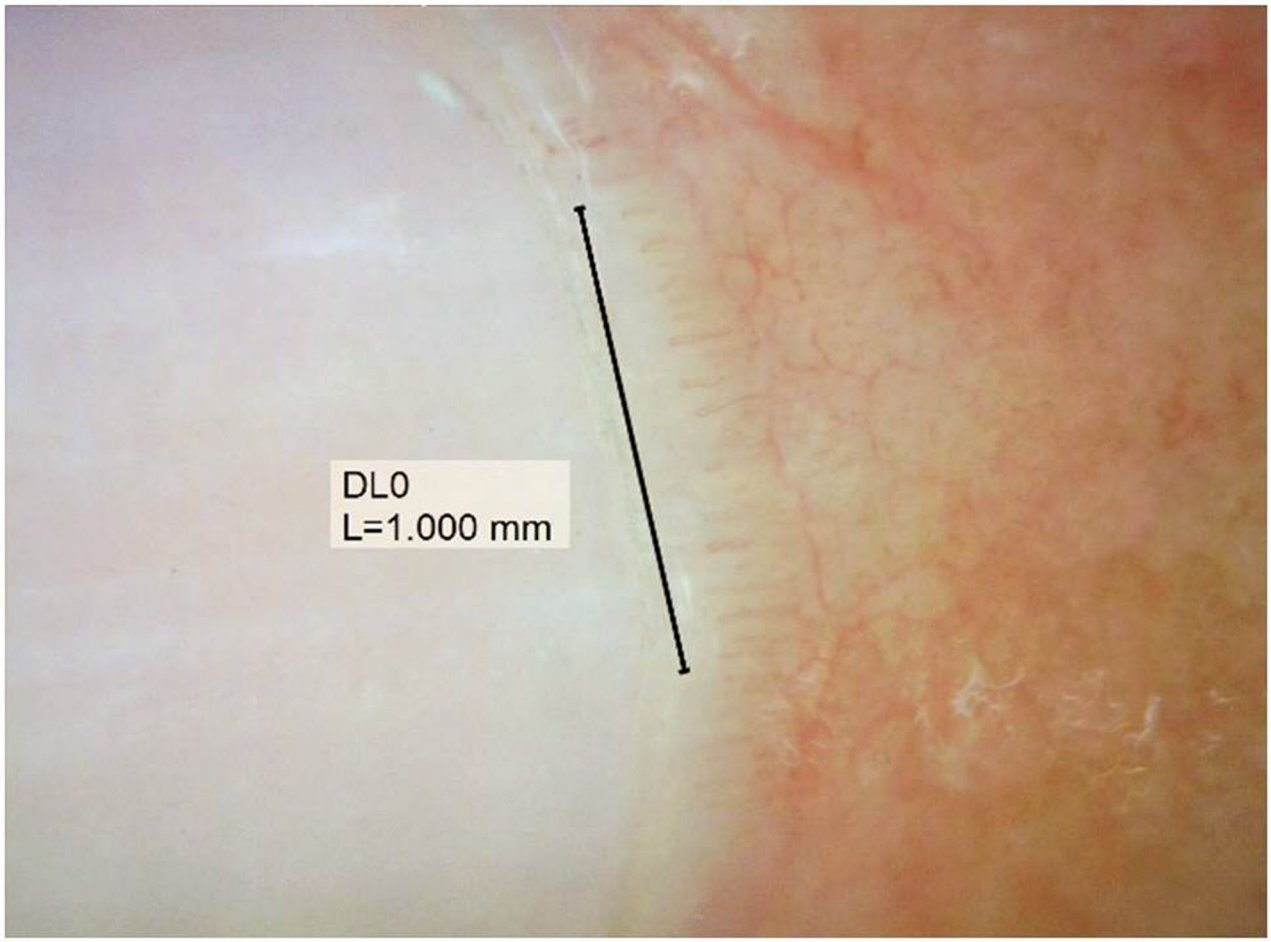

FIGURE 4 | Assessment of capillary density, counting the visible end row capillaries under a 90° angle.

TABLE 1 | Comparison of demographic data of patients with connective tissue diseases and healthy controls.

Variable	SLE (*N* = 54)	DM (*N* = 32)	SSc (*N* = 51)	Controls (*N* = 108)
Mean age (year ± SD)	34.9 ± 15.5	52.2 ± 16.9	56.8 ± 12.5	35.2 ± 10.4
Sex				
• Male	6 (11.1%)	8 (25%)	9 (17%)	41 (37.9%)
• Female	48 (88.9%)	24 (75%)	42 (83%)	67 (62.1%)
• F/M ratio	8:1	3:1	4.6:1	1.6:1
Mean disease duration (year ± SD)	7.6 ± 8.9	3.8 ± 4.5	7.2 ± 6.0	–
Fitzpatrick skin type	III–V	III–V	III–V	III–V
Southeast asian descent	54 (100%)	32 (100%)	51 (100%)	108 (100%)

DM, dermatomyositis; F, female; M, male; SD, standard deviation; SLE, systemic lupus erythematosus; SSc, systemic sclerosis.

area revealed higher odds for SLE over SSc, while extensive avascular area (grades 2–3) had significantly greater odds for SSc and DM (**Supplementary Table 2**).

The correlation between NFC findings and disease activity of CTDs is shown in **Table 4**. The presence of enlarged capillaries was significantly associated with higher median

TABLE 2 | Comparison of onychoscopic features between connective tissue diseases and healthy controls.

Onychoscopic features	SLE (*N* = 54)	DM (*N* = 32)	SSc (*N* = 51)	*p*-Value (among CTDs)	Controls (*N* = 108)	*p*-Value (CTDs vs. controls)
Tortous capillaries *N* (%)	48 (88.8%)	31 (96.8%)	50 (98%)	0.125	96 (88.8%)	0.125
Bushy capillaries *N* (%)	27 (50%)	21 (65.6%)	10 (19.6%)	<0.001*	4 (3.7%)	<0.001*
Elongated capillaries *N* (%)	12 (22.2%)	3 (9.3%)	4 (7.8%)	0.073	4 (3.7%)	0.003*
Subpapillary plexus *N* (%)	28 (51.8%)	9 (28.1%)	8 (15.6%)	<0.001*	15 (13.8%)	<0.001*
Hemorrhage *N* (%)	10 (18.5%)	11 (34.4%)	26 (50.9%)	0.002*	3 (2.7%)	<0.001*
Enlarged capillaries *N* (%)	25 (46.2%)	21 (65.6%)	38 (74.5%)	0.01*	27 (25%)	<0.001*
Disorganized capillaries *N* (%)	43 (79.6%)	31 (96.8%)	46 (90.1%)	0.05	21 (19.4%)	<0.001*
Avascular areas *N* (%)	41 (75.9%)	30 (93.7%)	49 (96%)	0.004*	10 (9.2%)	<0.001*
Density (mean ± SD)	6.83 ± 1.95	5.31 ± 1.86	5.09 ± 1.69	0.592	7.43 ± 1.20	<0.001*

*CTDs, connective tissue diseases; DM, dermatomyositis; SD, standard deviation; SLE, systemic lupus erythematosus; SSc, systemic sclerosis. *Statistically significant.*

TABLE 3 | Multinomial logistic regression analysis of onychoscopic features in SLE, DM, and SSc patients.

Onychoscopic features	SLE vs. DM	SLE vs. SSc	DM vs. SSc
Tortous capillaries	OR: 0.25	OR: 0.16	OR: 0.62
	p-Value: 0.22	*p*-Value: 0.095	*p*-Value: 0.73
	95% CI: 0.02–2.24	95% CI: 0.01–1.37	95% CI: 0.03–10.27
Bushy capillaries	OR: 0.52	OR: 4.10	OR: 7.82
	p-Value: 0.16	*p*-Value: 0.002*	*p*-Value: <0.001*
	95% CI: 0.21–1.29	95% CI: 1.71–9.81	95% CI: 2.86–21.38
Elongated capillaries	OR: 2.76	OR: 3.35	OR: 1.21
	p-Value: 0.14	*p*-value: 0.049*	*p*-Value: 0.80
	95% CI: 0.71–10.66	95% CI: 1.005–11.20	95% CI: 0.25–5.82
Subpapillary plexus	OR: 2.75	OR: 5.78	OR: 2.10
	p-Value: 0.03*	*p*-Value: <0.001*	*p*-Value: 0.17
	95% CI: 1.07–7.02	95% CI: 2.29–14.58	95% CI: 0.71–6.18
Hemorrhage	OR: 0.43	OR: 0.21	OR: 0.50
	p-Value: 0.10	*p*-Value: 0.001*	*p*-Value: 0.14
	95% CI: 0.15–1.18	95% CI: 0.09–0.52	95% CI: 0.20–1.25
Enlarged capillaries	OR: 0.45	OR: 0.29	OR: 0.65
	p-Value: 0.08	p-Value: 0.004*	*p*-Value: 0.38
	95% CI: 0.18–1.11	95% CI: 0.12–0.67	95% CI: 0.24–1.71
Disorganized capillaries	OR: 0.12	OR: 0.42	OR: 3.36
	p-Value: 0.053	*p*-Value: 0.14	*p*-Value: 0.27
	95% CI: 0.01–1.02	95% CI: 0.13–1.32	95% CI: 0.37–30.25
Avascular areas	OR: 0.21	OR: 0.12	OR: 0.61
	p-Value: 0.05	*p*-Value: 0.009*	*p*-Value: 0.63
	95% CI: 0.04–1.00	95% CI: 0.02–0.60	95% CI: 0.08–4.57
Density	OR: 1.21	OR: 1.74	OR: 0.22
	p-Value: 0.09	*p*-value: <0.001*	*p*-Value: 0.52
	95% CI: 0.91–2.42	95% CI: 1.12–2.35	95% CI: −0.48 to 0.93

DM, dermatomyositis; OR, odds ratio; SLE, systemic lupus erythematosus; SSc, systemic sclerosis; 95% CI, 95% confidence interval.
**Statistically significant.*

SLEDAI scores in SLE patients ($p = 0.01$). However, no specific feature was related to DM and SSc cutaneous changes using the CAT score and modified Rodnan skin score, respectively.

DISCUSSION

Nailfold capillaroscopic examination using a USB digital microscopy has been demonstrated to provide high-quality

TABLE 4 | Onychoscopic findings in relations to disease activity in SLE, DM, and SSc patients.

Onychoscopic features	SLE			DM			SSc		
	Median SLEDAI score in patients with the features (IQR)	Median SLEDAI score in patients without the features (IQR)	*p*-Value	Median CAT score in patients with the features (IQR)	Median CAT score in patients without the features (IQR)	*p*-Value	Median modified Rodnan score in patients with the features (IQR)	Median modified Rodnan score in patients without the features (IQR)	*p*-Value
Tortuous capillaries	3.5 (0–8)	10 (5–14)	0.03*	3 (2–5)	0 (0–0)	0.08	4 (1–12)	10 (10)	0.42
Bushy capillaries	4 (1–14)	4 (0–6)	0.18	3 (2–5)	3 (2–5)	0.82	7.5 (2–13)	3 (1–10)	0.27
Elongated capillaries	4 (1–11.5)	4 (1–8)	0.68	4 (2–5)	3 (2–5)	0.64	3 (0–10.5)	5 (2–11)	0.41
Subpapillary plexus	4 (0–9)	4 (2–9)	0.80	3 (2–5)	3 (1–5)	0.44	2 (0.5–7)	6 (2–12.5)	0.21
Hemorrhage	4.5 (2–10)	4 (0.5–8.5)	0.52	3 (2–5)	4 (2–5)	0.84	4 (1–8)	6 (2–13)	0.60
Enlarged capillaries	7 (2–14)	2 (0–6)	0.01*	4 (2–5)	2 (1–4)	0.11	5 (2–12.5)	4.5 (0.5–9)	0.50
Disorganized capillaries	4 (1–11)	2 (0–6)	0.23	3 (2–5)	0 (0–0)	0.08	5 (1–11)	6 (2–11.5)	0.69
Avascular areas	4 (2–10)	2 (0–6)	0.07	3 (2–5)	2 (0–4)	0.34	6 (2–12)	1 (0–2)	0.15
Decrease density	4.5 (0–13)	3 (1.5–6)	0.24	3 (2–5)	3 (1–4.5)	0.62	5 (2–12)	3.5 (0–7)	0.43

CAT, cutaneous assessment tool for myositis; DM, dermatomyositis; IQR, interquartile range; SLE, systemic lupus erythematosus; SLEDAI-2K, Systemic Lupus Erythematosus Disease Activity Index 2000; SSc, systemic sclerosis.
**Statistically significant.*

images and comparable ability to differentiate between patients with SSc and healthy controls in previous studies with a small number of subjects (12, 42, 43). The method offers a cheaper and more readily available device comparing with videocapillaroscopy. Our study on a relatively high number of patients demonstrates the significant value of a USB digital microscope used as onychoscopy for the detection of nailfold capillary abnormalities among the three most common CTDs, namely SLE, DM, and SSc. To the best of our knowledge, this is the first study to compare NFC abnormalities among CTDs and the normal population with this method. Although information regarding the comparison of NFC features in patients with autoimmune CTDs vs. healthy controls has been previously reported in Caucasian and Japanese individuals (44, 45), there is no data in the Southeast Asian population. We confirm that numerous onychoscopic microvascular parameters in the morphologic indexes (i.e., bushy capillaries, elongated capillaries, subpapillary plexus, and hemorrhage), diameter patterns (i.e., enlarged capillaries), architectural forms (i.e., disorganized and avascular pattern), and decreased capillary density were distinct features for CTDs and rarely seen in normal individuals.

Previous reports have documented an increase in tortuosity as one of the important NFC findings in CTDs, particularly for SLE patients (9, 10). Our results have suggested otherwise, tortuous capillary morphology was a fairly common finding in healthy controls and should not be considered a valuable index to identify CTDs. The scleroderma pattern consists of two or more of the following features, enlarged capillaries, bushy capillaries, capillary hemorrhage, disorganized capillaries, and avascular area, presented in at least two nailfolds (6). These characteristic microvascular changes are well recognized for SSc. DM is considered a scleroderma-spectrum disorder; therefore, the scleroderma pattern is also commonly observed in DM patients (8, 46, 47). In the present study, we confirm that the majority (over 90%) of SSc and DM patients possessed NFC features of the scleroderma-type pattern. In multinomial logistic regression analysis, the scleroderma-type features on onychoscopy, namely, hemorrhage, enlarged capillary, and avascular area were not suggestive of SSc over DM or vice versa. However, only the bushy capillary morphology revealed significantly higher odds for DM (OR: 7.82, 95% CI: 2.86–21.38; $p < 0.001$). Therefore, we postulate that although DM is considered a scleroderma-spectrum disorder, possessing similar nailfold capillaroscopic features to SSc, bushy capillary formation is a valuable NFC finding that favored DM over SSc.

Evidence to date has shown that capillary nailfold changes in SLE patients present a smaller percentage of the scleroderma-type pattern and hold fewer specific characteristics (9, 10, 27–29, 39, 45, 48, 49). However, our results were discordant with previous reports. Of 51 SLE patients, 79.6%, 75.9%, 50%, 46.2%, and 18.5% had disorganized architecture, avascular areas, bushy capillaries, enlarged capillaries, and hemorrhage as their NFC findings, respectively. Therefore, using the aforementioned findings, over three-fourths of our SLE patients would fulfill the definition of the scleroderma pattern of NFC. In line with several previous reports, the higher prevalence of scleroderma-type pattern in SLE patients may be in part due to a relatively high number of SLE patients (40.5%) possessing Raynaud's phenomenon and/or anti-U1RNP antibody (50, 51). It would be informative to further explore whether or not scleroderma-type pattern on nail fold of SLE reflexes an SLE subset with subclinical features of SSc such as Raynaud's phenomenon**.** As our data showed that the scleroderma-type pattern may not invariably differentiate scleroderma-spectrum disorders from SLE, we suggest that individual microvascular nailfold changes

and their severity should be considered rather than focusing on a specific pattern spectrum. SLE-type capillary nailfold pattern has been mentioned earlier consisting of tortuous, meandering capillaries, increase diameter, and prominent subpapillary plexus (9, 11, 28, 49). Our study results were concordant with the literature, but with regards to only the elongated capillary and prominent subpapillary plexus being more common in SLE. We also demonstrated that bushy capillary, elongated capillary, and prominent subpapillary plexus were patterns possessing significantly higher odds for SLE compared with SSc patients, while the prominent subpapillary plexus was the sole NFC finding that significantly favored SLE over DM. Moreover, in quantitative analysis for the degree of avascular areas, the absence of avascular area revealed significant odds for SLE over SSc, while extensive avascular areas favored both SSc and DM over SLE.

Microvascular changes play a central role in the pathophysiology of SLE, DM, and SSc. The similarities and dissimilarities on the NFC features may reflect their microvascular pathology. Endothelial injury is thought to be the initial vascular insult in SSc. Endothelial cell apoptosis, vasoconstriction, and vasculopathy are pronounced in SSc. A vast amount of tissue hypoxia in SSc patients may parallel the predominant nailfold avascular areas and the decrease capillary density seen on onychoscopy. Angiogenesis consequently occurs as compensation to chronic hypoxia, but the process is defective and dysregulated in SSc patients. An endothelial activation factor, namely vascular endothelial growth factor (VEGF), is highly expressed and has shown to be associated with decreased nailfold capillary density in patients with SSc (52).

VEGF is considered a key regulator of angiogenesis for SLE and DM as well. Kuryliszyn-Moskal et al. demonstrated that endothelial activation markers, namely VEGF, endothelin-1, E-selectin, and thrombomodulin were associated with increased capillaroscopic changes in SLE. Moreover, patients with moderate to severe capillaroscopic abnormalities (e.g., elongated, tortuous, meandering, ramified, and/or disarranged capillaries) showed higher levels of VEGF (23). In DM, microvascular injury is mediated by the humeral process with secondary vascular depletion, hypoxia, and myofiber necrosis. Subsequently, local angiogenesis occurs as compensation for vascular reduction. Angiogenic factors such as VEGF and angiogenin may play a role in the pathogenesis of DM and correspond to their onycoscopic changes (53). Therefore, similar to SSc, onychoscopic findings in DM may display both ischemia (e.g., avascular area and disorganized capillaries) and aberrant angiogenesis (e.g., enlarged capillaries and bushy capillaries). Nevertheless, further studies to determine the true pathomechanism and biomarkers that reflect the microvascular changes in CTDs are warranted.

The correlation of NFC alterations with the disease activity in SLE, DM, and SSc has been reported with variable results. In the present study, SLE patients with higher SLEDAI scores were associated with the presence of enlarged capillaries on onychoscopy than those without. Our results were in line with the literature showing higher disease activity defined by the SLEDAI, Systemic Lupus Activity Measures, and the European Consensus Activity Measures in SLE patients with NFC changes (11, 23, 27, 29). Documents on the microvascular nailfold abnormalities and disease activity in DM and SSc have been rather inconsistent. In DM and/or polymyositis, while several studies have shown a significant correlation between capillary damage with disease activity (e.g., myositis damage index, myositis disease activity assessment tools, and the global disease activity), many others have not (8, 54–59). Reports on the relationship between NFC and disease severity in SSc have been quite controversial, ranging from significant predictive association to no association. The significant heterogeneity reported are due to the differences in disease duration, specific organ complication (e.g., pulmonary vascular/parenchymal disease, myocardial dysfunction, and cutaneous sclerosis), scoring systems, and the parameter used in NFC (20, 60–64). In the present study, we found no correlation between nailfold capillaroscopic patterns with DM and SSc skin activity score, using the CAT score and modified Rodnan skin score, respectively. Further studies with validated disease severity/outcome parameters, analysis technique, and scoring system are much needed to determine the relationship between NFC features and the disease severity and organ-specific complications among CTDs.

The present study is subjected to several limitations. We did not determine NFC abnormalities of other chronic rheumatic disorders such as Sjogren's syndrome, rheumatoid arthritis, and antiphospholipid syndrome. Additional limitations were its cross-sectional, single-center study nature, with population restricted to Southeast Asians, and lack of prospective monitoring in order to evaluate alterations of NFC features and their relationship with disease activity over time. Our designated severity measures could not reflect the severity of disease in all aspects. Finally, being conducted in a tertiary care center means the study was prone to referral bias.

CONCLUSION

Our study confirms that a USB digital microscope used as onychoscopy is a valuable tool to detect nailfold capillary changes in SLE, DM, and SSc patients. Several morphologic patterns and their severity can help differentiate among CTDs. Therefore, the device may serve as a relevant diagnostic instrument and could be implemented in clinical practice. However, determining the prognostic significance of onychoscopy requires a large cohort study with validating assessment on disease severity and organ-specific complication.

DATA AVAILABILITY STATEMENT

The raw data supporting the conclusions of this article will be made available by the authors, without undue reservation.

ETHICS STATEMENT

The studies involving human participants were reviewed and approved by the Mahidol University Institutional Review

Board for Ethics in Human Research. The patients/participants provided their written informed consent to participate in this study.

AUTHOR CONTRIBUTIONS

PS: Conceptualization, writing-review and editing. PS, KC, and WF: methodology. PS and PL: validation. KC and WF: formal analysis PS, KC, WF, and PL: investigation. KC and WF: data curation and writing-original draft preparation. All authors have read and agreed to the published version of the manuscript.

SUPPLEMENTARY MATERIAL

The Supplementary Material for this article can be found online at: https://www.frontiersin.org/articles/10.3389/fmed.2021.683900/full#supplementary-material

REFERENCES

1. Nagy Z, Czirják L. Nailfold digital capillaroscopy in 447 patients with connective tissue disease and Raynaud's disease. *J Eur Acad Dermatol Venereol.* (2004) 18:62–8. doi: 10.1111/j.1468-3083.2004.00853.x
2. Zhao T, Lin FA, Chen HP. Pattern of nailfold capillaroscopy in patients with systemic lupus erythematosus. *Arch Rheumatol.* (2020) 35:568–74. doi: 10.46497/ArchRheumatol.2020.7763
3. Corominas H, Ortiz-Santamaría V, Castellví I, Moreno M, Morlà R, Clavaguera T, et al. Nailfold capillaroscopic findings in primary Sjögren's syndrome with and without Raynaud's phenomenon and/or positive anti-SSA/Ro and anti-SSB/La antibodies. *Rheumatol Int.* (2016) 36:365–9. doi: 10.1007/s00296-015-3396-9
4. Pavlov-Dolijanovic S, Damjanov NS, Stojanovic RM, Vujasinovic Stupar NZ, Stanisavljevic DM. Scleroderma pattern of nailfold capillary changes as predictive value for the development of a connective tissue disease: a follow-up study of 3,029 patients with primary Raynaud's phenomenon. *Rheumatol Int.* (2012) 32:3039–45. doi: 10.1007/s00296-011-2109-2
5. Shenavandeh S, Habibi S, Habibi Y, Nazarinia M. Mechanic hands: clinical and capillaroscopy manifestations of patients with connective tissue diseases presented with and without mechanic hands. *Clin Rheumatol.* (2019) 38:2309–18. doi: 10.1007/s10067-018-04422-z
6. Chojnowski MM, Felis-Giemza A, Olesińska M. Capillaroscopy - a role in modern rheumatology. *Reumatologia.* (2016) 54:67–72. doi: 10.5114/reum.2016.60215
7. van den Hoogen F, Khanna D, Fransen J, Johnson SR, Baron M, Tyndall A, et al. 2013 classification criteria for systemic sclerosis: an American College of Rheumatology/European League against Rheumatism collaborative initiative. *Arthritis Rheum.* (2013) 65:2737–47. doi: 10.1002/art.38098
8. Mugii N, Hasegawa M, Matsushita T, Hamaguchi Y, Horie S, Yahata T, et al. Association between nail-fold capillary findings and disease activity in dermatomyositis. *Rheumatology (Oxford).* (2011) 50:1091–8. doi: 10.1093/rheumatology/keq430
9. Lambova SN, Müller-Ladner U. Capillaroscopic pattern in systemic lupus erythematosus and undifferentiated connective tissue disease: What we still have to learn? *Rheumatol Int.* (2013) 33:689–95. doi: 10.1007/s00296-012-2434-0
10. Cutolo M, Melsens K, Wijnant S, Ingegnoli F, Thevissen K, De Keyser F, et al. Nailfold capillaroscopy in systemic lupus erythematosus: A systematic review and critical appraisal. *Autoimmun Rev.* (2018) 17:344–52. doi: 10.1016/j.autrev.2017.11.025
11. Riccieri V, Spadaro A, Ceccarelli F, Scrivo R, Germano V, Valesini G. Nailfold capillaroscopy changes in systemic lupus erythematosus: correlations with disease activity and autoantibody profile. *Lupus.* (2005) 14:521–5. doi: 10.1191/0961203305lu2151oa
12. Berks M, Dinsdale G, Marjanovic E, Murray A, Taylor C, Herrick AL. Comparison between low cost USB nailfold capillaroscopy and videocapillaroscopy: a pilot study. *Rheumatology (Oxford).* (2020). doi: 10.1093/rheumatology/keaa723
13. Micali G, Lacarrubba F. Dermatoscopy: Instrumental Update. *Dermatol Clin.* (2018) 36:345–8. doi: 10.1016/j.det.2018.05.001
14. Sriphojanart T, Khunkhet S, Suchonwanit P, A. retrospective comparative study of the efficacy and safety of two regimens of diphenylcyclopropenone in the treatment of recalcitrant alopecia areata. *Dermatol Reports.* (2017) 9:7399. doi: 10.4081/dr.2017.7399
15. Chanprapaph K, Udompanich S, Visessiri Y, Ngamjanyaporn P, Suchonwanit P. Nonscarring alopecia in systemic lupus erythematosus: A cross-sectional study with trichoscopic, histopathologic, and immunopathologic analyses. *J Am Acad Dermatol.* (2019) 81:1319–29. doi: 10.1016/j.jaad.2019.05.053
16. Suchonwanit P, Udompanich S, Thadanipon K, Chanprapaph K. Trichoscopic signs in systemic lupus erythematosus: a comparative study with 109 patients and 305 healthy controls. *J Eur Acad Dermatol Venereol.* (2019) 33:774–80. doi: 10.1111/jdv.15421
17. Udompanich S, Chanprapaph K, Suchonwanit P. Hair and Scalp Changes in Cutaneous and Systemic Lupus Erythematosus. *Am J Clin Dermatol.* (2018) 19:679–94. doi: 10.1007/s40257-018-0363-8
18. Jasso-Olivares JC, Tosti A, Miteva M, Domínguez-Cherit J, Díaz-González JM. Clinical and Dermoscopic Features of the Scalp in 31 Patients with Dermatomyositis. *Skin Appendage Disord.* (2017) 3:119–24. doi: 10.1159/000464469
19. Kwiatkowska M, Rakowska A, Walecka I, Rudnicka L. The diagnostic value of trichoscopy in systemic sclerosis. *J Dermatol Case Rep.* (2016) 10:21–5. doi: 10.3315/jdcr.2016.1225
20. Herrick AL, Moore TL, Murray AK, Whidby N, Manning JB, Bhushan M, et al. Nail-fold capillary abnormalities are associated with anti-centromere antibody and severity of digital ischaemia. *Rheumatology (Oxford).* (2010) 49:1776–82. doi: 10.1093/rheumatology/keq139
21. Manfredi A, Sebastiani M, Cassone G, Pipitone N, Giuggioli D, Colaci M, et al. Nailfold capillaroscopic changes in dermatomyositis and polymyositis. *Clin Rheumatol.* (2015) 34:279–84. doi: 10.1007/s10067-014-2795-8
22. Souza EJ, Kayser C. [Nailfold capillaroscopy: relevance to the practice of rheumatology]. *Rev Bras Reumatol.* (2015) 55:264–71. doi: 10.1016/j.rbre.2014.09.005
23. Kuryliszyn-Moskal A, Ciolkiewicz M, Klimiuk PA, Sierakowski S. Clinical significance of nailfold capillaroscopy in systemic lupus erythematosus: correlation with endothelial cell activation markers and disease activity. *Scand J Rheumatol.* (2009) 38:38–45. doi: 10.1080/03009740802366050
24. Ingegnoli F. Capillaroscopy abnormalities in relation to disease activity in juvenile systemic lupus erythematosus. *Microvasc Res.* (2013) 87:92–4. doi: 10.1016/j.mvr.2013.02.004
25. Ciołkiewicz M, Kuryliszyn-Moskal A, Klimiuk PA. Analysis of correlations between selected endothelial cell activation markers, disease activity, and nailfold capillaroscopy microvascular changes in systemic lupus erythematosus patients. *Clin Rheumatol.* (2010) 29:175–80. doi: 10.1007/s10067-009-1308-7
26. Chanasumon N, Sriphojanart T, Suchonwanit P. Therapeutic potential of bimatoprost for the treatment of eyebrow hypotrichosis. *Drug Des Devel Ther.* (2018) 12:365–72. doi: 10.2147/DDDT.S156467
27. Shenavandeh S, Habibi S. Nailfold capillaroscopic changes in patients with systemic lupus erythematosus: correlations with disease

activity, skin manifestation and nephritis. *Lupus.* (2017) 26:959–66. doi: 10.1177/0961203316686702
28. Tariq S, Tervaert JWC, Osman M. Nailfold Capillaroscopy in Systemic Lupus Erythematosus (SLE): a point-of-care tool that parallels disease activity and predicts future complications. *Curr Treat Options Rheumatol.* (2019) 5:336–45. doi: 10.1007/s40674-019-00133-x
29. Moneib HA, Salem SA, Aly DG, Khedr HT, Wafaey HA, Hassan HE. Assessment of serum vascular endothelial growth factor and nail fold capillaroscopy changes in systemic lupus erythematosus with and without cutaneous manifestations. *J Dermatol.* (2012) 39:52–7. doi: 10.1111/j.1346-8138.2011.01322.x
30. Petri M, Orbai AM, Alarcón GS, Gordon C, Merrill JT, Fortin PR, et al. Derivation and validation of the Systemic Lupus International Collaborating Clinics classification criteria for systemic lupus erythematosus. *Arthritis Rheum.* (2012) 64:2677–86. doi: 10.1002/art.34473
31. Leclair V, Lundberg IE. New Myositis Classification Criteria-What We Have Learned Since Bohan and Peter. *Curr Rheumatol Rep.* (2018) 20:18. doi: 10.1007/s11926-018-0726-4
32. Cutolo M, Sulli A, Smith V. How to perform and interpret capillaroscopy. *Best Pract Res Clin Rheumatol.* (2013) 27:237–48. doi: 10.1016/j.berh.2013.03.001
33. von Bierbrauer A, Barth P, Willert J, Baerwald C, Mennel HD, Schmidt JA. Electron microscopy and capillaroscopically guided nailfold biopsy in connective tissue diseases: detection of ultrastructural changes of the microcirculatory vessels. *Br J Rheumatol.* (1998) 37:1272–8. doi: 10.1093/rheumatology/37.12.1272
34. Etehad Tavakol M, Fatemi A, Karbalaie A, Emrani Z, Erlandsson BE. Nailfold capillaroscopy in rheumatic diseases: which parameters should be evaluated? *Biomed Res Int.* (2015) 2015:974530. doi: 10.1155/2015/974530
35. Kabasakal Y, Elvins DM, Ring EF, McHugh NJ. Quantitative nailfold capillaroscopy findings in a population with connective tissue disease and in normal healthy controls. *Ann Rheum Dis.* (1996) 55:507–12. doi: 10.1136/ard.55.8.507
36. Lee P, Leung FY, Alderdice C, Armstrong SK. Nailfold capillary microscopy in the connective tissue diseases: a semiquantitative assessment. *J Rheumatol.* (1983) 10:930–8.
37. Ingegnoli F, Gualtierotti R, Lubatti C, Zahalkova L, Meani L, Boracchi P, et al. Feasibility of different capillaroscopic measures for identifying nailfold microvascular alterations. *Semin Arthritis Rheum.* (2009) 38:289–95. doi: 10.1016/j.semarthrit.2007.10.008
38. Emrani Z, Karbalaie A, Fatemi A, Etehadtavakol M, Erlandsson BE. Capillary density: An important parameter in nailfold capillaroscopy. *Microvasc Res.* (2017) 109:7–18. doi: 10.1016/j.mvr.2016.09.001
39. Mikdashi J, Nived O. Measuring disease activity in adults with systemic lupus erythematosus: the challenges of administrative burden and responsiveness to patient concerns in clinical research. *Arthritis Res Ther.* (2015) 17:183. doi: 10.1186/s13075-015-0702-6
40. Huber AM, Dugan EM, Lachenbruch PA, Feldman BM, Perez MD, Zemel LS, et al. The Cutaneous Assessment Tool: development and reliability in juvenile idiopathic inflammatory myopathy. *Rheumatology (Oxford).* (2007) 46:1606–11. doi: 10.1093/rheumatology/kem179
41. Khanna D, Furst DE, Clements PJ, Allanore Y, Baron M, Czirjak L, et al. Standardization of the modified Rodnan skin score for use in clinical trials of systemic sclerosis. *J Scleroderma Relat Disord.* (2017) 2:11–8. doi: 10.5301/jsrd.5000231
42. Bhakuni DS, Vasdev V, Garg MK, Narayanan K, Jain R, Mullick G. Nailfold capillaroscopy by digital microscope in an Indian population with systemic sclerosis. *Int J Rheum Dis.* (2012) 15:95–101. doi: 10.1111/j.1756-185X.2011.01699.x
43. Jakhar D, Grover C, Singal A. Nailfold capillaroscopy with USB dermatoscope: A cross-sectional study in healthy adults. *Indian J Dermatol Venereol Leprol.* (2020) 86:33–8. doi: 10.4103/ijdvl.IJDVL_240_18
44. Sekiyama JY, Camargo CZ, Eduardo L, Andrade C, Kayser C. Reliability of widefield nailfold capillaroscopy and video capillaroscopy in the assessment of patients with Raynaud's phenomenon. *Arthritis Care Res (Hoboken).* (2013) 65:1853–61. doi: 10.1002/acr.22054
45. Ohtsuka T. Dermoscopic detection of nail fold capillary abnormality in patients with systemic sclerosis. *J Dermatol.* (2012) 39:331–5. doi: 10.1111/j.1346-8138.2011.01357.x
46. HASEGAWA M. Dermoscopy findings of nail fold capillaries in connective tissue diseases. *J Dermatol.* (2011) 38:66–70. doi: 10.1111/j.1346-8138.2010.01092.x
47. Manfredi A, Sebastiani M, Cassone G, Pipitone N, Giuggioli D, Colaci M, et al. SAT0298 Nailfold capillaroscopic alterations in dermatomyositis and polymyositis. *Ann Rheum Dis.* (2014) 73:700–1. doi: 10.1136/annrheumdis-2014-eular.4305
48. Ingegnoli F, Zeni S, Meani L, Soldi A, Lurati A, Fantini F. Evaluation of nailfold videocapillaroscopic abnormalities in patients with systemic lupus erythematosus. *J Clin Rheumatol.* (2005) 11:295–8. doi: 10.1097/01.rhu.0000191193.93720.95
49. Wu PC, Huang MN, Kuo YM, Hsieh SC Yu CL. Clinical applicability of quantitative nailfold capillaroscopy in differential diagnosis of connective tissue diseases with Raynaud's phenomenon. *J Formos Med Assoc.* (2013) 112:482–8. doi: 10.1016/j.jfma.2012.02.029
50. Furtado RN, Pucinelli ML, Cristo VV, Andrade LE, Sato EI. Scleroderma-like nailfold capillaroscopic abnormalities are associated with anti-U1-RNP antibodies and Raynaud's phenomenon in SLE patients. *Lupus.* (2002) 11:35–41. doi: 10.1191/0961203302lu144oa
51. Chojer P, Mahajan BB. Nail fold dermoscopy in collagen vascular disorders: A cross-sectional study. *Indian J Dermatol Venereol Leprol.* (2019) 85:439. doi: 10.4103/ijdvl.IJDVL_495_18
52. Choi JJ, Min DJ, Cho ML, Min SY, Kim SJ, Lee SS, et al. Elevated vascular endothelial growth factor in systemic sclerosis. *J Rheumatol.* (2003) 30:1529–33.
53. Miossi R, de Souza FHC, Shinjo SK. Nailfold capillary changes in adult new-onset dermatomyositis: a prospective cross-sectional study. *Clin Rheumatol.* (2019) 38:2319–26. doi: 10.1007/s10067-019-04537-x
54. Ganczarczyk ML, Lee P, Armstrong SK. Nailfold capillary microscopy in polymyositis and dermatomyositis. *Arthritis Rheum.* (1988) 31:116–9. doi: 10.1002/art.1780310116
55. Brunner HI, Feldman BM, Bombardier C, Silverman ED. Sensitivity of the Systemic Lupus Erythematosus Disease Activity Index, British Isles Lupus Assessment Group Index, and Systemic Lupus Activity Measure in the evaluation of clinical change in childhood-onset systemic lupus erythematosus. *Arthritis Rheum.* (1999) 42:1354–60. doi: 10.1002/1529-0131(199907)42:7<1354::AID-ANR8>3.0.CO;2-4
56. Selva-O'Callaghan A, Fonollosa-Pla V, Trallero-Araguás E, Martínez-Gómez X, Simeon-Aznar CP, Labrador-Horrillo M, et al. Nailfold capillary microscopy in adults with inflammatory myopathy. *Semin Arthritis Rheum.* (2010) 39:398–404. doi: 10.1016/j.semarthrit.2008.09.003
57. Suchonwanit P, Hector CE, Bin Saif GA, McMichael AJ. Factors affecting the severity of central centrifugal cicatricial alopecia. *Int J Dermatol.* (2016) 55:e338–43. doi: 10.1111/ijd.13061
58. Schmeling H, Stephens S, Goia C, Manlhiot C, Schneider R, Luthra S, et al. Nailfold capillary density is importantly associated over time with muscle and skin disease activity in juvenile dermatomyositis. *Rheumatology (Oxford).* (2011) 50:885–93. doi: 10.1093/rheumatology/keq407
59. Shenavandeh S, Zarei Nezhad M. Association of nailfold capillary changes with disease activity, clinical and laboratory findings in patients with dermatomyositis. *Med J Islam Repub Iran.* (2015) 29:233.
60. Castellví I, Simeón-Aznar CP, Sarmiento M, Fortuna A, Mayos M, Geli C, et al. Association between nailfold capillaroscopy findings and pulmonary function tests in patients with systemic sclerosis. *J Rheumatol.* (2015) 42:222–7. doi: 10.3899/jrheum.140276
61. Smith V, Pizzorni C, De Keyser F, Decuman S, Van Praet JT, Deschepper E, et al. Reliability of the qualitative and semiquantitative nailfold videocapillaroscopy assessment in a systemic sclerosis cohort: a two-center study. *Ann Rheum Dis.* (2010) 69:1092–6. doi: 10.1136/ard.2009.115568

62. Greidinger EL, Gaine SP, Wise RA, Boling C, Housten-Harris T, Wigley FM. Primary pulmonary hypertension is not associated with scleroderma-like changes in nailfold capillaries. *Chest.* (2001) 120:796–800. doi: 10.1378/chest.120.3.796
63. Lovy M, MacCarter D, Steigerwald JC. Relationship between nailfold capillary abnormalities and organ involvement in systemic sclerosis. *Arthritis Rheum.* (1985) 28:496–501. doi: 10.1002/art.1780280505
64. Sato LT, Kayser C, Andrade LE. Nailfold capillaroscopy abnormalities correlate with cutaneous and visceral involvement in systemic sclerosis patients. *Acta Reumatol Port.* (2009) 34:219–27.

Conflict of Interest: The authors declare that the research was conducted in the absence of any commercial or financial relationships that could be construed as a potential conflict of interest.

Publisher's Note: All claims expressed in this article are solely those of the authors and do not necessarily represent those of their affiliated organizations, or those of the publisher, the editors and the reviewers. Any product that may be evaluated in this article, or claim that may be made by its manufacturer, is not guaranteed or endorsed by the publisher.

frontiers in Medicine

ORIGINAL RESEARCH
published: 26 August 2021
doi: 10.3389/fmed.2021.670300

Accuracy of Deep Neural Network in Triaging Common Skin Diseases of Primary Care Attention

Mara Giavina-Bianchi, Eduardo Cordioli and André P. dos Santos*

Department of Telemedicine, Hospital Israelita Albert Einstein, São Paulo, Brazil

Access to dermatological care can be challenging in certain regions of the world. The triage process is usually conducted by primary care physicians; however, they may not be able to diagnose and assign the correct referral and level of priority for different dermatosis. The present research aimed to test different deep neural networks to obtain the highest level of accuracy for the following: (1) diagnosing groups of dermatoses; (2) correct referrals; and (3) the level of priority given to the referral compared to dermatologists. Using 140,446 images from a teledermatology project, previously labeled with the clinical diagnosis, and their respective referrals, namely biopsy, in-person dermatologist visits or monitoring the case via teledermatology along with the general physician, 27 different scenarios of neural networks were derived, and the algorithm accuracies in classifying different dermatosis, according to the group of the diagnosis they belong to, were calculated. The most accurate algorithm was then tested for accuracy in diagnosis, referral, and level of priority given to 6,945 cases. The GoogLeNet architecture, trained with 24,000 images and 1,000 epochs, using weight random initialization and learning rates of 10^{-3} was found to be the most accurate network, showing an accuracy of 89.72% for diagnosis, 96.03% for referrals and 92.54% for priority level in 6,975 image testing. Our study population, however, was confined to individuals with chronic skin conditions and, therefore, it has limited value as a triage tool because it has not been tested for acute conditions. Deep neural networks are accurate in triaging, correct referral and prioritizing common chronic skin diseases related to primary care attention. They can also help health-care systems optimize patients' access to dermatologists.

Keywords: primary care attention, common skin lesions, dermatology, deep neural network, articial intelligence

OPEN ACCESS

Edited by:
Je-Ho Mun,
Seoul National University Hospital,
South Korea

Reviewed by:
Takashi Hashimoto,
Osaka City University, Japan
Harald Kittler,
Medical University of Vienna, Austria
Sejung Yang,
Yonsei University, South Korea

****Correspondence:***
Mara Giavina-Bianchi
marahgbianchi@gmail.com

Specialty section:
This article was submitted to Dermatology, a section of the journal Frontiers in Medicine

Received: *20 February 2021*
Accepted: *30 June 2021*
Published: *26 August 2021*

Citation:
Giavina-Bianchi M, Cordioli E and Santos APd (2021) Accuracy of Deep Neural Network in Triaging Common Skin Diseases of Primary Care Attention. Front. Med. 8:670300. doi: 10.3389/fmed.2021.670300

INTRODUCTION

Health access is a serious challenge for most of the worldwide population. It becomes even more evident when the necessary assistance requires a specialized professional. In Brazil, the specialty of Dermatology was the second-most referred to by primary care physicians, amounting to 17.78% of all the referrals with the average waiting time being more than 100 days for an appointment (1, 2).

A large number of dermatologist referrals occur mainly due to the wide variety of dermatoses, which makes the diagnosis challenging for primary care physicians. A study conducted by the Brazilian Society of Dermatology indicated that, in 2018, only 9.1% Brazilian municipalities had specialists in dermatology (3). This heterogeneous distribution of the medical population,

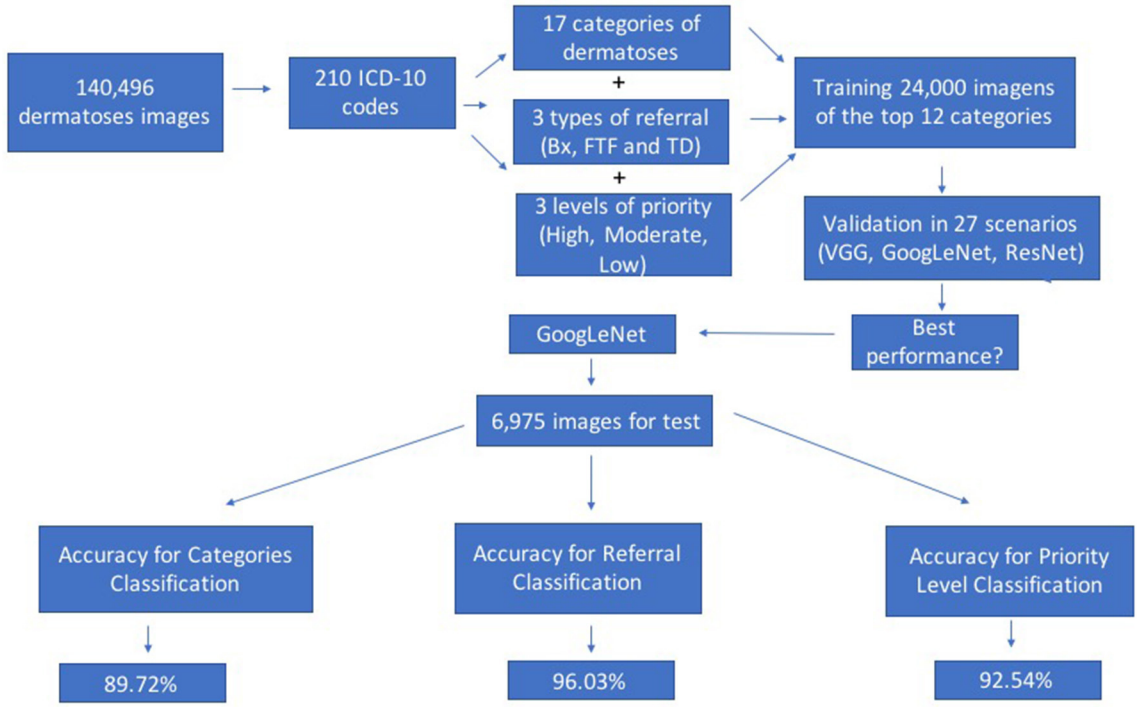

GRAPHICAL ABSTRACT | Graphical Abstract showing the research flow from the dataset base images, classification of the dermatoses according to categories, referral and level of priority; training and validation in different scenarios to the final test, using the algorithm with the best performance.

especially in remote areas, contributes to the increase in seeking means of care such as telemedicine. The effectiveness, accuracy, and reliability of dermatological diagnosis via telemedicine have been widely studied and are considered equivalent to those performed by dermatologists in face-to-face consultations (4–6).

The digital nature of these services, added to the recent developments in the field of image processing, provide an extremely fertile environment for research related to the application of artificial intelligence (AI) in the identification and diagnosis of skin lesions. In 2016, Shrivastava developed an algorithm based on support vector machine (SVM) capable of identifying psoriasis with 99.81% accuracy (7).

In 2018, in a research by Han et al., a classification algorithm built with deep neural networks showed 91% accuracy in the task of differentiating pigmented lesions between benign and malignant using a sample of 21,306 images (8). A large body of research in the literature points to a satisfactory accuracy of AI algorithms in identifying various types of skin diseases, ranging from simple onychomycosis (9) to melanomas (10–12).

However, previous studies generally focused on one disease or a limited group of diseases. To study the application of these technologies in the larger context of public health, a broader approach is needed to classify the dermatoses in established categories and suggest appropriate treatment approaches. In addition to focusing on the diagnosis of a single disease, it was observed that many studies have utilized image acquisition protocols and equipment designed specifically for AI in order to enhance the accuracy of classification algorithms. However, these image-acquisition protocols are too time consuming for health-care professionals to implement, and the equipment used are not available in most primary health-care units. This hinders the implementation of the algorithm in the public health system.

The authors identified an opportunity to evaluate the performance of these techniques in a broader context which does not classify lesions as belonging or not belonging to a specific diagnosis, rather in a more comprehensive classification, using simple protocols that can be applied by day-to-day primary health-care professionals.

The image acquisition equipment used in the present study are available among primary care networks. The purpose of the study was to optimize stages of the diagnostic process to provide health-care professionals with a diagnostic support tool that is capable of correctly and quickly screening and referring to cases to the specialist, according to their priority level.

The primary goal of the current work was to evaluate the accuracy of different algorithms of deep neural networks for triage and support diagnosis of skin lesions. The second aim was to test the accuracy of the algorithm for the best performance on the diagnosis, referral and level of priority, compared to those performed by dermatologists, using a test with clinical images *in silico*.

MATERIALS AND METHODS

Acquisition of Clinical Images for the Development of the Neural Network

The present study was approved by the Ethics Committee of the Hospital Israelita Albert Einstein (project number: 3541-18). 140,446 images were utilized corresponding to 57,568 skin lesions, obtained between July 2017 and August 2018 from a philanthropic assistance project between Albert Einstein Israel-Brazilian Benevolent Society and the São Paulo City Hall. The project and its results have been described in detail previously (1).

Briefly, patients requiring primary care attention and waiting for an appointment with a dermatologist in the public health-care system of the city were directed to three municipal hospitals, where photos of their skin lesions were collected by health technicians using the default Samsung Galaxy S7 smartphone camera in conventional offices. These images, together with the demographic data and a brief clinical history, were uploaded to the Amazon Web Services platform and diagnosed by 13 dermatologists who had to choose among three possible referrals: (1) biopsy of the lesion; (2) a face-to-face visit to the dermatologist; or (3) suggesting the best conduct for the treatment and/or monitoring the cases via teledermatology along with the primary care physician. The 57,568 diagnosed lesions were classified into 210 International Classification of Diseases-10 (ICD-10) codes, which were grouped into 17 categories based on the nature of the dermatoses for better evaluation of the results. The categories are described in **Table 1** and are the targets for predicting the diagnosis in the present study. The total number of images in each category, their corresponding percentage, the number of images used to test the algorithm and referrals with their respective priorities, according to our dermatologists' standards of care are shown in **Table 1**. The ICD-10 codes and the main diseases that make up each category are listed in **Supplementary Table 1**.

Development of Artificial Neural Networks

To mitigate the problem of lack of focus on injuries, all the images were cut individually using Microsoft Paint so that only the region of interest related to the lesion was preserved for analysis. Following this, in order to standardize the network input, images were resized to 224 × 224 pixels. The errors obtained in the classification of the training set and validation were calculated using the mean square error equation (MSE). It was chosen among the various loss functions used for the classification field because it was the most frequent suppervisioned learning in medical literature at the time of the experiment. More technical information on algorithm pipeline is found in **Supplementary Material 2**.

The programming language used was Python; all neural network models were trained and tested on Keras API using Tensorflow as the backend in two Amazon instances: p 2.xlarge with a single Nvidia Tesla k80 GPU, g3.4xlarge with a single Nvidia Tesla M60 GPU.

Experiments

Two initial exploratory experiments conducted previously to the following are presented in **Supplementary Material 3**.

TABLE 1 | Categories of target classes dermatological diseases, their contribution in the dataset of images, referral and level of priority, according to our dermatologists' standard of care.

	Category	Total images dataset (*n*)	Total images dataset (%)	Test images (*n*)	Referral	Priority
1	Benign tumor	31,998	22.78	1,600	TD	low
2	Eczema	25,217	17.95	1,261	TD	moderate
3	Pigmentation disorder	19,825	14.12	992	TD	low
4	Superficial infection/Infestation	18,963	13.50	949	TD	moderate
5	Inflammatory disorder	15,228	10.84	762	TD	moderate
6	Benign cyst	7,776	5.54	389	FTF	low
7	External cause	5,916	4.21	296	TD	low
8	Genetic cause	5,077	3.61	254	TD	low
9	Not grouped	2,474	1.76	123	TD	low
10	Metabolic cause	2,438	1.74	121	FTF	low
11	Malignant tumor	2,375	1.69	118	BIOPSY	high
12	Pre-malignant (actinic keratosis)	2,200	1.57	110	BIOPSY	high
13	Connective tissue disorder	371	0.26	0	FTF	high
14	Adverse drug reaction	339	0.24	0	TD	moderate
15	Deep/systemic infection	128	0.09	0	FTF	high
16	Bullous disease	61	0.04	0	TD	high
17	Factitial dermatitis	60	0.04	0	TD	low
18	Total	140,446	100%	6,975	–	–

TD, teledermatology; FTF, face-to-face dermatologist.

TABLE 2 | Results of the first experiment to test the accuracy of different neural networks according to architecture, weights and learning rate.

Scenario	Architecture	weight Initialization	Learning rate	Training accuracy	Validation accuracy	Training error	Validation error	Validation specificity	Validation sensitivity
1	**VGG**	**FFE**	**10^{-3}**	**99.97%**	**87%**	**0.0120**	**0.7359**	**96.76%**	**87.76%**
2	VGG	EMRW	10^{-3}	76.61%	66.66%	0.5899	0.8782	91.50%	68.2%
3	VGG	RI	10^{-3}	97.72%	86.45%	0.0722	0.7367	96.51%	86.6%
4	GoogLeNet	FFE	10^{-3}	100%	88%	0.0002	0.6811	88.59%	97.01%
5	GoogLeNet	EMRW	10^{-3}	92.46%	58.33%	0.1943	2,027	89.75%	62%
6	**GoogLeNet**	**RI**	**10^{-3}**	**98.09%**	**90.62%**	**0.0774**	**0.4928**	**97.73%**	**90.86%**
7	ResNet	FFE	10^{-3}	19.53%	20%	1.6094	1.6094	80%	20%
8	ResNet	EMRW	10^{-3}	98.55%	25%	0.0288	8,040	80%	20%
9	ResNet	RI	10^{-3}	15.27%	14%	1.6094	1.6094	79%	16%
10	VGG	FFE	10^{-6}	51.92%	60%	1,2061	1,181	89.95%	62.26%
11	VGG	EMRW	10^{-6}	56.85%	51.04%	1.1603	1.2	87.98%	54.33%
12	VGG	RI	10^{-6}	20%	26%	1.6094	1,6093	80%	20%
13	GoogLeNet	FFE	10^{-6}	88.16%	84%	0.3768	0.4937	95.94%	85%
14	GoogLeNet	EMRW	10^{-6}	66.21%	40.62%	0.899	1,66716	85.13%	43.3%
15	GoogLeNet	RI	10^{-6}	43.28%	38.54%	1.3286	1.6240	84.65%	40.59%
16	ResNet	FFE	10^{-6}	17.37%	26%	1.6109	1,608	80.26%	21%
17	ResNet	EMRW	10^{-6}	79.77%	25%	0.5516	1,99700	80%	20%
18	ResNet	RI	10^{-6}	34.87%	30%	1,44680	1.6094	82.74%	33.32%
19	VGG	FFE	10^{-9}	20%	20%	1,77511	1,66637	80%	20%
20	VGG	EMRW	10^{-9}	20.24%	20.83%	1.6809	1,66434	80%	20%
21	VGG	RI	10^{-9}	20.76%	14.58%	1,694	1.6094	80%	20%
22	GoogLeNet	FFE	10^{-9}	19.81%	25%	1.7363	1.6406	81.12%	25.2%
23	GoogLeNet	EMRW	10^{-9}	18.26%	11.45%	1,66825	1.7704	77.47%	11.20%
24	GoogLeNet	RI	10^{-9}	20.22%	16.66%	1,685	2,22818	79.50%	17.60%
25	ResNet	FFE	10^{-9}	22.7%	19%	1.6269	0.04	79.75%	19%
26	ResNet	EMRW	10^{-9}	18.85%	14%	2.1515	1.8448	79.69%	18.66%
27	ResNet	RI	10^{-9}	19.42%	15%	1,833	2,33286	79.35%	16.79%

FFE, fixed feature extractors; EMRW, extension of the model and reinitialization of weights; RI, random initialization.
The bold in lines for scenarios 1 and 6 of the this table, they were the best results obtained in the first experiment.

First Experiment

To test the accuracy of different neural networks, 24,000 random images were utilized to train the 12 groups of most frequently identified dermatoses (**Table 1**), corresponding to 99.32% of the total volume of the diagnosed diseases. The 12 groups were composed of the classes: benign tumor, eczema, pigmentation disorder, superficial infection/infestation, inflammatory disorder, benign cyst, external cause, genetic cause, not grouped, metabolic cause, malignant tumor and pre-malignant. The category "Pre-malignant" had only 2,200 images and was the only one in which the same images were used both in the training and validation sets (**Table 1**).

Twenty seven scenarios were evaluated based on architectural variations, the initialization strategy, the weights, and the learning rates. The VGG, GoogLeNet and ResNet architectures were evaluated using weight initialization of fixed feature extractors (FFE), extension of the model and reinitialization of weights (EMRW), and random initialization (RI). We have chosen those architectures based on previous works (8, 9, 13), which showed interesting results with them. As the first experiment intended to be exploratory, we used different initialization techniques, including random initialization, which could be seen as not seen suitable for our dataset. IMAGEnet was the base assembly to apply for weight initialization. The learning rate value was adjusted between test scenarios. The parameter variations were 1e-03, 1e-06, and 1e-09, respectively.

The other parameters of the architectures followed the configuration presented in the literature (14). For training, momentum rate with a value of 0.9 and images of the dataset were processed in groups of 32 images simultaneously were used. The training was carried out over 1,000 epochs. To avoid data unbalance due to the disparity between the number of images in each group, the same number of images were used in each of the 12 groups for training and validation. For the validation, 200 random images, which were not present in the training set of each group, were used.

Second Experiment

During the second experiment, in the final test with the algorithm yielding the best performance among the deep neural networks, 5% of images from each category of dermatoses were used with 7.022 images belonging to the 17 groups, as shown in **Table 1**. The five groups presented at the bottom of the table (connective tissue disorder, adverse drug reaction, deep/systemic infection, bullous disease and factitial dermatitis), however, were disregarded due to the small number of cases, resulting in a total of 6,975 cases tested.

RESULTS

First Experiment

Table 2 presents the results of 27 different scenarios tested in the first experiment to determine which neural network achieves the best performance.

In the training phase, the best accuracy was observed in scenarios with a learning rate of 10^{-3}. All three architectures showed an accuracy of 98–100%. However, when verifying the values of the validation phase, the GoogLeNet architecture

TABLE 3 | Confusion matrix of this diagnostic accuracy for GoogLeNet architecture.

	Genetic cause	Metabolic cause	Traumatic cause	Benign cyst	Pigmentation disorder	Eczema	Superficial infection	Inflammation of unknown cause	Not grouped	Benign tumor	Malignant tumor	Pre-malignant tumor
Genetic cause	236	1		9		53	9		3	38		
Metabolic cause		119	2			34	7	6	4		4	
External cause	1		272			3	5		1	14		2
Benign cyst	5			352	27	24	23	12	5			
Pigmentation disorder			4	7	898	36	29	20	5	11	2	
Eczema			2	2		1,041			3			
Superficial infection/infestation			13		29		859		2			
Inflammation disorder	3			9		2		690				
Not grouped	9		3	7	23	68		34	94		3	3
Benign tumor		1			11				1	1,488		0
Malignant tumor					4		15		2	20	108	4
Pre-malignant				3			2		3	29	1	101

Values of the color shade are the true positive results.

TABLE 4 | Confusion matrices for referrals and level of priority using GoogLeNet architecture.

		Results predicted by AI		
	Referral	**Teledermatology**	**Dermatotolgy**	**Biopsy**
Dermatologists' Choice (ground truth)	Teledermatology	6,013	36	10
	Dermatology	149	471	4
	Biopsy	75	3	214
	Total	6,237	510	228
	Priority	Low	Moderate	High
	Low	3,354	364	12
	Moderate	64	2,887	2
	High	61	17	214
	Total	3,479	3,268	228

obtained the best performance out of all using the RI approach, with 90.62% accuracy.

Second Experiment

The GoogLeNet network, using IR weight initialization was, then, tested in 6,945 images, obtaining an accuracy of 89.72%. **Table 3** shows the confusion matrix in the diagnostic accuracy of the test in different categories of dermatoses.

Observing the distribution of errors in **Table 3**, a regularity can be noticed in the number of errors and hits for each class except for "ungrouped," which shows not only a smaller number of hits among the lesions but also in a greater number of classes classified as other lesions with this label.

An analysis was conducted of the referral and its priority proposed by the algorithm regardless of the lesion category. Regarding referrals, eight groups (6,237 images) indicated referral for teledermatology, two groups (510 images) for face-to-face dermatologist appointments and two groups (228 images) for biopsy. Among the 12 groups of lesions assessed in the test dataset, up to six had low priority (3,479 images), four had moderate service priority (3.268 images), and two had high priority calls (228 images). The distribution of the priority indication of the service and the routing suggested in the classification of the images are presented in **Table 4**.

The overall accuracy was 96.03% (6,013+471+214 = 6,698/6,975) for the referral of the patient and 92.54% (3,354+2,887+214 = 6,455/6,975) for the priority definition task. The referral confusion matrix showed equivalent specificity percentages in all possible outcomes, 96.41% (6,013/6,237) for referral to the teledermatologist, 92.35% (471/510) to attend dermatologist in person and 93.86% (214/228) for biopsy. As for the priority, it was noted that 93.86% (214/228) high priority lesions received a pertinent indication in the algorithm. However, 78 cases classified as high priority by the dermatologists were classified as low (61) and moderate (17), determining a specificity of 73.23% (214/292).

DISCUSSION AND CONCLUSIONS

The present study tested 27 scenarios of deep-learning algorithms to determine the most efficient one for classifying common skin lesions in primary care attention into one of the predefined categories, reaching an accuracy of 90.6% in the validation phase and 89.7% in the test phase for 6,975 cases. These results were considered good compared to those in the literature. One of the studies in the literature aimed to use deep neural networks to classify 26 common dermatoses in primary care, with an overall accuracy of 0.66 in 963 cases (15). In another study, 3,501 cases were tested (using two different validation sets) for 134 classes of skin lesions, showing an accuracy of 56.7% in one test group and 44.8% in the other (16). In another research with 5,014 validated cases, AI obtained 76.9% accuracy in classifying 40 common dermatoses (17). Further, in a recently conducted study, 340 teledermatology images were tested for 174 different dermatological diseases, obtaining an accuracy of 41.2% (18).

Currently, a large number of articles show the development of algorithms for diagnostic support of diseases such as melanoma or a group of disorders such as skin cancer mainly using dermoscopic images (19–21). However, the use of dermoscopy may not be feasible on a large scale such as public health. For this reason, the present study used clinical images. Notably, the definitive diagnosis of malignant lesions to date is obtained by histopathology examination, i.e., through the microscopic analysis of the lesion in part or in totality after its surgical excision (biopsy). Therefore, although physicians or an algorithm may suggest skin cancer, the diagnosis is only confirmed by histopathology. Thus, if the biopsy referral is correct, this may be more significant than the diagnosis *per se*. An added advantage, especially in cases where the wait is sometimes as long as 6 months or more, can be if the priority of the disease is determined in addition to providing the correct referral. In cases of skin cancer, if the algorithm correctly points to high priority, it can benefit the patient as well as the health system as a whole. Thus, we consider our results with an accuracy of 96.0% for referrals and 92.5% for priority to be significant, as this data has not yet been reported in the literature.

Another fundamental aspect of the current study is the search for a simpler and low-cost means to obtain images: those clicked by health technicians using the standard photographic camera of a smartphone in regular offices. The use of common technology, with easy access and operability makes it viable to scale the present study. As the images and data were

obtained by health technicians, the demand for the physician's specialized workforce is reduced, possibly also lowering costs in the public system.

In terms of the development of neural networks, several challenges were identified in the present study such as the labeling of skin lesions by dermatologists which was done through ICD-10. Initially, it was expected that the present work would be able to create a classifier that can identify the ICD of each lesion. However, after the reports were extracted, it was found that, in addition to the large number of classes ($n = 210$), some ICD codes had a limited number of copies—around two or three images—disabling the training of an algorithm for their identification. Another situation was the low number of cases ($n = 2{,}200$) in the premalignant category, for which the same images had to be used for both validation and testing. Although this situation is against the basic rules of deep learning algorithm development, we used the same images for validation and test datasets because we did not have enough number of cases in the pre-malignant class to divide it into the different datasets, as we had in the other classes in order to prevent imbalance among the classes.

Also, the category "not grouped" performed poorly in accuracy due to the greater heterogeneity of the images that make up this data set. This class encompassed images showing no lesions at times, or lesions which did not characterize a specific classification, and nail disorders that could not be specified in other groups (**Supplementary Table 1**). Thus, less similarity was observed between the images in the data set and, in some cases, with lesions of other classes.

There are limitations to our work. Our study population was confined to individuals with chronic skin conditions and, therefore, it has limited value as a triage tool because it has not been tested for acute conditions and might not not work in this setting. It is also important to note that the algorithm was in no way intended to take over the physician's role. Its objective lies only in the screening of chronic dermatological lesions, offering health professionals a supporting tool in the confirmation of clinical diagnosis and increasing their productivity in the evaluation of patients. This can optimize medical access for the more severe, surgical, or complex cases and direct them to the right referral and priority.

There are several future possibilities based on the present study. For clinical research, the most obvious pathway will be to apply the algorithm in real-life settings to compare its performance with that of physicians and assess its degree of accuracy. Second, in case of good performance, the use of the algorithm should be verified as this tool would modify medical management. In the field of computing, many possibilities are present for increasing the algorithm's accuracy: use of other network architectures such as ResNeXT, DenseNet and SE-Net; use of demographic data and clinical history of patients; and use of data augmentation for groups of dermatoses with less representation.

DATA AVAILABILITY STATEMENT

The raw data supporting the conclusions of this article will be made available by the authors, without undue reservation.

ETHICS STATEMENT

The studies involving human participants were reviewed and approved by Ethics Committee of the Hospital Israelita Albert Einstein (project number: 3541-18). Written informed consent from the participants' legal guardian/next of kin was not required to participate in this study in accordance with the national legislation and the institutional requirements.

AUTHOR CONTRIBUTIONS

MG-B was responsible for study's design, data collection, and writing and reviewing the article. AS was responsible for study's design, data collection, and performing the experiments and reviewing. EC was responsible for study's design, data collection, and reviewing the article. All authors contributed to the article and approved the submitted version.

SUPPLEMENTARY MATERIAL

The Supplementary Material for this article can be found online at: https://www.frontiersin.org/articles/10.3389/fmed.2021.670300/full#supplementary-material

REFERENCES

1. Giavina-Bianchi M, Santos AP, Cordioli E. Teledermatology reduces dermatology referrals and improves access to specialists. *EClin Med.* (2020) 29–30:100641. doi: 10.1016/j.eclinm.2020.100641
2. Vieira R, Lima TMN, Gazzinelli A. The waiting time for specialized medical consultations in a small municipality of Minas Gerais, Brazil. *Rev Mineir Enfermagem.* (2015) 19:65–71. doi: 10.5935/1415-2762.20150006
3. Schmitt JV, Miot HA. Distribution of Brazilian dermatologists according to geographic location, population and HDI of municipalities: an ecological study. *An Bras Dermatol.* (2014) 89:1013–5. doi: 10.1590/abd1806-4841.20143276
4. Giavina-Bianchi M, Sousa R, Cordioli E. Part I: accuracy of teledermatology in inflammatory dermatoses. *Front Med.* (2020) 7:585792. doi: 10.3389/fmed.2020.585792
5. Giavina-Bianchi M, Azevedo MFD, Sousa RM, Cordioli E. Part II: accuracy of teledermatology in skin neoplasms. *Front Med.* (2020) 7:598903. doi: 10.3389/fmed.2020.598903
6. Levin YS, Warshaw EM. Teledermatology: a review of reliability and accuracy of diagnosis and management. *Dermatol Clin.* (2009) 27:163–76, vii. doi: 10.1016/j.det.2008.11.012
7. Shrivastava VK, Londhe ND, Sonawane RS, Suri JS. Computer-aided diagnosis of psoriasis skin images with HOS, texture and color features: a first comparative study of its kind. *Comp Meth Prog Biomed.* (2016) 126:98–109. doi: 10.1016/j.cmpb.2015.11.013
8. Han SS, Kim MS, Lim W, Park GH, Park I, Chang SE. Classification of the clinical images for benign and malignant cutaneous tumors using a deep learning algorithm. *J Invest Dermatol.* (2018) 138:1529–38. doi: 10.1016/j.jid.2018.01.028

9. Han SS, Park GH, Lim W, Kim MS, Na JI, Park I, et al. Deep neural networks show an equivalent and often superior performance to dermatologists in onychomycosis diagnosis: automatic construction of onychomycosis datasets by region-based convolutional deep neural network. *PLoS ONE*. (2018) 13:e0191493. doi: 10.1371/journal.pone.0191493
10. Tschandl P, Codella N, Akay BN, Argenziano G, Braun RP, Cabo H, et al. Comparison of the accuracy of human readers versus machine-learning algorithms for pigmented skin lesion classification: an open, web-based, international, diagnostic study. *Lancet Oncol.* (2019) 20:938–47. doi: 10.1016/S1470-2045(19)30333-X
11. Tschandl P, Rinner C, Apalla Z, Argenziano G, Codella N, Halpern A, et al. Human-computer collaboration for skin cancer recognition. *Nat Med.* (2020) 26:1229–34. doi: 10.1038/s41591-020-0942-0
12. Marchetti MA, Codella NCF, Dusza SW, Gutman DA, Helba B, Kalloo A, et al. Results of the 2016 international skin imaging collaboration international symposium on biomedical imaging challenge: comparison of the accuracy of computer algorithms to dermatologists for the diagnosis of melanoma from dermoscopic images. *J Am Acad Dermatol.* (2018) 78:270–7.e1. doi: 10.1016/j.jaad.2017.08.016
13. Mahbod A, Schaefer G,Wang C, Ecker R, Ellinger I. Skin lesion classification using hybrid deep neural networks. In: *Presented at: 44th International Conference on Acoustics, Speech, and Signal Processing (ICASSP 2019)*. Brighton (2017).
14. Simonyan K, Zisserman A. Very deep convolutional networks for large-scale image recognition. In: *Presented at: Computer Vision and Pattern Recognition (csCV)*. San Diego, CA (2014).
15. Liu Y, Jain A, Eng C, Way DH, Lee K, Bui P, et al. A deep learning system for differential diagnosis of skin diseases. *Nat Med.* (2020) 26:900–8. doi: 10.1038/s41591-020-0842-3
16. Han SS, Park I, Lim W, Kim MS, Park GH, Chae JB, et al. Augment intelligence dermatology : deep neural networks empower medical professionals in diagnosing skin cancer and predicting treatment options for 134 skin disorders. *J Invest Dermatol.* (2020) 140:1753–61. doi: 10.1016/j.jid.2020.01.019
17. Pangti R, Mathur J, Chouhan V, Kumar S, Rajput L, Shah S, et al. A machine learning-based, decision support, mobile phone application for diagnosis of common dermatological diseases. *J Eur Acad Dermatol Venereol.* (2020) 35:536–45. doi: 10.1111/jdv.16967
18. Muñoz-López C, Ramírez-Cornejo C, Marchetti MA, Han SS, Del Barrio-Díaz P, Jaque A, et al. Performance of a deep neural network in teledermatology: a single-centre prospective diagnostic study. *J Eur Acad Dermatol Venereol.* (2020) 35:546–53. doi: 10.1111/jdv.16979
19. Chu YS, An HG, Oh BH, Yang S. Artificial intelligence in cutaneous oncology. *Front Med.* (2020) 7:318. doi: 10.3389/fmed.2020.00318
20. Esteva A, Kuprel B, Novoa RA, Ko J, Swetter SM, Blau HM, et al. Corrigendum: dermatologist-level classification of skin cancer with deep neural networks. *Nature.* (2017) 546:686. doi: 10.1038/nature22985
21. Han SS, Moon IJ, Lim W, Suh IS, Lee SY, Na JI, et al. Keratinocytic skin cancer detection on the face using region-based convolutional neural network. *JAMA Dermatol.* (2019) 1:29–37. doi: 10.1001/jamadermatol.2019.3807

Conflict of Interest: The authors declare that the research was conducted in the absence of any commercial or financial relationships that could be construed as a potential conflict of interest.

Advantages of publishing in Frontiers

OPEN ACCESS
Articles are free to read for greatest visibility and readership

FAST PUBLICATION
Around 90 days from submission to decision

HIGH QUALITY PEER-REVIEW
Rigorous, collaborative, and constructive peer-review

TRANSPARENT PEER-REVIEW
Editors and reviewers acknowledged by name on published articles

Frontiers
Avenue du Tribunal-Fédéral 34
1005 Lausanne | Switzerland

Visit us: www.frontiersin.org
Contact us: frontiersin.org/about/contact

REPRODUCIBILITY OF RESEARCH
Support open data and methods to enhance research reproducibility

DIGITAL PUBLISHING
Articles designed for optimal readership across devices

FOLLOW US
@frontiersin

IMPACT METRICS
Advanced article metrics track visibility across digital media

EXTENSIVE PROMOTION
Marketing and promotion of impactful research

LOOP RESEARCH NETWORK
Our network increases your article's readership